



## **Contaminant mass discharge of chlorinated solvents from sources in clay till** Concepts, quantification and risk assessment

**Rosenberg, Louise**

*Publication date:*  
2023

*Document Version*  
Publisher's PDF, also known as Version of record

[Link back to DTU Orbit](#)

*Citation (APA):*  
Rosenberg, L. (2023). *Contaminant mass discharge of chlorinated solvents from sources in clay till: Concepts, quantification and risk assessment*. Technical University of Denmark.

---

### **General rights**

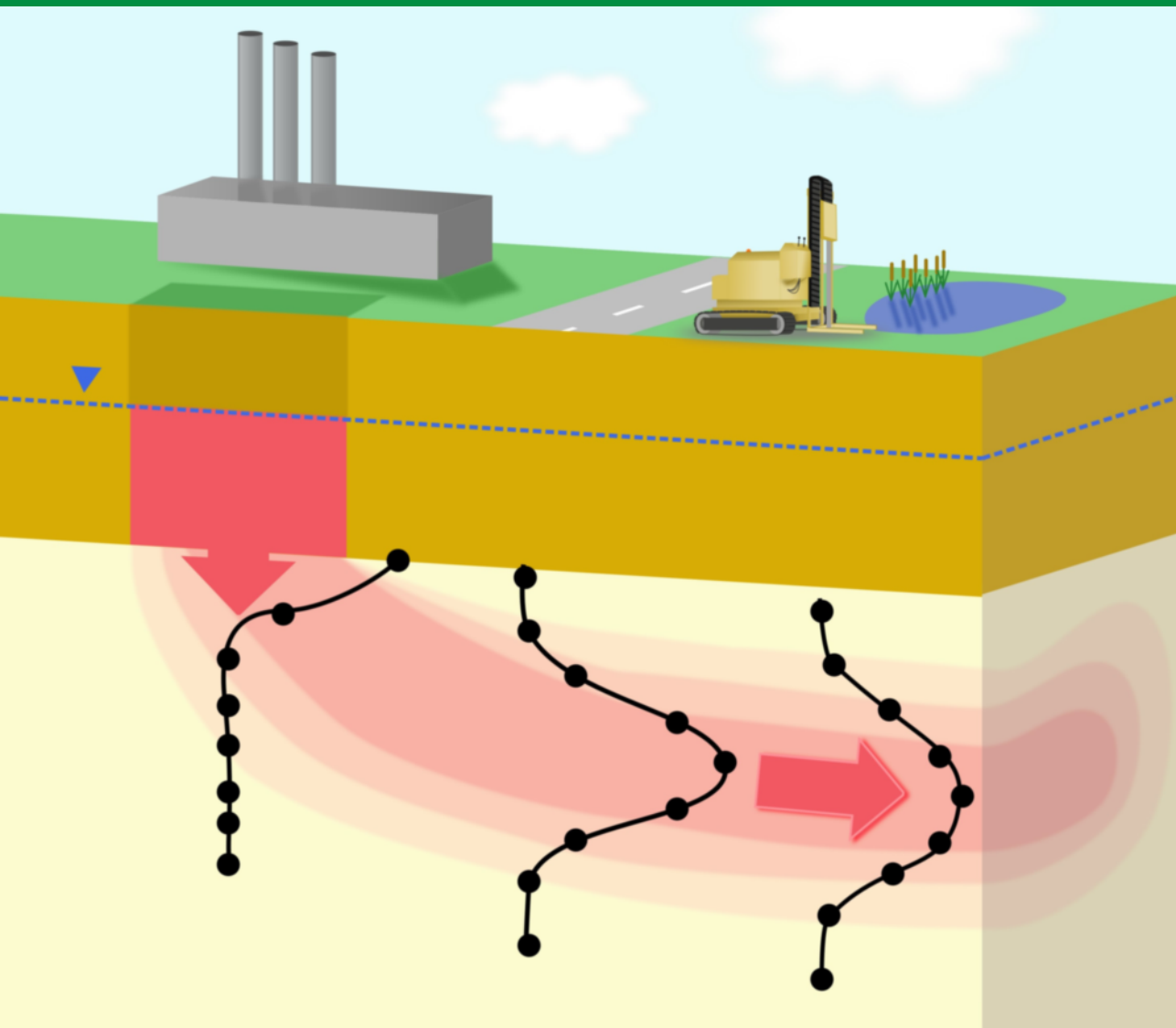
Copyright and moral rights for the publications made accessible in the public portal are retained by the authors and/or other copyright owners and it is a condition of accessing publications that users recognise and abide by the legal requirements associated with these rights.

- Users may download and print one copy of any publication from the public portal for the purpose of private study or research.
- You may not further distribute the material or use it for any profit-making activity or commercial gain
- You may freely distribute the URL identifying the publication in the public portal

If you believe that this document breaches copyright please contact us providing details, and we will remove access to the work immediately and investigate your claim.

# Contaminant mass discharge of chlorinated solvents from sources in clay till: Concepts, quantification and risk assessment

Louise Rosenberg - Phd Thesis



# Contaminant mass discharge of chlorinated solvents from sources in clay till: Concepts, quantification and risk assessment

Louise Rosenberg

PhD Thesis  
August 2023

DTU Sustain  
Department of Environmental and Resource Engineering  
Technical University of Denmark

**Contaminant mass discharge of chlorinated solvents from sources in clay tills: Concepts, quantification and risk assessment**

**Louise Rosenberg**

PhD Thesis, August 2023

Address: DTU Sustain  
Department of Environmental and Resource Engineering  
Technical University of Denmark  
Bygningstorvet, Building 115  
2800 Kgs. Lyngby  
Denmark

Phone reception: +45 4525 1600

Homepage: <https://www.sustain.dtu.dk>  
E-mail: [reception@env.dtu.dk](mailto:reception@env.dtu.dk)

Cover: STEP

# Preface

The work presented in this PhD thesis was carried out at the Department of Environmental and Resource Engineering at the Technical University of Denmark (DTU Sustain) in the period January 2018 to July 2023. Professor Poul L. Bjerg (DTU Sustain) was the main supervisor and Associate Professor Mette M. Broholm (DTU Sustain) was the co-supervisor.

The project was funded by the Capital Region of Denmark and the Department of Environmental and Resource Engineering (DTU Sustain).

The thesis is organized in two parts: the first part puts into context the findings of the PhD in an introductory review; the second part consists of the papers listed below. These will be referred to in the text by their paper number written with the Roman numerals **I-VI**. Paper **III** partly deals with how to interpret the georadar signals to investigate the geology of clay till sites. The georadar interpretation will only play a minor role in the introductory review, however, it is included in the thesis, as the paper contributes to the understanding of the geology at the field site.

- I Rosenberg, L., Broholm, M.M., Tuxen, N., Kerrn-Jespersen, I.H., Lilbæk, G., and Bjerg, P.L., 2022. Vertical Hydraulic Gradient Estimation in Clay Till, Using MiHPT Advanced Direct-Push Technology. Groundwater Monitoring and Remediation 42, no.1: 29–37. DOI: 10.1111/gwmr.12470.**
- II Rosenberg, L., Mosthaf, K., Broholm, M.M., Fjordbøge, A.S., Tuxen, N., Kerrn-Jespersen, H., Rønde, V.K., and Bjerg, P.L., 2023. A Novel Concept for Estimating the Contaminant Mass Discharge of Chlorinated Ethenes Emanating from Clay till Sites. Journal of Contaminant Hydrology 252, 1-10. DOI: 10.1016/j.jconhyd.2022.104121.**
- III Jensen, B.B., Rosenberg, L., Tsitonaki, A., Tuxen, N., Bjerg, P.L., Nielsen, L., Hansen, T.M., and Looms, M.C., 2023. High-resolution geological information from crosshole ground penetrating radar in clayey tills. Groundwater Monitoring and Remediation. DOI: 10.1111/gwmr.12588.**

- IV** Mosthaf, K., **Rosenberg**, L., Broholm, M.M., Lilbæk, G., Christensen, A.G., Fjordbøge, A.S., and Bjerg, P.L., 2023. Quantification of contaminant mass discharge from point sources in aquitard/aquifer systems based on vertical concentration profiles and 3D modeling. Submitted.

In addition to these papers, the following written work has been carried out in the duration of the PhD study:

Locatelli, L., Binning, P.J., Sanchez-Vila, X., Søndergaard, G.L., **Rosenberg**, L. and Bjerg, P.L., 2019. A Simple Contaminant Fate and Transport Modelling Tool for Management and Risk Assessment of Groundwater Pollution from Contaminated Sites. *Journal of Contaminant Hydrology* 221, 35–49. DOI: 10.1016/j.jconhyd.2018.11.002.

Jensen, B.B., **Rosenberg**, L., Nielsen, L., Tuxen, N., Tsitonaki, K., Hansen, T.M., and Looms, M.C., 2022. The Impact of Water-Filled Boreholes on GPR Data in a Clayey-till Environment. In 19th International Conference on Ground Penetrating Radar. Golden, Colorado. DOI: 10.1190/gpr2022-061.1.

# Acknowledgements

First I would like to thank my supervisors Poul L. Bjerg and Mette M. Broholm for great supervision, feedback on my work and the ability to provide a nice work environment. We have had many scientific discussions that have helped me and guided me back on track when needed and listened to my ideas and/or concerns. You have always made sure that the work-life balance was on point and provided a great work environment. Furthermore, a thank goes to Klaus Mosthaf who have been providing me with insightful comments and ideas throughout the project.

On my external stay to the Capital Region of Denmark, I met a lot of great people who have made it a joy for me visit and have made me feel welcome. A special thanks goes to Nina Tuxen, Henriette Kernn-Jespersen and Vinni Rønne for great cooperation and input for the project.

Acknowledgements also goes to Bolette B. Jensen and Majken C. Looms from University of Copenhagen for the nice co-operation on the use of cross-hole georadar in clay till. Additionally, collaboration with consultants and field technicians from NIRAS has been insightful and enjoyable.

A praise goes out to all my colleagues at DTU Sustain through the years. In the field, Bent and Jens have been excellent co-workers, finding solutions and performing exceptional field and lab work. I would like to thank my nice office mates through the years as a PhD student, Alex, Vinni, Majken and Cecilie who made sure that I never walked alone to the café for a nice coffee.

Last but not least, I would like to thank my family and friends for the mental support during the project. Especially my parents and in-laws for helping at home when I needed longer days or went for conferences. A special thanks goes to Mathias, Eigil and Ove for always being there for me.

Thank you all!

# Summary

Worldwide, contaminated sites pose a threat to water resources, in particular groundwater. Legacy chemicals, like chlorinated ethenes, exceeding the groundwater quality criteria are vastly found in groundwater. To limit the risk posed to ecosystem health, including humans, clean-ups are needed. However, funds are not unlimited and prioritization of the contaminated sites posing a risk to a given receptor is needed. To better perform a prioritization of contaminated sites, the concept of Contaminant Mass Discharge (CMD) has been suggested as a prevailing metric. A variety of methods to quantify CMD are needed in order to perform risk assessments at different knowledge levels.

In the Northern Hemisphere, many sites are located in clay till settings. Understanding the transport of contaminants in the low-permeability clay till is complex, but vital, in order to protect the underlying aquifer and drinking water abstraction wells. High-permeability features, such as sand lenses and fractures can act as preferential transport pathways. Via diffusion, and later on back-diffusion, the clay till matrix can act as a secondary source increasing the duration of the contaminant emanating to the aquifer. Setting up efficient approaches for investigation of contaminant sources in clay till settings to inform the conceptual site model is key for a reliable risk assessment.

The aim of this thesis is to improve the risk assessment of chlorinated ethene sources in clay till posing a risk to groundwater resources. This was done by: exploring governing and relevant transport processes of chlorinated ethenes in clay till/aquifer systems; assessing field investigation approaches for evaluation of the hydrogeology and contamination at a clay till site; evaluating current methods for quantification of CMD in aquifers and suggesting incorporation of the methods in the Danish risk assessment scheme for contaminated sites. A chlorinated ethane contaminated site in Vassingerød, Denmark, was used as field case for this study.

A comprehensive study of transport and fate processes of chlorinated ethenes in clay till and underlying aquifers was conducted. The study showed a time-dependency of dominant processes governing transport of chlorinated ethenes in clay till. Diffusion (enhanced by sorption) and back-diffusion in clay till play a crucial role in distributing and releasing the contaminant. In many cases, contamination with chlorinated ethenes occurred several decades ago, resulting in a more evenly distributed mass of contamination within the clay



till. The uncertainty in estimating the stored mass of the contaminant in the source zone of clay till is partly attributed to the sorption coefficient of the soil. In the aquifer, steep concentration gradients in both the horizontal and vertical directions are often observed, indicating low dispersivity values and minimal dilution at local scale.

Through comprehensive field and laboratory studies the vertical hydraulic gradient, sorption coefficient of chlorinated ethenes, and high-resolution, depth-discrete water samples were investigated. Furthermore, a solute transport model was set up to investigate the quantification and governing parameters for CMD at the site and evaluate the effect of fracture aperture and sorption in the clay till. The studies showed that the vertical hydraulic gradient provide insights into the presence of fractures and enhances the accuracy of estimating the infiltration rate at the site. An advancement of using the direct-push method Membrane Interface Probe Hydraulic Profiling Tool (MiHPT) proved valuable for estimating the vertical hydraulic gradient. High-resolution, depth-specific concentration profiles can be considered a footprint of the flow field and provide valuable information about the source zone at the site. Sorption plays a significant role for the mass distribution of contaminants, leaching time and the break-through of contamination into the aquifer. For large fracture apertures, the model showed that the transport primarily happened in the fractures, whereas for smaller fracture apertures, the model showed that the advective and diffusive transport in the clay till was the governing processes.

A need for a CMD quantification method for initial site investigations at clay till sites was identified and led to the development of the ProfileFlux method. This method allows for a time-efficient estimate of CMD that enables the prioritization of contaminated sites based on the associated receptors at a catchment scale. A suggestion for incorporating different CMD methods for different stages of risk assessment frameworks has been provided. CMD has been used for several years by the scientific community, however, it is a new way of thought for many practitioners. Thus, the implementation of CMD in risk assessment is still in its early stage in management of groundwater resources by authorities. Further knowledge sharing and development of protocols could help broaden the use of CMD as a metric for risk assessment of contaminated sites.

In conclusion, this PhD thesis has identified the governing transport and fate processes for legacy spills of chlorinated ethenes in clay till. The work introduced the possibility of using the MiHPT to achieve estimates of the vertical hydraulic gradient in the clay till, and presented the new ProfileFlux method useful for a cost-effective determination of CMD. This can improve the risk assessment of contaminated sites with chlorinated ethene sources located in clay till settings. Prioritizing clean-ups, and thereby using the resources and money properly, will ultimately support the protection of the groundwater.

Finally, for future research topics it is recommended to keep focus on the determination of vertical transport in clay till, further testing of the ProfileFlux method, and develop methods for uncertainty estimates regarding CMD estimates. It was also suggested to develop a protocol for the use of CMD for risk assessment purposes in management of contaminated sites.

# Dansk sammenfatning

Verden over udgør forurenede grunde en betydelig risiko for grundvandsressourcerne. Der bliver fundet kemikalier i niveauer, der overstiger de gældende grundvandskvalitetskriterier. Det drejer sig ofte om miljøfremmede stoffer, der tidligere er brugt i store mængder fx chlorerede ethener, pesticider og perfluorerede stoffer (PFAS). For at beskytte natur og mennesker er gode metoder til risikovurdering og eventuelt oprensning af forureningerne nødvendige. De økonomiske midler er begrænsede, og der er således brug for at prioritere mellem de forurenede grunde, der udgør en risiko for en given receptor. Hertil er forureningsflux en velegnet parameter at benytte, hvilket der, gennem de senere år, er kommet større fokus på. For at vurdere forureningsfluxen på forskellige stadier af risikovurdering og vidensniveau, er der behov for en bred vifte af metoder.

På den nordlige halvkugle findes der mange lokaliteter med moræneler i undergrunden. Forureningstransporten i den lavpermeable moræneler er kompleks, men vigtig at forstå for at beskytte det underliggende grundvandsmagasin. Sandlinser og sprækker kan danne præferentielle transportveje for forureningen. En sekundær forureningskilde kan dannes i morænelerens matrix via diffusion og senere tilbage-diffusion, hvilket vil forlænge varigheden af forureningens påvirkning af grundvandsmagasinet. For den konceptuelle forståelse og risikovurdering af forureninger i moræneler, kræver det målrettede og effektive metoder, samt veltilrettelagte undersøgelser.

Formålet med denne ph.d. afhandling er at forbedre risikovurderingen af forureningskilder i moræneler med chlorerede ethener, der påvirker grundvandsmagasiner. Der har været fokus på tre hovedemner. Første hovedemne var at afsøge relevante transportprocesser af chlorerede ethener i moræneler. Andet hovedemne var at vurdere undersøgelsesmetoder til bestemmelse af de hydrogeologiske og forureningsmæssige forhold ved forureningskilder i moræneler. Sidste hovedemne var at evaluere eksisterende metoder til kvantificering af forureningsflux, samt forslag til inkorporering af disse metoder i den danske tilgang til risikovurdering af forurenede grunde. En forurening med chlorerede ethener i moræneler blev benyttet som feltlokalitet for at foretage udvikling og afprøvning af nye metoder.

Der er foretaget en omfattende undersøgelse af chlorerede etheners forureningstransport og skæbne i moræneler og det underliggende grundvandsmagasin. Undersøgelsen viste, at betydningen af de forskellige processer er afhængig af forureningens alder. Diffusion (forstærket af sorption) og tilbage-diffusion i moræneler spiller en vigtig rolle for fordelingen og afgivelsen af forureningen. Mange forureninger med chlorerede ethener er flere årtier gamle. Forureningen er således blevet nogenlunde jævnt fordelt i morænele- ren via diffusion. Ved vurdering af den lagrede masse af chlorerede ethener i morænele- ren er der en betydelig usikkerhed forbundet i sorptionskoefficien- ten, som beskriver fordelingen mellem porevand og lermatrice. I grundvands- magasinet observeres ofte stejle koncentrationsgradienter både horisontalt og vertikalt, hvilket indikerer, at dispersiviteterne er små, og at der sker en mini- mal fortynding.

Den vertikale hydrauliske gradient, sorptionskoefficienter for chlorerede ethener til moræneler og brug af dybdediskrete vandprøver er blevet under- søgt gennem omfattende felt- og laboratorieundersøgelser. Videre blev foru- reningstransporten på testlokaliteten simuleret ved anvendelse af en numerisk model for at bestemme størrelsen og de styrende parametre for forurenings- fluxen samt effekten af sprækker og sorption i moræneler. Undersøgelserne viste, at man via den vertikale hydrauliske gradient kan få viden om tilstede- værelsen af betydelige sprækker og forbedre estimatet af infiltrationen. Den vertikale hydraulisk gradient kan vurderes ved brugen af MiHPT (Membrane Interface Probe Hydraulic Profiling Tool) ved mindre justeringer af feltproce- duren. Dybdediskrete koncentrationsprofiler afspejler strømningsforholdene, og giver værdifuld information angående forureningskilden. Sorption har en stor indflydelse på gennembruds- og nedsivningstiden samt fordelingen af forureningsmassen. Modellen viste, at der ved brug af stor sprækketykkelse sker en betydelig forureningstransport gennem sprækkerne, hvor i mod der ved en lille sprækketykkelse primært sker transport gennem advektive og dif- fusive processer.

ProfileFlux metoden blev udviklet til at estimere forureningsflux af chlore- rede ethener fra morænelerslokaliteter ved indledende forureningsundersøgel- ser. Metoden bidrager til en effektiv risikovurdering, hvor der fokuseres på at benytte forureningsflux til at prioritere forurenede grunde i et indvindingsop- land. Forskellige metoder til vurdering af forureningsflux er blevet forslået benyttet til risikovurdering på forskellige vidensniveauer. Det er for mange

aktører dog stadig en ”ny” tankegang at anvende forureningsflux til risikovurdering af forurenede grunde, selvom forureningsflux har været brugt forskningsmæssigt i mange år. Vidensdeling om erfaringer og opsætning af protokoller kan være vigtige redskaber til at udbrede brugen af forureningsflux ved undersøgelser og håndtering af forurenede grunde.

Samlet set har denne ph.d. afhandling identificeret betydende processer for forureningstransport og skæbne af gamle forureninger i moræner, introduceret brugen af MiHPT til vurdering af den vertikale hydrauliske gradient i moræner og opsat ProfileFlux metoden til effektivt at bestemme forureningsflux. Dette kan være med til at forbedre risikovurderingerne af forureningskilder i moræner. En saglig og velovervejet prioritering af oprensninger af forurenede grunde vil ultimativt lede til bedre beskyttelse af grundvandressourcen.

På baggrund af det udførte arbejde, er der opsat forslag til yderligere undersøgelser og forskningsemner. Disse inkluderer øget fokus på bestemmelse af den vertikale transport, afprøvning af ProfileFlux metoden og vurdering af usikkerheden forbundet til estimerne af forureningsflux. Desuden foreslås det at udvikle en protokol for brugen af forureningsflux til risikovurdering af forurenede grunde. En sådan protokol skal indeholde en detaljeret beskrivelse af, hvordan undersøgelser af forureningsflux skal foretages, og hvordan resultaterne kan benyttes til håndtering af forurenede grundens påvirkning af grundvandressourcen.

# Table of contents

<b>Preface</b> .....	<b>i</b>
<b>Acknowledgements</b> .....	<b>iii</b>
<b>Summary</b> .....	<b>iv</b>
<b>Dansk sammenfatning</b> .....	<b>vii</b>
<b>Table of contents</b> .....	<b>x</b>
<b>Abbreviations</b> .....	<b>xi</b>
<b>1 Introduction</b> .....	<b>1</b>
1.1 Background and motivation .....	1
1.2 Aim and research objectives .....	3
1.3 Thesis outline .....	3
<b>2 Risk assessment of contaminated sites</b> .....	<b>4</b>
2.1 Risk assessment approaches.....	4
2.2 Contaminant Mass Discharge .....	6
2.3 Scale and framework for risk assessment .....	7
<b>3 Transport and fate of chlorinated ethenes in clay till settings</b> .....	<b>9</b>
3.1 Spill of chlorinated ethenes in clay till.....	9
3.2 Mass estimate of the contaminant .....	11
3.3 Sorption .....	11
3.4 Degradation of chlorinated ethenes .....	12
3.5 Transport of chlorinated ethenes in the underlying aquifer .....	13
<b>4 The contaminated study site</b> .....	<b>15</b>
<b>5 Investigation approaches and strategies in clay till settings</b> .....	<b>18</b>
5.1 Geological characterization of clay till .....	18
5.2 Hydrological investigations of clay till .....	20
5.3 Seepage velocity .....	25
5.4 Subsurface transport of chlorinated ethenes .....	26
<b>6 Methods, approaches and application of CMD</b> .....	<b>32</b>
6.1 Methods for estimating the CMD in aquifers .....	32
6.2 Application of CMD for risk assessment .....	38
6.3 Moving onwards and upwards .....	41
<b>7 Conclusions</b> .....	<b>43</b>
<b>8 Recommendations for future work</b> .....	<b>45</b>
<b>9 References</b> .....	<b>47</b>
<b>10 Papers</b> .....	<b>57</b>

# Abbreviations

Cis-DCE	Cis-1,2-Dichloroethylene
CMD	Contaminant Mass Discharge
CMF	Contaminant Mass Flux
DMS	N,N-dimethylsulfamide
DNAPL	Dense Non-Aqueous Phase Liquid
EC	Electrical Conductivity
EPM	Equivalent Porous Media
ERT	Electrical Resistivity Tomography
GPR	Ground-Penetrating Radar
GSA	Grain Size Analysis
GWP	Groundwater Profiler
HPT	Hydraulic Profiling Tool
LUC	Large Undisturbed Column
MCL	Maximum Concentration Level
MiHPT	Membrane Interface Probe Hydraulic Profiling Tool
PCE	Tetrachloroethylene
PFAS	Per- and Polyfluorinated Substances
PID	Photoionization Detector
POC	Point of Compliance
TCE	Trichloroethylene
VC	Vinyl Chloride

# 1 Introduction

## 1.1 Background and motivation

Worldwide groundwater is an important water resource, especially for drinking water. In Denmark, it is the primary drinking water resource. Therefore, it is of high priority to protect the groundwater from xenobiotic organic contaminants such as chlorinated ethenes. Pérez and Eugenio (2018) estimated that around 2.8 million sites in the European Union are potentially contaminated. In 2022, nearly 40,000 Danish sites were registered as either contaminated or suspected contaminated (Olsen et al. 2023).

In the year 2000, the European Union agreed upon the Water Framework Directive – a directive set up to protect and manage waters, and to streamline the legislation in the member countries (European Commission 2022). Risk assessment of contaminated sites is essential in order to protect different receptors such as groundwater. The financial resources for investigation and remediation are limited. Hence, prioritization of the many contaminated sites are crucial for using the funds wisely and ensure better protection of groundwater resources (Overheu et al. 2014).

Several contaminated sites around the world, e.g. in North America and Europe, are located in low-permeability fractured settings, such as clay till (Chambon et al. 2011). Geological and hydrogeological conditions are crucial for the transport and fate of the contaminants (Thomsen et al. 2012). In clay till, fractures, fissures, macro pores, and lenses create preferential travel paths, with a higher hydraulic conductivity, compared to the matrix (e.g. Kessler et al. 2012; Ding et al. 2022). The matrix can in addition act as a secondary source, as the contaminants will be stored in and diffuse back from the matrix (Parker et al. 2008). As back-diffusion is a slow process, a secondary source will pose a threat to the underlying aquifer for several decades. Hence, the geological setting at the contaminated site is important as the distribution of the contaminants is strongly influenced by the hydraulic properties of the subsurface.

Sites contaminated with chlorinated ethenes are mostly considered as legacy sites, where the contaminant spills predominantly happened between the 1940s and 1980s (McGuire et al. 2004; Sale et al. 2008). Several decades after the spill, most of the chlorinated ethenes would not be present as a separate phase dense non-aqueous phase liquid (DNAPL) due to dissolution (Chapman and



Parker 2005). The chlorinated ethenes will be distributed by diffusive processes and stored in the low permeable matrix (Parker et al. 2008; Sale et al. 2008; ITRC 2010).

Contaminant mass discharge (CMD) has been introduced as a useful metric for risk assessment in sand and gravel aquifers. Determination of CMD in aquifers relies on hydraulic properties and contaminant concentrations from multiple screens or sampling points placed in a control plane downgradient the site (Troldborg et al. 2010; Verreydt et al. 2012) or devices for measuring contaminant flux (CMF), such as the Passive Flux Meter (Annable et al. 2005). Determining the CMD from a source in clay till relies typically on the infiltration rate, contaminant distribution and source area. These methods require historical review, elaborate field work, laboratory analyses and interpretation, which are time consuming and expensive. Thus, development of a method for determining the CMD from the source in clay till to the underlying aquifer, as a part of the initial site characterisation process, would provide a more useful risk assessment in an early stage of a contaminated site investigation. If the site is found to be of low risk for the groundwater aquifer due to a low CMD, the need for further investigations would be eliminated or substantially reduced, leading to cost savings.

Today, the use of the CMD approach in clay till is limited by lack of useful and time efficient field methods and approaches. Thus, development of approaches to determine important field site parameters valuable for estimating the CMD is essential. New methods and rethinking of concepts are needed in order to perform more reliable and time efficient risk assessments for contaminant sources located in clay till settings.

## 1.2 Aim and research objectives

The overall objective of this PhD thesis is to improve risk assessment of chlorinated ethene sources located in clay till settings by:

- Explore the governing transport and fate processes of chlorinated ethene sources in clay till/aquifer systems for risk assessment of contaminated sites potentially posing a risk to groundwater resources (**I, II, IV**)
- Assess field investigation approaches for examining the contamination and hydrogeology of clay till sites (**I, III**)
- Evaluate methods for estimating and quantifying the CMD of chlorinated ethene sources in clay till and underlying aquifers and suggest how to incorporate these estimates into current risk assessment schemes for protection of groundwater resources (**II, IV**)

## 1.3 Thesis outline

The focus of this PhD thesis is on chlorinated ethenes even though the title states chlorinated solvents. This choice was taken as chlorinated ethenes were the main contaminants at the field site used for the PhD project. The thesis is divided into eight chapters. Chapter 2 describes the current risk assessment framework, defines contaminant mass discharge and introduces the Danish guidelines for risk assessment. An overview of relevant transport and fate processes, in both clay till and the underlying aquifer, focusing on chlorinated ethenes are given in chapter 3. Chapter 4 provides a brief introduction to the field site used for the research carried out during this PhD project, which is in focus in the following chapters. In chapter 5 a presentation of different field and investigative approaches are presented. An overview of different methods for estimating the contaminant mass discharge, suggestions of applicable methods for different stages of risk assessment, and discussions on how to move forward with contaminant mass discharge as a meaningful metric for risk assessment are introduced in chapter 6. Lastly, conclusions are drawn in chapter 7, and ideas for further work on this subject is suggested in chapter 8.

## 2 Risk assessment of contaminated sites

This chapter will explore the current state of risk assessment strategies in general and a definition of contaminant mass discharge (CMD) will be given. Furthermore, a presentation of the current Danish risk assessment framework is presented along with the scope of local and catchment scale risk assessment.

### 2.1 Risk assessment approaches

When performing a risk assessment of a contaminated site it is important to identify the relevant receptors, to which the contamination may pose a risk. Relevant receptors include; groundwater, surface water, nature conservation areas, and ultimately human health. The focus of this work being on groundwater. The risk that a contaminated site poses to a certain receptor is a combination of the risk for the compound to reach the receptor(s) and a hazardous assessment of the specific compound (Critto and Suter II 2009).

Commonly, a source-pathway-receptor concept is used to evaluate if the contaminant source has a pathway to the receptor, hence if the contamination is likely to pose a risk (McKnight et al. 2010; Verreydt et al. 2012; Hussain et al. 2017; Mahammedi et al. 2020). This requires characterization of all three components to investigate the possible pathway from the source to e.g. the groundwater.

Risk assessment of contaminated sites typically relies on concentration-based analysis, where the evaluation outcome is often a forecast or measurement of contaminant levels at a specific location referred to as Point of Compliance (POC) (ITRC 2010; Locatelli et al. 2019). The POC must meet established threshold concentrations in order to secure the receptor (e.g. water quality). These are referred to as maximum concentration level (MCL) and depending on the compound the MCL can be set on a national or international level. Different locations of the POC may be used. In Figure 1, different locations of the POC are shown. P0, P1A, and P1B are used in the source zone, respectively right at the source, at the groundwater table immediately below the source, and in the aquifer below the source. P2 is a point located in the contaminant plume in a given distance from the source zone. In Denmark, this distance is 100 m from the downgradient edge of the source zone area (Rosenberg et al. 2016). Investigating the concentration level at a POC when performing a risk assessment at a contaminated site is a relatively inexpensive approach. However, a concentration-based risk assessment has its shortcomings such as:

- The maximum concentration found at a POC may be affecting only a small volume of the aquifer and/or be located in an area with low flow conditions.
- If the placement of POC is outside the mass center of the contamination, there is a possibility for underestimation of the risk, as the potential hotspot is not identified.

To meet these challenges, Pankow and Cherry (1996) described a flux-based concept for risk assessment of contaminated sites. Since then, several researchers have suggested the use of CMD for risk assessment and prioritization of contaminated sites (e.g. Einarson and Mackay 2001; Troldborg et al. 2008; Newell et al. 2011; Einarson 2017; Rønne et al. 2017). When evaluating the CMD at a contaminated site, the contaminants located in high-permeability zones have a larger impact on the risk assessment than the contaminants located in the low-permeability zones. This allows for a spatially averaged, flow-weighted concentration focusing on where the mass is distributed and transported (Einarson 2017). Despite the large interest for CMD in the community, many still adhere to the concentration-based risk assessment, due to reasons such as lack of expertise by practitioners or lack of agreement on how CMD relates to a MCL (Horst et al. 2021), see chapter 6.3.

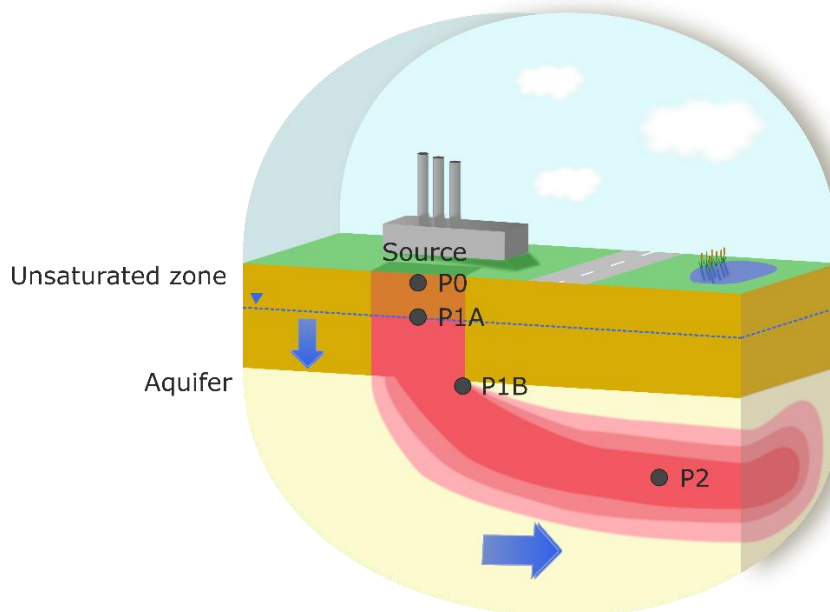


**Figure 1.** Different locations of Point of Compliance (POC) at a contaminated site. P0 is right below the source, P1A is at the top of the water table under the source zone, P1B is in the aquifer below the source zone, and P2 is in the aquifer at a certain/site specific distance downgradient from the source zone.

## 2.2 Contaminant Mass Discharge

Contaminant mass flux (CMF) and contaminant mass discharge (CMD) are both metrics which usage has increased through the years. CMF is a vector quantity that describes the contaminant mass moving per area per time and has the units [mass/time/area]. Hence, CMF gives a point specific vector quantity that is limited to a defined area (Stauffer 2006; ITRC 2010). CMD is defined as the mass of a contaminant per unit time [mass/time] passing through an area perpendicular to the flow direction (Basu et al. 2006; ITRC 2010; Rosenberg et al., II). Perceived as the CMF integrated over a given contaminated area, often covering the entire area of a contaminant plume, CMD is given as:

$$CMD = \int_A q \cdot c \cdot A \quad (1)$$

Where  $q$  is the water flux [volume/area/time],  $c$  is the concentration [mass/volume] and  $A$  is the area of interest [area].

Depending on the resource of interest,  $q$  can be e.g. the groundwater flux, infiltration or in-stream flux in order to investigate the CMD in an aquifer, from a source zone or in a stream, respectively.

When estimating the CMD in an aquifer, the most common method utilizes a network of multi-level screens placed in a transect downgradient of the source zone (ITRC 2010). From hereon, this method is referred to, as the transect method. A schematic drawing of the transect method is shown in Figure 2. The transect is divided into sub-areas often found through the installed network of multi-level screens. The CMD in the aquifer is found using:

$$CMD = \sum_{i=1}^N q_i \cdot c_i \cdot A_i \quad (2)$$

Where  $A_i$  is the area of the  $i^{\text{th}}$  sub-area,  $q_i$  is the water flux in the  $i^{\text{th}}$  sub-area,  $c_i$  is the concentration in the  $i^{\text{th}}$  sub-area and  $N$  is the number of sub-areas in the CMD transect.

Other methods on how to investigate the CMD in aquifers are described in chapter 6.

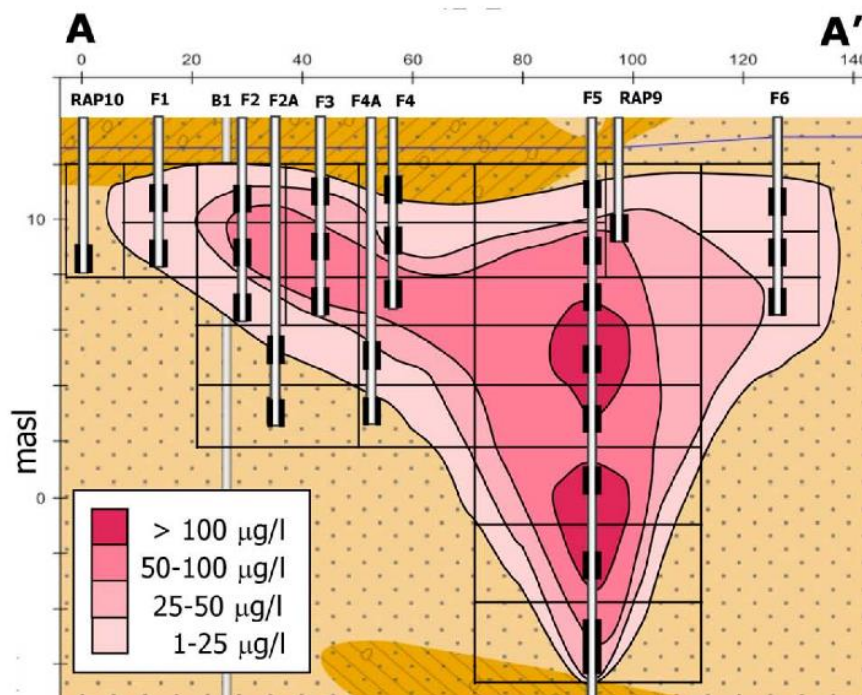


**Figure 2.** CMD found using the transect method in the aquifer. Each monitoring screen covers a sub-area (square around the screen) of the total contaminated transect area. Modified from Troldborg et al. (2010).

### 2.3 Scale and framework for risk assessment

Per tradition, risk assessments of contaminated sites are frequently carried out at local scale, focusing on one site at a time only. However, having the focus on only the local scale does not allow for a comprehensive prioritization of the contaminated sites, as the prioritization should be at a catchment scale focusing on the relevant receptor (e.g. water supply well) (Einarson and Mackay 2001).

To meet the challenges of risk assessments only focusing on the local scale several screening tools have been developed over the years (e.g. Arey et al. 2005; Frind et al. 2006; Li et al. 2021). A CMD-based screening tool called CatchRisk combines the risk posed to abstracted groundwater from each site in a catchment area (Troldborg et al. 2008). A local scale leaching model estimates the CMD from an identified site in the catchment and a transport model covering the catchment area estimates the impact on the supply well (Figure 3). Additionally, it can serve as a framework for investigating the source of contamination in the catchment and identifying unknown sources of contaminants.

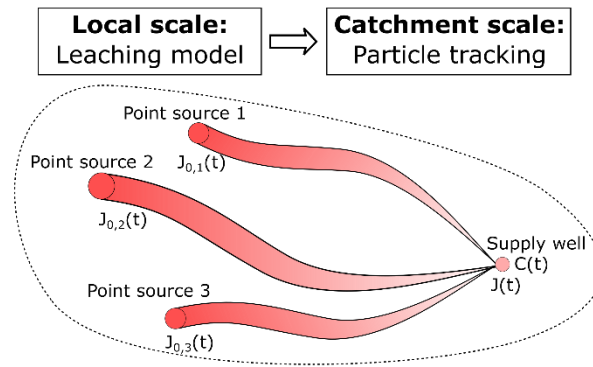


**Figure 3.** Conceptual set up of the CMD-based CatchRisk model. It comprises of two models: a local scale leaching model used for the individual contaminated sites, and a catchment scale transport model. Modified from Troldborg et al. (2008).

As previously stated, prioritization of contaminated sites are necessary to ensure appropriate protection of the environment. In Denmark, it is primarily the five administrative regions that handle the risk assessment and clean-up of contaminated sites. In order to help the regions prioritizing the contaminated sites the Danish EPA has developed a guiding hand book (Overheu et al. 2012; Overheu et al. 2014). It allows for evaluation and prioritization within the administrative area (see Figure 4) as well as the catchment areas using multiple approaches and principles, including CMD. The handbook is meant as a guide and the regions are free to choose how to conduct the prioritizations. A description of how risk assessment in the Capital Region of Denmark is carried out, can be found in chapter 6.2.

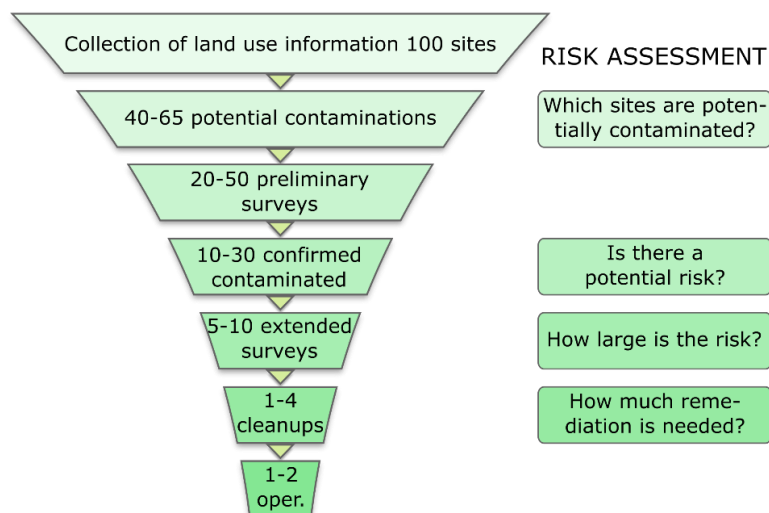


**Figure 4.** An overview of the administrative workflow for the risk assessment framework used in Denmark. The numbers in each phase indicates the number of sites out of 100 potentially contaminated sites. Oper. means operation. Modified from Overheu et al. (2014).

# 3 Transport and fate of chlorinated ethenes in clay till settings

Chlorinated ethenes have been used widely throughout the world within industries such as drycleaners and the metal industry. The use of chlorinated ethenes started in the early 1900s (Doherty 2000) and were widely applied in the period between 1940 and 1980 (McGuire 2004; Sale 2008). As a result of this intensive usage they are now a contaminant group found frequently in groundwater (Pankow and Cherry 1996; Murray et al. 2019; Ottosen et al. 2021) especially at sites where an aquitard is on top of the aquifer (Chapman 2005; Parker 2008; Damgaard et al. 2013a; Damgaard et al. 2013b). In this chapter, relevant transport processes within the saturated clay till as well as the underlying aquifer is described.

## 3.1 Spill of chlorinated ethenes in clay till

The hydrogeology at a contaminated site has a significant impact on the transport of the Dense Non-Aqueous Phase Liquid (DNAPL). Sale et al. (2008) suggested using the 14-compartment model to characterize the distribution of chlorinated solvents into vapour, separate phase DNAPL, aqueous, and sorbed phases dependent on time from spill. The 14-compartment model is divided into source zone and plume, and set up for five different geological types. Figure 5 depicts the 14-compartment model for clay till-like geological settings. This guides the conceptual understanding of the distribution of DNAPL.

Zone/Phase	Early				Middle				Late			
	Source zone		Plume		Source zone		Plume		Source zone		Plume	
	Low perm	High perm	High perm	Low perm	Low perm	High perm	High perm	Low perm	Low perm	High perm	High perm	Low perm
Vapor	0	2	1	0	2	2	2	2	3	2	2	3
DNAPL	0	4			2	3			1	1		
Aqueous	0	2	1	0	2	3	3	2	3	2	2	3
Sorbed	0	2	1	0	2	3	3	2	3	2	2	3

0 Not impacted    1 <1-10 µg/L    2 <10-100 µg/L    3 <100-1000 µg/L    4 >1000 µg/L

**Figure 5.** Relevant phases to take into account when investigating a contaminant sources in clay till-like settings. This is also known as the 14-compartment model. The importance of the phases varies depending on the time since the spill. The figure is made with inspiration from ESTCP (2011) and (Tsitonaki et al. 2013).



At an early stage, chlorinated ethenes will move downward into the subsurface, as a Dense Non-Aqueous Phase Liquid, DNAPL. The movement in a low permeable subsurface is highly dependent on the presence of high-permeability features such as fractures, sand lenses, and sand stringers, see Figure 6a (Kessler 2012; Rosenberg et al. I). The separate phase DNAPL will move downward through the vertical fractures or pool in the horizontal features. Due to a high concentration gradient between the high and low permeable features, contaminants will move into the clay matrix by diffusion (Parker et al. 2004; Cherry et al. 2006) enhanced by sorption (Filippini et al. 2020). For the middle time stage, the mass of the DNAPL contamination is distributed more evenly between the low and high permeable features and only small amounts of separate phase DNAPL is present (Figure 6b). When the separate phase DNAPL is no longer present (late phase), the concentration gradient between the low and high permeable features will shift, and the diffusion process will occur from the matrix to the high permeable features. As diffusion occurs at a low rate, the so-called back-diffusion and desorption will cause long-term secondary source zones within the clay till, Figure 6c (Parker 2008; Adamson et al. 2015; Rosenberg et al. II).

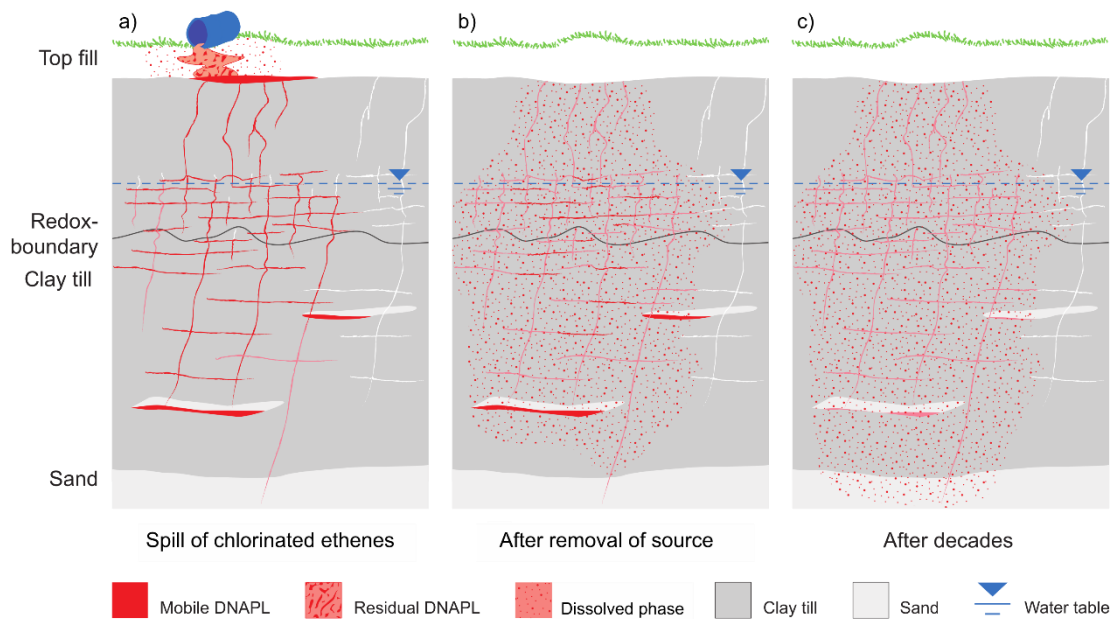


**Figure 6.** Transport of chlorinated ethenes through clay till and into the underlying aquifer. The three pictures display different periods showcasing the relevant contaminant transport pathways from spill until a stable plume has been formed. Modified from Damgaard (2012).

Taking into account that spills with chlorinated ethenes predominantly happened several decades ago and 90 % of 191 investigated chlorinated solvent

sites showed stable plumes (McGuire et al. 2004) most sites will be at a middle to late stage (ESTCP 2011). The solute transport in clay till is primarily vertical both through vertical fractures, the clay till matrix (driven by the vertical hydraulic gradient), and diffusion. For aquitards with relatively high porosity the contaminant transport can be simulated using the advection-dispersion equation in an equivalent porous media (EPM) model (Cherry et al. 2006).

### 3.2 Mass estimate of the contaminant

Estimating the mass of chlorinated ethenes in the source zone adds crucial conceptual understanding and provides an estimate of the duration of the contamination. The total mass can be found as:

$$M_{Total} = M_{vapor} + M_{DNAPL} + M_{aqueous} + M_{sorbed} \quad (3)$$

As the focus is on old spills of chlorinated ethenes (Figure 6c) it is assumed that no separate phase DNAPL is present and the mass in the saturated clay till is the dissolved ( $M_{aqueous}$ ) and sorbed mass ( $M_{sorbed}$ ). However, separate phase DNAPL has a large effect on the mass estimate and the presence hereof should be assessed during site investigations (Jørgensen et al. 2010).

To estimate the contaminant mass the contaminated area is divided into sub-volumes that are assumed to have an evenly distributed concentration. In order to decrease the uncertainty of the mass estimate, the amount of sub-volumes should increase with increasing heterogeneity. For each sub-volume equilibrium between soil and water is assumed. Therefore, having e.g. a water sample ( $C_w$ ) in one sub-volume, the sorbed concentration ( $C_s$ ) can be found by using the sorption coefficient ( $K_d$ ):

$$C_s = K_d \cdot C_w \quad (4)$$

Hence,  $K_d$  is linearly correlated to the concentrations of the two media meaning that an underestimation of  $K_d$  will lead to an underestimation of the sorbed concentration and an overestimation of the aqueous concentration.

### 3.3 Sorption

Sorption of chlorinated ethenes will affect the mass transfer of contaminants from the matrix to the high permeable features (Chambon et al. 2010; Lu et al. 2011) and, therefore, extend the duration of how long the contaminants will act as a secondary source zone in the clay till. Furthermore, the sorption contributes to retardation of the contaminant transport. Lu et al. (2011) conducted sorption experiments on clay tills with seven different chlorinated solvents.

The results showed that the chlorinated ethenes had a higher sorption coefficient,  $K_d$ , than what was found using typical regressions between fraction of organic carbon,  $f_{oc}$ , as reported for instance by Abdul et al. (1987). Piwoni and Banerjee (1989) showed that if  $f_{oc}$  is low (<0.1 %), it has a negligible impact on the sorption and the octanol-water partitioning coefficient,  $\log(K_{ow})$ , can be used to estimate the  $K_d$  value. Lu et al. (2011) also compared the  $K_d$  values using the correlation by Piwoni and Banerjee (1989) and found that they were under-estimated. This indicates that not only  $f_{oc}$  or  $\log(K_{ow})$  are affecting the sorption of chlorinated ethenes. Clay content may have an influence on the sorption, hence storage and transport, of chlorinated ethenes.

### 3.4 Degradation of chlorinated ethenes

Degradation of chlorinated ethenes is an important process when assessing the risk that a contaminated site poses to a relevant receptor. It can take place through abiotic and biotic pathways under aerobic and anaerobic conditions. The most typical degradation is reductive dechlorination that is a biotic process occurring under anaerobic conditions (Dolinová et al. 2017). The chlorine is substituted with a hydrogen, one atom at a time until it is degraded to ethene or ethane (see Figure 7). For reductive dechlorination to occur, the redox conditions, availability of electron donor and presence of specific bacteria are important (Chambon et al. 2013; Ottosen et al. 2021).

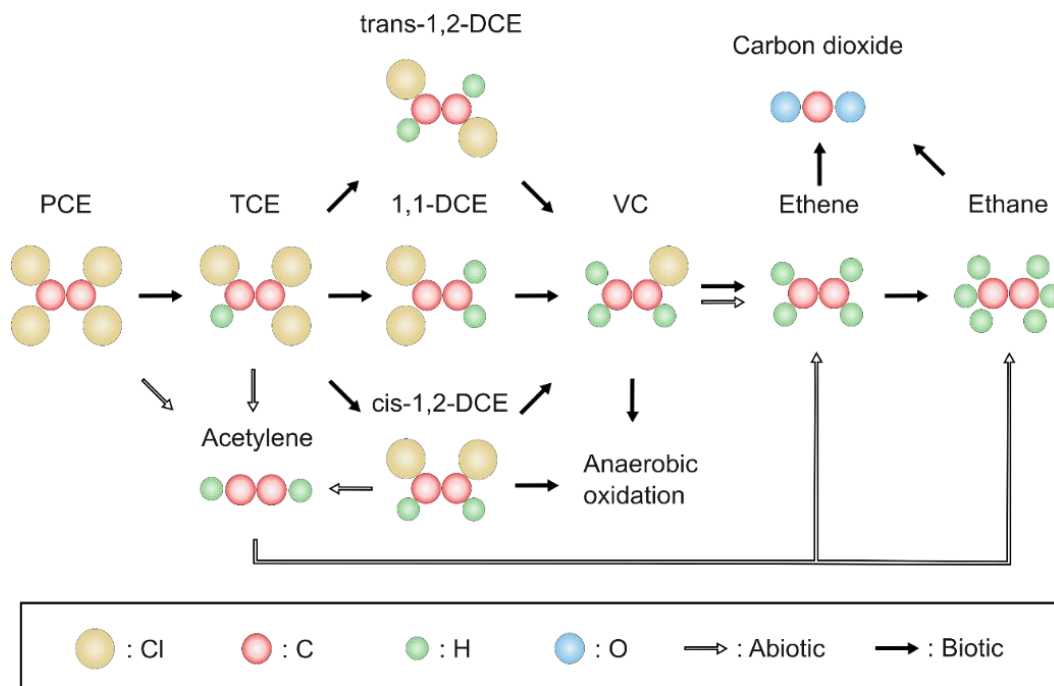


**Figure 7.** Abiotic and biotic degradation of chlorinated ethenes under anaerobic conditions. Modified from Ottosen (2020).

## 3.5 Transport of chlorinated ethenes in the underlying aquifer

When the dissolved chlorinated ethenes reaches the porous aquifer the dominant processes are advection and dispersion. It will migrate primarily in the ground water flow direction as a result of advective transport (Domenico and Schwartz 1997). This is governed by Darcy's law and the velocity of the groundwater flow is found using equation (5).

$$v = -\frac{K}{n} \cdot \frac{\partial h}{\partial l} \quad (5)$$

Where  $K$  is the hydraulic conductivity of the aquifer [length/time],  $n$  is the porosity of the aquifer [volume/volume] and  $\frac{\partial h}{\partial l}$  is the hydraulic gradient in the aquifer [length/length]. When assessing the groundwater velocity, the most uncertain parameter is the hydraulic conductivity, as this can vary several orders of magnitude within a short distance. The porosity has less uncertainty and only vary around a factor of two when the aquifer material is known. The hydraulic gradient is easy to determine, however, caution must be taken regarding seasonal variations.

### 3.5.1 Dispersion

Dispersion refers to the process of mixing that occurs due to variations of velocities in the aquifer which causes spreading of the contaminants in all directions. Understanding and predicting the extent and rate of dispersion is important in evaluating the transport and fate of contaminants in aquifers. The central parameter for describing dispersion in the aquifer is dispersivity. The dispersivity vary in quantity between the longitudinal, transversal and vertical direction, with the longitudinal being significant larger than the two latter (Gelhar et al. 1992). Studies have shown that the longitudinal dispersivity is scale dependent (Gelhar et al. 1992; Schulze-Makuch 2005; Chakraborty and Das 2018) reporting a longitudinal dispersivity in the meter range for studies with a scale of 100 m. Studies of transversal and vertical dispersivities are few. The majority of published studies shows the use of values in the millimetre to centimetre range (e.g. Garabedian et al. 1991; Jensen et al. 1993; Rotaru et al. 2014; Rosenberg et al. **II**; Zech et al. 2023). The small values of the transversal and vertical dispersivities are important to consider when designing observation networks and remediation schemes (Gelhar et al. 1992). Transversal and

vertical spreading will be limited by the dispersivities, resulting in steep concentration gradients from the centre to the fringes of the plume (see Figure 8). Acquiring depth-discrete concentration measurements using short screens (cm scale) with small increments demonstrate the limited vertical spreading observed in the field (Tuxen et al. 2006; Anneser et al. 2008; Zech et al. 2019; Rosenberg et al. II).

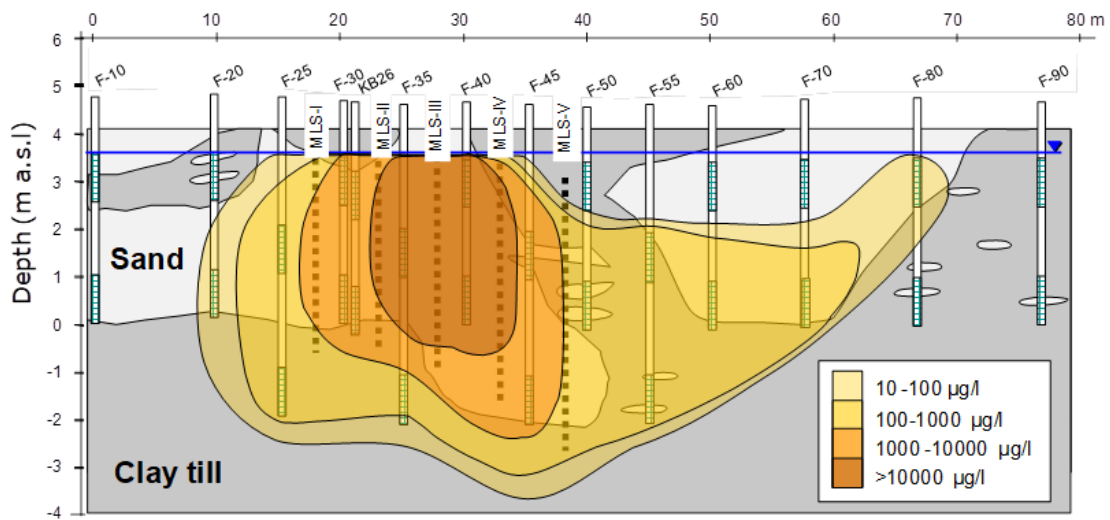


**Figure 8.** Transect of plume in Skuldelev, Denmark, showing a steep gradient from the centre to the fringes of the plume (Troldborg et al. 2012).

## 4 The contaminated study site

A contaminated site in Vassingerød, Denmark, was used for the research and field investigations carried out in this study. In 1962 cutting and laminating of Styrofoam began, see timeline in Figure 9 (Mosthaf et al. **IV**). Between 1970 and 1972 activities that indicate storage and usage of chlorinated ethenes outside the building on the north-eastern end of the site was initiated (see Figure 10a for aerial photo). Furthermore, in 1972 an oil tank was buried at the site. In 1988, the oil tank was removed and in 1996 the outside storage and activities with use of chlorinated ethenes ended (Rosenberg et al. **II**). The site is located on top of an aquifer within a drinking water catchment area which in Denmark makes the site of high interest to risk asses and potentially remediate. Therefore, in 2015, investigations began aimed at defining the risk from the contamination at the site. Extended surveys and field investigations (see Table 1), including the work carried out as part of this PhD, started in 2017.

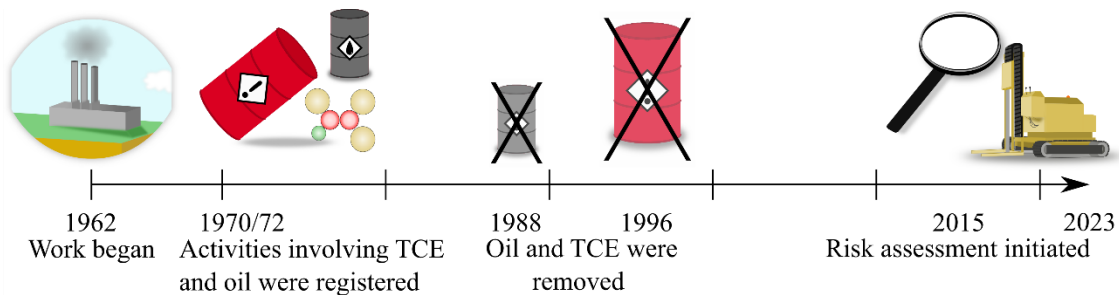


**Figure 9.** Timeline of the contaminant site in Vassingerød, and activities associated with the spill at the site. Modified from Mosthaf et al. (**IV**).

The geology at the site (shown in Figure 10c) is comprised of 10 – 12 m thick clay till, enclosed with several sand/silt lenses and layers. Investigations of the geology,  $f_{oc}$ , and  $K_d$  suggest that the clay till is divided in two by a sand/silt layer: upper and lower. From the clay till, the geology transitions into a sandy aquifer within a transition zone of 1 – 2 m in thickness which is confirmed by the grain size analysis and Membrane Interface Probe Hydraulic Profiling Tool logs (MiHPT). The sandy aquifer has a thickness of more than 35 m and is underlain by a limestone aquifer (Mosthaf et al. **IV**).

The clay till is partly saturated with the groundwater table at approximately 35.5 m asl which is the same depth as the silt layer in the source zone area. Between the clay till and the aquifer there is a downward vertical hydraulic gradient between 0.33 and 0.58, whereas no vertical hydraulic gradient has been found within the aquifer. The groundwater flow direction at the site is

south-southwest (Rosenberg et al. I). The hydraulic conductivity at the site was investigated using both slug tests and grain size analysis. In the top of the aquifer (approximately the top 4-5 m), the hydraulic conductivity was found to be nearly 3 times higher than the lower part of the investigated aquifer.

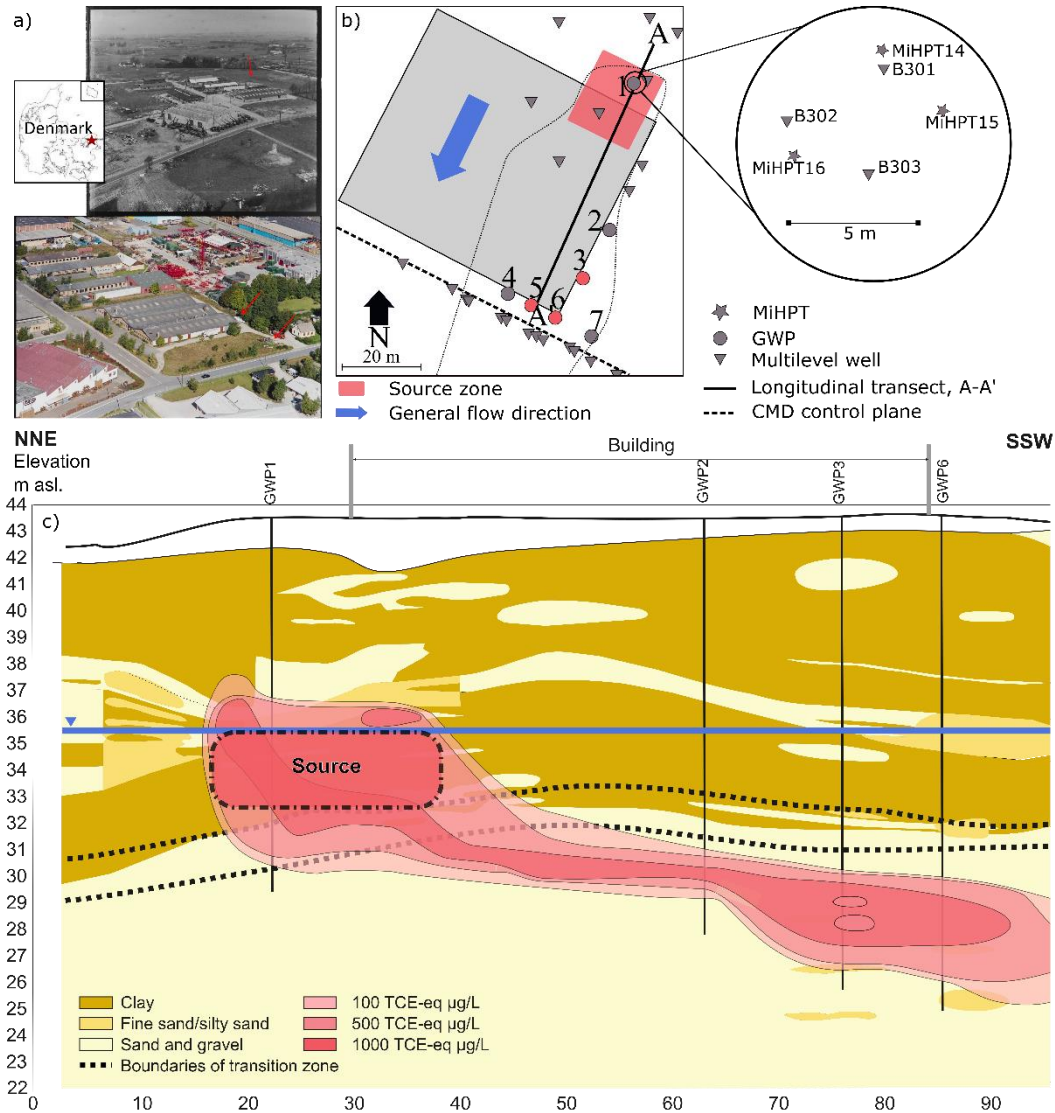


**Figure 10.** Overview of the field site in Vassingerød, Denmark. a) shows older aerial photos of the field site. b) some sampling points are shown at field scale and within the source zone. c) depicts the geology in transect A-A' and the contaminant plume. Modified from NIRAS (2019), Rosenberg et al. (II), Jensen et al. (III), and Mosthaf et al. (IV).

Contaminant investigations have been carried out throughout the site (see Figure 10b). Different contaminant compounds were found at the site; chlorinated ethenes, chlorinated ethanes and oil compounds. All of the compounds were found to exceed the Danish groundwater quality criteria, however, the primary

contamination at the site was established to be chlorinated ethenes (mostly trichloroethylene, TCE) (Rosenberg et al. II). Discretized Photoionization Detector measurements (PID) and soil samples showed, that the contamination in the source is in the lower clay till. Furthermore, water samples taken with 25 cm intervals in the source zone area showed a steep concentration gradient through the transition layer.

Investigation of the degradation products cis-1,2-dichloroethylene and vinyl chloride (cis-DCE and VC) was conducted showing sporadic points with concentrations of especially cis-DCE, and a change in the isotope ratio (NIRAS 2019). However, the degradation was not evident throughout the site and have been concluded to be of minimal importance for the current study.

A transect of multilevel wells was placed downgradient of the source zone in order to estimate the CMD at the site and perform the risk assessment. Other studies have been carried out with a starting point in this transect:

- One study examined the uncertainty of the CMD estimate by using a geostatistical approach (Bøllingtoft 2020).
- Another study used a transect at the site, downgradient from the area of interest for this study, for a pilot scale study of remediation of the TCE plume by injection of activated carbon and bioamendments for enhanced reductive dechlorination (Ottosen et al. 2021).

**Table 1:** Investigations performed at the contaminated site, including activities used as part of the risk assessment and the research described in this thesis. Different actors have carried out the investigations, including consultancy companies, students, technicians, and researchers.

Investigation	Activity
History of the site	Interviews with owner, viewing of old aerial photos
Geology	Bore logs, geological determination of soil samples, grain size analysis, MiHPT logs, GPR
Hydrology	Measurement of water table, monitoring water table with divers, slug test, grain size analysis, MiHPT logs
Contaminant distribution	Vapor air samples, soil samples, water samples, MiHPT logs, sorption experiments, fraction of organic carbon, geostatistical analysis of the source area
Other	Geostatistical analysis of the estimated mass in the source zone, installation of iFLUX



# 5 Investigation approaches and strategies in clay till settings

The conceptual understanding of the hydrogeology and the contaminant spreading at a contaminated site is key for a well-executed risk assessment. A conceptual model for a contaminated site should be informed with the geological settings, hydrogeological understanding and contaminant distribution. For a contaminant source in clay till settings, especially the conceptual understanding of the clay till is important. In addition to field site investigations, contaminant transport models can be useful to interpret the contaminant spreading at the site. This chapter will investigate these aspects for contaminant sources in clay till settings.

## 5.1 Geological characterization of clay till

Through investigations of the clay till, it is possible to identify important geological features such as fractures, sand lenses and stringers, and thickness of the till. For investigation and characterization of the geological layers drilling of boreholes or taking a core sample will provide information on the geology and give an indication of the vertical heterogeneity at the point of sampling. The lithology of the soil sample could be investigated in the field or described in detail by a geologist (Høyer et al. 2019). Conducting grain size analysis (GSA) on soil samples will add information to the geological composition of the sample (Switzer and Pile 2015), and should be viewed as a supplementary information to the geological description based on borelog samples. Additional information of the vertical heterogeneity of the subsurface can be obtained through direct push technologies such as the Hydraulic Profiling Tool (HPT), see Figure 11 and Figure 12 for examples of such logs (McCall and Christy 2020). This site specific information together with the understanding of the regional geology will help build a good geological model.

Some studies (Christiansen et al. 2012; Kessler et al. 2012; Aamand et al. 2022) have used excavations for examining the heterogeneity and in particular sand lenses and fractures of a clay till. However, this is not a common practice for contaminated site investigations as excavations are expensive and primarily done for remediation means (Kessler 2012). Another method is to perform tracer tests on large undisturbed columns (LUC), which allow for a study of the important transport pathways in a clay till column such as fractures and

micro pores (Jørgensen et al. 2002; 2019; Mosthaf et al. 2021). As with excavations, this is also not a common practice when investigating a contaminated site.

Using the point specific information to build the conceptual understanding of the geology at the site can have its downfalls with e.g. misinterpretation/missing identification of the sand bodies and other high permeability features (Jensen et al. **III**). Various geophysical methods exist and have been found useful for investigation of the subsurface geology and used e.g. to create highly detailed large scale geological models (Maurya et al. 2018; Hyojin et al. 2019). An overview of geophysical methods is reported in e.g. Thompson et al. (2023). Surface methods have the limitation that the vertical resolution decreases with depth and identification of small-scale heterogeneities are problematic.

Conversely, crosshole methods provides a constant resolution with the depth of a borehole (Jensen et al. **III**). Amongst commonly used crosshole methods are the ground-penetrating radar (GPR) which has previously been used to gather information on the geology in so-called low-loss environments, such as unconsolidated sands and gravels, see review in Svendsen et al. (2023). GPR has been tested in high-loss environments like clay till, and proven valuable to investigate the geology between boreholes (Looms et al. 2018; Svendsen et al. 2023; Jensen et al. **III**). Jensen et al. (**III**) made a field-scale test of the GPR and compared it with a comprehensive data set including borehole logs, grain size analysis and HPT data, see Figure 11. The study showed, that the GPR method can be used to interpret the geology between the boreholes down to a vertical stretch of decimetres, and therefore identifying high-permeability layers in the clay till. Furthermore, the plausibility of the high-permeability layers can be assessed, indicating influential horizontal transport pathways. Currently, the GPR can be used with a distance between boreholes of 4-8 meters, and are therefore useful when investigating the geology at a smaller scale than a standard site scale. Other commonly used crosshole methods are electrical resistivity tomography (ERT) and seismic tomography, see e.g. Slater et al. (2000), Wang and Rao (2006), and Lévy et al. (2022).

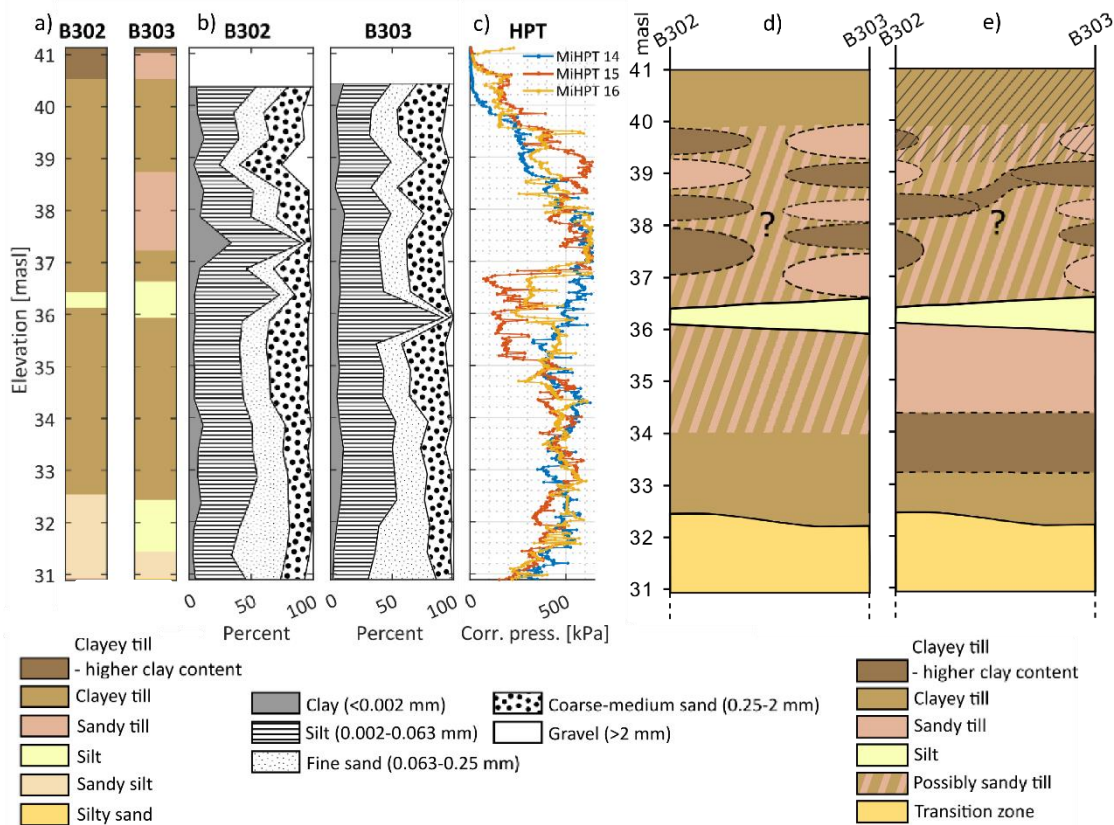


**Figure 11.** Investigation of the composition of a clay till in Vassingerød. Initial investigations of the clay till was done with borehole logs (a), grain size analysis with 0.5 m vertical spacing (b), and HPT logs placed close to the boreholes, maximum of 4 m away (c). (d) shows the conceptual understanding of the geology between the two boreholes prior to the GPR investigation. The improved conceptual understanding of the geology between the boreholes provided by the GPR is shown in (e). Modified from Jensen et al. (III).

## 5.2 Hydrological investigations of clay till

Hydrological conditions and parameters relevant for field site investigations are many, and the relevance of these depends on the wanted knowledge and/or output of the investigations. In this subchapter, only hydrological parameters and investigations relevant for the determination of CMD are presented, i.e. infiltration, hydraulic conductivity, hydraulic gradient, and the seepage velocity.

### 5.2.1 Infiltration through clay till

Examining equation (1), the relevant water flux,  $q$ , for the determination of vertical CMD from a clay till is the infiltration,  $I$  [length/time]. The infiltration is often determined through the use of regional/national data and/or regional groundwater models (Rosenberg et al. I). However, it is in particular crucial to assess the site specific infrastructure that can have an impact on the infiltration

through the clay till. Infrastructure such as paved areas and buildings can reduce the infiltration through the clay till and have a significant impact on the conceptual understanding and the estimated risk at the site, see Frederiksen et al. (2023).

### 5.2.2 Vertical hydraulic gradient in clay till

Alternatively, the infiltration can be determined using the following equation:

$$I = K_v \cdot i_v \quad (6)$$

Where  $K_v$  [length/time] is the vertical hydraulic conductivity and  $i_v$  [length/length] is the vertical hydraulic gradient in the clay till. Determination of the vertical hydraulic gradient is given as:

$$i_v = \frac{\Delta h}{\Delta d} \quad (7)$$

Where  $\Delta h$  [m] is the difference in the measured hydraulic heads and  $\Delta d$  [m] is the thickness of the clay till. Studies of the vertical hydraulic gradient in aquitards have used measurements of the hydraulic head from depth-discrete wells, along with the depth of the low-permeability media (Meyer et al. 2008; Meyer 2014; Filippini 2020).

A study of the vertical hydraulic gradient in clay till was carried out using the Membrane Interface Probe Hydraulic Profiling Tool (MiHPT) (Rosenberg et al. 2011). The MiHPT is a direct-push method that can add information on the subsurface regarding both the contaminant level and the permeability (McCall et al. 2014). When descending into the subsurface, the needed pressure for injecting a certain flow of water is measured in order to evaluate the permeability. When reaching the saturated part of the subsurface, dissipation tests are performed in order to correct the measured pressure for the pressure caused by the water column. Subtracting the atmospheric pressure from the stabilized pressure found through the dissipation test yields an estimate of the hydraulic head at the depth of the dissipation test (McCall and Christy 2020). Aiming at dissipation tests in the high permeable layers in the clay till and aquifer will allow for good estimates of the hydraulic head and subsequently vertical hydraulic gradient.

The thickness of the clay till was estimated through a combination of two logs: the corrected pressure log (Corr. Press. in Figure 12) and the electrical conductivity (EC in Figure 12). A high pressure is an indication of low-permeability and an increase in EC can indicate an increase in clay content and/or increase

in the ionic strength of the porewater (McCall 2010; Maurya et al. 2018; McCall and Christy 2020). The vertical hydraulic gradients found using the MiHPT compared well with those found using a multilevel well (example in Figure 12), showing that the MiHPT can be a useful tool for examining the vertical hydraulic gradient. It should be noted, however, that the MiHPT is applicable in unconsolidated formations and has a limitation in how deep it can be pushed (around 20-25 m). For consolidated formations and/or deeper investigations other methods such as depth-discrete multilevel samplers should be used to measure the water table (see 5.4.3 for suggestions on such samplers).

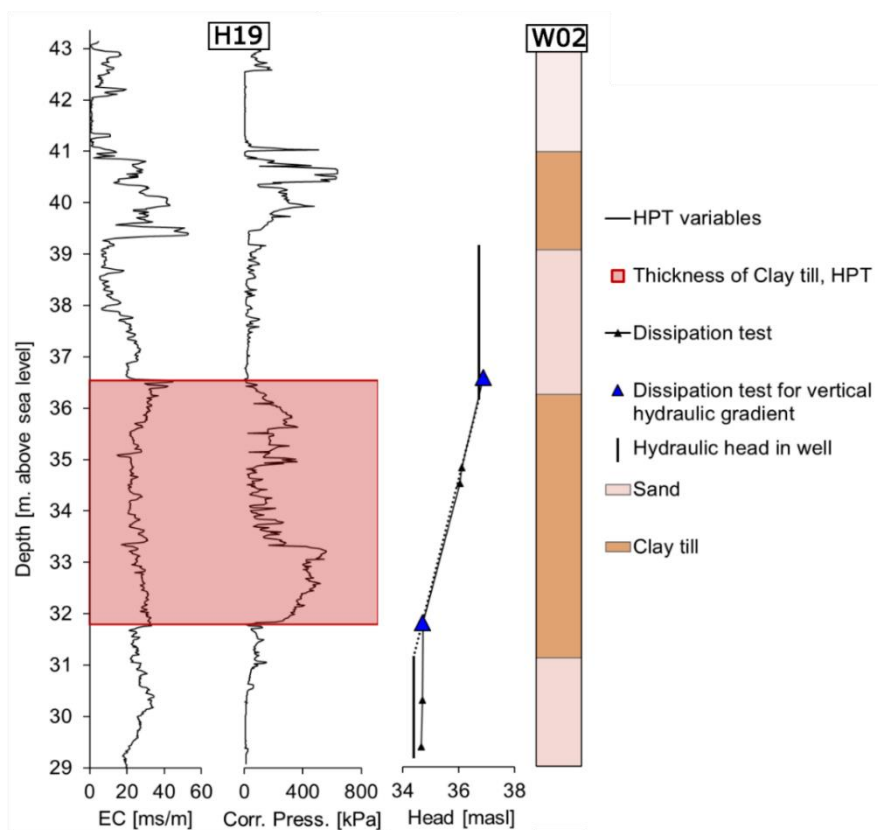


**Figure 12.** Comparison of two methods for determining the vertical hydraulic gradient in clay till: H19 refers to MiHPT and W02 refers to a multilevel well. The graph to the left shows the electrical conductivity through the subsurface, and helps indicating zone of higher clay content. The Corr. Press. plot shows the corrected pressure of the MiHPT, where higher pressure indicates lower permeability. In the plot showing the head found from both methods, the estimated hydraulic head from the dissipation tests are also shown. To the right is the borehole log for the multilevel well.

Finally, the vertical hydraulic gradient is also useful for investigating the likely presence of fractures in an aquitard and if the aquitard is disconnected. If the vertical hydraulic gradient is high, it indicates a fairly connected aquitard and vice versa (Cherry et al. 2006; Meyer et al. 2008). However, when the vertical

hydraulic gradient is larger than one, attention should be drawn to further investigations of the aquitard. Hart et al. (2008) has in a technical commentary demonstrated how a natural vertical hydraulic gradient larger than one is not technically correct despite it being reported in several studies. A gradient higher than one indicates a change in the hydraulic conductivity over the sample depth which is likely to occur in aquitards like clay till (due to e.g. sand lenses). Therefore, it is important to increase discretization when characterizing the changes in the permeability of the clay till. The investigations performed in Rosenberg et al. (I) are valuable for this. Using the MiHPT to investigate the permeability and adding dissipation tests where possible, when reaching high permeable layers, allows for evaluation of the vertical hydraulic gradient in discrete intervals.

### 5.2.3 Hydraulic conductivity in clay till

To estimate the infiltration, the vertical hydraulic conductivity of the clay till is also needed, see equation (6). This is a more challenging parameter to investigate and determine the site specific quantity of, as it is often very time- and resource-consuming (Keller et al. 1989). Quantifying the hydraulic conductivity in clay till can be done at three different scales: lab, in-situ, and regional scale (Ferris et al. 2020). Studies have shown that the hydraulic conductivity determined at lab scale are lower than hydraulic conductivity determined in-situ or at regional scale. This indicates that the hydraulic conductivity determined in the lab, mainly describes the hydraulic conductivity in the matrix neglecting important transport pathways in the clay till (Van der Kamp 2001; Neuzil 2019). For determination of hydraulic conductivity in the lab, methods like oedometer consolidation test and the triaxial apparatus can be used. At a regional scale it is typically modelling of seasonal water level fluctuations that is used (Ferris et al. 2020). See Van der Kamp (2001) for suggestions of primarily in-situ methods for determination of hydraulic conductivity in aquitards.

Ferris et al. (2020) have compiled studies of hydraulic conductivity of the clay till in the Interior Plains region of Saskatchewan, Canada. The compilation comprises of 15 study sites spanning over an area of approximately 160.000 m<sup>2</sup>. In total, 393 estimates of hydraulic conductivity found at three different scales: lab, in-situ, and regional (from model simulations), are compared in the study, see Figure 13. The geometric mean of the hydraulic conductivities found at lab scale was around two orders of magnitude lower than the geometric mean at both in-situ and regional scale. Additionally, the study also found, that there is a distinct difference in the hydraulic conductivity with depth, a greater depth

results in a lower hydraulic conductivity. This implies that the effect of the fracture network decreases with increasing depth in the clay till. Ferris et al. (2020) found that many of the shallow tills were often oxidized. However, the description of the samples were not consistent enough to draw any conclusions on that matter.

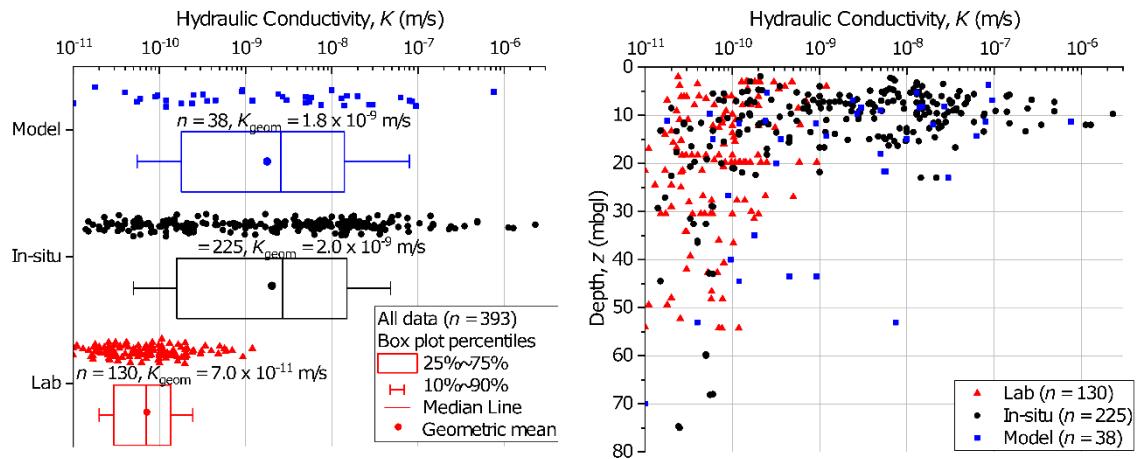


**Figure 13.** Collection of hydraulic conductivity based on a total of 393 estimates. To the left, results are divided into scale: lab, in-situ (field), and model (regional). To the right, the results are plotted with depth. Modified from Ferris et al. (2020)

When investigating the hydraulic conductivity it is important to keep in mind, the scale at which it is determined and if it is the vertical, horizontal or bulk hydraulic conductivity. In the literature there is not a strict use of the direction of the hydraulic conductivity, and one must be aware of e.g. which test method is used (as an example LUC will give a vertical hydraulic conductivity). When a horizontal or total hydraulic gradient is given, the anisotropy factor can be used to estimate the vertical hydraulic conductivity. See Chapuis and Gill (1989) for relevant anisotropy values.

#### 5.2.4 Coherency of key parameters

Even though the vertical hydraulic conductivity is a difficult parameter to quantify at a standard contaminated site investigation, knowing the interval and correlation with depth is important. Furthermore, the vertical hydraulic gradient is a central parameter to investigate as it can give valuable information on the clay formation. It provides helpful insight to whether or not, the estimated infiltration is plausible (Rosenberg et al. II). For a plausibility check of the infiltration rate, Figure 14 can be used. It depicts the relationship between infiltration, vertical hydraulic gradient and vertical hydraulic conductivity for

clay till. The figure shows, that a low vertical hydraulic gradient and an assumed high infiltration rate requires the vertical hydraulic conductivity to be in the high range and vice versa.

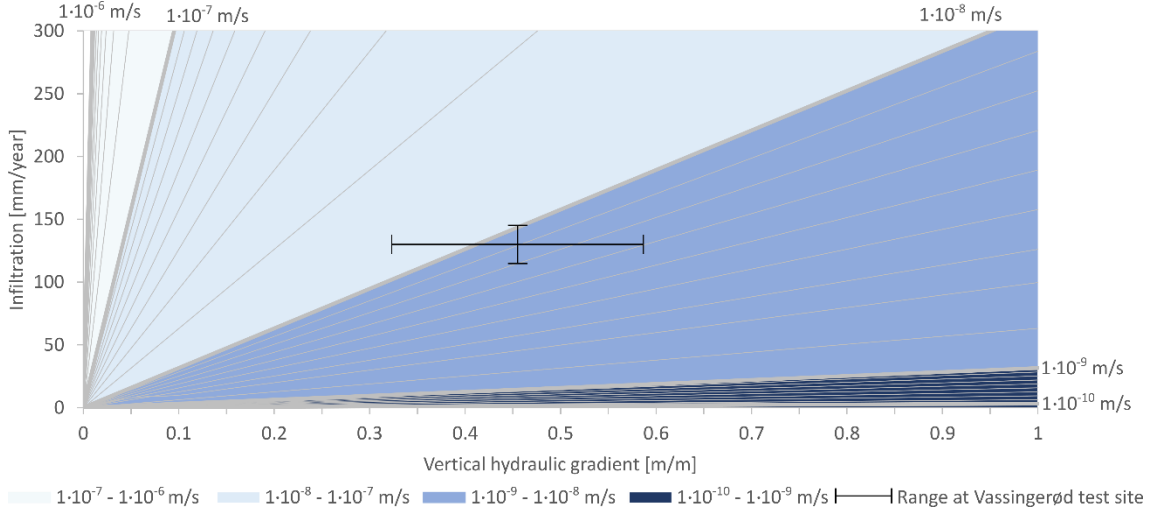


**Figure 14.** Relationship between infiltration, vertical hydraulic gradient and vertical hydraulic conductivity for clay till. The different shades of blue represent the bulk vertical hydraulic conductivity. The findings of vertical hydraulic gradient and estimated infiltration rates at the Vassingerød field site is marked with the black lines.

### 5.3 Seepage velocity

For the investigation of the horizontal CMD in the aquifer, the relevant water flux,  $q$ , is the Darcy's velocity found as:

$$q = K_h \cdot i_h \quad (8)$$

Where  $K_h$  [length/time] is the hydraulic conductivity in the aquifer and  $i_h$  [length/length] is the hydraulic gradient.

The hydraulic gradient in the aquifer is typically found by measuring the water table in the aquifer at various points (at least three). When examining at a small scale, narrow area, or investigating an aquifer with a small hydraulic gradient, small measurement errors may result in wrong conclusions on the flow field (Silliman and Mantz 2000; Labaky et al. 2009). Drawing up the isopotential lines of the water table will help investigating the groundwater flow direction and the hydraulic gradient. Alternatively, the flow direction and hydraulic gradient can be found using the HydrogeoEstimatorXL (free download from: <https://kuscholarworks.ku.edu/handle/1808/22049>) (Devlin and Schillig 2017).



The hydraulic conductivity in the field can be found using a variety of different field methods such as slug tests (e.g. Hinsby et al. 1992; Mosthaf et al. **IV**) (e.g. Hinsby et al. 1992 ), pumping test (e.g. Rovey and Cherkauer 1995), grain size analysis (e.g. Devlin 2015; Mosthaf et al. **IV**), and permeameter tests (Freeze and Cherry 1979). As for the hydraulic conductivity in the aquitard, which has been found to be scale dependent, so is the hydraulic conductivity in the aquifer. Rovey and Cherkauer (1995) found, that the hydraulic conductivity increases with increasing test radius until approximately 220 m. For test radius larger than 220 m, the hydraulic conductivity was not found to increase further. This is most likely due to the effect of the heterogeneities in the aquifer having a larger effect on smaller scale.

## 5.4 Subsurface transport of chlorinated ethenes

In accordance with equation (2), estimation of CMD requires the concentration of the contaminant and the relevant total area or sub-area. For such investigations soil and water samples from the clay till and groundwater samples can be utilized. See e.g. Fjordbøge et al. (2017) for sampling in clay till, Verreydt et al. (2011) for review on passive samplers, and Troldborg et al. (2010) on application of sub-areas in the aquifer.

The transport of chlorinated ethenes through clay till is highly dependent on the heterogeneity and the sorption. This chapter will focus on the vertical transport through fractures and the matrix. Furthermore, a description of how vertical concentration profiles in the transition and aquifer zones can add valuable information to the conceptual model at a contaminated site is provided.

### 5.4.1 Transport in matrix, sand inclusions, and fractures

Simulating the transport through clay till can be done through the use of an equivalent porous media (EPM) model where fractures are not directly accounted for. This is a simplified way to simulate the contaminant transport in the clay till where it is assumed that high-permeability features are absent or have a minor effect on the vertical contaminant transport. This was tested by Mosthaf et al. (**IV**) who simulated the contamination at the Vassingerød test site. The simulations were carried out using a 3D model divided into four interconnected layers (clay till, transition layer, upper aquifer, and lower aquifer), history at the site, and the comprehensive field data. Due to the age of the spill it was assumed that the TCE had spread evenly throughout the source zone area and depth of the saturated clay till due to diffusion and sorption. The transient transport in the clay till was simulated using the advection-dispersion

equation (including mechanical dispersion and diffusion). Vertical concentration profiles downgradient from the source zone were compared with simulated concentration profiles that showed a good fit. In preliminary studies, Mosthaf et al. (IV) investigated the influence of isolated horizontal sand lenses in the clay till, that showed to have only minor impact on the vertical contaminant transport in the clay till. The study found that the flow-field contrast between the aquitard and aquifer was more influential than the small-scale heterogeneities within the aquitard.

Fractures in clay till can contribute to fast transport of contaminants as well as distribution of the contaminants to the matrix due to diffusion and sorption processes (Mosthaf et al. 2021). The fracture spacing and aperture can have a strong influence on the contaminant transport through clay till as well as the continuity of the fractures.

A comprehensive study of LUC experiments and excavations at several primarily Danish field sites has shown that the fracture spacing increases with depth. Close to the surface the fracture spacing is in the tens of centimetre scale. However, from the depth of around 3 m reported fracture spacing is around 1-3 m for the majority of the sites. The same study investigated the fracture aperture with depth (to a maximum depth of 6 m below ground surface) and found that the fracture aperture is predominantly between 5-25  $\mu\text{m}$  when reaching a depth of around 4 m below ground surface (Aamand et al. 2022).

Mosthaf et al. (2021) simulated the transport of pesticides in two different, but visually similar, LUCs; one taken close to the surface with large fracture aperture (110  $\mu\text{m}$ ); and one from around 5 m below ground level with a small fracture aperture (10-18.5  $\mu\text{m}$ ). The study showed that the fracture aperture had a great impact on the dominating transport processes. In the column with the large fracture aperture, the transport occurred primarily in the fractures with some matrix diffusion on a long time scale. In the column with the small fracture aperture, the advective transport in the matrix and diffusion had a distinct influence.

A simulation of how different source zone realizations affects the downgradient concentration profiles (see chapter 5.4.3 on these) and CMD were set up based on the Vassingerød field site. The source zone realizations were produced through a 2D discrete fracture-matrix model and implemented as an input function to the aquifer simulated with a 3D model (Mosthaf et al. IV). Fracture apertures in the range between 5 and 25  $\mu\text{m}$  were investigated. Figure 15c shows that a fracture aperture of 8  $\mu\text{m}$  results in a nearly homogeneous

distribution of the TCE in the lower part of the clay till after 50 years. Furthermore, an increase in fracture aperture results in TCE contamination at a larger depth interval due to matrix diffusion. As seen from Figure 15d, an increase in fracture aperture leads to a faster breakthrough at the bottom of the clay till to the top of the aquifer and a longer tailing period. The fast breakthrough is due to fracture transport and the tailing is caused by the matrix back-diffusion (Parker et al. 2008; Chambon et al. 2011).

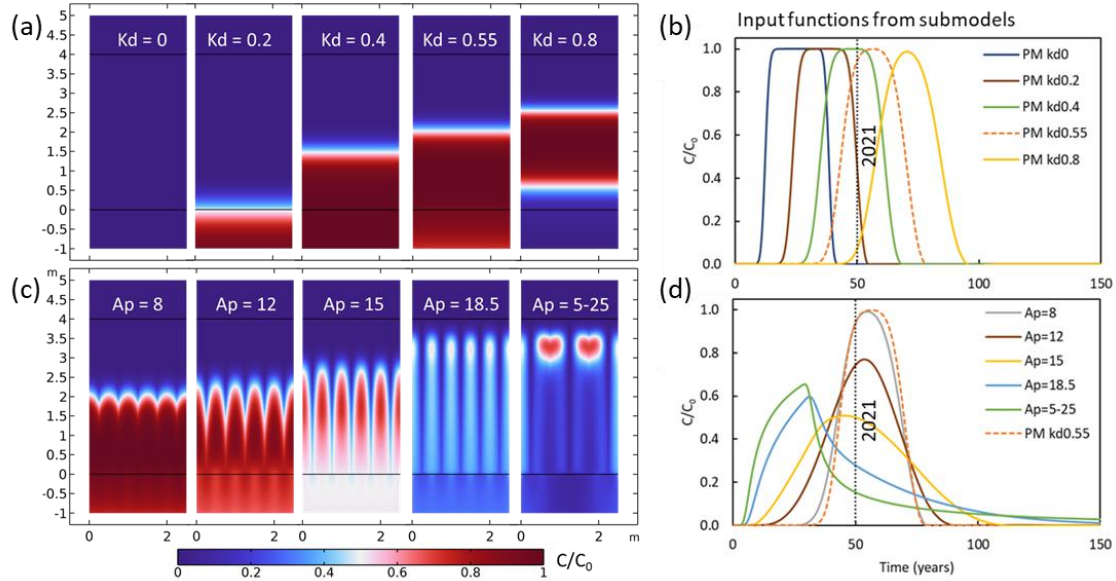


**Figure 15.** Investigation of the effect of sorption ((a) and (b)) and fracture aperture ((c) and (d)) at the field site in Vassingerød. (a) and (c) show the source zone after 50 years from the spill with respect to sorption and fracture aperture, respectively. (b) and (d) show the breakthrough curves from the source zone into the underlying aquifer with different sorption coefficients and fracture aperture respectively.

#### 5.4.2 Sorption of chlorinated ethenes in clay till

Sorption can have a large effect on the diffusion time between the clay till matrix and fractures/high-permeability zones, the estimate of stored mass, contaminant advective transport, and the clean-up timeframe as described in 3.3. Therefore, investigation of the effect and size of  $K_d$  value is of high importance.

By simulating the transport through the clay till at Vassingerød field site, Mosthaf et al. (IV) showed that the  $K_d$  value of TCE had a significant impact on the contaminant distribution in the clay till and the leaching to the underlying aquifer. A lower  $K_d$  value resulted in a faster transport through the clay till, and a greater vertical distribution of the contaminant, see Figure 15a. With a  $K_d$  value of 0 L/kg (no sorption) TCE would no longer prevail as a secondary

source zone this long after the spill (2021) which is contradicting field observations from the field site. With a higher  $K_d$  value, the time span during which the contaminant is leaching to the aquifer is likewise increased.

Through laboratory experiments Mosthaf et al. (IV) found an average  $K_d$  value of TCE in the lower clay till at the Vassingerød field site to be 0.8 L/kg (ranging from 0.55 to 1.1 L/kg) with a varying clay content between 5 and 10.8 %. As shown in Table 2, this  $K_d$  value compares well with the one found by Lu et al. (2011). However, the clay content is remarkably lower at the field site in Vassingerød and the  $f_{oc}$  remarkably higher. The differences in  $f_{oc}$  and clay content between the two studies and how this affects the  $K_d$  value should be investigated further in order to establish reasonable guidelines for the estimation of  $K_d$  values in clay till. Examining the  $K_d$  value found using Abdul's formula is between 12 and 52 times lower than the lab tests from both studies. This indicates that the clay content (large surface area) has an influence on the sorption, as previously stated by Lu et al. (2011). Therefore, a relatively high  $K_d$  value is needed when evaluating the time span of contamination, stored mass in the source zone, contaminant transport, and developing schemes for remedial action.

**Table 2.** Comparison between average  $K_d$  values for TCE in clay till and the site specific parameters  $f_{oc}$  and clay content as well as the resulting  $K_{oc}$ . Furthermore, a calculation of the  $K_d$  value through the use of Abdul's formula from the measured  $f_{oc}$  levels in the two studies. First number is the average and the interval of the samples are given as [min – max].

Source of information	Method	$K_{d,TCE}$ [L/kg]	$f_{oc}$ [%]	Log $K_{oc}$ [L/kg]	Clay [%]
Mosthaf et al. (IV)	Lab test	0.8 [0.55 – 1.1]	0.18 [0.11 – 0.21]	2.64 [2.48 – 2.88]	5.0 – 10.8
	Abdul's formula	0.064 [0.050 – 0.074]			
Lu et al. (2011)	Lab test	0.83 [0.62 – 0.96]	0.05 [0.03 – 0.08]	3.18 [2.95 – 3.48]	23.0 – 27.0
	Abdul's formula	0.016 [0.007 – 0.028]			

The metabolites of TCE (cis-DCE and VC) have smaller  $K_d$  values in clay till than TCE (Lu et al. 2011). Therefore, when evaluating e.g. the stored mass estimate in the source zone where degradation is taking place, the different  $K_d$  values of the chlorinated ethenes should be accounted for.

### 5.4.3 Use of high-resolution, depth-discrete concentration profiles

Obtaining high-resolution, depth-discrete concentration profiles has been shown to be of great value at different sites (Rivett et al. 1994; Chapman and Parker 2005; Bjerg et al. 2011; Broholm et al. 2016; Rønde et al. 2017; Steelman et al. 2020). The high-resolution, depth-discrete samples provide valuable information on the heterogeneity, transport properties at the site, and identification of degradation at the plume fringes (Tuxen et al. 2006; Anneser et al. 2008). Identifying such relevant processes at the local scale is not easily obtainable when e.g. taking water samples using the traditional long screened wells, as the sample is mixed across the screen length. Hence, the water sample is potentially abstracted from several different flow zones and the maximum concentration may be underestimated (Reilly et al. 1989; Church and Granato 1996).

At clay sites, high-resolution, depth-discrete concentration profiles have shown the importance of back-diffusion of TCE by sampling the clay interbedded in a sandy aquifer for TCE (Chapman and Parker 2005). Adamson et al. (2015) used high-resolution, depth-discrete samples to investigate the source zone history of chlorinated ethenes and ethanes that were suspected to have been spilled several decades ago. Both studies show steep concentration gradients at the transition between clay and the over-/underlying transmissive zone.

Recognizing that the vertical concentration profiles are a footprint of the site-specific parameters is important. Such parameters include the flow, contaminant strength and the CMD from the source zone (McNab et al. 2000; Rosenberg et al. **II**). Relevant field methods for taking high-resolution, depth-discrete water samples can be seen in the review by Broholm et al. (2016) complemented with a description of the Groundwater Profiler (GWP) in Dutta et al. (2021).

Rosenberg et al. (**II**) investigated the impact of the field site specific parameters on the vertical concentration profiles in a sandy aquifer overlain by a clay till. Three main characteristics of the vertical concentration profiles were selected; thickness of plume, maximum concentration, and depth of the maximum concentration. The effect of 12 parameters were tested by performing a sensitivity analysis on a simulated 2D plume. Figure 16 shows the results of the sensitivity analysis, with the level of influence ( $\mu^*$ ) and the uncertainty of the influence ( $\sigma$ ).

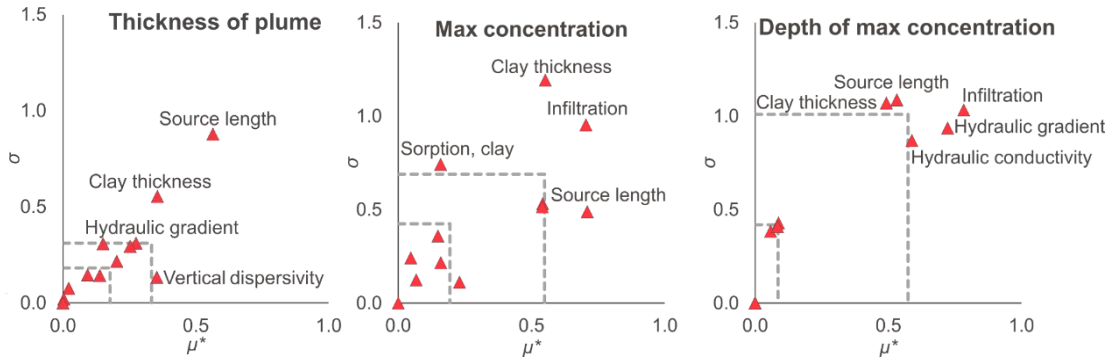


**Figure 16.** Sensitivity analysis of the parameters affecting the estimated CMD, thickness of the plume, maximum concentration, and depth of the maximum concentration. If the triangle is connected to a label, it means that it has a strong influence on the result ( $\mu^*$ ) and/or the influence is bound with a high uncertainty ( $\sigma$ ). The outer dashed grey lines indicate the third quartile and the inner dashed grey lines indicate the first quartile. Modified from Rosenberg et al. (II).

For all three characteristics of the vertical concentration profiles it is primarily parameters that are determinable through field site investigations that are of high importance. However, some of the influential parameters are difficult to determine. The infiltration at the site can be approximated by investigating the depth to the maximum concentration when knowing the horizontal flow conditions at the site, which are easier to determine (Rosenberg et al. II). The vertical dispersivity in the aquifer should be kept in the mm-cm scale, as described in chapter 3.5. The sorption coefficient only affects the arrival of the plume but not the shape.

For investigations in heterogeneous aquifers with e.g. low conductivity layers, the vertical concentration profiles may be affected by the heterogeneity to a degree, where it is difficult to localize the characteristics of the vertical concentration profiles. Nonetheless, the high-resolution, depth-discrete concentration profiles still add valuable information on the contaminant distribution and the flow conditions at the site.

High-resolution, depth-discrete concentration profiles can provide valuable information on the site-specific parameters. This can help identify the relevant parameters at the site and improve the conceptual understanding of the contaminant distribution at the site.

# 6 Methods, approaches and application of CMD

Investigating the CMD from a contaminated site can be motivated by different reasons such as improving the conceptual models (ITRC 2010), risk assessment for a downgradient receptor (Einarson and Mackay 2001; Newell et al. 2011; Rønne et al. 2017), and assessment of remediation in the source zone or plume (Kao and Wang 2001; Fjordbøge 2017). When assessing the risk to a downgradient receptor, the focus can be on different types of water bodies. The focus of this chapter is on estimation of CMD to/in aquifers. For detailed description of estimations of CMD to/in streams, see (Milosevic et al. 2012; Rønne et al. 2017; Sonne et al. 2017).

## 6.1 Methods for estimating the CMD in aquifers

As stated in chapter 2.2, CMD in an aquifer can be estimated through the use of many different field methods, see list in Table 4. Each of the methods have different advantages and disadvantages as shown in the table. The ProfileFlux method will be described in the next chapter. For an in-depth description of the other methods, please consult the suggested references. The application of some of the methods for risk assessment are described in chapter 6.2.

At the Vassingerød field site, different methods have been used to estimate the CMD. All methods found estimates of CMD within comparable ranges. The transect method has been used in the traditional way using sub-areas for each monitoring screen. Additionally, a geostatistical model has been applied to the transect method to get a 95 % confidence interval of the CMD estimate. Read more on the geostatistical analysis in Bøllingtoft (2020). The results shown in Table 3 suggests, that all of the applied methods are valid to inform the risk assessment with a CMD estimate.

**Table 3.** Estimate of the CMD at the field site in Vassingerød, Denmark, using different methods.

Method	CMD [g/year]	References
Transect	143	NIRAS (2019)
Transect with an confidence interval	81 – 297	Bøllingtoft (2020)
Solute transport model	117 – 148	Mosthaf et al. (IV)
ProfileFlux method	117 – 170	Rosenberg et al. (II)

**Table 4.** Description of different methods to estimate CMD in an aquifer along with some relevant references describing the methods in detail and/or applying the method.

Method	Description	Advantages	Disadvantages	Examples of references
Transect method	A transect of wells, preferably multilevel-wells, are placed perpendicular to the groundwater flow direction. Concentration measurements are collected along with estimations of Darcy velocity from each well, resulting in an estimate of CMF. The sub-areas/CMFs represented by each well screen are summed up to find the CMD for the transect area.	<ul style="list-style-type: none"> <li>• Useful to follow contaminant evolution or remedial action</li> </ul>	<ul style="list-style-type: none"> <li>• Requires many sampling points to reduce uncertainty</li> <li>• Expensive</li> </ul>	Einarson and Mackay (2001); Basu et al. (2006)
Passive flux meters (PFM)	A permeable device containing sorption material and tracer is submerged into a well. As the groundwater flows through the device the contaminants are being sorbed and tracer is released. The device is installed for a period of time resulting in a time-averaged water flux and CMF. If placed in a transect the CMD can be estimated.	<ul style="list-style-type: none"> <li>• Time-averaged concentration and flow parameters</li> <li>• Readily installed in groundwater monitoring wells</li> </ul>	<ul style="list-style-type: none"> <li>• Flow-field in borehole casting is difficult to estimate</li> <li>• Risk of degradation the contaminant while sorbed to the PFM.</li> </ul>	Annable et al. (2005); Basu et al. (2006); Verreydt et al. (2015)
Integral pump test	To perform an integral pump test, a well is placed so the contaminant plume is captured by the pump test. The water is extracted at a controlled rate and analysed with time. Based on an analytical solution the CMD is back calculated.	<ul style="list-style-type: none"> <li>• Fewer wells</li> <li>• No interpretation of contaminant concentrations between sampling points</li> <li>• Continuous sampling</li> </ul>	<ul style="list-style-type: none"> <li>• Large amount of contaminated water to manage</li> <li>• Risk of changing plume chemistry</li> <li>• Little information on the spatial distribution of the plume</li> </ul>	Bockelmann et al. (2001); Béland-Pelletier et al. (2011)
Isocontours	Using the isocontour lines produced for the source zone or plume. For each isocontour line, the CMD is found assuming the isocontour line as the average concentration in that specific area. The CMD estimates from the isocontour lines are summed up resulting in a total CMD.	<ul style="list-style-type: none"> <li>• Useful when e.g. infrastructure is challenging</li> <li>• Isocontours for source zone to estimate vertical CMD from source</li> </ul>	<ul style="list-style-type: none"> <li>• Higher uncertainty than using multilevel screens</li> </ul>	ITRC (2010)



Solute transport models	Applying the field specific knowledge of flow and contaminant data into a solute transport model. Different models exist and the detailing of the input and output vary as well as whether it is a 1D, 2D or 3D model.	<ul style="list-style-type: none"> <li>• Possible to investigate the CMD at different distances</li> </ul>	<ul style="list-style-type: none"> <li>• Variation in the need of data</li> <li>• Many assumes heterogeneous system</li> </ul>	Locatelli et al. (2019); Mosthaf et al. (IV)
ProfileFlux method	Using high-resolution, depth-discrete concentration profiles downgradient of a contaminant source combined with a 2D solute transport model. When the simulated vertical concentration profile matches the measured, the CMD at the site can be estimated.	<ul style="list-style-type: none"> <li>• Effective first estimate</li> <li>• Informing the conceptual model</li> <li>• Cost-effective</li> </ul>	<ul style="list-style-type: none"> <li>• Uncertainty in locating the centre line of the plume</li> <li>• Assumptions that might not be valid for all sites</li> </ul>	Rosenberg et al. (II)

---

### 6.1.1 ProfileFlux method

The ProfileFlux method is a new method for estimating the CMD in an aquifer, with a source zone located in an overlying clay till. It utilizes the shape and concentrations of the vertical concentration profiles in the aquifer along with field site measured flow conditions (Rosenberg et al. **II**). The concept is depicted in Figure 17 with the following steps:

- a) Investigations of the flow conditions at the site and approximate source zone delineation.
- b) Measuring the vertical concentration profiles in the assumed centerline of the plume as well as across the plume.
- c) Adding the site specific parameters to a solute transport model to generate simulated concentration profiles. The simulated vertical concentration profiles are fitted to the measured vertical concentration profiles within an acceptable range. This will result in a CMD estimate along with a breakthrough curve with indication of the duration of the contamination (see Figure 18).

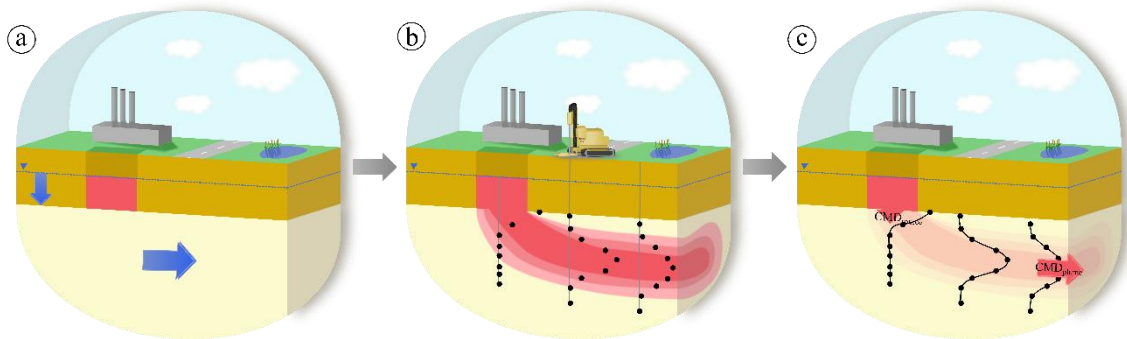


**Figure 17.** Illustration of the three steps of the ProfileFlux method used to estimate the CMD at a clay till site. a) Investigations of the flow field at the site and approximate delineation of the source zone. b) Measurements of the vertical concentration profiles down-gradient from the source. c) Simulating the contaminant transport at the site and comparing the simulated and measured vertical concentration profiles to get an estimate of the CMD from the source.

The ProfileFlux method relies on assumptions on the flow conditions and contaminant distribution:

- Taking into account only the saturated portion of the clay till and aquifer.

- Primarily vertical flow in the clay till and horizontal flow in the aquifer. The occurrence of sand lenses can have an influence and add horizontal transport pathways (Kessler 2012) and can shift the source zone.
- Clay till can be moderately heterogeneous, but not with too many larger fractures or dominating horizontal transport pathways. If the saturated zone of the clay till is overlain by more than 4 meters of clay till, the occurrence of larger fractures are less likely as described in chapter 5.4.1, and this assumption is justifiable.
- Applicable for legacy contaminations, hence last phase in Figure 6, where the contaminant source zone is primarily dominated by back diffusion and advective transport through the matrix. The plume in the aquifer is at steady state. As chlorinated ethenes have predominately been spilled several decades ago (see chapter 3) it is applicable for many sites.

Performing MiHPT logs at the site are useful to investigate the relevant vertical investigation area to obtain the measured vertical concentration profiles. This is possible for VOCs like chlorinated ethenes (McCall et al. 2014). However, for compounds such as pesticides prior investigation with the MiHPT will not add any value regarding the vertical contaminant distribution.

When comparing the simulated and measured vertical concentration profiles, it allows for the user to evaluate the knowledge level at the site. Therefore, the ProfileFlux method can also be used to evaluate if further investigations are needed and can help informing the conceptual model for the contaminated site.

Applying the ProfileFlux method at a contaminated site will allow for an initial estimate of the CMD in a less expensive way than the traditional transect method. However, if the initial CMD estimate is high or bound with too much uncertainty, it is advised to make a new CMD estimate using the traditional transect method.

The ProfileFlux method is still new and application at other sites than the field site is needed. The testing should include other contaminants than chlorinated ethenes, e.g. pesticides or Per- and Polyfluorinated Substances (PFAS). Furthermore, the method is also applicable at sites with other geological settings than clay till. The geological setting should however, constitute of a contaminant source located in an aquitard with primarily vertical transport overlying an aquifer with primarily horizontal transport.

The ProfileFlux method has been further developed for a pesticide plume application in similar geological settings as Vassingerød field site by Frederiksen

et al. (2023). Through the use of a solute transport model simulating the fracture-matrix interplay and several vertical concentration profiles (in total 249 groundwater samples) the understanding of fate and transport of N,N-dimethylsulfamide (DMS) was improved. The contaminated site consisted of several sources and the comparison between measured and simulated concentration profiles helped to identify the source location and strength of a point source and two diffuse sources.

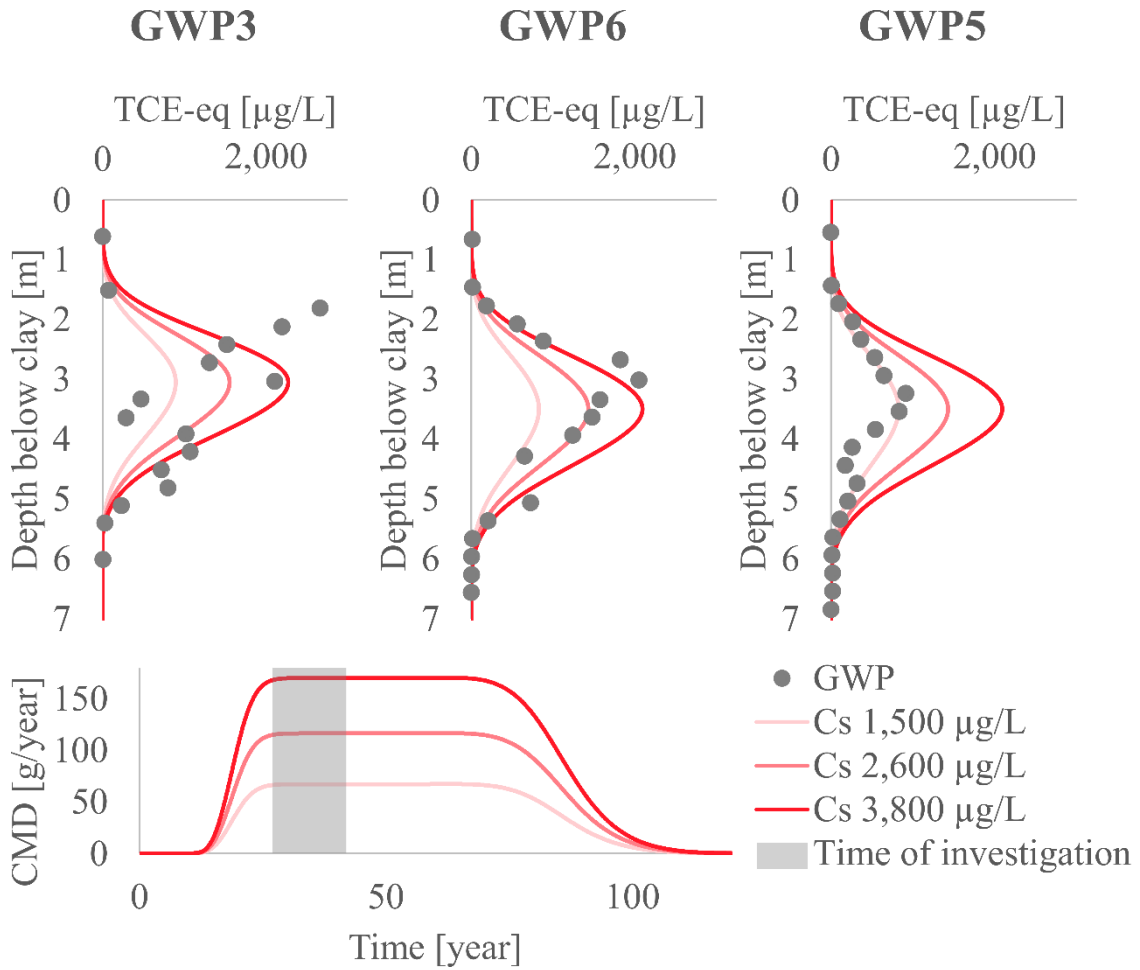


**Figure 18.** Comparison between simulated and measured vertical concentration profiles (top) along with a breakthrough curve of the CMD at the Vassingerød field site (bottom).

## 6.2 Application of CMD for risk assessment

The methods mentioned in chapter 6.1 are useful for different steps of a risk assessment of contaminated sites. The application of the CMD as a metric for risk assessment and implementation of the different CMD methods in the Danish administrative risk assessment framework (Figure 4) are identified in this chapter.

### 6.2.1 CMD as a risk assessment metric

The idea to use CMD for risk assessment of contaminated sites is still at an early stage, though it has been suggested as an effective metric for more than 20 years (Horst et al. 2021). Especially when it comes to prioritizing clean-up of different contaminated sites affecting the same receptor, the CMD approach is more valuable than a single concentration (Einarson and Mackay 2001; Troldborg et al. 2008).

Different approaches to use the abstraction rate (or flow rates of other receptors) to estimate a resulting concentration from the estimated CMD has previously been suggested in the literature (Einarson and Mackay 2001; Verreydt et al. 2012; Einarson 2017; Horst et al. 2021). This allows for a comparison with e.g. drinking water standards and therefore has a strong similarity to the “traditional” mind set of using a measured concentration at a given POC. Hence, this will increase the ease of implementation of CMD as a metric for risk assessment (Horst et al. 2021).

In Figure 19 the resulting concentrations of the abstracted groundwater is shown as a function of the estimated CMD and abstraction rate of the supply well or water work. It is made with the Danish quality criteria of chlorinated ethenes in mind (1 µg/L for PCE, TCE, and cis-DCE and 0.2 µg/L for VC), however, other concentration levels are also shown. The maximum abstraction rate (3 mio m<sup>3</sup>/year) is chosen based on the maximum value for abstraction rates in the Capital Region of Denmark. The grey line marks the extraction rate of 200,000 m<sup>3</sup>/year that is set as a standard abstraction rate for a future water work. The figure shows that for an abstraction rate of 200,000 m<sup>3</sup>/year a CMD greater than 200 g/year will result in the quality criteria for PCE, TCE, and cis-DCE to be exceeded. For VC the limit for CMD, using the same extraction rate, is 40 g/year.

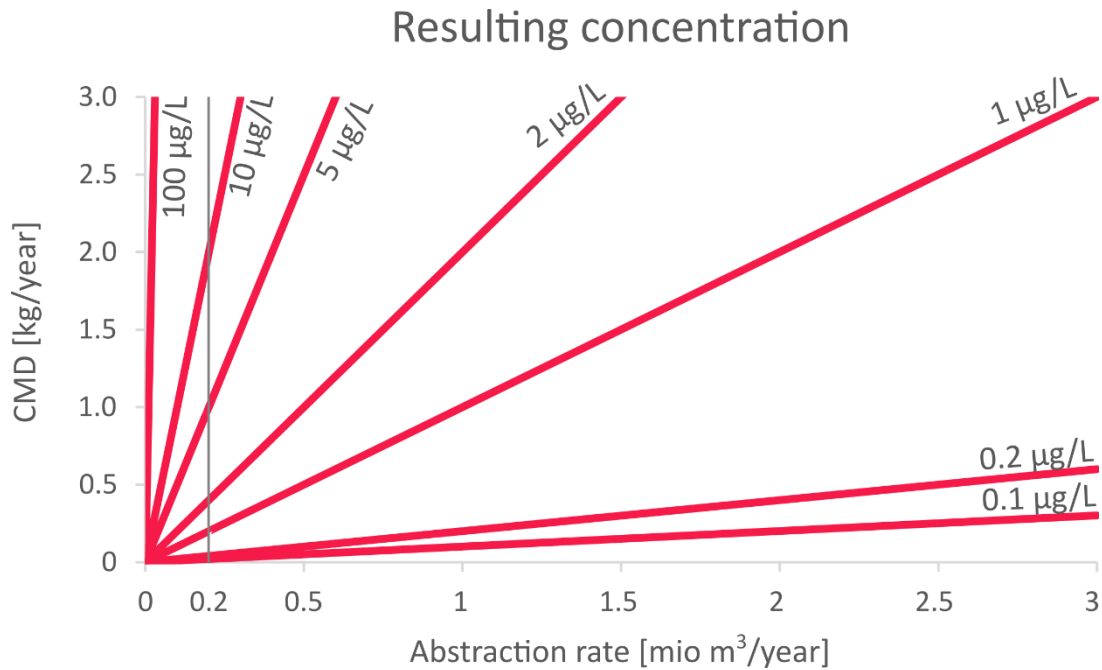


**Figure 19.** The resulting concentration with different abstraction rates for CMD estimate between 0 and 3 kg/year. The exemplification of the resulting concentration is based on the Danish groundwater quality criteria for chlorinated ethenes (1 µg/L for PCE, TCE, and cis-DCE and 0.2 µg/L for VC), as well as some higher standards applicable for other compounds. The maximum abstraction rate is set to 3 mio m<sup>3</sup>/year as this the maximum value of a water works in the Capital Region of Denmark. The grey line indicates the standard abstraction rate of 200,000 m<sup>3</sup>/year used in the Capital Region of Denmark. Inspiration from (Einarson and Mackay 2001).

### 6.2.2 CMD methods for the Danish risk assessment framework

The Capital Region of Denmark has started to apply CMD as a metric for risk assessment of contaminated sites at a site specific local scale, a catchment scale, and at different knowledge levels of the investigations. At the local scale, the approach is, as described later, with the use of an abstraction rate to evaluate the resulting concentration. At the catchment scale, the Capital Region of Denmark investigates the contaminated sites within a catchment area in order to prioritize the remedial actions, similar to the approach suggested by Troldborg et al. (2008).

At an early stage of investigating a contaminated site (preliminary surveys), it is beneficial to get a fairly rough estimate of the CMD, and therefore an overall idea of whether further field investigations are needed at the site. In Denmark, the risk assessment model GrundRisk (Rosenberg et al. 2016; Locatelli et al. 2019) is soon to be implemented for the preliminary surveys of the risk assessment framework, see Figure 20. The GrundRisk model estimates a groundwater

concentration at a POC 100 m downgradient from the source, the CMD in the aquifer, and the resulting concentration in the water abstracted with a given rate.

At the stage of confirmed contaminated, the ProfileFlux method is beneficial, as it allows for a cost-effective investigation that combines measurements and interpretation of these using a solute transport model (Rosenberg et al. **II**). The estimated CMD from the ProfileFlux method will inform the risk assessment and the learnings from comparing the measured and the simulated concentration profiles will guide the user in choosing potential additional field investigations.

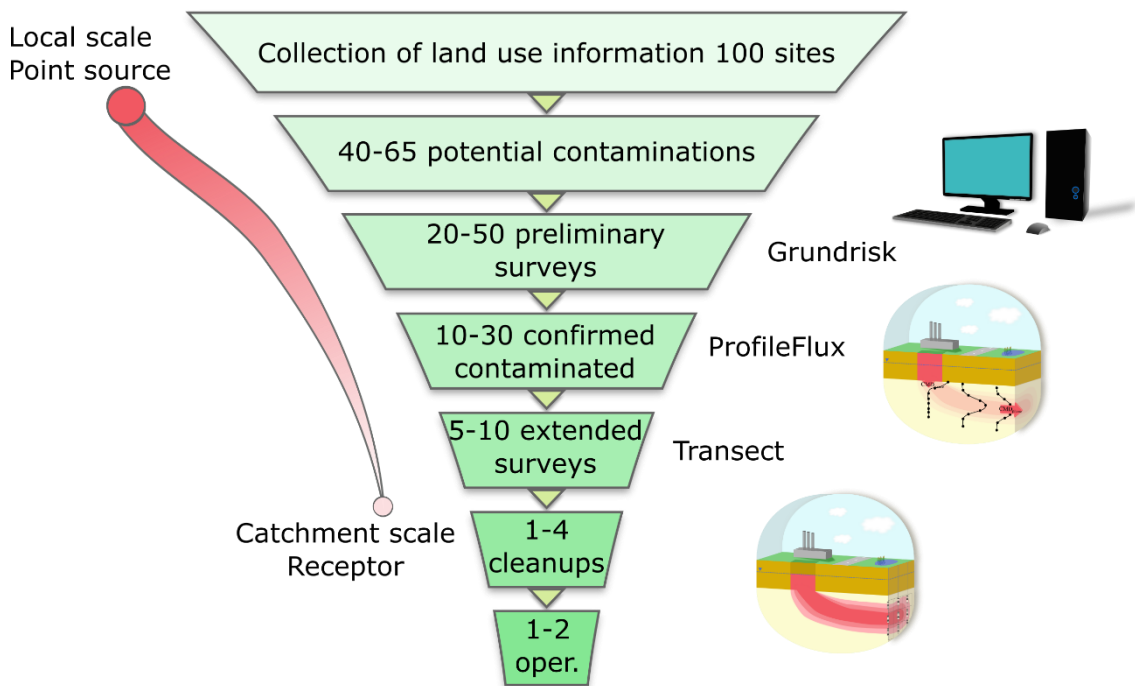


**Figure 20.** Exemplification of how three CMD methods can be applied at different stages of a risk assessment, from a Danish point of view. Moving towards extended surveys and clean-ups requires prioritization of the contaminated sites, hence, the focus is shifting from local scale to catchment scale. Modified from and inspired by Troldborg et al. (2008) and Overheu et al. (2014).

The transect method (including the PFM) are beneficial to use at a more elaborate field site investigation needed for extended surveys. Furthermore, the methods are useful for investigating the evolution of the contaminant plume and/or the effect of a given remediation scheme in progress. The PFM can be used in a transect instead of traditional concentration measurements and Darcy velocity estimates. Moreover, PFMs can be installed in certain monitoring wells to estimate the contaminant mass flux (CMF). The CMF can be compared

with the  $CMF_{max}$  (maximum acceptable CMF) as suggested by (Verreydt et al. 2012).

In the Capital Region of Denmark, the estimate of CMD is used in combination with a risk-CMD that is found as described in chapter 6.2.1 using the actual or standard abstraction rate. If the risk-CMD is larger than the estimated CMD, the risk associated with the contamination is acceptable. However, other factors are also included in the risk assessment at the stage of extended surveys such as knowledge of CMD estimates from other contaminated sites in the area. Furthermore, the risk assessment relies on a qualitative assessment of the knowledge level at the site e.g. if the source zone is delineated or if the infiltration is well-established.

### 6.3 Moving onwards and upwards

As previously stated in chapter 2.1 the community has suggested moving toward using CMD as a risk assessment metric for several years, however, it is still not broadly implemented. Horst et al. (2021) identified three main reasons for why CMD (denoted mass flux in the scientific paper) has not been implemented as a metric for risk assessment:

- 1) *“Despite the availability of guidance and technology, there is still a lack of **widespread technical adeptness by the practitioner community.**”*
- 2) *“Another key limitation is the hesitancy of some responsible parties to **invest in the effort required to develop a robust mass flux assessment.**”*
- 3) *“There is **general lack of alignment on how mass flux fits with compliance metrics particularly in the most common framework where numeric water quality standards (e.g., maximum contaminant level [MCLs]) are applied at specific compliance points.**”*

The lack of technical adeptness (point 1) is most likely due to the lack of alignment on how to use the resulting CMD (point 3). If there is no market for investigation or use of the estimated CMD, there is no motivation for the practitioners to adapt the CMD metric in the work. Furthermore, a protocol describing the use of an appropriate CMD method depending on the level of knowledge and risk assessment would guide the practitioners. The protocol should include step-by-step instructions, data requirement, quality control measures and uncertainties.

The scientific community has for several years developed new robust methods, or improvements of exiting methods, to determine CMD and the associated



uncertainties (point 2) and work is still in progress. Many good and valid methods exist but more focus on developing a protocol for the methods (as described in the previous section) should be pushed for. This would require the national, and maybe even international, government/authorities to invest resources and address these issues.

Point 3 mentioned by Horst et al. (2021) is the most critical point to solve. As stated previously, many researchers have suggested the use of CMD, and receptor flow rates to calculate a concentration at the receptor. This has now been implemented in the Capital Region of Denmark in their most recent guideline for risk assessment (Region Hovedstaden 2021). In order to extend the use of CMD metric, the experiences from parties actually practising it should be shared and discussed on national and international level. Hopefully, continued interest and added learning will drive the risk assessments towards applying the CMD as a metric.

## 7 Conclusions

The aim of this thesis was to improve the risk assessment of chlorinated ethene sources in clay till settings in order to protect the groundwater resources. The conclusion on the specific objectives are summarized below:

### *Governing processes of chlorinated ethenes at clay till sites*

- Diffusion and back-diffusion plays an important role of distributing and releasing the chlorinated ethenes in clay till. Many chlorinated ethene contaminations are several decades old and these processes have resulted in a more uniformly distributed mass of contamination in the clay till.
- Uncertainty of the estimate of stored contaminant mass in the clay till source zone are related to the uncertainties regarding determination of the sorption coefficient.
- Realistic values for the dispersivities in the aquifer are important, when simulating a contaminant plume in the aquifer. Often, steep concentration gradients in the transverse and vertical direction are observed indicating low dispersivity values and very limited dilution at local scale.

### *Field approaches for clay till sites*

- A novel method to determine the vertical hydraulic gradient has been presented. It is an advancement of the procedure while using the direct-push MiHPT that is already widely used.
- An important parameter to determine for a risk assessment of a contaminated field site is the vertical hydraulic gradient. It will give an indication of the presence of fractures and make the estimated infiltration rate at the site more reliable.
- A numerical 3D model using advective-dispersive transport was able to simulate the observed vertical concentration profiles. To investigate the influence of fractures and sorption in the clay till, a 2D sub-model was set up.
- Determination of the thickness of the clay till is important as fracture spacing and aperture has been observed to decrease with depth. Few fractures and small fracture aperture will result in contaminant moving primarily by diffusive and advective transport in the clay till matrix.

- The sorption has a high influence on the leaching time, time frame of the spill and mass estimate. Clay till has been shown to have a higher sorption coefficient of chlorinated ethenes than what is estimated using traditional methods correlated with  $f_{oc}$  and  $\log(K_{ow})$ .
- High-resolution, depth-discrete concentration profiles can be used to improve the conceptual model for clay till sites. The profiles can be perceived as a footprint of the flow field and source zone information at the site.

### ***Methods and application of CMD informed risk assessment***

- Through comprehensive field investigation and modelling the Profile-Flux method has been developed. It is a method for determining the CMD at clay till sites.
- For an initial estimate of CMD at clay till sites, the ProfileFlux method that utilizes the information retrieved from high-resolution, depth-discrete concentration profiles in the aquifer can be used. The method permits for a time-efficient risk assessment based on the CMD estimate of an old spill.
- Using CMD as a metric in the risk assessment framework will allow for a prioritization of clean-up of contaminated sites for the associated receptor(s) at a catchment scale. Applying and adapting the CMD methods to different knowledge levels depending on the step in the risk assessment framework will be a cost-effective approach.
- Development of a comprehensive protocol describing the different CMD methods, their applicability, data needs, and uncertainty will help guide the practitioners and decision makers towards incorporating CMD as a metric.

## 8 Recommendations for future work

Working with the topic of risk assessment of chlorinated ethene sources located in clay till settings, with a focus on groundwater resources protection, have allowed for the following ideas for future research topics and perspectives:

- ***Vertical transport in clay till***

The vertical transport in clay till is highly depending of infiltration, vertical hydraulic gradient and vertical hydraulic conductivity. Currently, the hydraulic conductivity in clay till has been investigated at different scales and with varying focus on the flow direction (horizontal, vertical). Future work regarding development of new methods to investigate the in-situ vertical hydraulic conductivity will be useful. This could involve investigations on performance of long term slug tests in clay till. Combining investigations of vertical hydraulic gradient and a readily accessible in-situ field investigation of the vertical hydraulic conductivity will improve the estimation of infiltration at clay till sites.

- ***Sorption of contaminants in clay till***

Sorption of chlorinated ethenes to clay till has an impact on the duration of the secondary source emanating from the clay till and the estimated stored mass, hence, using a realistic estimate of  $K_d$  is crucial. An increased focus on the use of suitable  $K_d$  values for chlorinated ethenes in clay till is recommended. Also, investigation of the transport and storage of other sorbing compounds in clay till should include an evaluation of whether the chosen  $K_d$  value is adequate.

- ***High-resolution, depth-discrete concentration profiles (ProfileFlux)***

Performing investigations of the vertical concentration profiles at a contaminated site can add valuable information to the conceptual understanding and risk assessment. Performing high-resolution, depth-discrete investigations should be prioritized. This includes overcoming the habits of using long screens for site investigations and moving towards using shorter sampling intervals and lengths. The ProfileFlux method is new, and further testing should be carried out at other field sites to investigate further advantages and limitations. Such testing includes other compounds such as BTEX, PFAS, and pesticides. Furthermore, the ProfileFlux method should be tested at other aquitard-aquifer systems (inclusion of unsaturated zone).

- ***Uncertainty related to CMD estimates***

The CMD from the different methods has a related uncertainty that needs to be taken into consideration. Sampling density has a big impact on the uncertainty related to the estimate. Furthermore, the site specific parameters are determined with a degree of uncertainty. For each of the methods, the uncertainty of the CMD estimate related to the uncertainty of the parameters should be investigated. This requires further focus in particular for large and deep plumes with sparse monitoring network. The use of supporting information from geophysical methods, in situ probes and detectors should also be considered in future studies.

- ***Development of protocols for investigations of CMD***

CMD has proven to be a useful metric for risk assessment of contaminated sites. However, it is not fully integrated in the risk assessment process. A comparative study to determine the advantages and limitations of each method under different site conditions and knowledge levels could be the foundation of a comprehensive protocol. The protocol could be a guide for the practitioners to follow when estimating CMD. It should provide step-by-step instructions, data requirements, quality control measures and uncertainty. In addition, collaboration with national and international regulatory agencies to develop guidelines and policies are key for a concerted effort in fully using the untapped potential of CMD for risk assessment of contaminated sites.

## 9 References

- Aamand, J., N. Badawi, P. Roll Jakobsen, P.R. Jørgensen, K. Mosthaf, L. Troldborg, and M. Rolle. 2022. Mapping Groundwater Vulnerability to Pesticide Contamination through Fractured Clays - CLAYFRAC. The Danish Environmental Protection Agency. DOI: <https://mst.dk/service/publikationer/publikationsarkiv/2022/feb/clayfrac/>.
- Abdul, A.S., T.L. Gibson, and D.N. Rai. 1987. Statistical Correlations for Predicting the Partition Coefficient for Nonpolar Organic Contaminants between Aquifer Organic-Carbon and Water. *Hazardous Waste and Hazardous Materials* 4, no.3: 211–22.
- Adamson, D.T., S.W. Chapman, S.K. Farhat, B.L. Parker, P. deBlanc, and C.J. Newell. 2015. Characterization and Source History Modeling Using Low-k Zone Profiles at Two Source Areas. *Groundwater Monitoring and Remediation* 35, no.2: 52–69. DOI: 10.1111/gwmr.12090.
- Annable, M.D., K. Hatfield, J. Cho, H. Klammler, B.L. Parker, J.A. Cherry, and P.S.C. Rao. 2005. Field-Scale Evaluation of the Passive Flux Meter for Simultaneous Measurement of Groundwater and Contaminant Fluxes. *Environmental Science and Technology* 39, no.18: 7194–7201. DOI: 10.1021/es050074g.
- Anneser, B., F. Einsiedl, R.U. Meckenstock, L. Richters, F. Wisotzky, and C. Griebler. 2008. High-Resolution Monitoring of Biogeochemical Gradients in a Tar Oil-Contaminated Aquifer. *Applied Geochemistry* 23, no.6: 1715–30. DOI: 10.1016/j.apgeochem.2008.02.003.
- Arey, J.S., and P.M. Gschwend. 2005. A Physical-Chemical Screening Model for Anticipating Widespread Contamination of Community Water Supply Wells by Gasoline Constituents. *Journal of Contaminant Hydrology* 76, no.1–2: 109–38. DOI: 10.1016/j.jconhyd.2004.08.002.
- Basu, N.B., P.S.C. Rao, I.C. Poyer, M.D. Annable, and K. Hatfield. 2006. Flux-Based Assessment at a Manufacturing Site Contaminated with Trichloroethylene. *Journal of Contaminant Hydrology* 86, no.1–2: 105–27. DOI: 10.1016/j.jconhyd.2006.02.011.
- Béland-Pelletier, C., M. Fraser, J. Barker, and T. Ptak. 2011. Estimating Contaminant Mass Discharge: A Field Comparison of the Multilevel Point Measurement and the Integral Pumping Investigation Approaches and Their Uncertainties. *Journal of Contaminant Hydrology* 122, no.1–4: 63–75. DOI: 10.1016/j.jconhyd.2010.11.004.
- Bjerg, P.L., N. Tuxen, L.A. Reitzel, H.J. Albrechtsen, and P. Kjeldsen. 2011. Natural Attenuation Processes in Landfill Leachate Plumes at Three Danish Sites. *Ground Water* 49, no.5: 688–705. DOI: 10.1111/j.1745-6584.2009.00613.x.
- Bockelmann, A., T. Ptak, and G. Teutsch. 2001. An Analytical Quantification of Mass Fluxes and Natural Attenuation Rate Constants at a Former Gasworks Site. *Journal of Contaminant Hydrology* 53, no.3–4: 429–53. DOI: 10.1016/S0169-7722(01)00177-2.
- Bøllingtoft, A.B. 2020. Quantification of Uncertainties in Determination of Contaminant Mass Discharge in Groundwater. Technical University of Denmark.

- Broholm, M.M., G.S. Janniche, K. Mosthaf, A.S. Fjordbøge, P.J. Binning, A.G. Christensen, B. Grosen, T.H. Jørgensen, C. Keller, G. Wealthall, and H. Kern-Jespersen. 2016. Characterization of Chlorinated Solvent Contamination in Limestone Using Innovative FLUTe® Technologies in Combination with Other Methods in a Line of Evidence Approach. *Journal of Contaminant Hydrology* 189: 68–85. DOI: 10.1016/j.jconhyd.2016.03.007.
- Chakraborty, P., and B.S. Das. 2018. Measurement and Modeling of Longitudinal Dispersivity in Undisturbed Saturated Soil: An Experimental Approach. *Soil Science Society of America Journal* 82, no.5: 1117–23. DOI: 10.2136/sssaj2018.05.0176.
- Chambon, J. C., M.M. Broholm, P.J. Binning, and P.L. Bjerg. 2010. Modeling Multi-Component Transport and Enhanced Anaerobic Dechlorination Processes in a Single Fracture-Clay Matrix System. *Journal of Contaminant Hydrology* 112, no.1–4: 77–90. DOI: 10.1016/j.jconhyd.2009.10.008.
- Chambon, J.C., P.J. Binning, P.R. Jørgensen, and P.L. Bjerg. 2011. A Risk Assessment Tool for Contaminated Sites in Low-Permeability Fractured Media. *Journal of Contaminant Hydrology* 124, no.1–4: 82–98. DOI: 10.1016/j.jconhyd.2011.03.001.
- Chambon, Julie C., P.L. Bjerg, C. Scheutz, J. Bælum, R. Jakobsen, and P.J. Binning. 2013. Review of Reactive Kinetic Models Describing Reductive Dechlorination of Chlorinated Ethenes in Soil and Groundwater. *Biotechnology and Bioengineering* 110, no.1: 1–23. DOI: 10.1002/bit.24714.
- Chapman, S.W., and B.L. Parker. 2005. Plume Persistence Due to Aquitard Back Diffusion Following Dense Nonaqueous Phase Liquid Source Removal or Isolation. *Water Resources Research* 41, no.12: 1–16. DOI: 10.1029/2005WR004224.
- Chapuis, R.P., and D.E. Gill. 1989. Hydraulic Anisotropy of Homogeneous Soils and Rocks: Influence of the Densification Process. *Bulletin of the International Association of Engineering Geology* 39, no.1: 75–86. DOI: 10.1007/BF02592538.
- Cherry, J.A., B.L. Parker, K.R. Brandbury, T.T. Eaton, M.B. Gotkowitz, D.J. Hart, and M.A. Borchardt. 2006. Contaminant Transport Through Aquitards: A State-of-the-Science Review. *AWWA Research Foundation*. Denver, Colorado.
- Christiansen, C.M., I. Damgaard, M.M. Broholm, T.C. Kessler, and P.L. Bjerg. 2012. Direct-Push Delivery of Dye Tracers for Direct Documentation of Solute Distribution in Clay Till Camilla. *Journal of Environmental Engineering* 138, no.1: 27–37. DOI: 10.1061/(ASCE)EE.1943-7870.0000451.
- Church, P.E., and G.E. Granato. 1996. Bias in Ground-Water Data Caused by Well-Bore Flow in Long-Screen Wells. *Ground Water* 34, no.2: 262–73. DOI: 10.1111/j.1745-6584.1996.tb01886.x.
- Critto, A., and G.W. Suter II. 2009. Environmental Risk Assessment. In *Decision Support Systems for Risk-Based Management of Contaminated Sites*, 29–52. Springer US.
- Damgaard, I. 2012. Enhanced Reductive Dechlorination in Clay till Contaminated with Chlorinated Solvents. Kgs. Lyngby, Denmark.
- Damgaard, I., P.L. Bjerg, C.S. Jacobsen, M.M. Broholm, N. Tuxen, C. Scheutz, J. Bælum, and D. Hunkeler. 2013a. Identification of Chlorinated Solvents Degradation Zones in Clay till by High Resolution Chemical, Microbial and Compound Specific Isotope Analysis. *Journal of Contaminant Hydrology* 146: 37–50. DOI: 10.1016/j.jconhyd.2012.11.010.

- Damgaard, I., P.L. Bjerg, C.S. Jacobsen, A. Tsitonaki, H. Kern-Jespersen, and M.M. Broholm. 2013b. Performance of Full-Scale Enhanced Reductive Dechlorination in Clay Till. *Ground Water Monitoring & Remediation* 33, no.1: 48–61. DOI: 10.1111/j1745.
- Devlin, J.F. 2015. HydrogeoSieveXL: An Excel-Based Tool to Estimate Hydraulic Conductivity from Grain-Size Analysis. *Hydrogeology Journal* 23, no.4: 837–44. DOI: 10.1007/s10040-015-1255-0.
- Devlin, J.F., and P.C. Schillig. 2017. HydrogeoEstimatorXL: An Excel-Based Tool for Estimating Hydraulic Gradient Magnitude and Direction. *Hydrogeology Journal* 25, no.3: 867–75. DOI: 10.1007/s10040-016-1518-4.
- Ding, X.H., S.J. Feng, and Q.T. Zheng. 2022. Forward and Back Diffusion of Reactive Contaminants through Multi-Layer Low Permeability Sediments. *Water Research* 222, no. June: 118925. DOI: 10.1016/j.watres.2022.118925.
- Doherty, R.E. 2000. A History of the Production and Use of Carbon Tetrachloride, Tetrachloroethylene, Trichloroethylene and 1,1,1-Trichloroethane in the United States: Part 1 - Historical Background; Carbon Tetrachloride and Tetrachloroethylene. *Environmental Forensics* 1, no.2: 69–81. DOI: 10.1006/enfo.2000.0010.
- Dolinová, I., M. Štrojsová, M. Černík, J. Němeček, J. Macháčková, and A. Ševců. 2017. Microbial Degradation of Chloroethenes: A Review. *Environmental Science and Pollution Research* 24, no.15: 13262–83. DOI: 10.1007/s11356-017-8867-y.
- Domenico, P.A., and F. Schwartz. 1997. Solute Transport. In *Physical and Chemical Hydrogeology*, 2nd ed., 215–37. New York: John Wiley and Sons Inc.
- Dutta, S., T.M. Christy, W. Mccall, and P. Kurup. 2021. Field Evaluation of 1 . 75 Groundwater Profiler and Field Screening Device for on - Site Contamination Profiling of Chromium ( VI ) in Groundwater. *Environmental Earth Sciences* 80, no.7: 1–18. DOI: 10.1007/s12665-021-09568-9.
- Einarson, M. 2017. Spatially Averaged, Flow-Weighted Concentrations – A More Relevant Regulatory Metric for Groundwater Cleanup. *Groundwater Monitoring and Remediation* 37, no.4: 11–14. DOI: 10.1111/gwmmr.12240.
- Einarson, M.D., and D.M. Mackay. 2001. Predicting Impacts. *Environmental Science & Technology* 35, no.3: 66–73.
- ESTCP. 2011. Decision Guide: A Guide for Selecting Remedies for Subsurface Releases of Chlorinated Solvents. *Department of Defense Environmental Security Technology Program (ESTCP)*, no. March. DOI: [http://www.clu-in.org/download/contaminantfocus/dnapl/Treatment\\_Technologies/DNAPL-ER-200530-DG.pdf](http://www.clu-in.org/download/contaminantfocus/dnapl/Treatment_Technologies/DNAPL-ER-200530-DG.pdf).
- European Commission. 2022. Introduction to the EU Water Framework Directive. [https://ec.europa.eu/environment/water/water-framework/info/intro\\_en.htm](https://ec.europa.eu/environment/water/water-framework/info/intro_en.htm) [20.12.2022].
- Ferris, D.M., G. Potter, and G. Ferguson. 2020. Characterization of the Hydraulic Conductivity of Glacial till Aquitards. *Hydrogeology Journal* 28, no.5: 1827–39. DOI: 10.1007/s10040-020-02161-7.



- Filippini, M., B.L. Parker, E. Dinelli, P. Wanner, S.W. Chapman, and A. Gargini. 2020. Assessing Aquitard Integrity in a Complex Aquifer – Aquitard System Contaminated by Chlorinated Hydrocarbons. *Water Research* 171: 1–12. DOI: 10.1016/j.watres.2019.115388.
- Fjordbøge, A.S., G.S. Janniche, T.H. Jørgensen, B. Grosen, G. Wealthall, A.G. Christensen, H. Kernn-Jespersen, and M.M. Broholm. 2017. Integrity of Clay Till Aquitards to DNAPL Migration: Assessment Using Current and Emerging Characterization Tools. *Groundwater Monitoring and Remediation* 37, no.3: 45–61. DOI: 10.1111/gwmr.12217.
- Frederiksen, M., C.N. Albers, K. Mosthaf, G.A.S. Janniche, N. Tuxen, H. Kernn-jespersen, U.E. Bollmann, M. Christophersen, and P.L. Bjerg. 2023. Long-Term Leaching through Clayey till of N,N-Dimethylsulfamide, a Persistent and Mobile Organic Compound (PMOC). *Journal of Contaminant Hydrology* 257: 1–15. DOI: 10.1016/j.jconhyd.2023.104218.
- Freeze, R.A., and J.A. Cherry. 1979. *Groundwater*. Upper Saddle River: Prentice Hall Inc.
- Frind, E.O., J.W. Molson, and D.L. Rudolph. 2006. Well Vulnerability: A Quantitative Approach for Source Water Protection. *Ground Water* 44, no.5: 732–42. DOI: 10.1111/j.1745-6584.2006.00230.x.
- Garabedian, S.P., D.R. LeBlanc, L.W. Gelhar, and M.A. Celia. 1991. Large-Scale Natural Gradient Tracer Test in Sand and Gravel, Cape Cod, Massachusetts. 2. Analysis of Spatial Moments for a Nonreactive Tracer. *Water Resources Research* 27, no.5: 911–24.
- Gelhar, L.W., C. Welty, and K.R. Rehfeldt. 1992. A Critical of Data on Field-Scale Dispersion in Aquifers. *Water Resources Research* 28, no.7: 1955–74.
- Hart, D.J., K.R. Bradbury, and M.B. Gotkowitz. 2008. Is One an Upper Limit for Natural Hydraulic Gradients? *Ground Water* 46, no.4: 518–20. DOI: 10.1111/j.1745-6584.2008.00433.x.
- Hinsby, K., P.L. Bjerg, L.J. Andersen, B. Skov, and E. V. Clausen. 1992. A Mini Slug Test Method for Determination of a Local Hydraulic Conductivity of an Unconfined Sandy Aquifer. *Journal of Hydrology* 136, no.1–4: 87–106. DOI: 10.1016/0022-1694(92)90006-H.
- Horst, J., M. Schnobrich, C. Divine, P. Curry, S. Sager, and A. Horneman. 2021. Mass Flux Strategies 20 Years On—Getting the Sand Out of the Gears. *Groundwater Monitoring and Remediation* 41, no.4: 13–21. DOI: 10.1111/gwmr.12491.
- Høyer, A.S., K.E.S. Klint, G. Fiandaca, P.K. Maurya, A. V. Christiansen, N. Balbarini, P.L. Bjerg, T.B. Hansen, and I. Møller. 2019. Development of a High-Resolution 3D Geological Model for Landfill Leachate Risk Assessment. *Engineering Geology* 249, no.December 2018: 45–59. DOI: 10.1016/j.enggeo.2018.12.015.
- Hussain, Y., S.F. Ullah, A.Q. Aslam, M.B. Hussain, G. Akhter, H.E. Martinez-Carvajal, F. Satgé, A. Ashraf, B. Iqbal, and M. Cárdenas-Soto. 2017. Vulnerability Assessment of an Agro-Stressed Aquifer Using a Source-Pathway-Receptor Model in GIS. *Modeling Earth Systems and Environment* 3, no.2: 595–604. DOI: 10.1007/s40808-017-0320-1.

- Hyojin, K., A.S. Høyer, R. Jakobsen, L. Thorling, J. Aamand, P.K. Maurya, A.V. Christiansen, and B. Hansen. 2019. 3D Characterization of the Subsurface Redox Architecture in Complex Geological Settings. *Science of the Total Environment* 693. DOI: 10.1016/j.scitotenv.2019.133583.
- ITRC. 2010. Use and Measurement of Mass Flux and Mass Discharge. *ITRC Technology Overview*. Vol. MASSFLUX-1. Washington D.C. DOI: <http://publication/uuid/B5586D8A-2803-4036-81E7-71A33795989D>.
- Jensen, B.B., L. Rosenberg, A. Tsitonaki, N. Tuxen, P.L. Bjerg, L. Nielsen, T.M. Hansen, and M.C. Looms. 2023. High-Resolution Geological Information from Crosshole Ground Penetrating Radar in Clayey Tills. *Ground Water Monitoring & Remediation*. DOI: 10.1111/gwmr.12588.
- Jensen, K.H., K. Bitsch, and P.L. Bjerg. 1993. Large-scale Dispersion Experiments in a Sandy Aquifer in Denmark: Observed Tracer Movements and Numerical Analyses. *Water Resources Research* 29, no.3: 673–96. DOI: 10.1029/92WR02468.
- Jørgensen, I. V, M.M. Broholm, and P.L. Bjerg. 2010. *DNAPL i kildeområder - konceptuelle modeller, karakterisering og estimering af forureningsmasse*. Technical University of Denmark.
- Jørgensen, P.R., M. Hoffmann, J.P. Kistrup, C. Bryde, R. Bossi, and K.G. Villholth. 2002. Preferential Flow and Pesticide Transport in a Clay-Rich till: Field, Laboratory, and Modeling Analysis. *Water Resources Research* 38, no.11: 28-1-28–15. DOI: 10.1029/2001wr000494.
- Jørgensen, P.R., K. Mosthaf, and M. Rolle. 2019. A Large Undisturbed Column Method to Study Flow and Transport in Macropores and Fractured Media. *Groundwater* 57, no.6: 951–61. DOI: 10.1111/gwat.12885.
- Kamp, G. Van der. 2001. Methods for Determining the in Situ Hydraulic Conductivity of Shallow Aquitards - An Overview. *Hydrogeology Journal* 9, no.1: 5–16. DOI: 10.1007/s100400000118.
- Kao, C.M., and Y.S. Wang. 2001. Field Investigation of the Natural Attenuation and Intrinsic Biodegradation Rates at an Underground Storage Tank Site. *Environmental Geology* 40, no.4–5: 622–31. DOI: 10.1007/s002540000226.
- Keller, C.K., G. Van Der Kamp, and J.A. Cherry. 1989. A Multiscale Study of the Permeability of a Thick Clayey Till. *Water Resources Research* 25, no.11: 2299–2317. DOI: 10.1029/WR025i011p02299.
- Kessler, T. C., K.E.S. Klint, B. Nilsson, and P.L. Bjerg. 2012. Characterization of Sand Lenses Embedded in Tills. *Quaternary Science Reviews* 53, no.C: 55–71. DOI: 10.1016/j.quascirev.2012.08.011.
- Kessler, Timo Christian. 2012. *Hydrogeological Characterization of Low-Permeability Clayey Tills: The Role of Sand Lenses*. DTU Environment. Denmark.
- Labaky, W., J.F. Devlin, and R.W. Gillham. 2009. Field Comparison of the Point Velocity Probe with Other Groundwater Velocity Measurement Methods. *Water Resources Research* 46, no.4: 1–9. DOI: 10.1029/2008WR007066.

- Lévy, L., R. Thalund-Hansen, T. Bording, G. Fiandaca, A. V. Christiansen, K. Rügge, N. Tuxen, M. Hag, and P.L. Bjerg. 2022. Quantifying Reagent Spreading by Cross-Borehole Electrical Tomography to Assess Performance of Groundwater Remediation. *Water Resources Research* 58, no.9: 1–23. DOI: 10.1029/2022WR032218.
- Li, T., Y. Liu, and P.L. Bjerg. 2021. Prioritization of Potentially Contaminated Sites: A Comparison between the Application of a Solute Transport Model and a Risk-Screening Method in China. *Journal of Environmental Management* 281, no.December 2020: 111765. DOI: 10.1016/j.jenvman.2020.111765.
- Locatelli, L., P.J.P.J. Binning, X. Sanchez-Vila, G.L.G.L. Søndergaard, L. Rosenberg, and P.L.P.L. Bjerg. 2019. A Simple Contaminant Fate and Transport Modelling Tool for Management and Risk Assessment of Groundwater Pollution from Contaminated Sites. *Journal of Contaminant Hydrology* 221, no.April 2018: 35–49. DOI: 10.1016/j.jconhyd.2018.11.002.
- Looms, M.C., A. Klotzsche, J. van der Kruk, T.H. Larsen, A. Edsen, N. Tuxen, N. Hamburger, J. Keskinen, and L. Nielsen. 2018. Mapping Sand Layers in Clayey till Using Crosshole Ground-Penetrating Radar. *Geophysics* 83, no.1: A21–26. DOI: 10.1190/GEO2017-0297.1.
- Lu, C., P.L. Bjerg, F. Zhang, and M.M. Broholm. 2011. Sorption of Chlorinated Solvents and Degradation Products on Natural Clayey Tills. *Chemosphere* 83, no.11: 1467–74. DOI: 10.1016/j.chemosphere.2011.03.007.
- Mahammedi, C., L. Mahdjoubi, C.A. Booth, H. Akram, and T.E. Butt. 2020. A Systematic Review of Risk Assessment Tools for Contaminated Sites – Current Perspectives and Future Prospects. *Environmental Research* 191, no.September: 110180. DOI: 10.1016/j.envres.2020.110180.
- Maurya, P.K., N. Balbarini, I. Møller, V. Rønde, A. V. Christiansen, P.L. Bjerg, E. Auken, and G. Fiandaca. 2018. Subsurface Imaging of Water Electrical Conductivity, Hydraulic Permeability and Lithology at Contaminated Sites by Induced Polarization. *Geophysical Journal International* 213, no.2: 770–85. DOI: 10.1093/gji/ggy018.
- McCall, Wes. 2010. Tech Guide for Calculation of Estimated Hydraulic Conductivity (Est . K) Log from HPT Data. DOI: [https://geoprobe.com/sites/default/files/storage/pdfs/tech\\_guide\\_estk\\_v5\\_0\\_0.pdf](https://geoprobe.com/sites/default/files/storage/pdfs/tech_guide_estk_v5_0_0.pdf).
- McCall, Wesley, and T.M. Christy. 2020. The Hydraulic Profiling Tool for Hydrogeologic Investigation of Unconsolidated Formations. *Groundwater Monitoring and Remediation* 40, no.3: 89–103. DOI: 10.1111/gwmr.12399.
- McCall, Wesley, T.M. Christy, D. Pipp, M. Terkelsen, A. Christensen, K. Weber, and P. Engelsen. 2014. Field Application of the Combined Membrane-Interface Probe and Hydraulic Profiling Tool (MiHpt). *Groundwater Monitoring and Remediation* 34, no.2: 85–95. DOI: 10.1111/gwmr.12051.
- McGuire, T.M., C.J. Newell, B.B. Looney, K.M. Vangelas, and C.H. Sink. 2004. Historical Analysis of Monitored Natural Attenuation: A Survey of 191 Chlorinated Solvent Sites and 45 Solvent Plumes. *Remediation* 15, no.1: 99–112. DOI: 10.1002/rem.20036.
- McKnight, U.S., S.G. Funder, J.J. Rasmussen, M. Finkel, P.J. Binning, and P.L. Bjerg. 2010. An Integrated Model for Assessing the Risk of TCE Groundwater Contamination to Human Receptors and Surface Water Ecosystems. *Ecological Engineering* 36, no.9: 1126–37. DOI: 10.1016/j.ecoleng.2010.01.004.

- McNab, W.W., D.W. Rice, and C. Tuckfield. 2000. Evaluating Chlorinated Hydrocarbon Plume Behavior Using Historical Case Population Analyses. *Bioremediation Journal* 4, no.4: 311–35. DOI: 10.1080/10889860091114284.
- Meyer, J.R. 2014. Characteristics of High Resolution Hydraulic Head Profiles and Vertical Gradients in Fractured Sedimentary Rocks. *Journal of Hydrology* 517: 493–507. DOI: 10.1016/j.jhydrol.2014.05.050.
- Meyer, J.R., B.L. Parker, and J.A. Cherry. 2008. Detailed Hydraulic Head Profiles as Essential Data for Defining Hydrogeologic Units in Layered Fractured Sedimentary Rock. *Environmental Geology* 56, no.1: 27–44. DOI: 10.1007/s00254-007-1137-4.
- Milosevic, N., N.I. Thomsen, R.K. Juhler, H.J. Albrechtsen, and P.L. Bjerg. 2012. Identification of Discharge Zones and Quantification of Contaminant Mass Discharges into a Local Stream from a Landfill in a Heterogeneous Geologic Setting. *Journal of Hydrology* 446–447: 13–23. DOI: 10.1016/j.jhydrol.2012.04.012.
- Mosthaf, K., M. Rolle, U. Petursdottir, J. Aamand, and P.R. Jørgensen. 2021. Transport of Tracers and Pesticides through Fractured Clayey till: Large Undisturbed Column (LUC) Experiments and Model-Based Interpretation. *Water Resources Research* 57: 1–18. DOI: 10.1029/2020WR028019.
- Mosthaf, K., L. Rosenberg, M.M. Broholm, G. Lilbæk, A.G. Christensen, A.S. Fjordbøge, and P.L. Bjerg. n.d. Quantification of Contaminant Mass Discharge from Point Sources in Aquitard/Aquifer Systems Based on Vertical Concentration Profiles and 3D Modeling. *Submitted*.
- Murray, A.M., C.B. Ottosen, J. Maillard, C. Holliger, A. Johansen, L. Brabæk, I.L. Kristensen, J. Zimmermann, D. Hunkeler, and M.M. Broholm. 2019. Chlorinated Ethene Plume Evolution after Source Thermal Remediation: Determination of Degradation Rates and Mechanisms. *Journal of Contaminant Hydrology* 227, no.March: 103551. DOI: 10.1016/j.jconhyd.2019.103551.
- Neuzil, C.E. 2019. Permeability of Clays and Shales. *Annual Review of Earth and Planetary Sciences* 47: 247–73. DOI: 10.1146/annurev-earth-053018-060437.
- Newell, C.J., S.K. Farhat, D.T. Adamson, and B.B. Looney. 2011. Contaminant Plume Classification System Based on Mass Discharge. *Ground Water* 49, no.6: 914–19. DOI: 10.1111/j.1745-6584.2010.00793.x.
- NIRAS. 2019. Afgrænsende Forureningsundersøgelse Industrivej 2, 3540 Lyngby. Region Hovedstaden. By request to regionh@regionh.dk.
- Olsen, J., A.-M. Westergaard, T. Laursen, J.R. Pedersen, M.L. Poulsen, and K. Jespersen. 2023. Bevar Jordforbindelsen - Regionernes Arbejde Med Jordforurening.
- Ottosen, C.B. 2020. Documentation and Quantification of in Situ Natural and Enhanced Degradation of Chlorinated Ethenes. Kgs. Lyngby, Denmark.
- Ottosen, Cecilie B., P.L. Bjerg, D. Hunkeler, J. Zimmermann, N. Tuxen, D. Harrekilde, L. Bennedsen, G. Leonard, L. Brabæk, I.L. Kristensen, and M.M. Broholm. 2021. Assessment of Chlorinated Ethenes Degradation after Field Scale Injection of Activated Carbon and Bioamendments: Application of Isotopic and Microbial Analyses. *Journal of Contaminant Hydrology* 240, no.March: 103794. DOI: 10.1016/j.jconhyd.2021.103794.

- Overheu, N.D., N. Tuxen, J. Flyvbjerg, J. Aabling, J.A. Andersen, J.K. Pedersen, T. Thyregod, P.J. Binning, and P.L. Bjerg. 2014. Risk-Based Prioritization of Ground Water Threatening Point Sources at Catchment and Regional Scales. *Science of the Total Environment* 485–486, no.1: 769–75. DOI: 10.1016/j.scitotenv.2014.03.083.
- Overheu, N.D., N. Tuxen, J. Flyvbjerg, P.J. Binning, and P.L. Bjerg. 2012. Håndbog for risikobaseret prioritering af grundvandstruende punktkilder. DOI: <http://www2.mst.dk/Udgiv/publikationer/2012/08/978-87-92903-40-2.pdf>.
- Pankow, J., and J. Cherry. 1996. *Dense Chlorinated Solvents and Other DNAPLs in Groundwater: History, Behavior and Remediation*. Waterloo: Waterloo Press.
- Parker, B.L., S.W. Chapman, and M.A. Guilbeault. 2008. Plume Persistence Caused by Back Diffusion from Thin Clay Layers in a Sand Aquifer Following TCE Source-Zone Hydraulic Isolation. *Journal of Contaminant Hydrology* 102, no.1–2: 86–104. DOI: 10.1016/j.jconhyd.2008.07.003.
- Parker, B.L., J.A. Cherry, and S.W. Chapman. 2004. Field Study of TCE Diffusion Profiles below DNAPL to Assess Aquitard Integrity. *Journal of Contaminant Hydrology* 74, no.1–4: 197–230. DOI: 10.1016/j.jconhyd.2004.02.011.
- Pérez, A.P., and N.R. Eugenio. 2018. Status of Local Soil Contamination in Europe. *JRC Technical Reports*. Luxembourg. DOI: 10.2760/093804.
- Piwoni, M.D., and P. Banerjee. 1989. Sorption of Volatile Organic Solvents from Aqueous Solution onto Subsurface Solids. *Journal of Contaminant Hydrology* 4, no.2: 163–79. DOI: 10.1016/0169-7722(89)90019-3.
- Region Hovedstaden. 2021. Rammekontraktbilag 1 SAB videregående jordforureningsundersøgelser 2021-2025. Hillerød.
- Reilly, T.E., O.L. Franke, and G.D. Bennett. 1989. Description of Hypothetical Groundwater System. *Journal of Hydraulic Engineering* 115, no.2: 270–76. DOI: 10.1061/(ASCE)0733-9429(1989)115:2(270).
- Rivett, M.O., S. Feenstra, and J.A. Cherry. 1994. Transport of a Dissolved-Phase Plume from a Residual Solvent Source in a Sand Aquifer. *Journal of Hydrology* 159, no.1–4: 27–41. DOI: 10.1016/0022-1694(94)90247-X.
- Rønne, V., U.S. McKnight, A.T. Sonne, N. Balbarini, J.F. Devlin, and P.L. Bjerg. 2017. Contaminant Mass Discharge to Streams: Comparing Direct Groundwater Velocity Measurements and Multi-Level Groundwater Sampling with an in-Stream Approach. *Journal of Contaminant Hydrology* 206, no.September: 43–54. DOI: 10.1016/j.jconhyd.2017.09.010.
- Rosenberg, L., K. Mosthaf, M.M. Broholm, A.S. Fjordbøge, N. Tuxen, H. Kern-Jespersen, V.K. Rønne, and P.L. Bjerg. 2023. A Novel Concept for Estimating the Contaminant Mass Discharge of Chlorinated Ethenes Emanating from Clay till Sites. *Journal of Contaminant Hydrology* 252: 1–10. DOI: 10.1016/j.jconhyd.2022.104121.
- Rosenberg, Louise, M.M. Broholm, N. Tuxen, I.H. Kern-Jespersen, G. Lilbæk, and P.L. Bjerg. 2022. Vertical Hydraulic Gradient Estimation in Clay Till, Using MiHPT Advanced Direct-Push Technology. *Groundwater Monitoring and Remediation* 42, no.1: 29–37. DOI: 10.1111/gwmmr.12470.

- Rosenberg, Louise, G.L. Søndergaard, P.J. Binning, J. Aabling, and P.L. Bjerg. 2016. GrundRisk: Beregningsmodel til risikovurdering af grundvandstruende forureninger. *Miljøprojekt 1864*.
- Rotaru, C., D.W. Ostendorf, and D.J. DeGroot. 2014. Chloride Dispersion across Silt Deposits in a Glaciated Bedrock River Valley. *Journal of Environmental Quality* 43, no.2: 459–67. DOI: 10.2134/jeq2013.07.0284.
- Rovey, C.W., and D.S. Cherkauer. 1995. SCALE DEPENDENCY OF HYDRAULIC CONDUCTIVITY MEASUREMENTS. *Ground Water* 33, no.5: 769–80.
- Sale, T., C. Newell, H. Stroo, R. Hinchee, and P. Johnson. 2008. Frequently Asked Questions Regarding Management of Chlorinated Solvents in Soils and Groundwater. Environmental Security Technology Certification Program.
- Schulze-Makuch, D. 2005. Longitudinal Dispersivity Data and Implications for Scaling Behavior. *Ground Water* 43, no.3: 443–56.
- Silliman, S.E., and G. Mantz. 2000. The Effect of Measurement Error on Estimating the Hydraulic Gradient in Three Dimensions. *Ground Water* 38, no.1: 114–20. DOI: 10.1111/j.1745-6584.2000.tb00208.x.
- Slater, L., A.M. Binley, W. Daily, and R. Johnson. 2000. Cross-Hole Electrical Imaging of a Controlled Saline Tracer Injection. *Journal of Applied Geophysics* 44, no.2–3: 85–102. DOI: 10.1016/S0926-9851(00)00002-1.
- Sonne, A.T., U.S. McKnight, V. Rønne, and P.L. Bjerg. 2017. Assessing the Chemical Contamination Dynamics in a Mixed Land Use Stream System. *Water Research* 125: 141–51. DOI: 10.1016/j.watres.2017.08.031.
- Stauffer, P.H. 2006. Flux Flummoxed: A Proposal for Consistent Usage. *Ground Water* 44, no.2: 125–28. DOI: 10.1111/j.1745-6584.2006.00197.x.
- Steelman, C.M., J.R. Meyer, P. Wanner, B.J. Swanson, O. Conway-White, and B.L. Parker. 2020. The Importance of Transects for Characterizing Aged Organic Contaminant Plumes in Groundwater. *Journal of Contaminant Hydrology* 235, no.October. DOI: 10.1016/j.jconhyd.2020.103728.
- Svendsen, E.B., L. Nielsen, B. Nilsson, K.H. Kjær, and M.C. Looms. 2023. Crosshole Ground-Penetrating Radar in Clay-Rich Quaternary Deposits: Toward Characterization of High-Loss Media. *Journal of Geophysical Research: Solid Earth* 128. DOI: 10.1029/2022JB025909.
- Switzer, A.D., and J. Pile. 2015. Grain Size Analysis. In *Handbook of Sea-Level Research*, edited by Ian Shennan, Anthony J. Long, and Benjamin P. Horton, 1st ed., 331. John Wiley & Sons, Ltd.
- Thompson, J., A. Mangel, and F.D. Day-Lewis. 2023. A Geophysical Remediation Monitoring Method Selection Tool (GRM-MST). *Groundwater* 61, no.1: 8–10. DOI: 10.1111/gwat.13268.
- Thomsen, N.I., N. Milosevic, and P.L. Bjerg. 2012. Application of a Contaminant Mass Balance Method at an Old Landfill to Assess the Impact on Water Resources. *Waste Management* 32, no.12: 2406–17. DOI: 10.1016/j.wasman.2012.06.014.
- Troldborg, M., G. Lemming, P.J. Binning, N. Tuxen, and P.L. Bjerg. 2008. Risk Assessment and Prioritisation of Contaminated Sites on the Catchment Scale. *Journal of Contaminant Hydrology* 101, no.1–4: 14–28. DOI: 10.1016/j.jconhyd.2008.07.006.

- Troldborg, M., W. Nowak, I. V. Lange, M.C. Santos, P.J. Binning, and P.L. Bjerg. 2012. Application of Bayesian Geostatistics for Evaluation of Mass Discharge Uncertainty at Contaminated Sites. *Water Resources Research* 48, no.9: 1–19. DOI: 10.1029/2011WR011785.
- Troldborg, M., W. Nowak, N. Tuxen, P.L. Bjerg, R. Helmig, and P.J. Binning. 2010. Uncertainty Evaluation of Mass Discharge Estimates from a Contaminated Site Using a Fully Bayesian Framework. *Water Resources Research* 46, no.1: 1–19. DOI: 10.1029/2010WR009227.
- Tsitonaki, K., M.G. Møller, and N. Tuxen. 2013. Sammenhænge mellem forureningsmasse og -flux for grundvandstruende forureninger. *Miljøprojekt 1479 2013*.
- Tuxen, N., H.J. Albrechtsen, and P.L. Bjerg. 2006. Identification of a Reactive Degradation Zone at a Landfill Leachate Plume Fringe Using High Resolution Sampling and Incubation Techniques. *Journal of Contaminant Hydrology* 85, no.3–4: 179–94. DOI: 10.1016/j.jconhyd.2006.01.004.
- Verreydt, G., J. Bronders, I. Van Keer, L. Diels, and P. Vanderauwera. 2011. Passive Samplers for Monitoring VOC in Groundwater: Prospects Related to Mass Flux Measurements. *IAHS-AISH Publication* 342: 391–94. DOI: 10.1111/j1745.
- Verreydt, G., I. van Keer, J. Bronders, L. Diels, and P. Vanderauwera. 2012. Flux-Based Risk Management Strategy of Groundwater Pollutions: The CMF Approach. *Environmental Geochemistry and Health* 34, no.6: 725–36. DOI: 10.1007/s10653-012-9491-x.
- Verreydt, Goedele, J. Bronders, I. van Keer, L. Diels, and P. Vanderauwera. 2015. Groundwater Flow Field Distortion by Monitoring Wells and Passive Flux Meters. *Groundwater* 53, no.6: 933–42. DOI: 10.1111/gwat.12290.
- Wang, Y., and Y. Rao. 2006. Crosshole Seismic Waveform Tomography - I. Strategy for Real Data Application. *Geophysical Journal International* 166, no.3: 1224–36. DOI: 10.1111/j.1365-246x.2006.03030.x.
- Zech, A., S. Attinger, A. Bellin, V. Cvetkovic, G. Dagan, P. Dietrich, A. Fiori, and G. Teutsch. 2023. Evidence Based Estimation of Macrodispersivity for Groundwater Transport Applications. *Groundwater* 61, no.3: 346–62. DOI: 10.1111/gwat.13252.
- Zech, A., S. Attinger, A. Bellin, V. Cvetkovic, P. Dietrich, A. Fiori, G. Teutsch, and G. Dagan. 2019. A Critical Analysis of Transverse Dispersivity Field Data. *Groundwater* 57, no.4: 632–39. DOI: 10.1111/gwat.12838.

## 10 Papers

- I Rosenberg, L., Broholm, M.M., Tuxen, N., Kerrn-Jespersen, I.H., Lilbæk, G., and Bjerg, P.L., 2022.** Vertical Hydraulic Gradient Estimation in Clay Till, Using MiHPT Advanced Direct-Push Technology. *Groundwater Monitoring and Remediation* 42, no.1: 29–37. DOI: 10.1111/gwmmr.12470.
- II Rosenberg, L., Mosthaf, K., Broholm, M.M., Fjordbøge, A.S., Tuxen, N., Kerrn-Jespersen, H., Rønde, V.K., and Bjerg, P.L., 2023.** A Novel Concept for Estimating the Contaminant Mass Discharge of Chlorinated Ethenes Emanating from Clay till Sites. *Journal of Contaminant Hydrology* 252. DOI: 10.1016/j.jconhyd.2022.104121.
- III Jensen, B.B., Rosenberg, L., Tsitonaki, A., Tuxen, N., Bjerg, P.L., Nielsen, L., Hansen, T.M., and Looms, M.C., 2023.** High-resolution geological information from crosshole ground penetrating radar in clayey tills. *Journal of Contaminant Hydrology* 252, 1-10. DOI: 10.1016/j.jconhyd.2022.104121.
- IV Mosthaf, K., Rosenberg, L., Broholm, M.M., Lilbæk, G., Christensen, A.G., Fjordbøge, A.S., and Bjerg, P.L., 2023.** Quantification of contaminant mass discharge from point sources in aquitard/aquifer systems based on vertical concentration profiles and 3D modeling. Submitted







# I

## Vertical Hydraulic Gradient Estimation in Clay Till, Using MiHPT Advanced Direct-Push Technology

Louise Rosenberg, Mette M. Broholm, Nina Tuxen, Ida  
Henriette Kernn-Jespersen, Gro Lilbæk, Poul L. Bjerg

Groundwater Monitoring and Remediation  
Vol. 42, No. 1, pp. 29-37, 2022

# Vertical Hydraulic Gradient Estimation in Clay Till, Using MiHPT Advanced Direct-Push Technology

by Louise Rosenberg , Mette M. Broholm, Nina Tuxen, Ida Henriette Kerrn-Jespersen, Gro Lilbæk and Poul L. Bjerg

## Abstract

The vertical transport of contaminants from source areas is employed in many risk assessment models and screening tools in order to estimate the contaminant mass discharge (CMD) into underlying aquifers. The key parameters for estimating CMD are the contaminant source area and concentration, and the vertical water flux, the latter of which depends on the vertical hydraulic conductivity and the vertical hydraulic gradient in the subsurface. This study focuses on advancing the use of the combined membrane interface probe hydraulic profiling tool (MiHPT) to investigate the vertical hydraulic gradient across a clay till overlying a sandy aquifer at a contaminated site in Denmark. Only the HPT is necessary for the estimate of vertical hydraulic gradient. The hydraulic head, clay till thickness, and resulting vertical hydraulic gradients found using the MiHPT compared well with observations from nearby nested wells. The parameter with the largest discrepancy was the thickness of the clay till. The advantage of the MiHPT is its relatively quick depth discrete access to information regarding subsurface permeability, vertical hydraulic gradients and contaminant distribution across a site. In this case study, performance of additional dissipation tests during the HPT log to acquire determination of the vertical hydraulic gradient increased the cost by 3% compared to standard HPT logs.

## Introduction

Worldwide, groundwater resources are at great risk of being contaminated, due to subsurface pollution from anthropogenic sources such as chlorinated solvents from e.g. dry cleaning and metal degreasing. Subsurface geology plays an important role in determining the risk of groundwater resource contamination. Aquitards have often been thought of as protective layers for underlying aquifers, but this is highly dependent on the hydrogeology and lithology of the aquitard (Cherry et al. 2006; Butler 2010; Filippini et al. 2020).

Heterogeneous geology, such as clay till, can affect contaminant transport in different ways: As a highway with contaminant transport traveling through vertical fractures, and as a channel network due to connected or embedded sand lenses (e.g., Chambon et al. 2010; Kessler et al. 2012; Damgaard et al. 2013). Furthermore, the porous matrix can act as a long-term, secondary source that leaches through back diffusion from the clay till matrix to the fractures—and thereby underlying aquifers (Chambon et al. 2011). This makes risk assessments in these settings difficult. Efficient and cost-effective approaches and methods to investigate contaminated sites in clay till settings are needed, particularly in early-stage screening investigations. A key challenge in this regard is assessing vertical transport from the clay till to the aquifer.

A useful metric to characterize the risk from a contaminated site is contaminant mass discharge (CMD), used mainly for sand and gravel aquifers and estimated at a vertical control plane in the plume down-gradient the source (e.g., Troldborg et al. 2010; Newell et al. 2011; Verreydt et al. 2012). The method can also be applied quantifying the vertical CMD from the source, with a focus on the contaminated area, concentration, and vertical water flux from a secondary source in risk assessment models (Kamath et al. 2006; Chambon et al. 2011; RISC5 2011; Locatelli et al. 2019). Commonly, either net infiltration, often determined through large scale hydraulic models, or the product of the vertical hydraulic gradient and vertical hydraulic conductivity (Darcy's law) (Overheu et al. 2014; Locatelli et al. 2019) is used as the vertical water flux in early-stage risk assessment. At later stage of the site investigation, estimates of the vertical water flux should be made specifically for the site. Using the vertical hydraulic gradient and vertical hydraulic conductivity is particularly relevant for contamination in areas that are paved or built up, where net infiltration is difficult to define or does not exist.

Measuring the hydraulic head variation over depth to determine vertical hydraulic gradients is a challenge using traditional nested wells as this requires several short screens. Recent studies have used depth discrete measurements of the hydraulic head within an aquitard, along with geological and hydraulic properties, to estimate the thickness and vertical hydraulic gradient of a low permeable zone, as well as to locate high permeable zones, for example, fractured areas, within the aquitard (Meyer et al. 2008; Meyer 2014; Filippini et al. 2020). Furthermore, the high resolution profiles of

*Article Impact Statement:* Using a MiHPT it is possible to determine the vertical hydraulic gradient from a clay till aquitard to the underlying groundwater aquifer.

hydraulic head have contributed to better understanding of the solute transport of contaminants through clayey aquitards (e.g., Keller et al. 1989; Parker et al. 2004). In clay till, several sand lenses are often embedded in the matrix, and the vertical hydraulic gradient between the sand lenses and the underlying aquifer can vary over a contaminated area. This variation is caused by the differences in the thickness of the clay till between the sand lenses and the aquifer. Determining the vertical hydraulic gradient in such a geological setting requires nested wells, well clusters or multilevel systems in order to measure the hydraulic head in both the sand lenses and the aquifer. The same notion applies, for example, when investigating the vertical hydraulic gradient within an aquifer. Furthermore, the measurements of hydraulic head within the aquitard are valuable to assess preferential flow paths within the aquitard. Consequently, in order to determine variations in the vertical hydraulic gradient at a site, several nested wells or other monitoring systems are required.

The membrane interface probe hydraulic profiling tool (MiHPT) that has been applied in this study is a direct push tool, and over the past years it has gained acceptance as a means of field characterization in the risk assessment of contaminated sites (McCall et al. 2014; McCall and Christy 2020). The MiHPT is a combination of a membrane interface probe (MIP) and a hydraulic profiling tool (HPT). The MIP has four detectors for different contaminant groups, such as aliphatic hydrocarbon, and they indicate the contaminant level at depth on a relative scale. The HPT describes the relative permeability of the subsurface as the probe descends, by detecting the necessary pressure needed to inject a certain flow of water. Furthermore, the MiHPT detects electrical conductivity (EC) at depth. The EC provides a measure of the soil EC which can be used as support to distinguish between sandy and clayey materials. In order to investigate the vertical hydraulic gradient only the HPT is necessary. However, as previously stated, the MiHPT was used for this study and it will be referred to as MiHPT throughout the paper.

The objectives of this paper are (1) to evaluate the use of the MiHPT direct push method as a tool to determine the vertical hydraulic gradient between sand lenses embedded in clay till and the underlying aquifer; (2) to estimate additional cost in reference to extra time required for data gathering. This was carried out through fieldwork and a comparison of the following: Measured and estimated hydraulic heads through MiHPT estimates and hydraulic head measurements of traditional nested wells (individual well casings within a single borehole); the thickness of the clay till estimated from MiHPT logs and borehole logs; and the resulting vertical hydraulic gradients obtained via the two previously mentioned methods. Furthermore, the application of the new method for determining vertical hydraulic gradients in other geological settings, as well as its use for estimates of hydraulic conductivity, CMD, and risk assessment, is discussed.

## Equipment and Method

### Contaminated Field Site

Field investigations were conducted at an industrial site located in Vassingerød, Denmark. A map of the site, showing well installations and infrastructure, is presented in

Figure 1. Industrial activity at the site (cutting and laminating Styrofoam) started in 1962.

Site investigations have shown groundwater contamination with trichloroethene (TCE) (NIRAS 2019). An extensive geological investigation of the site showed a sandy aquifer overlain by a clay till with embedded sand lenses (Figure 2). These sand lenses are fully or partly water-saturated. Several monitoring wells were installed, some with screens in the sand lenses and the aquifer, respectively. Geological and hydrogeological characterization along with quantification of contaminant mass distribution were completed in both the source zone and plume areas from ground surface into the underlying sandy aquifer. Apart from knowledge from the nested wells, this was done through the use of more than 20 MiHPT logs. However, not all of the MiHPT logs were operated with this study in mind. Therefore, seven MiHPT logs and seven nested wells were examined for this study.

### Determination of the Vertical Head and Hydraulic Gradient

The vertical hydraulic gradient is defined in Equation (1):

$$i_v = \frac{\Delta h}{\Delta d} \quad (1)$$

where  $i_v$  (m H<sub>2</sub>O/m distance) is the vertical hydraulic gradient,  $\Delta h$  (m H<sub>2</sub>O) is the change in the hydraulic head, and  $\Delta d$  (m distance) is the vertical distance between the

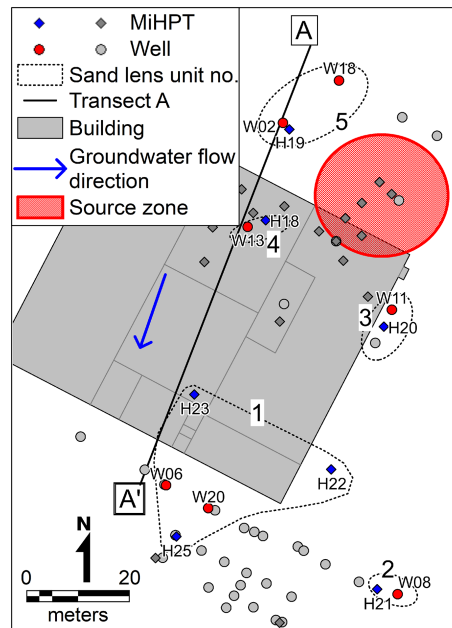


**Figure 1.** Illustration of the MiHPT logs and wells at the field site located in Vassingerød, North Zealand, Denmark. The sand lens units are described in detail in the section “Comparative analysis”. The colored points are the ones referred to in this study. The MiHPT logs performed prior to this study, did not include dissipation tests in the sand lenses. Therefore, no information on the hydraulic head in the sand lenses can be obtained from these MiHPT logs, however, they support the geological model for the site. The placement of the source zone is approximate.

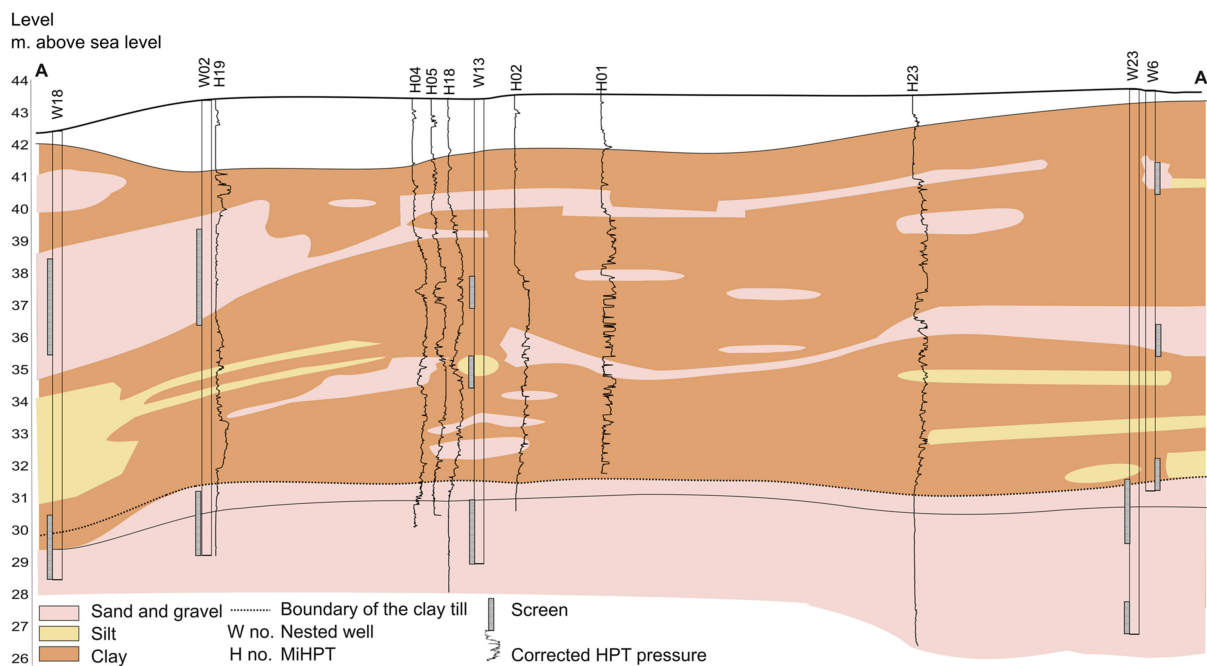


**Figure 2.** Geological profile from A-A' (see Figure 1) along the flow direction. It illustrates the clay till with embedded sand lenses underlain by a sandy aquifer. The geological profile was created through information taken from the bore logs from nested wells, corrected HPT pressure (described in the section “Determination of the vertical head and hydraulic gradient”), and soil samples. Only the nested wells (W) and the corrected HPT pressure (H) are depicted in the figure. The field investigation focused on the hydraulic head in the sand lenses and the underlying aquifer.

examined hydraulic heads. In clay till with embedded sand lenses, distance ( $\Delta d$ ) is assumed equal to the thickness of the low permeable clay till, as this controls any changes in the hydraulic head ( $\Delta h$ ) between the sand units (Cherry et al. 2006; Meyer 2014; Filippini et al. 2020). In this study, the change in the hydraulic head ( $\Delta h$ ) is the head in the sand lens subtracted from the head of the aquifer. Hence, a negative vertical hydraulic gradient value indicates a downward hydraulic gradient.

The hydraulic heads were estimated from dissipation tests carried out as a part of the MiHPT logs (e.g., the black and blue triangles in Figure 3). A dissipation test is used to measure the naturally occurring water pressure in a saturated zone which is used to correct the HPT pressure and provide an estimate of the hydraulic conductivity. When the probe reaches a high permeability zone situated below the water table, the probe and water flow are stopped and the pressure is recorded over time until stable pressure is obtained. This stabilized pressure is the hydrostatic pressure in the formation. Subtracting the atmospheric pressure found prior to the probe advancement through a pre- and post-log HPT reference test (see McCall and Christy 2020 for more information) from the stabilized pressure indicates the hydraulic head at the specific depth of the dissipation test. It is possible to perform several dissipation tests during a MiHPT probe advancement (McCall 2011) and thereby determine depth-specific pressure potentials/hydraulic heads in high-permeability zones (McCall and Christy 2020). The data processing software for the HPT is called *DI-viewer* (free download from <https://geoprobe.com/direct-image-viewer>). This software uses the atmospheric and hydrostatic pressure to correct the HPT pressure

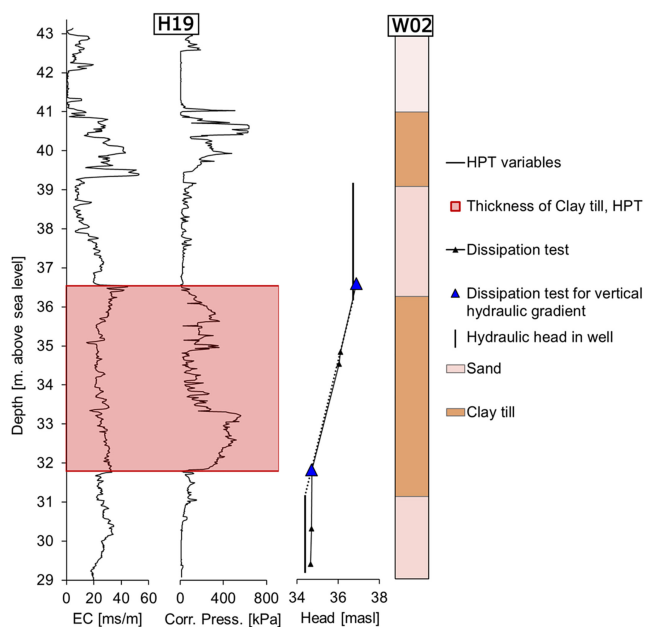


**Figure 3.** Illustration of the parameters used to estimate the vertical hydraulic gradient for the MiHPT log and well. The two graphs to the left are EC and corrected HPT pressure. The third graph is the hydraulic head for the MiHPT log (H19) and well W02, where the vertical line indicates screen placement and length. The blue triangles are the dissipation test used to estimate the vertical hydraulic gradient. The bore log of well W02 is shown to the right. The illustration shows the results for sand lens unit number 5 (see Figure 2).

for the pressure excess by the water column in the formation (corrected HPT pressure). For comparison, the hydraulic heads were measured in traditional nested wells

(vertical lines, Figure 3). In both cases, a vertical hydraulic gradient can be calculated with Equation (1), when the thickness of the intermediate low-permeability layer is known.

The thickness of the clay till used for the monitoring wells was found through the descriptive bore logs, where the lithology was noted every half meter and when changes were observed. For the MiHPT, the thickness of the clay till was estimated based on the corrected HPT pressure alongside the soil's EC. An increase in corrected HPT pressure indicates a decrease in permeability, while an increase in EC can indicate both an increase in the amount of clay particles and/or an increase in ionic strength of pore water (McCall 2010; Maurya et al. 2018; McCall and Christy 2020). The thickness of the clay till was estimated by a combination of an observed increase in the corrected HPT pressure along with an increase in the EC. No specific threshold of the corrected HPT pressure was used. The estimated thickness from the MiHPT is indicated with the red box overlying the logs in Figure 3.

### Comparative Analysis

For each of the seven MiHPT logs, relevant nested wells were chosen based on their placement at the site with respect to which sand lens they intercepted. The sand lens units were identified from the geological interpretations at the site and regular water level measurements in the nested wells monitored over a period of nearly two and a half years. The MiHPT logs were performed during two field campaigns (two different years). At each of the field campaigns, the hydraulic heads were measured in the nested wells close by the MiHPT logs within the same week as the MiHPT logs were carried out. The lateral distance between the MiHPT logs and nested wells within a sand lens unit varied between 1.8 and 35 m. An example of a comparison between a nested well and an adjacent MiHPT log is shown in Figure 3. The two graphs on the left of the figure illustrate results from the MiHPT log, the third shows the hydraulic head from the MiHPT and nested well, while the illustration on the right explains the geology described in the bore log.

The two measurements are different in the sense that the MiHPT is a point measurement and the nested well is an integrated measurement over the length of the screen. However, previous investigation at the site has showed no variation of hydraulic head over the depth of the sandy aquifer. Furthermore, one of the MiHPT logs had three dissipation tests carried out in the sand lens (Figure S4). This log showed no variation in the hydraulic head over the depth of the sand lens. Therefore, the comparison between the two methods at this field site is acceptable.

In total, five different sand lens units were compared (Figure 1), representing seven MiHPT logs and seven nested wells. Please note that the relevant well in sand lens unit 3 (W11) was dry at the time the H2O was performed, so the "measured" hydraulic head in W11 was set equal to the bottom of the screen. The water levels in the nested wells were, as mentioned previously, monitored regularly and W11 showed similar trends in decrease and increase of the hydraulic head as the nested wells nearby. Therefore, it was assumed that the hydraulic head in W11

followed observed changes in other sand lenses at the site, from August 2018 to November 2018. Subtracting the decrease in the observed hydraulic head in the nearby nested wells from the observed hydraulic head in W11 in August 2018, resulted in a hydraulic head equaling the bottom of the screen for W11. Therefore, the assumption seemed justified.

The comparison was done for both the estimated hydraulic heads in the sand lenses and the aquifer, the thickness of the clay till, and for the estimated vertical hydraulic gradient between the sand lenses and the aquifer. For each of these comparisons, the difference in head between the MiHPT and wells was calculated as (2):

$$\text{Diff\%} = \frac{\text{MiHPT} - \text{well}}{(\text{MiHPT} + \text{well}) / 2} \times 100\% \quad (2)$$

where *MiHPT* and *well* are the head, thickness of clay till, or vertical gradient estimated from the MiHPT and well, respectively. A negative number indicates that the results from the MiHPT measurements were lower than from the well measurements and vice versa.

### Estimation of Additional Time and Cost for the Dissipation Tests

Additional time in the field, required for the extra dissipation tests, was calculated as the difference between the time spent on the dissipation tests, viewing the results as a standard MiHPT log, and as an investigation into the vertical hydraulic gradient. The additional cost was calculated using an estimate of the cost of the dissipation tests for each of the MiHPT logs. As the investigations were carried out in Denmark, the cost was converted from Danish crowns (DKK) to US\$. The absolute cost will differ for other geologies and countries, as it is dependent on the permeability of the soil and the hourly price charged by technicians carrying out the work.

## Results

### Estimated Hydraulic Head

A comparison of the estimated hydraulic heads in the sand lenses from the MiHPTs and wells showed very good accordance (Figure 4a, Table S1 and Figures S1–S7). Differences between hydraulic head estimates from the MiHPTs compared to the wells were between  $-0.66\%$  and  $1.3\%$ .

The estimated hydraulic head from the two methods in the aquifer also compared very well. The differences between the estimates were small and varied between  $-1.3\%$  and  $0.78\%$ . Overall, both the results from the sand lenses and the results from the aquifer showed that the MiHPT made a good estimate of the hydraulic head. Furthermore, there was no trend in whether the hydraulic head from the MiHPT was higher or lower than what was measured by the traditional hydraulic head measurement in wells. This indicates that it is rather a local variation in the head than any uncertainty in the method causing differences in measurements.

The biggest difference in hydraulic head estimates in the sand lens was observed in sand lens unit 1 (Figure 4a

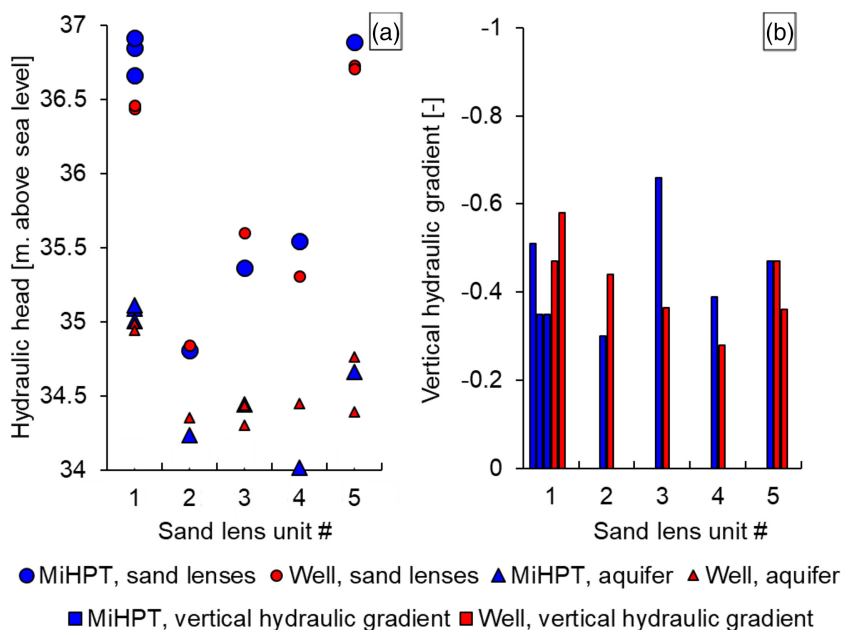


**Figure 4.** (a) The estimated hydraulic head found from the MiHPT logs and the wells. (b) The vertical hydraulic gradients estimated from the MiHPT logs and well. The negative values for the vertical hydraulic gradient indicate an overall downward vertical hydraulic gradient.

and Figures S1–S3). Here, the measured hydraulic head in the wells showed a slightly lower hydraulic head than the three MiHPT logs. This is a unit with a relatively large spatial volume (see Figure 1) where the geology is less well-known than for the other units. Therefore, differences in the hydraulic heads could imply that the investigated sand layer does not constitute a single sand lens but rather some smaller disconnected sand lenses. The biggest difference in hydraulic head estimates in the aquifer was observed in sand lens unit 4 (Figure 4 and Figure S6). The screen was placed in the transition zone between the clay till and the aquifer, where permeability is not as high as in the aquifer. The dissipation test was performed at the same depth as the screen was placed, but unfortunately stable values were not obtained, most likely causing the difference in the hydraulic head.

### Thickness of the Clay Layer

In sand lens unit 4, the difference between the thickness of the clay till layer estimated from the MiHPT and the well log (Figure S6) was very small (–2.6%). However, the thickness of the clay till was overall the parameter that differed the most in the comparison between MiHPT estimates and the well logs. The differences between the two methods were between –79% and 64%, and hence there was no trend in whether the MiHPT yielded a thicker or a thinner layer of clay till than the bore log of the well, which once again indicated no systematic difference between the methods. The thickness of the clay till is determined in different ways in the two methods: From the nested wells, geologic interfaces are estimated while drilling and the soil samples subsequently geologically evaluated. Whereas, for the MiHPT, it is determined from depth discrete logs of subsurface permeability and hydraulic properties. The interpreted thickness of the clay till therefore differed somewhat due to

differences in the methods. This results in some discrepancies in the calculated vertical hydraulic gradient, as shown in the section “Comparison of vertical hydraulic gradient estimates using the two methods”.

The largest differences were seen in sand lens units 3 and 5 (Figures S5 and S7, respectively). In both cases, the thickness estimated from the MiHPT was smaller than from the well logs. The detailing of the bore log in sand lens unit 3 was sparse. The thickness of the clay layer from one of the bore logs located in sand lens unit 5 was found to be very heterogeneous and consisting of clay and silt, which resulted in a larger thickness than found with MiHPT. Observations of the lithology in bore logs can vary according to the person describing the sediment as well as the recovery of the soil on the auger. Furthermore, drilling makes the sample interval more uncertain than for the MiHPT. The thickness of the clay till from the MiHPT is dependent on how the logs are interpreted. For instance, the chosen corrected HPT pressure at which you would expect clay materials, or whether the EC has been used to back up the estimated thickness of the clay till. However, the data from the MiHPT is more discretized than the samples from the bore logs.

The observed differences did not indicate a systematic divergence between the methods, as they showed both higher and lower estimates from the MiHPT than from the well; therefore, these differences were mainly due to local geological spatial variations and as mentioned before, the interpretation of the MiHPT logs and the bore logs.

### Comparison of Vertical Hydraulic Gradient Estimates Using the Two Methods

The resulting vertical hydraulic gradients (Figure 4b) showed good agreement between the two methods. The difference between the estimates was between –49% and 58%. There was no pattern in whether the use of the MiHPT



resulted in a higher or a lower vertical hydraulic gradient than the wells. The highest difference was seen in sand lens unit 3, which also had the highest difference in the thickness of clay till estimated from the two methods. Another difference was found in sand lens unit 1, which covers a large area. The large variation in both the hydraulic head and the vertical hydraulic gradient could imply that there is more than one sand lens in unit 1. It was determined that the highest gradient observed at the site is related to the thinnest separating clay unit.

### Estimated Cost of the Additional Dissipation Tests and Materials

The time spent to perform the additional dissipation tests required to evaluate the vertical hydraulic gradient at the field site was 76 min in total for four of the MiHPT logs (H18-H21), i.e. an average of 19 min per MiHPT log (Table 1). This resulted in an added cost of 39 USD (Danish price level), or an increase of 48%, when only considering the time spent on the dissipation tests. Taking into account the cost of the logs (the drilling and dissipation tests), the cost increase was only 3% for the total field work required for the four MiHPT logs, which took place over 3 days. This corresponds to an increase of the daily workload of 25 min for the drilling team. It should be noted that this added cost is without desktop time for interpretation however, this part is difficult to calculate as the new data also allows for estimation of the vertical CMD, which could not be determined properly without this information (see Discussion section). The time required for the dissipation test will be dependent on the soil permeability.

## Discussion

### Vertical Hydraulic Gradient Measurements

The results showed that the vertical hydraulic gradient can be determined with reasonable confidence in a clay till setting, using MiHPT and nested wells, respectively. Vertical hydraulic gradient estimation is relevant not only for clay till sites, but also in general for low-permeability aquitards.

**Table 1**

**Time and Cost of Performing One MiHPT Log, with and without the Focus on Estimating the Vertical Hydraulic Gradient**

	Dissipation Tests Needed	Time Spent on Dissipation Tests (min)	Dissipation Tests	Total, Drilling + Dissipation Test
Regular MiHPT	4 tests	27	82 USD	1518 USD
Vertical hydraulic gradient MiHPT	6 tests	46	121 USD	1558 USD
Additional test, time and cost	2 tests	19	48%	3%

Note: The estimate is based on an average of four of the MiHPT logs from the field site (H18–H21), taken over 3 days.

Baiocchi et al. (2013) simulated a hydrogeological system from Cimino-Vico (Italy), consisting of two aquifers separated by an aquitard (vulcanite and flysch). They found that the vertical hydraulic conductivity and thickness of the aquitard, and hence the vertical hydraulic gradient, were the main drivers of the interaction between the two aquifers. Cherry et al. (2006) and Meyer et al. (2008) discussed the use of detailed head profiles to locate contrasting hydraulic conductivity units and where aquitards are fractured or disconnected. The combination of the HPT pressure log and the dissipation test (i.e., hydraulic head measure) from the MiHPT offers the opportunity to generate continuous vertical profiles of permeability and hydraulic head both within and across an aquitard. Therefore, it is possible to use the MiHPT to evaluate the plausible path for water flow and contaminant transport within an aquitard. Hart et al. (2008) suggest that the best location for measuring the vertical hydraulic gradient is in the layer boundary, which can be difficult to determine beforehand when installing nested wells. Due to the uncertainty regarding the recovery of the soil on the auger, the exact location of the boundary layer between two units can be difficult to determine as precisely during drilling as is possible with the MiHPT. Furthermore, the screens in the nested wells give an average of the hydraulic head across the screen length, and therefore not the actual hydraulic head in the boundary layer. The permeability reading from the MiHPT can be helpful in investigating the optimal placement of the dissipation tests, but moreover, utilizing the MiHPT as described in this paper is also applicable when investigating the vertical hydraulic gradient within an aquifer.

### Application of the Vertical Hydraulic Gradient for CMD Estimates

At a contaminated site, both vertical and horizontal CMDs are widely used measures to perform a risk assessment. Vertical CMD is used to describe how much contamination is leaching from the source zone into the underlying aquifer (contaminant mass/time), and most often, it is described as (3) (e.g., Locatelli et al. 2019):

$$CMD_v = C \times A \times I \quad (3)$$

where  $CMD_v$  is vertical CMD,  $C$  is concentration (contaminant mass/volume),  $A$  is area (distance squared), and  $I$  is infiltration (distance/time), the latter of which is often determined at a regional scale, whereas both area and concentration are given for a specific site. In some instances, infiltration can be difficult to justify, due to paved areas and buildings on the surface and preferential pathways in the subsurface. In order for all three parameters to be site-specific, infiltration can be substituted by the vertical hydraulic gradient and vertical hydraulic conductivity, which will result in (4):

$$CMD_v = C \times A \times K_v \times i_v \quad (4)$$

where  $K_v$  is vertical hydraulic conductivity (length/time). The vertical hydraulic gradient can be determined for the site by using the MiHPT tool as described in this paper.

For the field site used in this study, elaborate field investigations and modeling of the site show a site-specific vertical hydraulic conductivity of the clay till between  $6.1 \times 10^{-9}$  m/s and  $8.2 \times 10^{-9}$  m/s. Other field and modeling studies of Danish clay tills have shown vertical hydraulic conductivities ranging between  $1.2 \times 10^{-7}$  and  $1.5 \times 10^{-9}$  m/s (Nilsson et al. 2001; Jørgensen et al. 2002, 2004; Mosthaf et al. 2020), which places the vertical hydraulic conductivity for this specific site in the low range.

Applying site-specific information of the source area, as well as concentrations therein and averaged estimated vertical hydraulic gradient found in this paper (440 m<sup>2</sup>, 3000 µg/L and 0.44, respectively), the resulting vertical CMD of TCE from the clay till into the aquifer is between 112 and 149 g/year. This compares well with the initial site investigation estimating a vertical CMD of 27–202 g/year (NIRAS 2019).

### MiHPT and Nested Wells as Tools for Site Investigations

Using the MiHPT as a tool with a focus on obtaining information about the vertical hydraulic gradient will provide the risk assessment of a contaminated site with crucial data. In addition, a variety of depth discrete information can be collected, including: Subsurface permeability, an estimate of hydraulic conductivity, and the distribution of contaminants at depth. Furthermore, the correlation of geological units can be done with a higher degree of certainty compared to the subjective geologically interpreted bore logs. However, some knowledge of the local geology is needed, as the MiHPT probe does not provide aquitard/aquifer material for geological description. With the MiHPT, it is possible to obtain information on variations in the vertical hydraulic gradient across a site with multiple different embedded sand lenses in clay till, as well as depth discrete information on the relative contaminant level and permeability of the subsurface. The pressure measurements for the MiHPT log are performed with the use of a pressure transducer. A calibrated transducer typically has an accuracy of  $\pm 7$  kPa or  $\pm 0.07$  m of water under static conditions. Applying this accuracy to the sand lens unit with the highest difference between the MiHPT and well measurements (sand lens unit 1), results in an increased difference between the methods from 1.3% to 1.5%. This is acceptable taking the uncertainty of the estimate of the clay layer thickness into account. The disadvantage of the MiHPT is that it is not a permanent installation, and therefore it is not possible to investigate changes in the relative contaminant levels and vertical hydraulic gradients over time at the same point.

The use of other direct push probes can also provide information on the vertical hydraulic gradient, as long as the probe shows subsurface permeability (e.g., corrected HPT pressure), the EC signal, and is able to perform a dissipation test or in other ways determining the hydraulic head. Such a probe could be: the combined HPT-GWS or Waterloo APS, which both allows for groundwater sampling in the high permeable layers of the aquifer, or simply the HPT or CPT.

An advantage of the nested well is the ability to monitor changes in both contamination and the hydraulic head over time. In addition, information from soil samples is obtained when drilling is carried out. The disadvantage of the nested well is that information is only available for the specific

depths and lengths of the screens installed (low discretization and integrated measurements over the screen length).

Overall, the two methods are useful at different times during a site investigation. The MiHPT can be used as a screening tool to do an initial investigation at a contaminated site in respect to which further site investigations are needed as well as the placement of these. The logs from the MiHPT can be used to assist in the placement of the nested wells or other permanent monitoring systems such as multilevel systems. Furthermore, the MiHPT logs can be used to determine whether or not these monitoring systems are even needed for further investigation of the site in question.

### Conclusion

This field study investigated the possibility of estimating the vertical hydraulic gradient between two aquifers separated by a low-permeability layer such as clay till, using the MiHPT tool. A comparison between the MiHPT and nested wells paired in five different sand lens units showed very good accordance between the two approaches. Hence, it is possible to investigate the relative contaminant level, the hydrogeology of the subsurface, and the vertical hydraulic gradient, using the MiHPT. The daily added workload in the field for investigating the vertical hydraulic gradient in our case was 25 min, but this would of course vary depending on the permeability of the soil and aquifer material in question.

It is expected that the results shown in this paper will also apply to complex unconsolidated geologies other than clay tills, as well as open up the possibility of obtaining vertical hydraulic gradients within aquifers. The cost is expected to be less for a less complex geology, as this would most likely require fewer dissipation tests.

This study advocates for the use of the vertical hydraulic gradient combined with vertical hydraulic conductivity, in order to estimate the vertical CMD from the source zone into an underlying aquifer. Both the MiHPT and the nested well offer the ability to obtain vertical hydraulic gradients. Using the MiHPT, with a focus on the vertical hydraulic gradient, as a screening tool, supplemented with nested wells and/or other field methods to quantify the specific contaminant concentrations at a site, allows for a better risk assessment.

### Supporting Information

Additional Supporting Information may be found in the online version of this article. Supporting Information is generally not peer reviewed.

**Figure S1:** Illustration of the parameters used to estimate the vertical hydraulic gradient for the MiHPT log and two wells. The two graphs to the left are EC and corrected HPT pressure. The third graph is the hydraulic head for the MiHPT log (H23), well W06 (black) and well W20 (blue), where the vertical line indicates screen placement and length. The blue triangles are the dissipation test used to estimate the vertical hydraulic gradient. The bore logs of the wells are shown to the right. The illustration shows the results for sand lens unit number 1 (see Figure 2).

**Figure S2:** Illustration of the parameters used to estimate the vertical hydraulic gradient for the MiHPT log and two wells. The two graphs to the left are EC and corrected HPT pressure. The third graph is the hydraulic head for the MiHPT log (H22), well W06 (black) and well W20 (blue), where the vertical line indicates screen placement and length. The blue triangles are the dissipation test used to estimate the vertical hydraulic gradient. The bore logs of the wells are shown to the right. The illustration shows the results for sand lens unit number 1 (see Figure 2).

**Figure S3:** Illustration of the parameters used to estimate the vertical hydraulic gradient for the MiHPT log and two wells. The two graphs to the left are EC and corrected HPT pressure. The third graph is the hydraulic head for the MiHPT log (H25), well W06 (black) and well W20 (blue), where the vertical line indicates screen placement and length. The blue triangles are the dissipation test used to estimate the vertical hydraulic gradient. The bore logs of the wells are shown to the right. The illustration shows the results for sand lens unit number 1 (see Figure 2).

**Figure S4:** Illustration of the parameters used to estimate the vertical hydraulic gradient for the MiHPT log and well. The two graphs to the left are EC and corrected HPT pressure. The third graph is the hydraulic head for the MiHPT log (H21) and well W08, where the vertical line indicates screen placement and length. The blue triangles are the dissipation test used to estimate the vertical hydraulic gradient. The bore log of the well is shown to the right. The illustration shows the results for sand lens unit number 2 (see Figure 2).

**Figure S5:** Illustration of the parameters used to estimate the vertical hydraulic gradient for the MiHPT log and well. The two graphs to the left are EC and corrected HPT pressure. The third graph is the hydraulic head for the MiHPT log (H20) and well W11, where the vertical line indicates screen placement and length. The blue triangles are the dissipation test used to estimate the vertical hydraulic gradient. The bore log of the well is shown to the right. The illustration shows the results for sand lens unit number 3 (see Figure 2).

**Figure S6:** Illustration of the parameters used to estimate the vertical hydraulic gradient for the MiHPT log and well. The two graphs to the left are EC and corrected HPT pressure. The third graph is the hydraulic head for the MiHPT log (H18) and well W13, where the vertical line indicates screen placement and length. The blue triangles are the dissipation test used to estimate the vertical hydraulic gradient. The bore log of the well is shown to the right. The illustration shows the results for sand lens unit number 4 (see Figure 2).

**Figure S7:** Illustration of the parameters used to estimate the vertical hydraulic gradient for the MiHPT log and two wells. The two graphs to the left are EC and corrected HPT pressure. The third graph is the hydraulic head for the MiHPT log (H19), well W02 (black) and well W18 (blue), where the vertical line indicates screen placement and length. The blue triangles are the dissipation test used to estimate the vertical hydraulic gradient. The bore logs of the wells are shown to the right. The illustration shows the results for sand lens unit number 5 (see Figure 2).

**Table S1:** The difference in estimate of hydraulic head, thickness of clay layer and vertical hydraulic gradient.

## References

- Baiocchi, A., F. Lotti, and V. Piscopo. 2013. Impact of groundwater withdrawals on the interaction of multi-layered aquifers in the Viterbo geothermal area (Central Italy). *Hydrogeology Journal* 21, no. 6: 1339–1353. <https://doi.org/10.1007/s10040-013-1000-5>
- Butler, A.P. 2010. Groundwater vulnerability and protection. *Groundwater Modelling in Arid and Semi-Arid Areas* 9780521111: 75–86. <https://doi.org/10.1017/CBO9780511760280.007>
- Chambon, J.C., P.J. Binning, P.R. Jørgensen, and P.L. Bjerg. 2011. A risk assessment tool for contaminated sites in low-permeability fractured media. *Journal of Contaminant Hydrology* 124, no. 1–4: 82–98. <https://doi.org/10.1016/j.jconhyd.2011.03.001>
- Chambon, J.C., M.M. Broholm, P.J. Binning, and P.L. Bjerg. 2010. Modeling multi-component transport and enhanced anaerobic dechlorination processes in a single fracture-clay matrix system. *Journal of Contaminant Hydrology* 112, no. 1–4: 77–90. <https://doi.org/10.1016/j.jconhyd.2009.10.008>
- Cherry, J.A., B.L. Parker, K.R. Bradbury, T.T. Eaton, M.B. Gotkowitz, D.J. Hart, and M.A. Borchardt. 2006. *Contaminant Transport through Aquitards: A State-of-the-Science Review*. Denver, Colorado: AWWA Research Foundation.
- Damgaard, I., P.L. Bjerg, C.S. Jacobsen, M.M. Broholm, N. Tuxen, C. Scheutz, J. Bælum, and D. Hunkeler. 2013. Identification of chlorinated solvents degradation zones in clay till by high resolution chemical, microbial and compound specific isotope analysis. *Journal of Contaminant Hydrology* 146: 37–50. <https://doi.org/10.1016/j.jconhyd.2012.11.010>
- Filippini, M., B.L. Parker, E. Dinelli, P. Wanner, S.W. Chapman, and A. Gargini. 2020. Assessing aquitard integrity in a complex aquifer – Aquitard system contaminated by chlorinated hydrocarbons. *Water Research* 171: 1–12. <https://doi.org/10.1016/j.watres.2019.115388>
- Hart, D.J., K.R. Bradbury, and M.B. Gotkowitz. 2008. Is one an upper limit for natural hydraulic gradients? *Ground Water* 46, no. 4: 518–520. <https://doi.org/10.1111/j.1745-6584.2008.00433.x>
- Jørgensen, P.R., T. Helstrup, J. Urup, and D. Seifert. 2004. Modeling of non-reactive solute transport in fractured clayey till during variable flow rate and time. *Journal of Contaminant Hydrology* 68, no. 3–4: 193–216. [https://doi.org/10.1016/S0169-7722\(03\)00146-3](https://doi.org/10.1016/S0169-7722(03)00146-3)
- Jørgensen, P.R., M. Hoffmann, J.P. Kistrup, C. Bryde, R. Bossi, and K.G. Villholth. 2002. Preferential flow and pesticide transport in a clay-rich till: Field, laboratory, and modeling analysis. *Water Resources Research* 38, no. 11: 28-1–28-15. <https://doi.org/10.1029/2001wr000494>
- Kamath, R.K., C.J. Newell, B.B. Looney, K.M. Vangelas, and D.T. Adamson. 2006. *BIOBALANCE: A Mass Balance Toolkit, for Evaluating Source Depletion, Competition Effects, Long-Term Sustainability, and Plume Dynamics. User's Manual*. Houston, Texas, United States of America: Groundwater Services Inc.
- Keller, C.K., G. Van Der Kamp, and J.A. Cherry. 1989. A multiscale study of the permeability of a thick clayey till. *Water Resources Research* 25, no. 11: 2299–2317. <https://doi.org/10.1029/WR025i011p02299>
- Kessler, T.C., K.E.S. Klint, B. Nilsson, and P.L. Bjerg. 2012. Characterization of sand lenses embedded in tills. *Quaternary Science Reviews* 53: 55–71. <https://doi.org/10.1016/j.quascirev.2012.08.011>
- Locatelli, L., P.J. Binning, X. Sanchez-Vila, G.L. Søndergaard, L. Rosenberg, and P.L. Bjerg. 2019. A simple contaminant fate and transport modelling tool for management and risk assessment of groundwater pollution from contaminated sites. *Journal*

- of *Contaminant Hydrology* 221, no. 2018: 35–49. <https://doi.org/10.1016/j.jconhyd.2018.11.002>
- Maurya, P.K., N. Balbarini, I. Møller, V. Rønde, A.V. Christiansen, P.L. Bjerg, E. Auken, and G. Fiandaca. 2018. Subsurface imaging of water electrical conductivity, hydraulic permeability and lithology at contaminated sites by induced polarization. *Geophysical Journal International* 213, no. 2: 770–785. <https://doi.org/10.1093/gji/ggy018>
- McCall, W., and T.M. Christy. 2020. The hydraulic profiling tool for Hydrogeologic investigation of unconsolidated formations. *Groundwater Monitoring and Remediation* 40, no. 3: 89–103. <https://doi.org/10.1111/gwmr.12399>
- McCall, W., T.M. Christy, D. Pipp, M. Terkelsen, A. Christensen, K. Weber, and P. Engelsen. 2014. Field application of the combined membrane-interface probe and hydraulic profiling tool (MiHpt). *Groundwater Monitoring and Remediation* 34, no. 2: 85–95. <https://doi.org/10.1111/gwmr.12051>
- McCall, W. 2011. Application of the Geoprobe® HPT Logging System For Geo-Environmental Investigations. <http://geoprobe.com/literature/mk3184-application-of-hpt-for-geo-environmental-investigations>.
- McCall, W. 2010. Tech Guide for Calculation of Estimated Hydraulic Conductivity (Est. K) Log from HPT Data. [https://geoprobe.com/sites/default/files/storage/pdfs/tech\\_guide\\_estk\\_v5\\_0\\_0.pdf](https://geoprobe.com/sites/default/files/storage/pdfs/tech_guide_estk_v5_0_0.pdf). (accessed September 18, 2020)
- Meyer, J.R. 2014. Characteristics of high resolution hydraulic head profiles and vertical gradients in fractured sedimentary rocks. *Journal of Hydrology* 517: 493–507. <https://doi.org/10.1016/j.jhydrol.2014.05.050>
- Meyer, J.R., B.L. Parker, and J.A. Cherry. 2008. Detailed hydraulic head profiles as essential data for defining hydrogeologic units in layered fractured sedimentary rock. *Environmental Geology* 56, no. 1: 27–44. <https://doi.org/10.1007/s00254-007-1137-4>
- Mosthaf, K., M. Rolle, U. Petursdottir, J. Aamand, and P.R. Jørgensen. 2020. Transport of tracers and pesticides through fractured clayey till: Large undisturbed column (LUC) experiments and model-based interpretation. *Water Resources Research* 57: 1–18. <https://doi.org/10.1029/2020WR028019>
- Newell, C.J., S.K. Farhat, D.T. Adamson, and B.B. Looney. 2011. Contaminant plume classification system based on mass discharge. *Ground Water* 49, no. 6: 914–919. <https://doi.org/10.1111/j.1745-6584.2010.00793.x>
- Nilsson, B., R.C. Sidle, K.E. Klint, C.E. Bøggild, and K. Broholm. 2001. Mass transport and scale-dependent hydraulic tests in a heterogeneous glacial till – Sandy aquifer system. *Journal of Hydrology* 243, no. 3–4: 162–179. [https://doi.org/10.1016/S0022-1694\(00\)00416-9](https://doi.org/10.1016/S0022-1694(00)00416-9)
- NIRAS. 2019. *Afgrænsende Forureningsundersøgelse Industrivej 2, 3540 Lyngø*. Allerød, Denmark: Region Hovedstaden.
- Overheu, N.D., N. Tuxen, J. Flyvbjerg, J. Aabling, J.A. Andersen, J.K. Pedersen, T. Thyregod, P.J. Binning, and P.L. Bjerg. 2014. Risk-based prioritization of ground water threatening point sources at catchment and regional scales. *Science of the Total Environment* 485–486, no. 1: 769–775. <https://doi.org/10.1016/j.scitotenv.2014.03.083>
- Parker, B.L., J.A. Cherry, and S.W. Chapman. 2004. Field study of TCE diffusion profiles below DNAPL to assess aquitard integrity. *Journal of Contaminant Hydrology* 74, no. 1–4: 197–230. <https://doi.org/10.1016/j.jconhyd.2004.02.011>
- RISC5. 2011. Risk-Integrated Software for Clean-Ups. Version 5. User's Guide.
- Troldborg, M., W. Nowak, N. Tuxen, P.L. Bjerg, R. Helmig, and P.J. Binning. 2010. Uncertainty evaluation of mass discharge estimates from a contaminated site using a fully Bayesian framework. *Water Resources Research* 46, no. 1: 1–19. <https://doi.org/10.1029/2010WR009227>
- Verreydt, G., I. van Keer, J. Bronders, L. Diels, and P. Vanderauwera. 2012. Flux-based risk management strategy of groundwater pollutions: The CMF approach. *Environmental Geochemistry and Health* 34, no. 6: 725–736. <https://doi.org/10.1007/s10653-012-9491-x>

## Biographical Sketches

**Louise Rosenberg**, corresponding author, is at the Technical University of Denmark, DTU Environment, Bygningstorvet 115, 2800 Kgs. Lyngby, Denmark; [lour@env.dtu.dk](mailto:lour@env.dtu.dk)

**Mette M. Broholm** is at the Technical University of Denmark, DTU Environment, Bygningstorvet 115, 2800 Kgs. Lyngby, Denmark

**Nina Tuxen** is at the Capital Region of Denmark, Kongens Vænge 2, 3400 Hillerød, Denmark

**Ida Henriette Kerrn-Jespersen** is at the Capital Region of Denmark, Kongens Vænge 2, 3400 Hillerød, Denmark

**Gro Lilbæk** is at NIRAS, Sortemosevej 19, 3450 Allerød, Denmark

**Poul L. Bjerg** is at the Technical University of Denmark, DTU Environment, Bygningstorvet 115, 2800 Kgs. Lyngby, Denmark

497 **Supporting Information:**

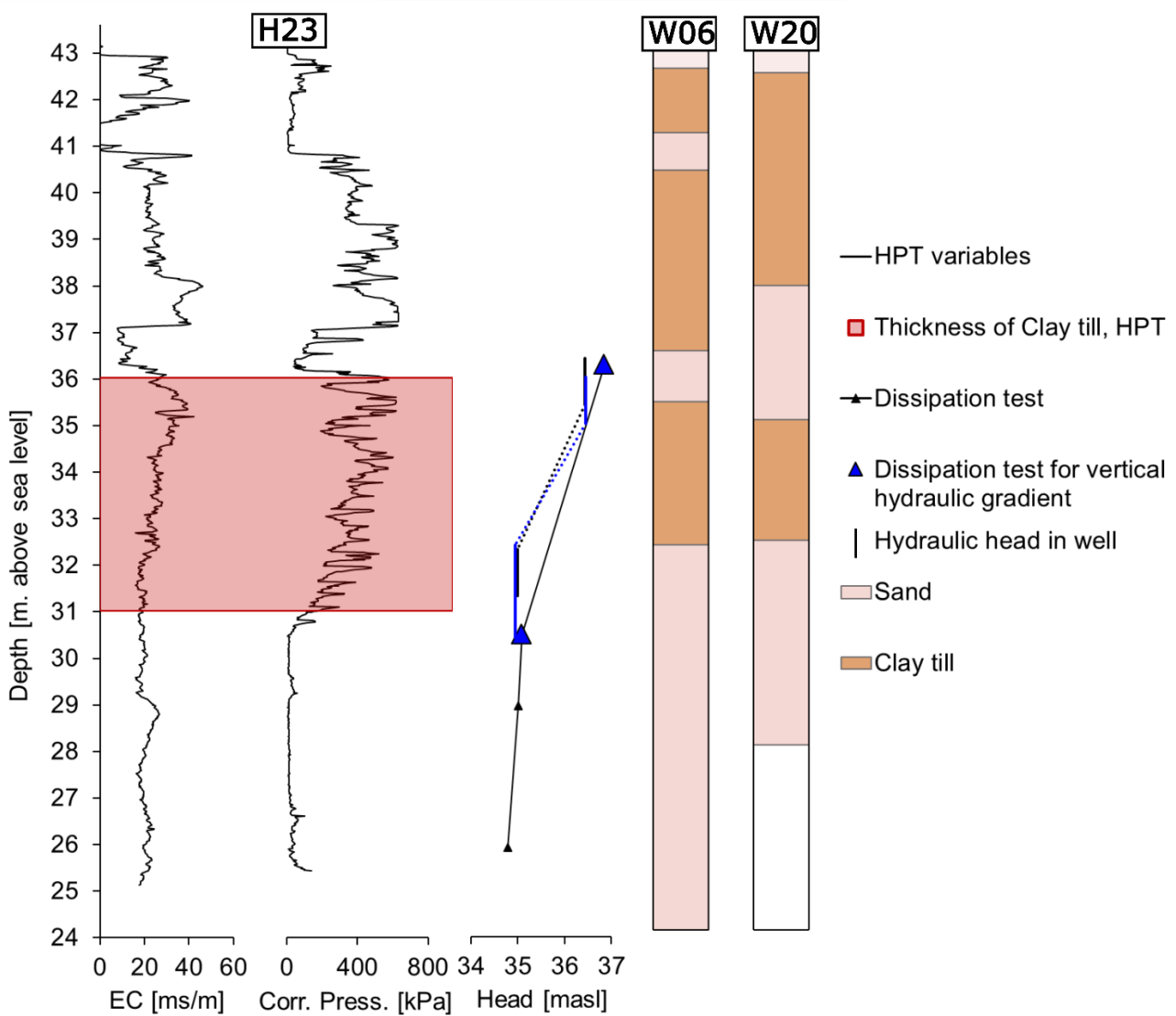
498 **Table S1**

499 **The difference in estimate of hydraulic head, thickness of clay layer and vertical hydraulic**  
500 **gradient.**

Sand lens unit #	Hydraulic head		Thickness of clay layer	Vertical hydraulic gradient
	Sand lens	Aquifer		
1	1.3 %	0.48 %	64 %	-49 %
2	-0.10 %	-0.35 %	50 %	-38 %
3	-0.66 %*	0.03 %	-79 %	58 %*
4	0.67 %	-1.25 %	-2.6 %	33 %
5	0.50 %	0.78 %	-14 %	27 %

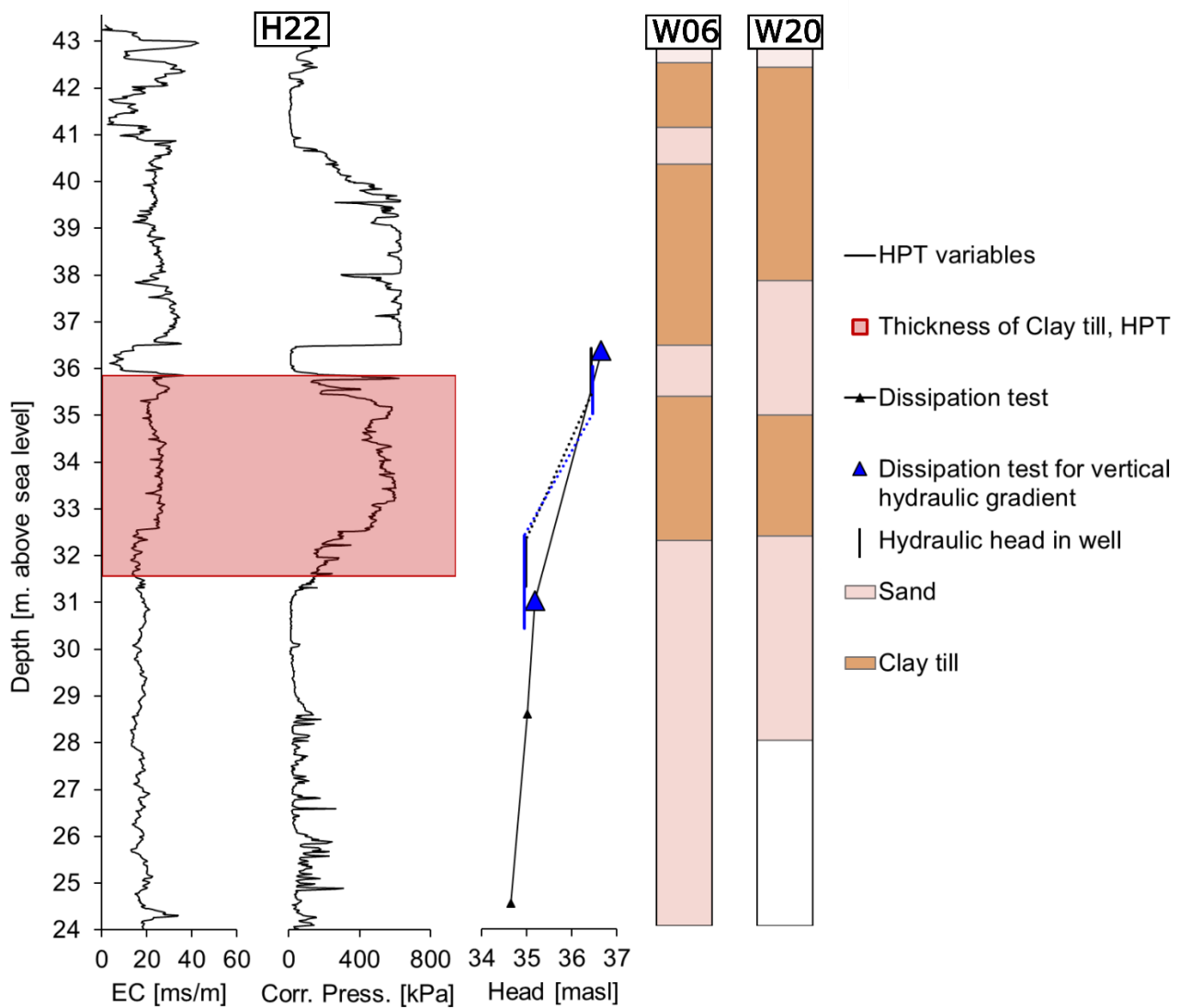
501 \* the screen located in the sand lens in the two relevant wells were dry at the time of the fieldwork.  
502 The hydraulic head in the sand lens has therefore been set to be equal the bottom of the lower of the  
503 two screens. The calculations show the difference from the MiHPT compared to that of the wells  
504 for each of the five sand lens units. As some units have more than one of each measurement per  
505 method, the stated value is the largest difference within the sand lens unit. A negative value is  
506 showing that the estimate from the MiHPT is smaller than that of the well.

507



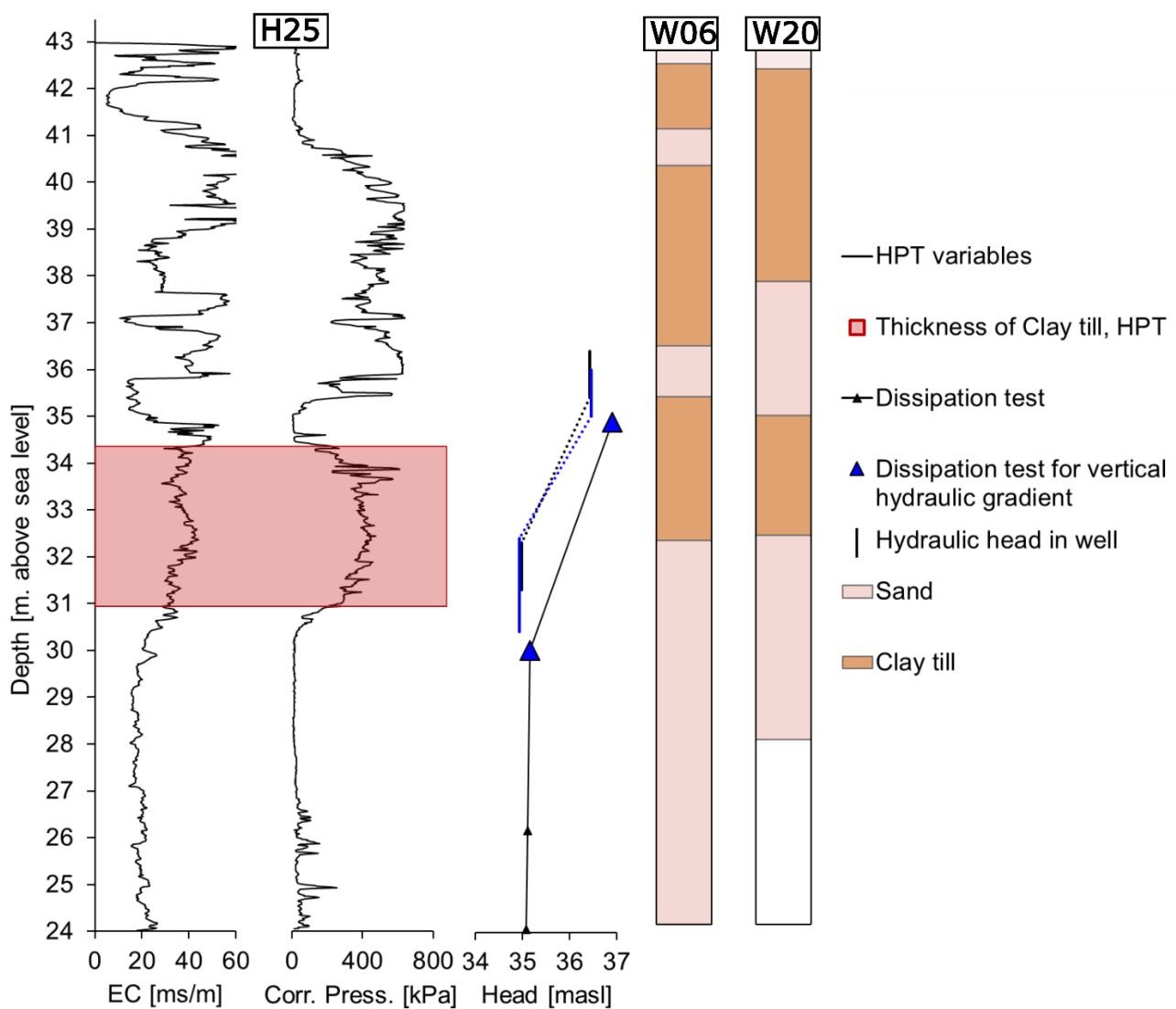
509

510 **Figure S1: Illustration of the parameters used to estimate the vertical hydraulic gradient for**  
 511 **the MiHPT log and two wells. The two graphs to the left are EC and corrected HPT pressure.**  
 512 **The third graph is the hydraulic head for the MiHPT log (H23), well W06 (black) and well**  
 513 **W20 (blue), where the vertical line indicates screen placement and length. The blue triangles**  
 514 **are the dissipation test used to estimate the vertical hydraulic gradient. The bore logs of the**  
 515 **wells are shown to the right. The illustration shows the results for sand lens unit number 1**  
 516 **(see Figure 2).**



517

518 **Figure S2: Illustration of the parameters used to estimate the vertical hydraulic gradient for**  
 519 **the MiHPT log and two wells. The two graphs to the left are EC and corrected HPT pressure.**  
 520 **The third graph is the hydraulic head for the MiHPT log (H22), well W06 (black) and well**  
 521 **W20 (blue), where the vertical line indicates screen placement and length. The blue triangles**  
 522 **are the dissipation test used to estimate the vertical hydraulic gradient. The bore logs of the**  
 523 **wells are shown to the right. The illustration shows the results for sand lens unit number 1**  
 524 **(see Figure 2).**

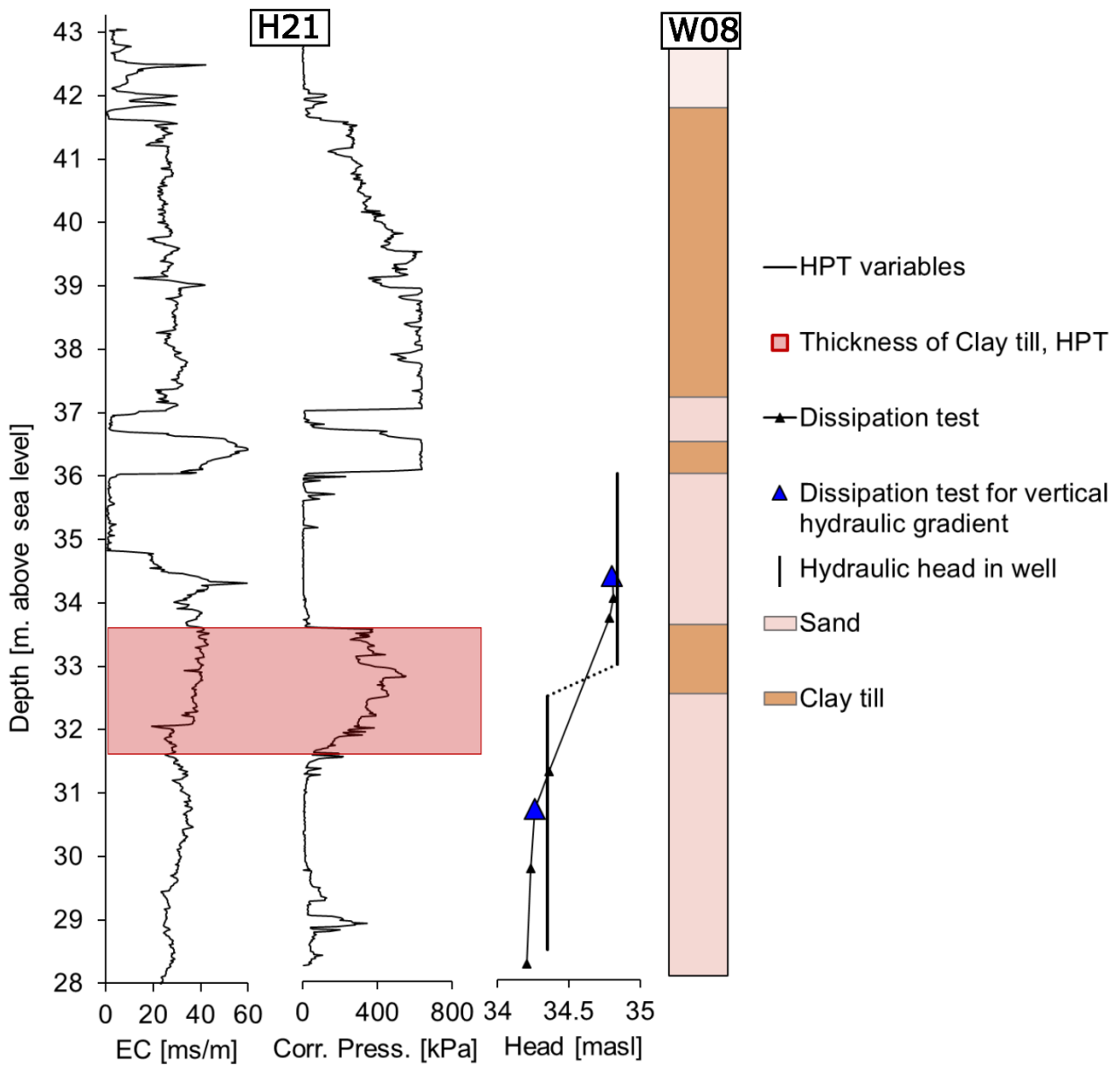


525

526 **Figure S3: Illustration of the parameters used to estimate the vertical hydraulic gradient for**  
 527 **the MiHPT log and two wells. The two graphs to the left are EC and corrected HPT pressure.**  
 528 **The third graph is the hydraulic head for the MiHPT log (H25), well W06 (black) and well**  
 529 **W20 (blue), where the vertical line indicates screen placement and length. The blue triangles**  
 530 **are the dissipation test used to estimate the vertical hydraulic gradient. The bore logs of the**  
 531 **wells are shown to the right. The illustration shows the results for sand lens unit number 1**  
 532 **(see Figure 2).**

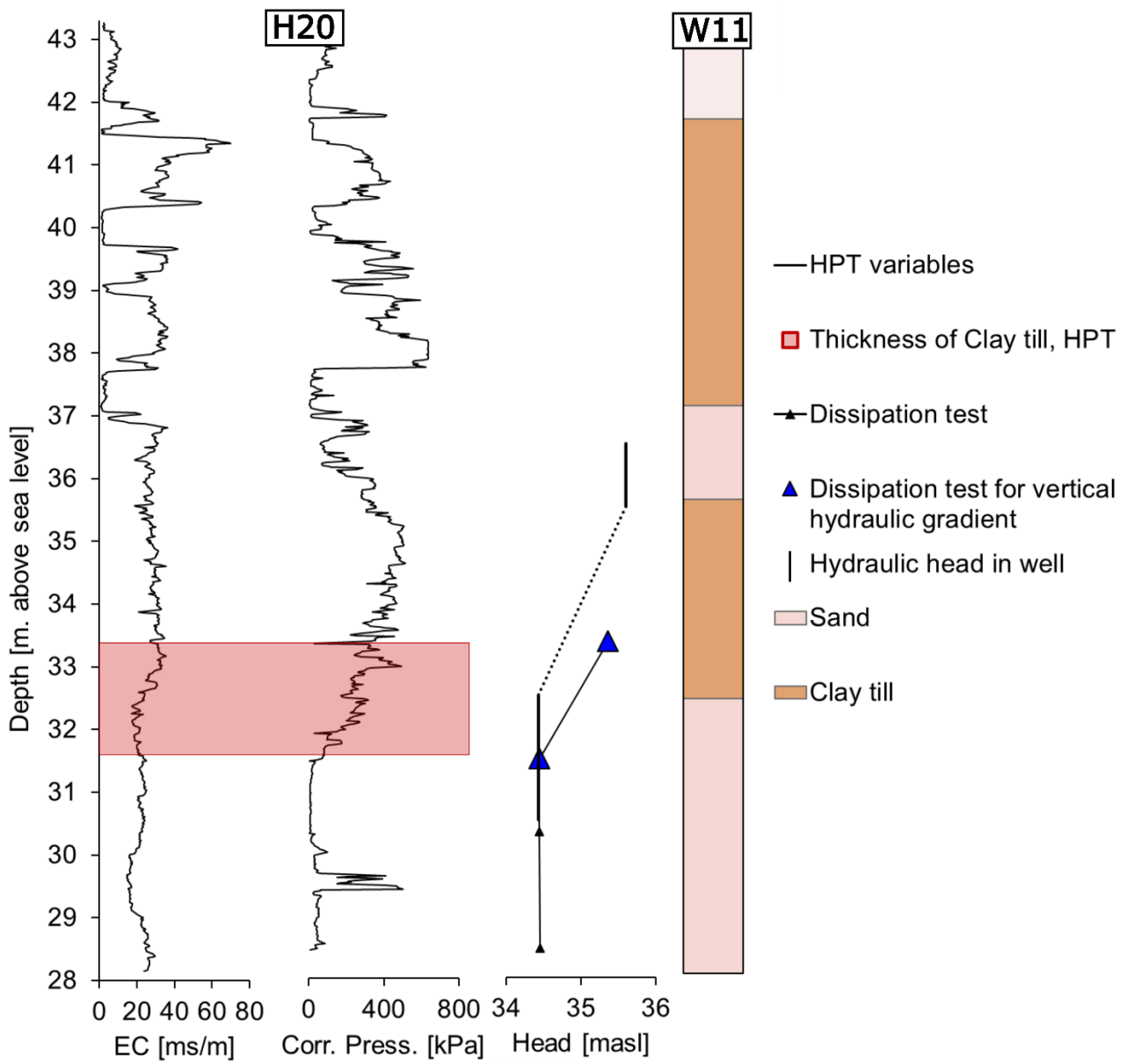
533





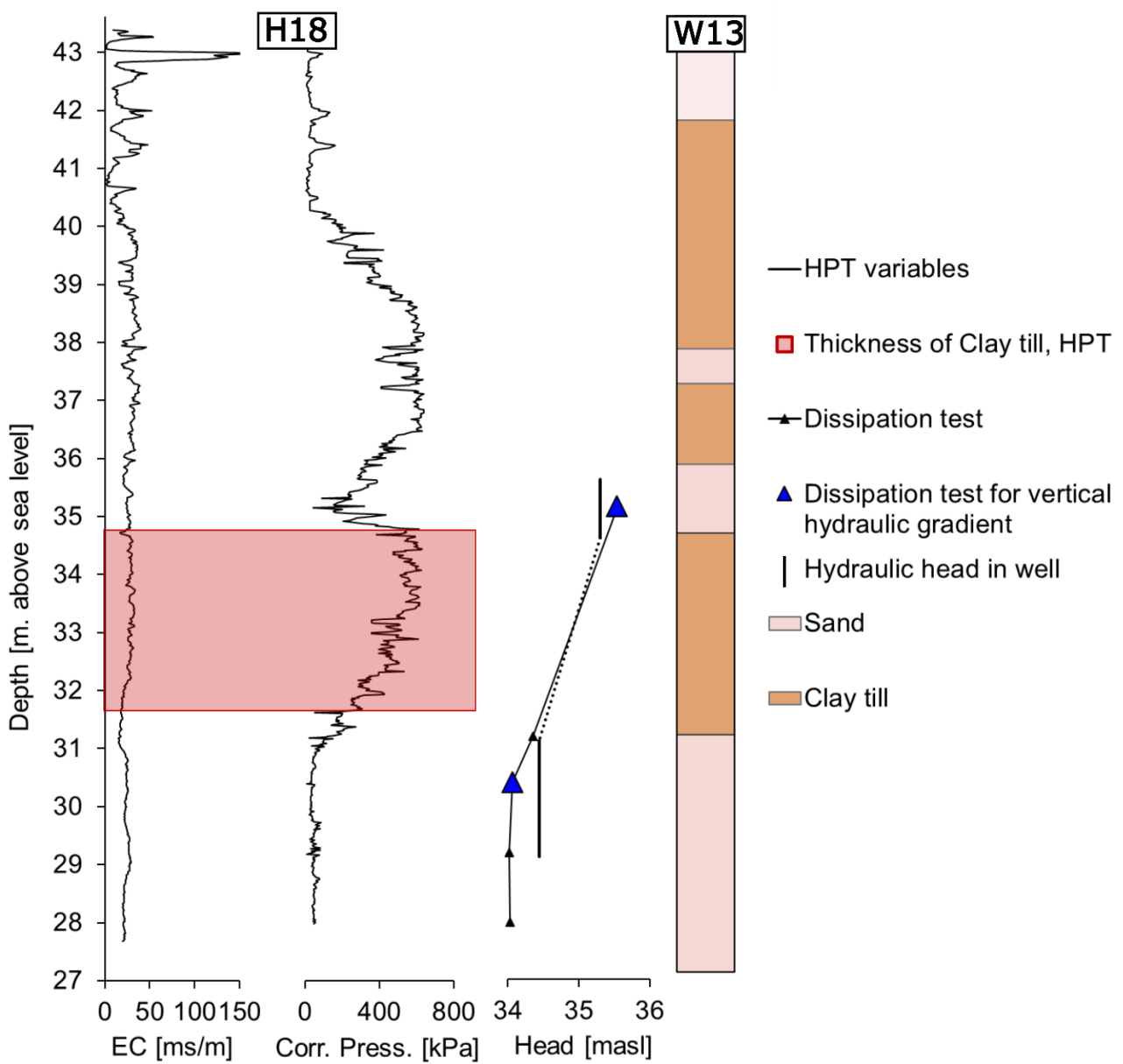
535

536 **Figure S4: Illustration of the parameters used to estimate the vertical hydraulic gradient for**  
 537 **the MiHPT log and well. The two graphs to the left are EC and corrected HPT pressure. The**  
 538 **third graph is the hydraulic head for the MiHPT log (H21) and well W08, where the vertical**  
 539 **line indicates screen placement and length. The blue triangles are the dissipation test used to**  
 540 **estimate the vertical hydraulic gradient. The bore log of the well is shown to the right. The**  
 541 **illustration shows the results for sand lens unit number 2 (see Figure 2).**



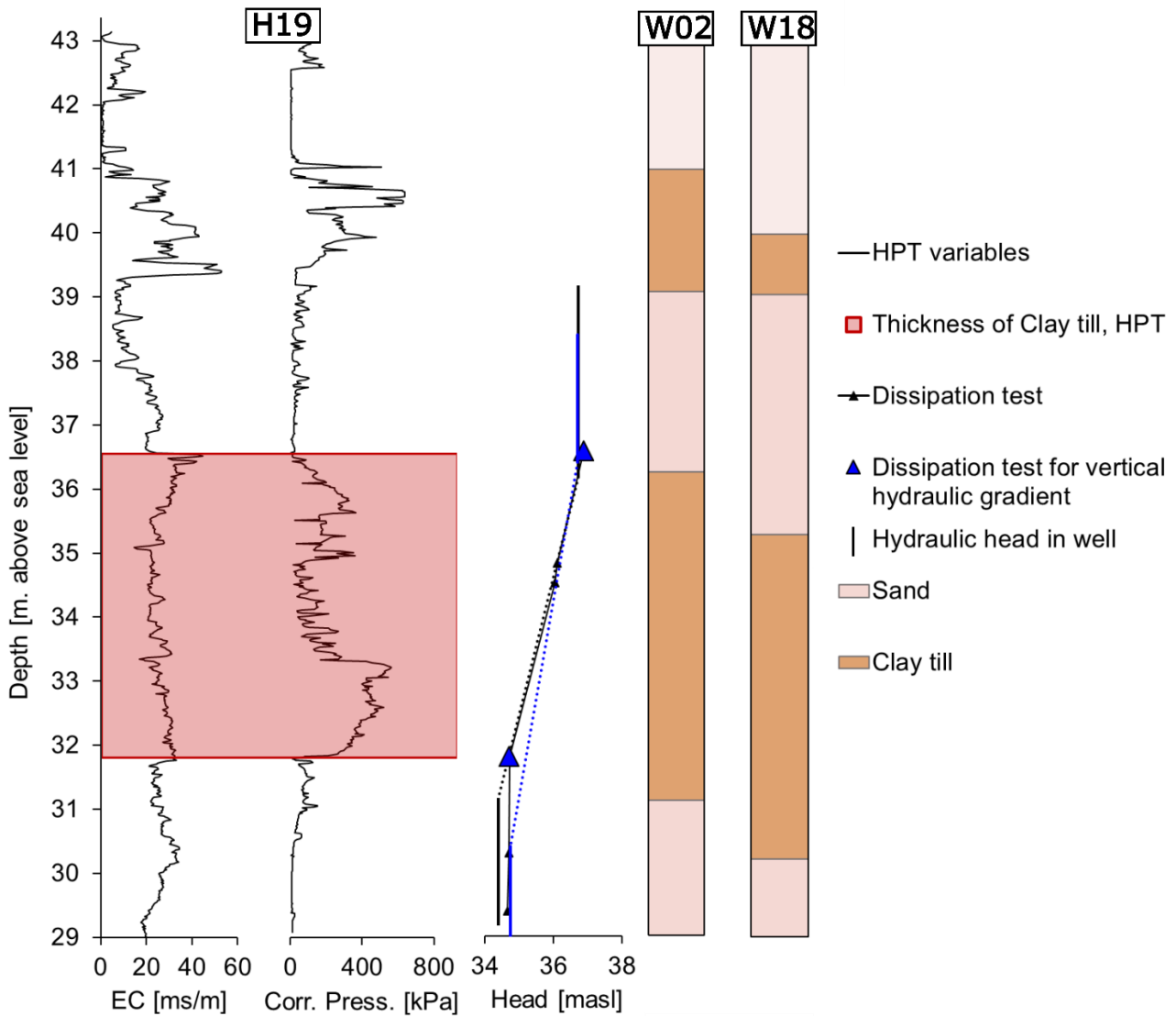
543

544 **Figure S5: Illustration of the parameters used to estimate the vertical hydraulic gradient for**  
 545 **the MiHPT log and well. The two graphs to the left are EC and corrected HPT pressure. The**  
 546 **third graph is the hydraulic head for the MiHPT log (H20) and well W11, where the vertical**  
 547 **line indicates screen placement and length. The blue triangles are the dissipation test used to**  
 548 **estimate the vertical hydraulic gradient. The bore log of the well is shown to the right. The**  
 549 **illustration shows the results for sand lens unit number 3 (see Figure 2).**



551

552 **Figure S6: Illustration of the parameters used to estimate the vertical hydraulic gradient for**  
 553 **the MiHPT log and well. The two graphs to the left are EC and corrected HPT pressure. The**  
 554 **third graph is the hydraulic head for the MiHPT log (H18) and well W13, where the vertical**  
 555 **line indicates screen placement and length. The blue triangles are the dissipation test used to**  
 556 **estimate the vertical hydraulic gradient. The bore log of the well is shown to the right. The**  
 557 **illustration shows the results for sand lens unit number 4 (see Figure 2).**



559

560 **Figure S7: Illustration of the parameters used to estimate the vertical hydraulic gradient for**  
 561 **the MiHPT log and two wells. The two graphs to the left are EC and corrected HPT pressure.**  
 562 **The third graph is the hydraulic head for the MiHPT log (H19), well W02 (black) and well**  
 563 **W18 (blue), where the vertical line indicates screen placement and length. The blue triangles**  
 564 **are the dissipation test used to estimate the vertical hydraulic gradient. The bore logs of the**  
 565 **wells are shown to the right. The illustration shows the results for sand lens unit number 5**  
 566 **(see Figure 2).**



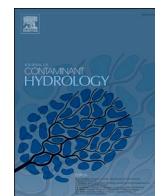


# II

## A Novel Concept for Estimating the Contaminant Mass Discharge of Chlorinated Ethenes Emanating from Clay till Sites

Louise Rosenberg, Klaus Mosthaf, Mette M. Broholm, Annika S. Fjordbøge, Nina Tuxen, Ida Henriette Kern-Jespersen, Vinni K. Rønde, Poul L. Bjerg

Journal of Contaminant Hydrology  
Vol. 252, pp. 1-10, 2023



## A novel concept for estimating the contaminant mass discharge of chlorinated ethenes emanating from clay till sites

Louise Rosenberg<sup>a,\*</sup>, Klaus Mosthaf<sup>a</sup>, Mette M. Broholm<sup>a</sup>, Annika S. Fjordbøge<sup>a</sup>, Nina Tuxen<sup>b</sup>, Ida Henriette Kerrn-Jespersen<sup>b</sup>, Vinni Rønde<sup>b</sup>, Poul L. Bjerg<sup>a</sup>

<sup>a</sup> Technical University of Denmark, Department of Environmental and Resource Engineering, Bygningstorvet 115, 2800 Kgs. Lyngby, Denmark

<sup>b</sup> Capital Region of Denmark, Kongens Vænge 2, 3400 Hillerød, Denmark

### ARTICLE INFO

#### Keywords:

Contaminant flux  
Depth-discrete concentration profiles  
Contaminant plume  
Risk assessment  
Groundwater solute transport model

### ABSTRACT

Interest in using contaminant mass discharge (CMD) for risk assessment of contaminated sites has increased over the years, as it accounts for the contaminant mass that is moving and posing a risk to water resources and receptors. The most common investigation of CMD involves a transect of multilevel wells; however, this is an expensive undertaking, and it is difficult to place it in the right position in a plume. Additionally, infrastructure at the site needs to be considered. To derive an initial CMD estimate at a contaminated site and to allow for the prioritization of further investigations and remedial actions, the ProfileFlux method has been developed. It is targeted at former industrial sites with a source zone in a low conductivity layer with primarily vertical flow overlying an aquifer with primarily horizontal groundwater flow. The ProfileFlux method was developed for mature chlorinated solvent plumes, typically originating from more than 30 to 50-year-old spills, as the usage of chlorinated solvents is mainly historical. Thus, it is assumed that the contaminant had time to distribute in the low conductivity layer by mainly diffusive processes. Today the contamination is continuously released to the underlying aquifer, where advection and dispersive (other than diffusive) processes are of higher importance. The approach combines high-resolution, depth-discrete vertical concentration profiles and a simple 2D flow and transport model to estimate CMD by comparing measured and simulated concentration profiles in the aquifer. The study presented herein includes a global sensitivity analysis, in order to identify crucial field parameters, and of particular importance in this regard are source length, groundwater flux and infiltration. The ProfileFlux method was tested at a well-examined industrial site primarily contaminated with trichloroethylene, thereby allowing a comparison between CMD from the ProfileFlux method and the traditional transect method. CMD was estimated at 117–170 g/year, when using the ProfileFlux method, against 143 g/year with the transect method, thus validating ProfileFlux method's ability to estimate CMD. In addition, applying the method identified weak points in the conceptual site model. The method will be incorporated into a user-friendly online tool directed at environmental consultants and decision-makers working on the risk assessment and prioritization of contaminated sites with the specific hydrogeological conditions of an aquifer with an overlying low permeability layer.

### 1. Introduction

Due to modern society's previous usage of chemicals, such as chlorinated solvents, petroleum hydrocarbons, per-/polyfluoroalkyl substances and pesticides, contaminated sites abound worldwide. Often, contamination is located in low permeability layers overlying aquifers (Falta, 2005; Chambon et al., 2010, 2011; Filippini et al., 2020), where contaminants can be stored and released over a long period of time. The migration of dissolved contaminants from these sites into underlying

aquifers poses a risk to groundwater systems and drinking water resources and ultimately human and environmental receptors. When risk assessing contaminated sites, contaminant mass discharge (CMD) can be used to evaluate the risk to receptors downgradient of a source and to prioritize the need to remediate different contaminated sites (Einarson and Mackay, 2001; Trolborg et al., 2008; Newell et al., 2011; Einarson, 2017; Rønde et al., 2017). Furthermore, it is used to evaluate source zone remediation and natural plume attenuation (Kao and Wang, 2001; National Research Council, 2005; Brooks et al., 2008; Fraser et al., 2008;

\* Corresponding author.

E-mail address: [lour@dtu.dk](mailto:lour@dtu.dk) (L. Rosenberg).

<https://doi.org/10.1016/j.jconhyd.2022.104121>

Received 30 August 2022; Received in revised form 24 October 2022; Accepted 28 November 2022

Available online 2 December 2022

0169-7722/© 2022 The Authors. Published by Elsevier B.V. This is an open access article under the CC BY license (<http://creativecommons.org/licenses/by/4.0/>).



Fjordbøge et al., 2012; Horneman et al., 2017). Although CMD provides an integrated flow and contaminant concentration response, which enables a risk-based assessment of the impact on water resources, most practitioners and decision-makers still adhere to generic concentration-based water quality standards at a given point downgradient of a source. Horst et al. (2021) listed three main factors explaining why the CMD approach is not fully incorporated into contaminated site risk assessments: 1) a lack of technical adeptness by practitioners, 2) the need to develop robust CMD assessments and 3) a lack of alignment regarding compliance metrics when using CMD.

CMD describes the mass of a contaminant transported through a control plane per unit of time. CMD is most commonly evaluated in a vertical control plane perpendicular to the groundwater flow direction in an aquifer downgradient of a source zone (e.g. Newell et al., 2011; Verreydt et al., 2012). In the control plane, point measurements covering the width and depth of the plume are often collected by using multiple sampling points over depth (traditional wells or multilevel samplers) (e.g. Kao and Wang, 2001; Freitas et al., 2011; Troldborg et al., 2012), albeit passive flux meters (PFMs) have also been developed and applied in this regard (e.g. Annable et al., 2005; Verreydt et al., 2011; Ottosen et al., 2020). Both methods require many measurement points to ensure adequate sample density and to minimize uncertainty in the CMD estimate (Li and Abriola, 2009; Troldborg et al., 2010, 2012; Brooks et al., 2015; Balbarini et al., 2018). Furthermore, the placement of a transect is difficult, as it should be neither too close nor too far away from the source zone, and so it often takes several attempts to achieve a proper transect for CMD determination. Hence, it can be an expensive metric to evaluate, and we therefore need faster and cheaper methods for an initial estimate of the CMD in order to evaluate and prioritize further investigation or remediation of contaminated sites at an early stage.

Field investigations and risk assessments in heterogeneous glacial sediments such as clay till have proven particularly difficult due to the existence of fractures, fissures and sand lenses which can potentially create preferential transport paths (Kessler et al., 2012). Furthermore, the matrix can store contaminants and act as a secondary source through back-diffusion (Falta, 2005; Chambon et al., 2010). Chambon et al. (2011) and Locatelli et al. (2019) have developed risk assessment models describing the vertical transport of dissolved contaminants through clay till, coupled with horizontal transport in the underlying aquifer. The focus of both models is on dissolved contaminant concentration in the aquifer, and they do not focus on CMD. For these heterogeneous geological settings and/or complex contaminant plumes, the high-resolution, depth-discrete characterization of both hydraulic properties and contaminant concentrations is important in order to improve our understanding of the key processes driving the CMD and to refine our conceptual site models (e.g. Suthersan et al., 2016; Steelman et al., 2020).

Coupling field site investigations with transport models is a valuable practice, as it helps to understand contaminant transport better. Essouayed et al. (2021) presented a method for an iterative source localization strategy at a chlorinated solvent site that merged field site measurements and 2D modeling, as well as used the results to improve the conceptual site model. However, this was done in a sandy aquifer with a focus on locating the source zone at a contaminated site and did not include depth-discrete sampling or the estimation of CMD. Thus, we see a need – as requested by Horst et al. (2021) – for new and robust methods for assessing CMD emanating from clay till sites, which can be adapted by practitioners using existing field techniques. The transect method is already used to evaluate CMD and is applied at many sites. However, as discussed it is an expensive method, and it is often difficult to get the placement of the wells correct and can take several field campaigns to fully delineate the plume and estimate the CMD.

With this in mind, we present a novel concept herein, namely the ProfileFlux method, to estimate the CMD of dissolved contaminants from a point source located in a low permeability layer into an

underlying aquifer without utilizing a traditional control plane of multiple expensive and permanently installed sampling points over depth. The estimate is done using knowledge of the source zone, the flow field and high-resolution, depth-discrete concentration profiles in the aquifer along the plume center line. This is coupled with a 2D solute transport model developed specifically for sources located in clay till settings. Comparing field site measurements with contamination simulations allows for a better understanding of contaminant migration and the conceptual site model. A CMD estimate is achievable with less intensive data collection than the traditional transect method and can indicate whether a traditional transect method estimation needs to be done. This paper aims to (1) present the approach and prerequisites of the CMD estimation method, (2) identify governing parameters via a global sensitivity analysis using a 2D solute transport model, and (3) apply the approach at a field site, including a discussion of the water balance and inferred updates of the conceptual site model.

The work is developed and tested on a typical Danish industrial site contaminated with trichloroethylene (TCE) located in clay till settings overlying a sandy aquifer in order to create a risk assessment tool that can be used for contaminated sites located in similar settings.

## 2. Conceptual model and the ProfileFlux method

The ProfileFlux method has been developed for geological settings where chlorinated solvents emanate from a low permeability clay till unit into a high permeability aquifer (e.g. sand or gravel) located below. The main idea is that high-resolution, depth-discrete concentration profiles are the footprints of site-specific parameters such as flow system, contaminant source strength and length and the actual CMD from the source zone (McNab et al., 2000). The ProfileFlux method comprises the following three steps:

- 1) Initial site investigations to characterize the contaminated site in terms of the approximate extent of the source zone, contaminant concentration in clay till, flow direction and hydraulic properties of the system (Fig. 1a).
- 2) An investigation into contaminants in the aquifer, where high-resolution, depth-discrete concentration profiles are gathered along the center line of the plume, both from within the source zone and at different distances downgradient thereof (Fig. 1b).
- 3) A comparison between measured and simulated concentration profiles in order to estimate CMD. A 2D solute transport model is used to simulate these concentration profiles by adjusting site-specific parameters within a given range until a good agreement between the simulated and measured profiles is achieved (Fig. 1c).

The infiltration through and downgradient the source zone will determine how the plume distributes vertically. Often, the infiltration rate is a difficult parameter to determine in clay till, as vertical hydraulic conductivity defining the actual infiltration is difficult to measure. Combining groundwater flow in the aquifer and the vertical concentration profile leads to a fair estimate of infiltration through clay till, as the former is often known with a relatively high degree of certainty. Thus, through a combination of measured and simulated concentration profiles, we can estimate CMD, update our conceptual site model and refine key parameters. In the following sections, assumptions, field parameters and model descriptions are addressed.

### 2.1. Assumptions for the ProfileFlux method

The ProfileFlux method was developed with simplicity in mind to produce a tool that can be used within the existing field site investigation framework and provide the end-user with an estimate of CMD out of the source zone and within the aquifer at a given distance from the source as an alternative a complement to the more expensive and tedious transect method. The ProfileFlux method is directed toward

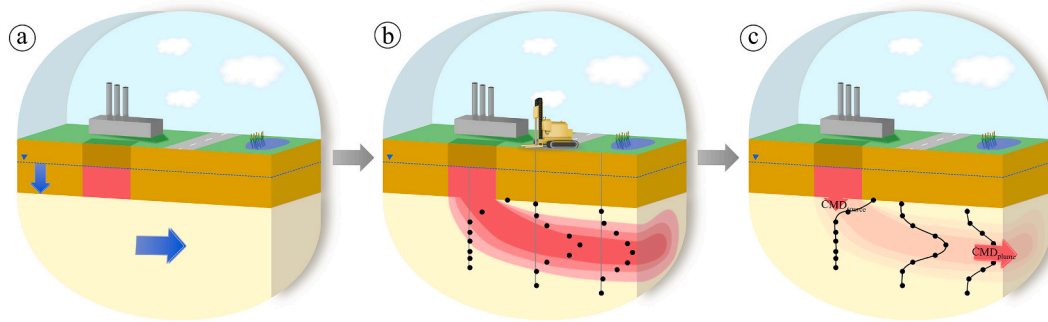


**Fig. 1.** Conceptual setup of the method: (a) Step 1, initial site investigation with approximate position of the source zone, vertical and horizontal water fluxes. (b) Step 2, contaminant investigation with high-resolution, depth-discrete concentration profiles gathered at different locations within and downgradient of the source. (c) Step 3, contaminant transport is simulated by a 2D transport model, and the measured and simulated contaminant profiles are compared and optimized.

legacy sites contaminated with chlorinated solvents, which in many parts of the world originate from the 1940s to the 1980s (McGuire et al., 2004; Sale et al., 2008). Thus, they are more than 40 years old and represent mature secondary sources, where non-aqueous phase solvents have been depleted by dissolution and the chlorinated compounds already distributed by diffusive processes and stored in the clay till matrix (Parker et al., 2008). Such source zones in clay till overlying aquifers are relevant for many sites in Northern Europe and North America (e.g. Hønning et al., 2007; Damgaard et al., 2013a, 2013b).

McGuire et al. (2004) examined 191 chlorinated solvent sites and found that most (90%) of the plumes were stable. Sale et al. (2008) suggested using a 14-compartment model to evaluate the contaminant distribution of chlorinated solvents in four different phases, in both the source zone and the plume. The four phases are dense non-aqueous phase liquid (DNAPL), vapour, aqueous and sorbed. The importance of each phase varies with the geological setting and time since the spill. For sources located in low permeability layers and in the middle to late stage of their life span, the stored mass in the matrix is the predominant source of contamination to the transmissive zone (ESTCP, 2011), as little to no DNAPL is present (Chapman and Parker, 2005). During the development of the ProfileFlux method, the aim was to get an initial robust estimate of CMD from the source and within the plume, which resulted in focusing on the saturated zone to keep the method simple. The ProfileFlux method therefore only takes dissolved and sorbed contaminants into consideration. Furthermore, degradation is disregarded in the model; however, if reductive dechlorination products are observed at a site, the sum of chlorinated compounds on a molar basis can be used as an input for step 3 (Chambon et al., 2013).

As reported by Kessler et al. (2012), fractures in clay till can act as a preferential transport pathway causing a faster breakthrough of contaminants to an underlying aquifer. However, a study of clay till at eight sites in Denmark and one in Canada showed that the fracture aperture often decreases with depth, with a clear change at a depth of 3 m below the ground surface (m bgs) (Klint et al., 2013; Aamand et al., 2022). The same study found that for 32 different locations, fracture spacing increased with depth from around 3 m bgs. Smaller fracture apertures and fewer fractures will result in a smaller impact on contaminant transport through clay till (Falta, 2005). When reaching clay till deeper than approximately 3 m bgs, the importance of these fractures on water flow decreases, and so they are not considered in the ProfileFlux method, and both clay till and the aquifer are assumed to act like a porous medium, therefore not accounting for fractures in clay till.

## 2.2. Required site characterization

Site-specific parameters are essential for the reliable simulation of the vertical concentration profile – and, ultimately, a credible estimate of CMD with the ProfileFlux method. This section addresses the required

field site parameters, which can be determined within the framework of a typical site investigation.

Relevant input and output parameters for the ProfileFlux method are shown in Fig. 2 and listed in Table 1. Parameters that are field site-specific and typically determined in investigations at contaminated sites are assigned a “Yes” in the “Field” column in Table 1. Other parameters are considered less site-specific and/or need elaborate field methods like tracer experiments to be determined. These are assigned a “No” in the “Field” column. In the following, typically measured field parameters are described.

Site investigation methods are diverse, and most of the input parameters can be determined using different field equipment/techniques. For initial site investigations (step 1), traditional screened wells will most likely be available. Borehole logs from these wells are useful in determining geology at the site and the thickness of clay till. Furthermore, properly constructed and screened wells can provide information on the flow field in the system by allowing measurements of the hydraulic head in both clay till and the aquifer. Devlin and Schillig (2017) presented an Excel spreadsheet for estimating groundwater flow direction and the head gradient, both of which are relevant for site investigations. Slug tests or other hydraulic test methods can be performed to determine hydraulic conductivity in the aquifer. Also, if hydraulic properties from prior investigations or models in the area are known beforehand, they can be considered. Soil concentrations should be measured to determine the amount of contaminant at the site and to delineate the source zone. The soil concentration can be converted into solute concentration using the sorption coefficient,  $k_d$ .

For unconsolidated settings such as clay till and sandy aquifers, direct-push methods are valuable, as they provide different depth-discrete information (McCall et al., 2014). For instance, using a membrane interface probe hydraulic profiling tool (MiHPT) is beneficial for investigating contaminated clay till and the transition zone into the aquifer. It provides a depth-discrete, qualitative signal of contaminant distribution for source zone delineation, along with an estimate of the permeability of the subsurface, for a more detailed determination of clay till thickness than offered by initial borehole logs. An MiHPT is also useful for examining the vertical hydraulic gradient at the site – as described in Rosenberg et al. (2022).

The ProfileFlux method relies on the use of high-resolution, depth-discrete concentration profiles (screen length of around 10 cm with a vertical spacing of 0.5–1 m) in the aquifer (step 2). Several multilevel sampling methods are available (Tuxen et al., 2006; Anneser et al., 2008), and Broholm et al. (2016) reviewed a range of commercially available devices. A new device, not mentioned in Broholm et al. (2016), is the groundwater profiler system (GWP) from GeoProbe®, namely a direct-push method that samples groundwater from high permeability settings through the use of a syringe pump or bladder pump. 20 sample ports are distributed on four sides of the probe, resulting in a screen

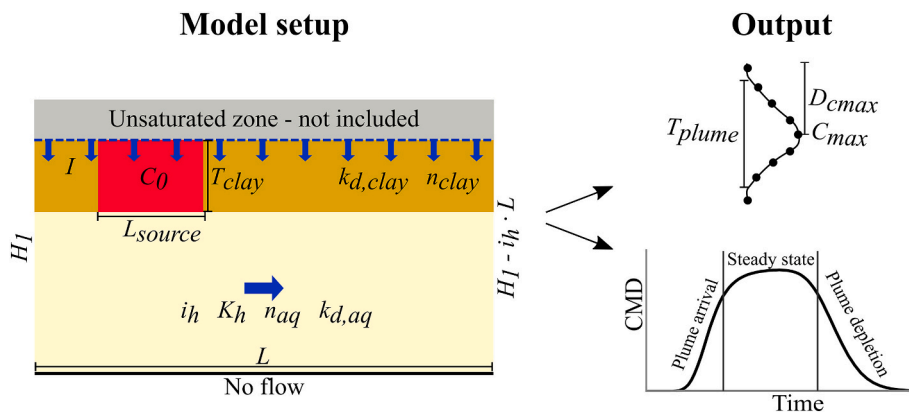


Fig. 2. Model setup with the parameters needed for the 2D transport model. Output from the model is both a simulated concentration profile and a breakthrough curve in the aquifer at a chosen distance downgradient from the source. The simulated concentration profile has three important features, i.e. plume thickness ( $T_{plume}$ ), maximum concentration ( $C_{max}$ ) and depth from the bottom of the clay till layer to  $C_{max}$  ( $D_{cmax}$ ). The first part of the breakthrough curve describes the CMD incline, as the contaminant moves from the source zone into and through the aquifer. The plateau part of the curve occurs when the model reaches a steady state at the maximum estimated CMD. The third part describes the decline of CMD in the aquifer. The ideal time for the ProfileFlux method is the second part, i.e. the steady state.

length of around 10 cm (Dutta et al., 2021). All devices benefit from prior knowledge of contaminant levels at depth, in order to select appropriate target depths for groundwater sampling, and the MiHPT is very useful in this regard as well as evaluating sampling depths with suitable permeability. When undertaking depth-discrete groundwater sampling, it is important to define concentrations that delineate the entire thickness of the plume and locate maximum concentrations. Furthermore, to make the most reliable estimate of CMD, one should target the expected center line of the contaminant plume, based on overall groundwater flow direction. MiHPT can support the decision on the placement of the depth-discrete groundwater samples and sampling across the expected centerline is advised in order to make sure that the center line has been found. Missing or deviating from the center line, in particular for narrow sources, will result in an underestimation of the

Table 1

Input parameters for the ProfileFlux method. Some parameters are field site-specific (marked as “Yes” in the “Field” column). All parameters have been given a suggested range of values to use for Danish conditions. Parameters marked with an x in the GSA column are used for a global sensitivity analysis.

Parameter	Symbol	Field	Suggested value range	GSA
<b>Source</b>				
Source concentration	$C_0$	Yes	0.1–10 mg/L*	x
Source length	$L_s$	Yes	5–40 m	x
<b>Clay till</b>				
Infiltration rate	$I$	No	30–300 mm/year	x
Vertical head gradient	$i_v$	Yes	0.1–1	
Vertical conductivity	$K_v$	No	$10^{-6} - 10^{-10}$ m/s	
Anisotropy	$K_v/K_h$	No	0.15	
	$clay$			
Porosity	$n_{clay}$	No	0.2–0.4	x
Longitudinal dispersivity	$\alpha_{l,clay}$	No	0.1 m <sup>a</sup>	
Vertical dispersivity	$\alpha_{v,clay}$	No	0.002 m <sup>a</sup>	
Thickness	$T_{clay}$	Yes	4–10 m	x
Sorption coefficient	$k_{d,clay}$	No	0–2 L/kg <sup>b</sup>	x
<b>Aquifer</b>				
Horizontal head gradient	$i_h$	Yes	0.8–5 ‰	x
Horizontal conductivity	$K_h$	Yes	$5 \cdot 10^{-6} - 1 \cdot 10^{-4}$ m/s	x
Anisotropy	$K_v/K_h, aq$	No	0.15	
Porosity	$n_{aq}$	No	0.2–0.4	x
Longitudinal dispersivity	$\alpha_{l,aq}$	No	0.1–1 m <sup>c</sup>	x
Vertical dispersivity	$\alpha_{v,aq}$	No	0.005–0.02 m <sup>c</sup>	x
Sorption coefficient	$k_{d,aq}$	No	0–0.5 L/kg <sup>b</sup>	x
Vertical concentration profiles		Yes		

\* With a  $k_{d,clay}$  of 1 L/kg, this range equals to 0.1–10 mg/kg.

<sup>a</sup> Modified from Mosthaf et al. (2021) to be ten times higher, due to a larger scale than their study.

<sup>b</sup> Lu et al. (2011).

<sup>c</sup> Chiang et al. (1989); Robertson et al. (1991); Rivett et al. (1994); Mallants et al. (2000); Schulze-Makuch (2005); Rotaru et al. (2014); Locatelli et al. (2019).

CMD (see section 4.2).

### 2.3. Flow and solute transport model

Modeling of the transport of chlorinated solvents through clay till and further downgradient in the aquifer is performed by a classic, transient 2D flow and solute transport model with a simplified setup (Mosthaf et al., 2021). The 2D model domain comprises a clay till layer and an aquifer (see Fig. 2). Mainly vertical flow and transport through the source area and the clay till are combined with the groundwater flow and transport in the aquifer. Thereby flow and solute transport are simulated in a vertical cross-section in the main groundwater flow direction, ideally through the center line of the plume. The model domain is extended beyond the source zone and the interval of interest covering the area of interest of the plume in order to reduce the influence of the constant head boundary, which would otherwise impede vertical flows in the vicinity, on the local flow field. A steady-state flow is assumed and described by Darcy’s law and the mass balance as:

$$\nabla \cdot (-\mathbf{K} \nabla h) = 0$$

with the hydraulic conductivity tensor  $\mathbf{K}$  and the hydraulic head  $h$  as the primary variable. Constant infiltration is applied at the top boundary, and no-flow is assumed through the bottom boundary. The hydraulic heads on the left and right boundaries are fixed, thus creating the overall horizontal hydraulic gradient in the aquifer. In the clay till overlying the aquifer, advective transport is mainly vertical and driven by infiltrating water, whereas, in the underlying sandy aquifer, the advective transport is predominantly horizontal.

Contaminant transport is described by the time-dependent advection-dispersion equation, which can account for sorption:

$$\phi R \frac{\partial c}{\partial t} + \nabla \cdot (\phi c \mathbf{v}) - \nabla \cdot (\phi \mathbf{D}_{eff} \nabla c) = q$$

with porosity  $\phi$ , concentration  $c$  (primary variable), retardation factor  $R$ , seepage velocity  $\mathbf{v}$ , effective hydrodynamic dispersion tensor  $\mathbf{D}_{eff}$  (mechanical dispersion and molecular diffusion) and sources/sinks  $q$ .

All boundaries in the transport domain are set to no-flow conditions. The contaminant source is implemented as a rectangular area with an initially uniform concentration of dissolved and sorbed chlorinated compounds covering the saturated clay till, assuming the chlorinated compounds in the mature contaminant source have been distributed in the matrix by diffusive processes, with the length of the determined source zone. All other areas are initially set to a concentration of 0, i.e. the simulation starts when contamination reaches the aquifer.

The model was implemented in COMSOL Multiphysics v6.0, which has been benchmarked with more complex setups against analytical solutions, experimental data, and other modeling tools (e.g. Chambon et al., 2010; Jørgensen et al., 2019). The model simulates both vertical

and horizontal transport and creates vertical concentration profiles downgradient of the source zone, which can then be compared to measured concentration profiles. Input parameters can be adjusted until good accordance between measured and simulated profiles is obtained, thus yielding CMD per meter width in the model. CMD is multiplied by the approximate width of the source zone, in order to make a final estimate of CMD at the investigated field site. As the transport model is transient, the approximate time when the spill happened should be known. Part of the modeling result is a breakthrough curve at the distance of the respective concentration profile, thereby allowing for evaluating whether contaminant leaching at the field site is in a stable situation/pseudo steady state (plateau part of breakthrough curve in Fig. 2).

The development of the 2D model approach was based on a comprehensive study at a field site, where a detailed 3D model was set up to simulate chlorinated solvent contamination emanating from clay till into a sandy aquifer. This was simplified to the 2D model described above. Comparisons of the 2D model's results with the 3D model's results showed a good agreement, with the main difference caused by transverse dispersion, which is not resolved in the vertical 2D model setup.

#### 2.4. Global sensitivity analysis

When comparing simulated and measured concentration profiles, it is important to identify parameters with a strong impact on the simulated concentration profiles and resulting CMD. For a successful

application of the ProfileFlux method, it is crucial that the most influential parameters on CMD and the depth of the concentration maximum can be easily determined. To identify the most relevant parameters, a global sensitivity analysis (GSA) was conducted. Moreover, the results from the GSA would provide guidance on which field parameter would be further investigated if simulated and measured concentration profiles did not match. The GSA method employed for this study was the Elementary Effects method, proposed by Morris (1991) and refined as suggested by Campolongo et al. (2007). It evaluates how a change in each input parameter affects output through the use of  $\mu^*$  and  $\sigma$ . In this case,  $\mu^*$  is the mean absolute sensitivity of the evaluated output parameter, while the standard deviation,  $\sigma$ , of the sensitivity of a parameter describes uncertainty in these changes (Campolongo et al., 2011).

The input parameters examined in the GSA are marked with an "x" in the "GSA" column in Table 1 along with the investigated parameter range. The examined output parameters are CMD, plume thickness ( $T_{plume}$ ), maximum concentration ( $C_{max}$ ) and depth of the maximum concentration ( $D_{cmax}$ ). The output parameters were evaluated at 50 m downgradient from the source 50 years after the spill had happened. For a thorough description of the GSA, see Supporting Information 1 (SI1).

Fig. 3 presents the results of the GSA analysis for each output parameter. The gray dashed lines mark the first and third quartiles of the resulting values of  $\mu^*$  and  $\sigma$ , and only parameters above the third quartile are shown with a label. The  $\mu^*$  and  $\sigma$  values for all parameters can be found in SI1. When analyzing the results, the most important value is  $\mu^*$ , as it describes the normalized mean impact of each

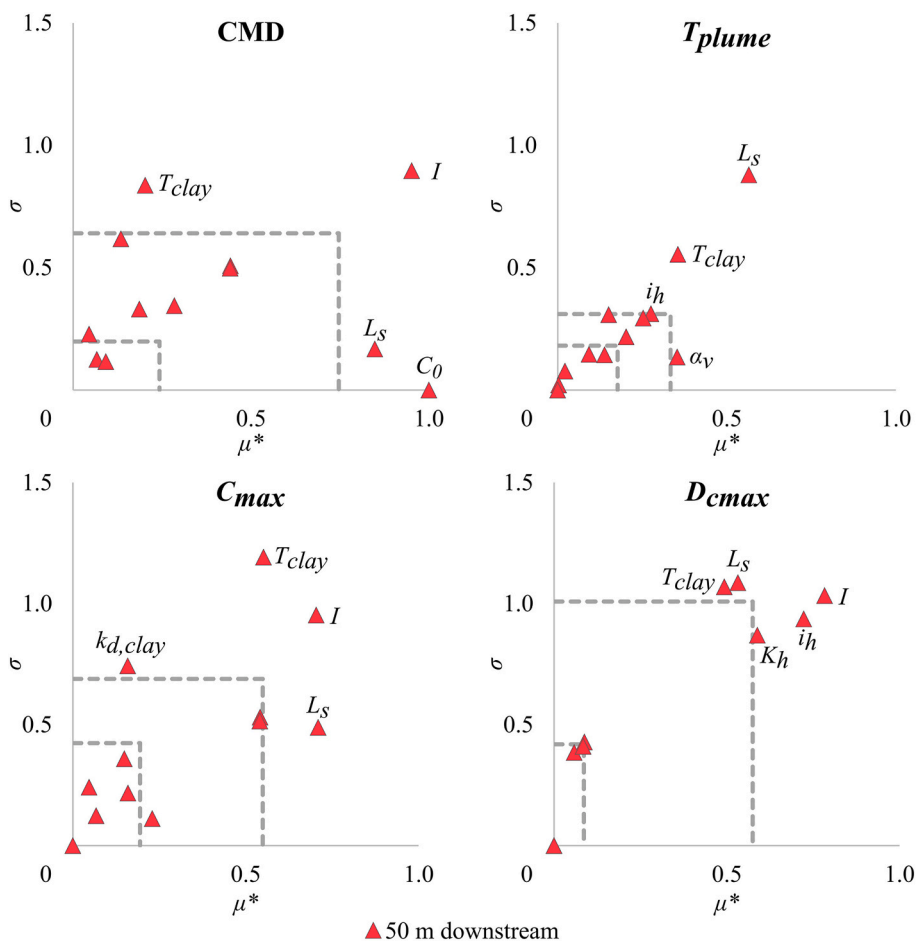


Fig. 3. Results of the GSA with 12 input parameters and four output parameters, 50 years after the spill. The scatter plots describe the relationship between the mean ( $\mu^*$ ) and standard deviation ( $\sigma$ ) of the sensitivity index of each parameter. A low mean means that the parameter does not have a big influence on output, and vice versa. A low standard deviation means that the effect on output does not vary, and vice versa.

parameter on the output, whereas a high  $\sigma$  value indicates non-linear effects or possible interactions with other parameters.

For all four output parameters, the infiltration rate,  $I$ , as well as the source length  $L_s$  (with the exemption of  $T_{plume}$ ), has a significant influence. The depth of the maximum concentration  $D_{cmax}$  is also sensitive to groundwater flow, characterized by  $i_h$  and  $K_h$ . The GSA of CMD shows that the low-sensitivity parameters are the porosities  $n_{clay}$  and  $n_{aq}$ , the distribution coefficient in the aquifer  $k_{d,aq}$  and vertical dispersivity in the aquifer (transverse to the flow direction)  $\alpha_{v,aq}$ . Parameters with a small influence on the vertical concentration profile ( $T_{plume}$ ,  $C_{max}$  and  $D_{cmax}$ ) are  $C_0$ ,  $n_{clay}$ ,  $n_{aq}$ ,  $k_{d,clay}$ ,  $k_{d,aq}$  and  $\alpha_{l,aq}$ , albeit the latter five of these are normally not determined during site investigations. The results of the GSA are discussed further in section 4.1.

### 3. Application of the ProfileFlux method at a chlorinated solvent site

To test the ProfileFlux method, it was applied to a TCE-contaminated site located in Denmark. In 1962, a factory was established to cut and laminate Styrofoam. TCE was used in the production and consequently released to the subsurface. A historical examination has shown that the TCE spill likely happened at some point between 1970 and 1996. The geology at the site consists of clay till, with a varying thickness of 10–12 m, overlying a sandy aquifer. The site is described in Rosenberg et al. (2022), in which a detailed conceptual geological model is provided. In Fig. 4a a plan view of the site is shown, and in Fig. 4b, a simplified longitudinal transect of the saturated part of the site is shown. The source was determined to be 20 m long and 16 m wide, the saturated depth of clay till 5 m, infiltration 140 mm/year and groundwater flow velocity 14 m/year. At the site, the average vertical hydraulic head gradient was 0.4 m/m, resulting in vertical hydraulic conductivity in the clay till of  $1.11 \cdot 10^{-8}$  m/s, which is in the lower range found at other Danish clay till sites (Nilsson et al., 2001; Jørgensen et al., 2002, 2004;

Mosthaf et al., 2021). This indicates that the simulated infiltration rate was in accordance with the field measurement relating to the vertical hydraulic head gradient. Sorption coefficients, which were measured for research purposes and are normally not expected in a typical site investigation, were  $k_{d,clay} = 0.87$  L/kg and  $k_{d,aq} = 0.22$  L/kg. The maximum measured solute concentration in the source was 4900  $\mu\text{g/L}$  TCE; therefore, no free phase DNAPL was expected to be present.

In total, GWPs were performed at seven locations after investigating the vertical extent of groundwater contamination using MiHPT logs. The MiHPT logs identified the approximate center line of the plume using the overall flow field as a starting point for the survey. One of the GWPs was placed at the source area (GWP1 on Fig. 4b), three were placed at different distances along the expected center line of the plume (GWP2–3 and GWP5 on Fig. 4b) and the other three were placed transversal to the groundwater flow direction at the same distance as GWP5 downgradient of the source. There was no indication of any particularly significant reductive dechlorination at the site; however, cis-1,2-dichloroethylene (cis-DCE) was detected in some of the groundwater samples. Therefore, the concentrations used in this example are noted as the sum of chlorinated ethenes (TCE-equivalents, TCE-eq).

Fig. 5 presents a comparison between the measured and simulated concentration profiles. Simulated concentration profiles with three different initial concentrations (1500  $\mu\text{g/L}$ , 2600  $\mu\text{g/L}$  and 3800  $\mu\text{g/L}$ ) are depicted, resulting in an estimated CMD of 67 g/year, 117 g/year and 170 g/year, respectively. The simulated concentration profiles are compared to two of the GWPs along the expected flow center line (GWP3 and GWP5) and GWP6 5 m to the east of GWP5. For both GWP3 and GWP6, the simulated concentration profiles captured the thickness of the measured concentration profile. GWP6 shows a close to Gaussian-shaped concentration profile, with the initial source concentration of 3800  $\mu\text{g/L}$  comparing well with the maximum measured concentration in terms of both depth and value. The simulation of the initial source concentration of 2600  $\mu\text{g/L}$  compares well with measurements at around

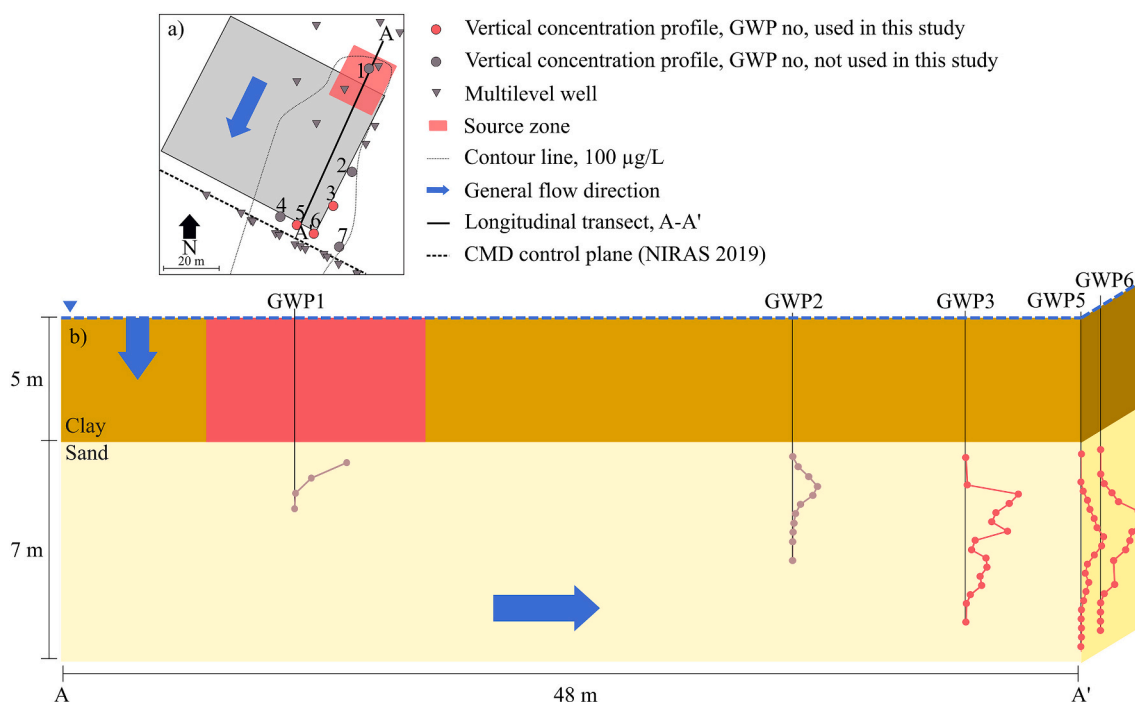
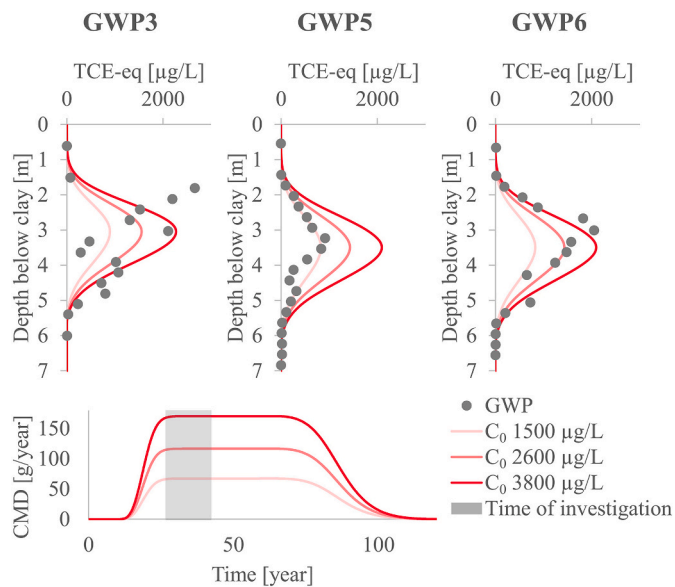


Fig. 4. a) Plan view of the study site with the placement of wells, GWPs, source zone, CMD control plane from NIRAS (2019) and the placement of the expected centerline, referred to as longitudinal transect. b) Longitudinal transect (A-A') showing the simplified geology at the industrial site in the expected center line of the plume. The blue arrows indicate the flow direction. The five graphs show the vertical concentration profiles of the sum of chlorinated ethenes in TCE-equivalents in the source zone, 22 m, 37 m and 48 m downgradient from the source. GWP3, GWP5 and GWP6, which are exemplified in the study, are shown in red, whereas GWP1 and GWP2 are shown in gray as they are not used for the CMD quantification. (For interpretation of the references to colour in this figure legend, the reader is referred to the web version of this article.)



**Fig. 5.** Comparing simulated profiles to the measured profiles at 37 and 48 m downgradient of the contaminant source. Three different source concentrations were applied in the simulation. Furthermore, the breakthrough curves for the three simulations at a distance 48 m downgradient from the source are shown, with the gray box indicating the time interval since the contamination approximately started leaching from the bottom of the saturated clay till (27–40 years). The x-axis on the breakthrough curve is time from the contaminant started leaching from the clay till into the aquifer.

3.5 m below the clay till layer, indicating that CMD at the site is between 117 g/year and 170 g/year. GWP3 showed a more asymmetrical concentration profile, with the maximum concentration not captured by the simulation. However, the simulation did reveal a large proportion of the measured values and the general shape of the concentration profile. Furthermore, the MiHPT at this point showed some heterogeneities in the aquifer when evaluating the MiHPT pressure log. For GWP5, the simulated profile with an initial concentration of 1500 µg/L (67 g/year) compared well with the measured concentration profile relating to the depth and value of the maximum concentration and the thickness of the plume. The resulting CMD, based on the two GWPs in the center line and simulations, was between 117 and 170 g/year, which is in the same range as previously estimated at the site. A consulting company, [NIRAS \(2019\)](#), estimated the CMD to be 143 g TCE/year by using the traditional transverse transect method at 50 m downgradient from the source zone. The plume was delineated and the CMD estimate was based on 26 well screens with individual concentration and hydraulic conductivity measurements. Whilst planning the field campaign, it was expected that GWP5 would be in the center line of the plume, but this was not the case, as GWP6 had higher concentrations and yielded higher CMD from the ProfileFlux method. Furthermore, GWP4 and GWP7 showed significantly lower concentrations, which confirms that the centerline is around the placement of GWP6.

According to historical data relating to the site, and knowledge of the thickness of the unsaturated and saturated zones, the contaminant started leaching from the saturated zone around 27–40 years ago. This is indicated as the gray box on the breakthrough curve in [Fig. 5](#), highlighting that contamination at the site is in a steady state for both the earliest and latest estimates of time. This is also evident from the simulated concentration profiles for GWP3 and GWP6, which reveal the same level of CMD at both 37 and 48 m downgradient of the source – equivalent to approximately 1.5 years' worth of transport in the aquifer.

## 4. Discussion

### 4.1. Robustness and uncertainty of the ProfileFlux method

Parameters with a strong effect on the results of CMD and the vertical concentration profiles ( $T_{plume}$ ,  $C_{max}$  and  $D_{cmax}$ ) were identified in the GSA ([Fig. 3](#)). Most influential parameters are often determined as a part of an initial field investigation at a contaminated site. Critical parameters which are difficult to estimate according to measurements, but which are nevertheless important, are infiltration rate  $I$  through the clay till and vertical dispersivity  $\alpha_{v,aq}$  in the aquifer. However, the unique combination between the infiltration rate in clay till,  $I$ , and the horizontal groundwater flux determines the shape of the vertical concentration profile and the depth of the maximum concentration  $D_{cmax}$ . Hence, a good approximation of the groundwater flux allows for determining infiltration through clay till by adjusting the infiltration rate until a good agreement between the simulated and measured  $D_{cmax}$  is reached. Establishing  $I$  based on the groundwater flux will furthermore lead to a better and more reliable determination of CMD, as  $I$  is the second most sensitive parameter when estimating CMD.

Regarding dispersivities in the aquifer, the vertical dispersivity  $\alpha_{v,aq}$  only affects  $T_{plume}$  significantly, which means that the other two parameters describing the vertical concentration profile ( $C_{max}$  and  $D_{cmax}$ ) can still be determined with reasonable certainty. Furthermore,  $\alpha_{v,aq}$  does not influence CMD estimates and should be kept at a certain low value (in the millimeter scale) based on literature ([Bjerg et al., 2011](#)). A high  $\alpha_{v,aq}$  value will lead to a poor comparison. The longitudinal dispersivity  $\alpha_{L,aq}$  is of minor importance and fairly good values exist from tracer experiments and field observations ([Jensen et al., 1993](#); [Bjerg et al., 2011](#)) and the literature review by [Schulze-Makuch \(2005\)](#).

In general, the least influential parameters are fortunately those requiring laboratory measurements ( $n_{clay}$ ,  $n_{aq}$ ,  $k_{d,clay}$ ,  $k_{d,aq}$ ), which suits the objectives of the ProfileFlux method. The method is developed for initial investigations of CMD at a contaminated site where comprehensive lab work has not been carried out.

From the GSA, the source length  $L_s$  is shown to have a significant impact on the results of both the vertical concentration profiles ( $T_{plume}$ ,  $C_{max}$  and  $D_{cmax}$ ) and the estimated CMD, and it is therefore important to obtain a good estimate of this parameter. In the case of the application at the Danish field site described in section 3,  $L_s$  was determined by using a combination of soil concentrations (above 1 mg TCE/kg soil), solute concentrations from clay till (above 1000 µg TCE/L) and MiHPT logs. When using ProfileFlux, the source zone should be viewed as the place at which the contaminant enters the aquifer. Sand lenses and other heterogeneities in clay till can cause a shift in the placement of the contaminant source at depth ([Kessler, 2012](#)). For this type of investigation, a field method such as MiHPT is useful for establishing the location of chlorinated ethenes.

An important quantity for the ProfileFlux method is the depth from the bottom of the clay till to the groundwater sampling points. At some sites, the transition from clay till to the underlying aquifer is very sharp (i.e. a narrow depth interval), while at other sites the change is gradual over a greater depth interval, resulting in a transition zone between the two geological units. The choice of the location of the bottom of the clay till will have an effect on the comparison between the measured and simulated vertical concentration profiles. When the transition zone has a significant thickness, it is suggested to treat half of it as clay till and the other half as the sandy aquifer when applying field site parameters to the 2D transport model (step 3). With an MiHPT, the transition zone can easily be observed using the pressure log ([Rosenberg et al., 2022](#)).

#### 4.2. Data requirements and field methods

The use of depth-discrete concentration profiles is essential for the ProfileFlux method, and should ideally be sampled along the expected center line of the contaminant plume. In total, four or five vertical concentration profiles with a high resolution (e.g. 50–100 cm intervals, with short screens of around 10 cm) should be made both along and across the center line of the contaminant plume, in order to increase the probability of hitting the center line. This is a critical point as deviations from the center line will reduce the CMD estimates. In particular for narrow sources it is recommended to optimize the position of the concentration profiles by MiHPT measurements across the center line. It should also be noted that the CMD is proportional to the source width and sensitive to the source length as discussed above. Thus, focus on the initial delineation and geometry of the source is recommended in the application of the ProfileFlux method. The vertical concentration profiles, should be performed at a distance away from the source that is in perspective to groundwater flow velocity. This is done by considering the same aspects as for the transect method; time from the spill, clay till thickness and the likelihood of the contaminant plume having reached/ passed the point of interest.

Multiple profiles along the center line of the plume at different distances away from the source zone will allow for evaluating whether the contaminant plume is growing, stable or depleting. From the application at the site presented in section 3, GWP3 and GWP6 (taken along the observed center line of the contaminant plume at distances from the source of 37 and 48 m), showed that the estimated CMD was the same, thereby indicating a stable plume between the two GWPs. The differences between the estimated CMDs based on GWP5 and GWP6 (same downgradient distance) were 67 and 170 g/year, respectively, which is a factor of 2.5 between two points that are 5 m apart. This is based on measured maximum concentrations of 915 and 2049  $\mu\text{g/L}$ , respectively, and shows the importance of more than one sampling point across the center line of the contaminant plume.

Site-specific parameters can be found by using various field methods as described previously. With parameters that most likely will show spatial variations (e.g.  $K_h$  at different locations), it is possible to consider several simulated concentration profiles and to evaluate which value results in the best accordance for all of the measured vertical concentration profiles. Using the comparison between the simulated and measured vertical concentration profiles can add knowledge of the contaminated site as poor accordance indicates knowledge gaps regarding geology, hydrogeology, the contaminant source or plume. Different combinations of infiltration rate and groundwater flux can lead to similar profiles. However, constraining the groundwater flux based on measurements of the hydraulic conductivity and the gradient allows constraining the solutions.

As mentioned previously, comparing the simulated and measured vertical concentration profiles, using the site-specific groundwater flux, allows for evaluating the infiltration rate  $I$ . This acquired value can be compared to the assumed/expected value of  $I$  as well as checked using measurements of  $i_v$  and  $K_v$ . If the resulting values of  $K_v$ ,  $I$  and  $i_v$  are within the expected ranges, the estimate of  $I$  is reasonable. Furthermore, if the simulated and measured vertical concentration profiles only compare well by extensively changing the field site parameters, this can be an indication that further field site investigations are required. This is also the case if these changes result in unrealistic input parameter values, e.g. overly high infiltration rates. This means that applying the ProfileFlux method can contribute to a much better conceptual site model, which is a very strong additional benefit of the approach.

#### 4.3. Can the ProfileFlux method be applied in other geological settings and for other contaminants?

Applying the ProfileFlux method to other geological settings is possible. However, it is important to keep in mind that the model is

made for a source zone located in a low permeability layer with a primarily vertical flow, and the aquifer has considerably higher hydraulic conductivity with a primarily horizontal and stable flow. This combination of a low permeability layer overlying a high permeability aquifer should be present when applying the ProfileFlux method to other geological settings, as a strong difference in hydraulic conductivity is important with regards to the soil type and our understanding of the stable source and plume. Both the low permeability layer and the aquifer should be only moderately heterogeneous, which for the low permeability layer means no significant fractures, and groundwater flow conditions need to be stable.

The method is also applicable to geological settings with fractures in the clay till. For such settings, the model has to be adjusted to account for fracture-matrix interactions e.g. with a discrete fracture-matrix model (Chambon et al., 2010, 2011, Locatelli et al., 2019), in order to include the effects of preferential flow and matrix diffusion on the contaminant leaching out of the source zone.

When the ProfileFlux method is used at chlorinated solvent sites, initial investigations using MiHPT are beneficial, as e.g. the halogen specific XSD detector can detect these. Other volatile contaminants e.g. BTEX/petroleum hydrocarbons can also be detected using MiHPT equipped with a suitable detector. Using MiHPT for initial screening of the contaminant distribution is not possible for non-volatile contaminants such as pesticides; however, the HPT is still valuable for a hydrogeological description of the site. The ProfileFlux method is still applicable for such contaminants, as the source zone and hydrogeological setting have the same effect on the contaminant spreading and the resulting vertical concentration profiles – as in the case of chlorinated ethenes. It should, however, be noted that degradation of the contaminants will affect the vertical concentration profiles as discussed in studies for pesticides (Tuxen et al., 2006) and for BTEX (Anneser et al., 2008).

#### 4.4. Contaminant mass discharge for risk assessment

Risk assessment of contaminated sites has been performed over several decades based on point concentrations and comparisons to maximum contaminant levels (MCLs). Point measurements are highly dependent on the media in which they are taken, as well as where they are placed in the plume (center or edges). In this regard, several concentration measurements can be taken across the width of the plume, without knowing which one to compare with the MCL (Einarson, 2017). Several researchers (Verreydt et al., 2012; Einarson, 2017; Horst et al., 2021) have called over the past decade for the use of flow-weighted, spatially averaged concentrations to perform risk assessments at contaminated sites, which CMD allows for.

The development of methods for evaluating CMD has come a long way, but there are still some uncertainties regarding how to perform a risk assessment based on a CMD estimate. Einarson and Mackay (2001) suggested using CMD in the aquifer and the flow rate of a supply well to evaluate resulting maximum concentration. The flow rate of the supply well could be replaced by the flow rate of a relevant receptor (Einarson, 2017) e.g. a stream (Rønde et al., 2017). Another suggestion from the literature is a contaminant plume classification system that divides CMD into ten separate magnitude categories relevant, for instance, to prioritizing between several contaminated sites (Newell et al., 2011). Recently, the Capital Region of Denmark has started to implement CMD as a metric for performing risk assessments through the use of an existing or a potential future groundwater well, thereby allowing for a comparison between a concentration derived from CMD and the MCL (Horst et al., 2021). Furthermore, the Capital Region of Denmark uses CMD and level of conceptual understanding of the site to evaluate the potential risk caused by contamination at a site.

As previously stated in the Introduction, one of the missing links mentioned by Horst et al. (2021), in terms of including CMD at contaminated sites, is the lack of robust CMD estimates. The ProfileFlux

method addresses this missing link by guiding the end-user to focus on high-resolution, depth-discrete concentration profiles and then couple this information with a standard flow and transport model. Within the project for which the ProfileFlux method was developed, a 2D transport model will be set up as a user-friendly tool publicly available, in order to include CMD estimates in a better way at contaminated sites located in clay till settings. Moving forward, the subject relating to how CMD can be used as a metric for risk assessment should be addressed by regulators so that the community truly adopts it as a key metric for risk assessing contaminated sites.

## 5. Conclusion

The ProfileFlux method for estimating the CMD at a contaminated site located in a clay till setting is presented herein. Compared to the traditional transect method, the ProfileFlux method is useful in the early stages of field investigations of mature plumes and does not require the installation of permanent multilevel wells. The combination of high-resolution, depth-discrete concentration profiles and a 2D flow and transport model is essential, as it engenders a better understanding of how the contaminant spreads, because the method exploits information extracted from concentration profiles (i.e. maximum concentration, depth of maximum concentration, plume thickness) downgradient of a contaminant source. A GSA highlighted the most important field characteristics for the ProfileFlux method in terms of both the shape of the vertical concentration profiles and the estimated CMD. It revealed that parameters determining water fluxes (both vertical and horizontal) and source length are crucial for ensuring a good CMD estimate when comparing the measured concentration profiles to their simulated counterparts. Using these, combined with the horizontal groundwater flux, can yield a good infiltration estimate – and subsequently a good CMD estimate. The method was applied at a thoroughly investigated contaminated site, resulting in an estimated CMD of 117–170 g/year, which compared well with the 143 g/year found using the more expensive and tedious transect method. Furthermore, the high-resolution, depth-discrete measurements taken in the plume perpendicular to the flow direction showed that the center of the plume was actually further east than expected, therefore, improving the conceptual understanding of the contaminant spread at the site. This paper exemplified that the CMD can be found using the ProfileFlux method. The next step, besides testing at other contaminated sites, is to implement the method in a tool for end-users to use in the risk assessment of contaminated sites.

## Funding

Funding for the project was provided by the Capital Region of Denmark and the Department of Environmental and Resource Engineering at the Technical University of Denmark.

## CRediT authorship contribution statement

**Louise Rosenberg:** Investigation, Visualization, Writing – original draft. **Klaus Mosthaf:** Methodology, Software, Formal analysis, Writing – review & editing. **Mette M. Broholm:** Conceptualization, Methodology. **Annika S. Fjordbøge:** Investigation. **Nina Tuxen:** Methodology, Project administration. **Ida Henriette Kern-Jespersen:** Methodology, Supervision. **Vinni Rønde:** Methodology. **Poul L. Bjerg:** Conceptualization, Methodology, Writing – review & editing.

## Declaration of Competing Interest

The authors declare that they have no known competing financial interests or personal relationships that could have appeared to influence the work reported in this paper.

## Data availability

The data used for this study is presented in the paper alongside the equations needed to set up the model.

## Appendix A. Supplementary data

Supplementary data to this article can be found online at <https://doi.org/10.1016/j.jconhyd.2022.104121>.

## References

- Aamand, J., Badawi, N., Roll Jakobsen, P., Jørgensen, P.R., Mosthaf, K., Troldborg, L., Rolle, M., 2022. Mapping Groundwater Vulnerability to Pesticide Contamination through Fractured Clays - CLAYFRAC. The Danish Environmental Protection Agency. DOI: <https://mst.dk/service/publikationer/publikationsarkiv/2022/feb/clayfrac/>.
- Annable, M.D., Hatfield, K., Cho, J., Klammler, H., Parker, B.L., Cherry, J.A., Rao, P.S.C., 2005. Field-scale evaluation of the passive flux meter for simultaneous measurement of groundwater and contaminant fluxes. *Environ. Sci. Technol.* 39 (18), 7194–7201. <https://doi.org/10.1021/es050074g>.
- Anneser, B., Einsiedl, F., Meckenstock, R.U., Richters, L., Wisotzky, F., Griebler, C., 2008. High-resolution monitoring of biogeochemical gradients in a tar oil-contaminated aquifer. *Appl. Geochem.* 23 (6), 1715–1730. <https://doi.org/10.1016/j.apgeochem.2008.02.003>.
- Balbarini, N., Rønde, V., Maurya, P., Fiandaca, G., Møller, I., Klint, K.E., Christiansen, A. V., Binning, P.J., Bjerg, P.L., 2018. Geophysics-based contaminant mass discharge quantification downgradient of a landfill and a former pharmaceutical factory. *Water Resour. Res.* 54, 5436–5456.
- Bjerg, P.L., Tuxen, N., Reitzel, L.A., Albrechtsen, H.-J., Kjeldsen, P., 2011. Natural Attenuation Processes in landfill leachate plumes at three Danish sites. *Ground Water* 49 (5), 688–705.
- Broholm, M.M., Janniche, G.S., Mosthaf, K., Fjordbøge, A.S., Binning, P.J., Christensen, A.G., Grosen, B., Jørgensen, T.H., Keller, C., Wealthall, G., Kern-Jespersen, H., 2016. Characterization of chlorinated solvent contamination in limestone using innovative FLUTE® Technologies in Combination with other methods in a line of evidence approach. *J. Contam. Hydrol.* 189, 68–85. <https://doi.org/10.1016/j.jconhyd.2016.03.007>.
- Brooks, M.C., Wood, A.L., Annable, M.D., Hatfield, K., Cho, J., Holbert, C., Rao, P.S.C., Enfield, C.G., Lynch, K., Smith, R.E., 2008. Changes in contaminant mass discharge from DNAPL source mass depletion: evaluation at two field sites. *J. Contam. Hydrol.* 102 (1–2), 140–153. <https://doi.org/10.1016/j.jconhyd.2008.05.008>.
- Brooks, M.C., Cha, K.Y., Wood, A.L., Annable, M.D., 2015. Screening-level estimates of mass discharge uncertainty from point measurement methods. *J. Contam. Hydrol.* 177–178 (June), 167–182. <https://doi.org/10.1016/j.jconhyd.2015.04.002>.
- Campolongo, F., Cariboni, J., Saltelli, A., 2007. An effective screening Design for Sensitivity Analysis of large models. *Environ. Model. Softw.* 22 (10), 1509–1518. <https://doi.org/10.1016/j.envsoft.2006.10.004>.
- Campolongo, F., Saltelli, A., Cariboni, J., 2011. From screening to quantitative sensitivity analysis. A unified approach. *Comput. Phys. Commun.* 182 (4), 978–988. <https://doi.org/10.1016/j.cpc.2010.12.039>.
- Chambon, J.C., Broholm, M.M., Binning, P.J., Bjerg, P.L., 2010. Modeling multi-component transport and enhanced anaerobic Dechlorination processes in a single fracture-clay matrix system. *J. Contam. Hydrol.* 112 (1–4), 77–90. <https://doi.org/10.1016/j.jconhyd.2009.10.008>.
- Chambon, J.C., Binning, P.J., Jørgensen, P.R., Bjerg, P.L., 2011. A risk assessment tool for contaminated sites in low-permeability fractured media. *J. Contam. Hydrol.* 124 (1–4), 82–98. <https://doi.org/10.1016/j.jconhyd.2011.03.001>.
- Chambon, Julie C., Bjerg, P.L., Scheutz, C., Bælum, J., Jakobsen, R., Binning, P.J., 2013. Review of reactive kinetic models describing reductive Dechlorination of chlorinated Ethenes in soil and groundwater. *Biotechnol. Bioeng.* 110 (1), 1–23. <https://doi.org/10.1002/bit.24714>.
- Chapman, S.W., Parker, B.L., 2005. Plume persistence due to aquitard Back diffusion following dense nonaqueous phase liquid source removal or isolation. *Water Resour. Res.* 41 (12), 1–16. <https://doi.org/10.1029/2005WR004224>.
- Chiang, C.Y., Salanitro, J.P., Chai, E.Y., Colthart, J.D., Klein, C.L., 1989. Aerobic biodegradation of benzene toluene and xylene in a Sandy aquifer data analysis and computer modeling. *Ground Water* 27 (6), 823–834.
- Damgaard, I., Bjerg, P.L., Jacobsen, C.S., Broholm, M.M., Tuxen, N., Scheutz, C., Bælum, J., Hunkeler, D., 2013a. Identification of chlorinated solvents degradation zones in clay till by high resolution chemical, microbial and compound specific isotope analysis. *J. Contam. Hydrol.* 146, 37–50. <https://doi.org/10.1016/j.jconhyd.2012.11.010>.
- Damgaard, I., Bjerg, P.L., Jacobsen, C.S., Tsitonaki, A., Kern-Jespersen, H., Broholm, M. M., 2013b. Performance of full-scale enhanced reductive Dechlorination in clay till. *Ground Water Monit. Remediat.* 33 (1), 48–61. <https://doi.org/10.1111/j1745>.
- Devlin, J.F., Schillig, P.C., 2017. HydrogeoEstimatorXL: an excel-based tool for estimating hydraulic gradient magnitude and direction. *Hydrogeol. J.* 25 (3), 867–875. <https://doi.org/10.1007/s10040-016-1518-4>.
- Dutta, S., Christy, T.M., Mccall, W., Kurup, P., 2021. Field evaluation of 1.75 groundwater profiler and field screening device for on - site contamination profiling of Chromium ( VI ) in groundwater. *Environ. Earth Sci.* 80 (7), 1–18. <https://doi.org/10.1007/s12665-021-09568-9>.



- Einarson, M., 2017. Spatially averaged, flow-weighted concentrations – a more relevant regulatory metric for groundwater cleanup. *Groundwater Monit. Remediat.* 37 (4), 11–14. <https://doi.org/10.1111/gwmr.12240>.
- Einarson, M.D., Mackay, D.M., 2001. Predicting impacts. *Environ. Sci. Technol.* 35 (3), 66–73.
- Essouayed, E., Ferré, T., Cohen, G., Guiserix, N., Atteia, O., 2021. Application of an iterative source localization strategy at a chlorinated solvent site. *J. Hydrol. X* 13. <https://doi.org/10.1016/j.jhydro.2021.100111>.
- ESTCP, 2011. Decision Guide: A Guide for Selecting Remedies for Subsurface Releases of Chlorinated Solvents. *Department of Defense Environmental Security Technology Program (ESTCP)* no. March. DOI. [http://www.clu-in.org/download/contaminantfocus/dnapi/Treatment\\_Technologies/DNAPL-ER-200530-DG.pdf](http://www.clu-in.org/download/contaminantfocus/dnapi/Treatment_Technologies/DNAPL-ER-200530-DG.pdf).
- Falta, R.W., 2005. Dissolved chemical discharge from fractured clay aquitards contaminated by DNAPLs. *Geophys. Monograph Series* 162, 165–174. <https://doi.org/10.1029/162GM15>.
- Filippini, M., Parker, B.L., Dinelli, E., Wanner, P., Chapman, S.W., Gargini, A., 2020. Assessing aquitard integrity in a complex aquifer – aquitard system contaminated by chlorinated hydrocarbons. *Water Res.* 171, 1–12. <https://doi.org/10.1016/j.watres.2019.115388>.
- Fjordbøge, A.S., Lange, I.V., Bjerg, P.L., Binning, P.J., Riis, C., Kjeldsen, P., 2012. ZVI-clay remediation of a chlorinated solvent source zone, skuldelev, denmark: 2. Groundwater contaminant mass discharge reduction. *J. Contam. Hydrol.* 140–141, 67–79. <https://doi.org/10.1016/j.jconhyd.2012.08.009>.
- Fraser, M., Barker, J.F., Butler, B., Blaine, F., Joseph, S., Cooke, C., 2008. Natural attenuation of a plume from an emplaced coal tar creosote source over 14 years. *J. Contam. Hydrol.* 100 (3–4), 101–115. <https://doi.org/10.1016/j.jconhyd.2008.06.001>.
- Freitas, J.G., Mocanu, M.T., Zoby, J.L.G., Molson, J.W., Barker, J.F., 2011. Migration and fate of ethanol-enhanced gasoline in groundwater: a modelling analysis of a field experiment. *J. Contam. Hydrol.* 119 (1–4), 25–43. <https://doi.org/10.1016/j.jconhyd.2010.08.007>.
- Hønning, J., Broholm, M.M., Bjerg, P.L., 2007. Role of diffusion in chemical oxidation of PCE in a dual permeability system. *Environ. Sci. Technol.* 41 (24), 8426–8432. <https://doi.org/10.1021/es0708417>.
- Horneman, A., Divine, C., Sandtangelo-Dreiling, T., Lloyd, S., Anderson, H., Smith, M.B., McCray, J., 2017. The case for flux-based remedial performance monitoring programs. *Groundwater Monit. Remediat.* 37 (3), 16–18. <https://doi.org/10.1111/gwmr.12225>.
- Horst, J., Schnobrich, M., Divine, C., Curry, P., Sager, S., Horneman, A., 2021. Mass flux strategies 20 years on—getting the sand out of the gears. *Groundwater Monit. Remediat.* 41 (4), 13–21. <https://doi.org/10.1111/gwmr.12491>.
- Jensen, K.H., Bitsch, K., Bjerg, P.L., 1993. Large-scale dispersion experiments in a Sandy aquifer in Denmark: observed tracer movements and numerical analyses. *Water Resour. Res.* 29 (3), 673–696. <https://doi.org/10.1029/92WR02468>.
- Jørgensen, P.R., Hoffmann, M., Kistrup, J.P., Bryde, C., Bossi, R., Villholth, K.G., 2002. Preferential flow and pesticide transport in a clay-rich till: field, laboratory, and modeling analysis. *Water Resour. Res.* 38 (11) <https://doi.org/10.1029/2001wr000494>, 28–1–28–15.
- Jørgensen, P.R., Helstrup, T., Urup, J., Seifert, D., 2004. Modeling of non-reactive solute transport in fractured clayey till during variable flow rate and time. *J. Contam. Hydrol.* 68 (3–4), 193–216. [https://doi.org/10.1016/S0169-7722\(03\)00146-3](https://doi.org/10.1016/S0169-7722(03)00146-3).
- Jørgensen, P.R., Mosthaf, K., Rolle, M., 2019. A large undisturbed column method to study flow and transport in macropores and fractured media. *Groundwater* 57 (6), 951–961. <https://doi.org/10.1111/gwat.12885>.
- Kao, C.M., Wang, Y.S., 2001. Field investigation of the natural attenuation and intrinsic biodegradation rates at an underground storage tank site. *Environ. Geol.* 40 (4–5), 622–631. <https://doi.org/10.1007/s002540000226>.
- Kessler, T.C., Klint, K.E.S., Nilsson, B., Bjerg, P.L., 2012. Characterization of sand lenses embedded in tills. *Quat. Sci. Rev.* 53 (C), 55–71. <https://doi.org/10.1016/j.quascirev.2012.08.011>.
- Kessler, Timo Christian, 2012. *Hydrogeological Characterization of Low-Permeability Clayey Tills: The Role of Sand Lenses.* DTU Environment, Denmark.
- Klint, K.E.S., Nilsson, B., Troldborg, L., Jakobsen, P.R., 2013. A poly morphological landform approach for hydrogeological applications in heterogeneous glacial sediments. *Hydrogeol. J.* 21 (6), 1247–1264. <https://doi.org/10.1007/s10040-013-1011-2>.
- Li, K.B., Abriola, L.M., 2009. A multistage multicriteria spatial sampling strategy for estimating contaminant mass discharge and its uncertainty. *Water Resour. Res.* 45 (6), 1–15. <https://doi.org/10.1029/2008WR007362>.
- Locatelli, L., Binning, P.J., Sanchez-Vila, X., Søndergaard, G.L., Rosenberg, L., Bjerg, P.L., 2019. A simple contaminant fate and transport modelling tool for management and risk assessment of groundwater pollution from contaminated sites. *J. Contam. Hydrol.* 221 <https://doi.org/10.1016/j.jconhyd.2018.11.002>.
- Lu, C., Bjerg, P.L., Zhang, F., Broholm, M.M., 2011. Sorption of chlorinated solvents and degradation products on natural clayey tills. *Chemosphere* 83 (11), 1467–1474. <https://doi.org/10.1016/j.chemosphere.2011.03.007>.
- Mallants, D., Espino, A., Hoorick, M.V., Feyen, J., Vandenberghe, N., Loy, W., 2000. Dispersivity estimates from a tracer experiment in a sandy aquifer. *Ground Water* 38 (2), 304–310.
- McCall, W., Christy, T.M., Pipp, D., Terkelsen, M., Christensen, A., Weber, K., Engelsen, P., 2014. Field application of the combined membrane-Interface probe and hydraulic profiling tool (MiHpt). *Groundwater Monit. Remediat.* 34 (2), 85–95. <https://doi.org/10.1111/gwmr.12051>.
- McGuire, T.M., Newell, C.J., Looney, B.B., Vangelas, K.M., Sink, C.H., 2004. Historical analysis of monitored natural attenuation: a survey of 191 chlorinated solvent sites and 45 solvent plumes. *Remediation* 15 (1), 99–112. <https://doi.org/10.1002/rem.20036>.
- McNab, W.W., Rice, D.W., Tuckfield, C., 2000. Evaluating chlorinated hydrocarbon plume behavior using historical case population analyses. *Bioremediation J.* 4 (4), 311–335. <https://doi.org/10.1080/10889860091114284>.
- Morris, M.D., 1991. Factorial sampling plans for preliminary computational experiments. *Technometrics* 33 (2), 161–174. <https://doi.org/10.1080/00401706.1991.10484804>.
- Mosthaf, K., Rolle, M., Petursdottir, U., Aamand, J., Jørgensen, P.R., 2021. Transport of tracers and pesticides through fractured clay till: large undisturbed column (LUC) experiments and model-based interpretation. *Water Resour. Res.* 57, 1–18. <https://doi.org/10.1029/2020WR028019>.
- National Research Council, 2005. *Contaminants in the Subsurface: Source Zone Assessment and Remediation.* The National Academies Press, Washington DC. <https://doi.org/10.17226/11146>.
- Newell, C.J., Farhat, S.K., Adamson, D.T., Looney, B.B., 2011. Contaminant plume classification system based on mass discharge. *Ground Water* 49 (6), 914–919. <https://doi.org/10.1111/j.1745-6584.2010.00793.x>.
- Nilsson, B., Sidle, R.C., Klint, K.E., Bøggild, C.E., Broholm, K., 2001. Mass transport and scale-dependent hydraulic tests in a heterogeneous glacial till – Sandy aquifer system. *J. Hydrol.* 243 (3–4), 162–179. [https://doi.org/10.1016/S0022-1694\(00\)00416-9](https://doi.org/10.1016/S0022-1694(00)00416-9).
- NIRAS, 2019.  *Afrgrænsende Forureningsundersøgelse Industrivej 2, 3540 Lyngby. Region Hovedstaden.* DOI: By request to regionh.dk.
- Ottosen, C.B., Rønde, V., McKnight, U.S., Annable, M.D., Broholm, M.M., Devlin, J.F., Bjerg, P.L., 2020. Natural attenuation of a chlorinated Ethene plume discharging to a stream: integrated assessment of hydrogeological, chemical and microbial interactions. *Water Res.* 186, 116332 <https://doi.org/10.1016/j.watres.2020.116332>.
- Parker, B.L., Chapman, S.W., Guilbeault, M.A., 2008. Plume persistence caused by Back diffusion from thin clay layers in a sand aquifer following TCE source-zone hydraulic isolation. *J. Contam. Hydrol.* 102 (1–2), 86–104. <https://doi.org/10.1016/j.jconhyd.2008.07.003>.
- Rivett, M.O., Feenstra, S., Cherry, J.A., 1994. Transport of a dissolved-phase plume from a residual solvent source in a sand aquifer. *J. Hydrol.* 159 (1–4), 27–41. [https://doi.org/10.1016/0022-1694\(94\)90247-X](https://doi.org/10.1016/0022-1694(94)90247-X).
- Robertson, W.D., Cherry, J.A., Sudicky, E.A., 1991. Ground-water contamination from two small septic systems on sand aquifers. *Ground Water* 29 (1), 82–92.
- Rønde, V., McKnight, U.S., Sonne, A.T., Balbarini, N., Devlin, J.F., Bjerg, P.L., 2017. Contaminant mass discharge to streams: comparing direct groundwater velocity measurements and multi-level groundwater sampling with an in-stream approach. *J. Contam. Hydrol.* 206 (September), 43–54. <https://doi.org/10.1016/j.jconhyd.2017.09.010>.
- Rosenberg, L., Broholm, M.M., Tuxen, N., Kerrn-Jespersen, I.H., Lilbæk, G., Bjerg, P.L., 2022. Vertical hydraulic gradient estimation in clay till, using MiHPT advanced direct-push technology. *Groundwater Monit. Remediat.* 42 (1), 29–37. <https://doi.org/10.1111/gwmr.12470>.
- Rotaru, C., Ostendorf, D.W., DeGroot, D.J., 2014. Chloride dispersion across silt deposits in a glaciated Bedrock River valley. *J. Environ. Qual.* 43 (2), 459–467. <https://doi.org/10.2134/jeq2013.07.0284>.
- Sale, T., Newell, C., Stroo, H., Hincee, R., Johnson, P., 2008. *Frequently Asked Questions Regarding Management of Chlorinated Solvents in Soils and Groundwater.* Environmental Security Technology Certification Program.
- Schulze-Makuch, D., 2005. *Longitudinal Dispersivity data and implications for scaling behavior.* *Ground Water* 43 (3), 443–456.
- Steelman, C.M., Meyer, J.R., Wanner, P., Swanson, B.J., Conway-White, O., Parker, B.L., 2020. The importance of transects for characterizing aged organic contaminant plumes in groundwater. *J. Contam. Hydrol.* 235 (October) <https://doi.org/10.1016/j.jconhyd.2020.103728>.
- Suthersan, S.S., Potter, S.T., Schnobrich, M., Wahlberg, J., Quinlan, J., Welty, N., Fewless, T., 2016. Rethinking conceptual site models in groundwater remediation. *Groundwater Monit. Remediat.* 36 (4), 22–30. <https://doi.org/10.1111/gwmr.12192>.
- Troldborg, M., Lemming, G., Binning, P.J., Tuxen, N., Bjerg, P.L., 2008. Risk assessment and prioritisation of contaminated sites on the catchment scale. *J. Contam. Hydrol.* 101 (1–4), 14–28. <https://doi.org/10.1016/j.jconhyd.2008.07.006>.
- Troldborg, M., Nowak, W., Tuxen, N., Bjerg, P.L., Helmig, R., Binning, P.J., 2010. Uncertainty evaluation of mass discharge estimates from a contaminated site using a fully Bayesian framework. *Water Resour. Res.* 46 (1), 1–19. <https://doi.org/10.1029/2010WR009227>.
- Troldborg, M., Nowak, W., Lange, I.V., Santos, M.C., Binning, P.J., Bjerg, P.L., 2012. Application of Bayesian Geostatistics for evaluation of mass discharge uncertainty at contaminated sites. *Water Resour. Res.* 48 (9), 1–19. <https://doi.org/10.1029/2011WR011785>.
- Tuxen, N., Albrechtsen, H.J., Bjerg, P.L., 2006. Identification of a reactive degradation zone at a landfill leachate plume fringe using high resolution sampling and incubation techniques. *J. Contam. Hydrol.* 85 (3–4), 179–194. <https://doi.org/10.1016/j.jconhyd.2006.01.004>.
- Verreydt, G., Bronders, J., Van Keer, I., Diels, L., Vanderauwera, P., 2011. *Passive Samplers for Monitoring VOC in Groundwater: Prospects Related to Mass Flux Measurements,* 342. IAHS-AISH Publication, pp. 391–394. <https://doi.org/10.1111/j1745>.
- Verreydt, G., van Keer, I., Bronders, J., Diels, L., Vanderauwera, P., 2012. Flux-based risk management strategy of groundwater pollutions: the CMF approach. *Environ. Geochem. Health* 34 (6), 725–736. <https://doi.org/10.1007/s10653-012-9491-x>.

## Supporting Information

### SI1: Global sensitivity analysis

12 parameters were examined in the GSA and are shown in Table SI1.  $i_v$  and  $K_v$  were not examined as they linearly correlate with  $I$ , and the dispersivities in the clay till were also not investigated due to the low flow conditions and the considered small scale. The dispersivities in the clay till will therefore not have a strong influence on the output. The 12 parameters were examined on how they influenced the output parameters:  $CMD$ ,  $T_{plume}$ ,  $C_{max}$  and  $D_{cmax}$  at three different locations (below the source zone, 20 and 50 m downgradient from the source), 50 years after the spill happened. The three locations were: right below the source zone (only relevant for  $CMD$ ), 20 m and 50 m from the downgradient edge of the source. The examined parameter ranges were those given in Table SI1. 650 runs of the model were performed (1 initial case plus 12 input parameters, run with 50 trajectories), however 78 of the runs were deemed unsuitable for the GSA due to a low resulting  $CMD$  of less than 1 g/year assuming a source width of 20 m (set in the same range as the limited impact category from (Newell et al. 2011)). The low  $CMD$  could be a result of either a very slow or fast transport resulting in the contaminant respectively not reaching or having already passed by the point of interest after 50 years. Therefore, the results have been based on 572 model runs covering the defined parameter space. In the GSA, the parameter space was subdivided in 50 trajectories with a random starting point within a specified range using Latin hypercube sampling (McKay et al. 1979).

The influence of all 12 input parameters on the four output parameters is shown in Figure SI1. Both ( $\mu^*$ ) and the standard deviation ( $\sigma$ ) are shown. In Table SI1, the effect on the output parameters are shown for each of the input parameters. (+) indicates that the output parameter increases (in the case of  $D_{cmax}$ , it means that the depth increases), (-) indicates that the output parameter decreases and (+ -) indicates, that the output parameter can increase or

decrease. The 0 indicated for  $C_0$  means that the change does not affect the output parameters due to the fact that  $C_0$  is simulated as the ratio between the concentration at a certain time and place and initial concentration,  $C/C_0$ .

*Table SII: Input parameters for the GSA and the parameter range. The four columns to the right indicates how the output parameters ( $CMD$ ,  $T_{plume}$ ,  $C_{max}$  and  $D_{cmax}$ ) are affected with an increase in the input parameter in question; + indicates an increase; - indicates a decrease; + - indicates that it is a parameter that has a large effect on the break-through curve; and 0 indicates no effect.*

Parameter	Symbol	Suggested value range	CMD	$T_{plume}$	$C_{max}$	$D_{cmax}$
<b>Source</b>						
Source concentration	$C_0$	0.1 – 10 mg/L	+	0*	0*	0*
Source length	$L_s$	5 – 40 m	+	+	+	+ -
<b>Clay till</b>						
Infiltration rate	$I$	30 – 300 mm/year	+ -	+	+ -	+
Porosity	$n_{clay}$	0.2 – 0.4	+ -	+	+ -	+
Thickness	$T_{clay}$	4 – 10 m	+	+	+	+ -
Sorption coefficient	$k_{d,clay}$	0 – 2 L/kg	+	-	+	-
<b>Aquifer</b>						
Horizontal head gradient	$i_h$	0.8 – 5 ‰	+	+	-	-
Horizontal conductivity	$K_h$	$5 \cdot 10^{-6} - 1 \cdot 10^{-4}$ m/s	+	+	-	-
Porosity	$n_{aq}$	0.2 – 0.4	+ -	+	-	+ -
Longitudinal dispersivity	$\alpha_{l,aq}$	0.1 – 1 m	+	+	+	+
Vertical dispersivity	$\alpha_{v,aq}$	0.005 – 0.02 m	+	+	-	+
Sorption coefficient	$k_{d,aq}$	0 – 0.5 L/kg	+ -	-	+ -	-

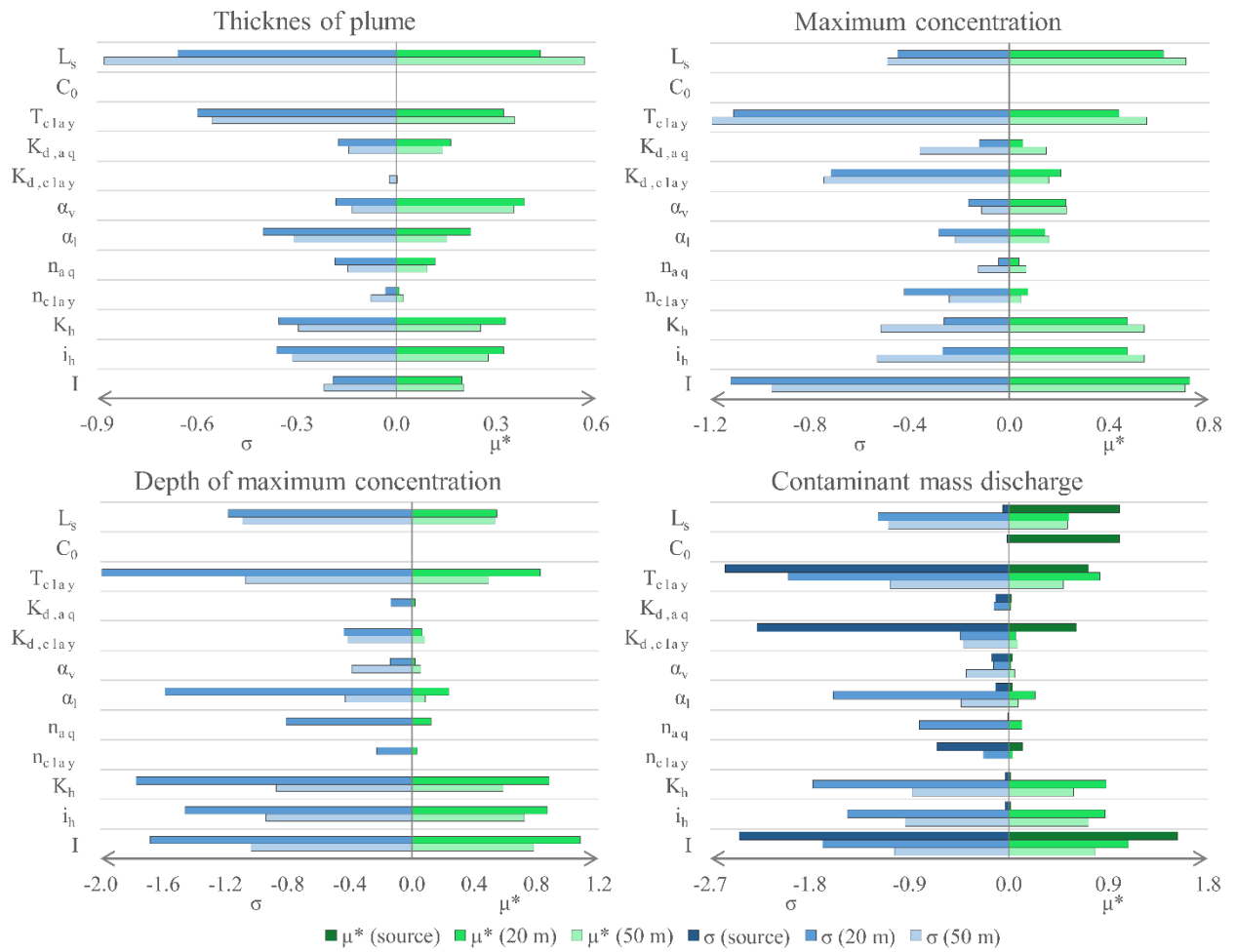
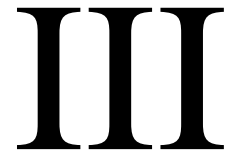


Figure S11: Input parameters effect on three output regarding the vertical concentration profile and the CMD estimate. The  $\mu^*$  (green) describes the effect (high number equals high effect) and the  $\sigma$  (blue) describes the variability of the changes (high number equals very varying effect on the output parameter).












High-resolution Geological Information  
from Crosshole Ground Penetrating Radar  
in Clayey Tills

Bolette B. Jensen, Louise Rosenberg, Aikaterini Tsi-  
tonaki, Nina Tuxen, Poul L. Bjerg, Lars Nielsen, Thomas  
M. Hansen, Majken C. Looms

Groundwater Monitoring and Remediation  
Accepted

# High-Resolution Geological Information from Crosshole Ground Penetrating Radar in Clayey Tills

by Bolette B. Jensen , Louise Rosenberg , Aikaterini Tsitonaki, Nina Tuxen, Poul L. Bjerg , Lars Nielsen , Thomas M. Hansen  and Majken C. Looms 

## Abstract

Heterogeneous glacial deposits dominate large parts of the Northern Hemisphere. In these landscapes, high-resolution characterization of the geology is crucial for understanding contaminant transport. Geological information is mostly obtained from multiple boreholes drilled during a site investigation, but such point-based data alone do not always provide the required resolution to map small-scale heterogeneity between boreholes. Crosshole ground penetrating radar (GPR) is suggested as a tool for adding credible geological information between boreholes at contaminated site investigations in industrial sites where infrastructure, such as electrical installations, can pose a challenge to other geophysical methods. GPR data are sensitive to the dielectric permittivity and the bulk electrical conductivity, which can be related to the distribution of water content and sand/clay occurrences. Here we present a detailed crosshole GPR dataset collected at an industrial contaminated site in a clay till setting. The data are processed using a novel inversion approach where information on changes in the velocity and attenuation of the radar signal are obtained independently. The GPR results are compared to borehole logs, grain size analyses, and relative permeability data from the site. The GPR data analysis provided valuable information on the understanding of the lateral geological variability. A silt layer with a thickness of a few decimeters, likely important for flow characterization, was confirmed and resolved by GPR data. Our findings suggest that crosshole GPR has the potential for contributing with high-resolution geological information by filling the data gap between boreholes, thereby becoming a relevant tool in contaminated site investigations.

## Introduction

Contaminated sites worldwide pose a risk to human health by threatening water resources, indoor environment and through direct exposure to contaminated soil. The European Union estimates approximately 2.5 million potentially contaminated sites need to be identified, investigated, and managed. In large parts of the Northern Hemisphere, the geology is characterized by heterogeneous glacial deposits (McCabe 1987; Shaw 1987; Houmark-Nielsen 2010), mainly clayey tills riddled with sand lenses of various sizes (Kessler et al. 2012; Klint et al. 2013). Heterogeneities, such as fractures and sand lenses, affect contaminant distribution and transport in these clayey tills, due to the contrast in hydraulic conductivity and biogeochemical properties (e.g., McKay

et al. 1993; Jørgensen et al. 2002; Harrington et al. 2007; Damgaard et al. 2013). High content of sand in the clayey till matrix also increases the hydraulic conductivity (Aamand et al. 2022). Mapping the extent and geometry of these sandy features, as well as the presence of continuous thick clay layers, is critical for understanding contaminant flow paths in the clayey till.

Information at contaminated sites is often limited to the locations of the boreholes drilled as part of a site investigation. From such boreholes, geological logs are obtained as well as information from soil and water samples. Additionally, direct push probes provide logs on, for example, bulk electrical conductivity and relative permeability (McCall et al. 2014; McCall and Christy 2020; Steelman et al. 2020). Common for all these data types is, that they provide depth-discrete information about the vertical variability of the subsurface, but little information about the lateral variability, which in practice is most often interpolated from these point data to build the conceptual geological model.

Geophysical methods can be used to obtain information on the subsurface variability between boreholes and have been applied to support conceptual site model development at contaminated sites. Høyer et al. (2019) used surface electromagnetic induction (EMI) data, direct current (DC) resistivity data, and transient electromagnetic (TEM) at a landfill situated in a clay till dominated setting. The interpretation of the geophysical data provided valuable information that was used

*Article impact statement:* Crosshole GPR is a promising tool for contaminated site investigations as it supports more reliable interpretation of geology between boreholes.

© 2023 The Authors. *Groundwater Monitoring & Remediation* published by Wiley Periodicals LLC on behalf of National Ground Water Association.  
doi: 10.1111/gwmm.12588

This is an open access article under the terms of the [Creative Commons Attribution](https://creativecommons.org/licenses/by/4.0/) License, which permits use, distribution and reproduction in any medium, provided the original work is properly cited.



in the development of a highly detailed 3D geological model for the area. In Maurya et al. (2018), results from an induced polarization survey in a major contaminant plume were used to support the geological modeling in the area. For these surface methods, the vertical resolution inevitably decreases with depth, and the penetration depth of, for example, surface ground penetrating radar (GPR) is limited in clayey till. Crosshole methods allow constant vertical resolution along the borehole depth, given appropriate spaced boreholes (Day-Lewis et al. 2005). Commonly used crosshole methods are seismic tomography (e.g., Wang and Rao 2006), electrical resistivity tomography (ERT) (e.g., Slater et al. 2000), and GPR tomography (e.g., Eppstein and Dougherty 1998).

Crosshole GPR investigations use electromagnetic (EM) pulses that are emitted from a transmitting antenna in one borehole and recorded by a receiving antenna in a nearby borehole. The recorded radar waveform carries a fingerprint of the medium through which the wave has traveled, depending on the spatial distribution of the subsurface dielectric properties. The EM wave velocity can be related to the dielectric permittivity of the subsurface, which can be translated to subsurface water content (e.g., Huisman et al. 2003). The attenuation of the EM wave provides additional information on the bulk electrical conductivity, which is different for sand and clay (e.g., Reynolds 2011), and crosshole GPR hence has the potential to distinguish between sandy and clayey features between boreholes (Looms et al. 2018; Jensen et al. 2022a). GPR is minimally-invasive and can be used in already existing boreholes, and can therefore be integrated in any ongoing site investigation. Crosshole GPR signals are generally thought not to be adversely affected by electrical installations at the site, which allows for the use of GPR investigations at urban and industrial sites. Furthermore, the fast data acquisition potentially allow for practical implementation at operational scale. Finally, the sensitivity of the GPR method is highest in the middle between the boreholes (Day-Lewis et al. 2005), and thus contributes with information in areas of low data density, which is an advantage compared to standard ERT methods where the resolution is highest close to the boreholes.

Crosshole GPR has been used for a wide range of applications, such as monitoring infiltration using time-lapse tracer studies (e.g., Hubbard et al. 2001; Chang et al. 2006; Gueting et al. 2017), characterizing subsurface moisture content (e.g., Alumbaugh et al. 2002), and for characterizing porosities in aquifers (e.g., Klotzsche et al. 2013; Zhou et al. 2020). Until recently, GPR was not applied in clay tills due to the attenuation of the signal, but Looms et al. (2018) and Svendsen et al. (2023) showed that GPR can be used in these environments, given sufficiently short borehole separation up to 5 to 7 m. Furthermore, Jensen et al. (2022a), recently developed a linear inversion algorithm that allows for fast interpretation of both GPR traveltime and amplitude data, which makes the method attractive for use as part of contaminated site investigations.

The scale of GPR investigations is limited, and the method is hence most relevant in small-scale investigations of, for example, a source zone at sites with highly heterogeneous geology, such as flow till (Klint et al. 2013), where interpolation between boreholes meters apart can be challenging. In a subglacially weakly deformed flow till, small-

scale sand lenses with lengths of 0.2 to 4 m and thicknesses of 2 to 50 cm have been identified (Kessler et al. 2012) and shown to be important for contaminant transport (Kessler 2012). Hydraulically important fractures most often have apertures smaller than what can be resolved using linear inversion of GPR data, hence the application of GPR to map hydraulically important heterogeneities is most relevant in layers where sand lenses act as preferential transport pathways as seen in, for example, Harrington et al. (2007) or Damgaard et al. (2013).

In this study, we present the first application of the linear inversion approach (Jensen et al. 2022a) to crosshole GPR traveltime and amplitude data at an industrial contaminated site situated in a clay till environment. The main aim is to assess whether the application and analysis of GPR data can provide supplementary high-resolution information on subsurface variations and delineate sandy structures, hence improve the understanding of the geology at the site at a small scale. Secondly, we identify and discuss the methods' limitations and advantages when used in an industrial contaminated site setting.

## Methods

### Field Site—Contamination and Geological Setting

Field investigations were conducted at an industrial site in Vassingerød, Denmark. The shallow geology is dominated by Quaternary deposits. The glacial sediments are composed of 30 to 35 m of sandy meltwater deposits, which is the main aquifer in the area, overlain by 10 to 15 m of clay till with embedded sand lenses. The clay till consists of two till units: a lower, consolidated unit (basal) and an upper, less consolidated till unit (flow or melt-out till) (NIRAS 2019). A transect from the geological model for the entire site is seen in Figure 1.

The field site has previously been thoroughly investigated in order to understand the spreading of an identified TCE contamination from the source zone in the clayey till to the underlying sand aquifer and to estimate the contaminant mass discharge (NIRAS 2019; Rosenberg et al. 2022, 2023). The GPR investigation in this study took place in the suspected source zone area in the clayey till. Further details of the site and contamination can be found in Rosenberg et al. (2022, 2023).

### Boreholes, Investigations, and Data Acquisitions

#### *Boreholes and Data*

In this study, we use the available data within the local investigation area set in the source zone (NIRAS 2019; Rosenberg et al. 2022) to make a more detailed local geological model (Figure 1, top). Specific borehole logs and grain size analyses associated with boreholes B301, B302, and B303 were included in this study, while relative permeability data were obtained from MiHPT14, MiHPT15, and MiHPT16. The locations are shown in Figure 1. Crosshole GPR data were acquired between boreholes B302 and B303, since the largest lateral geological variability was expected between these two boreholes. The investigated tomographic transect is illustrated in Figure 1 (top-right). We include information from B301 and MiHPT14-16 in the following

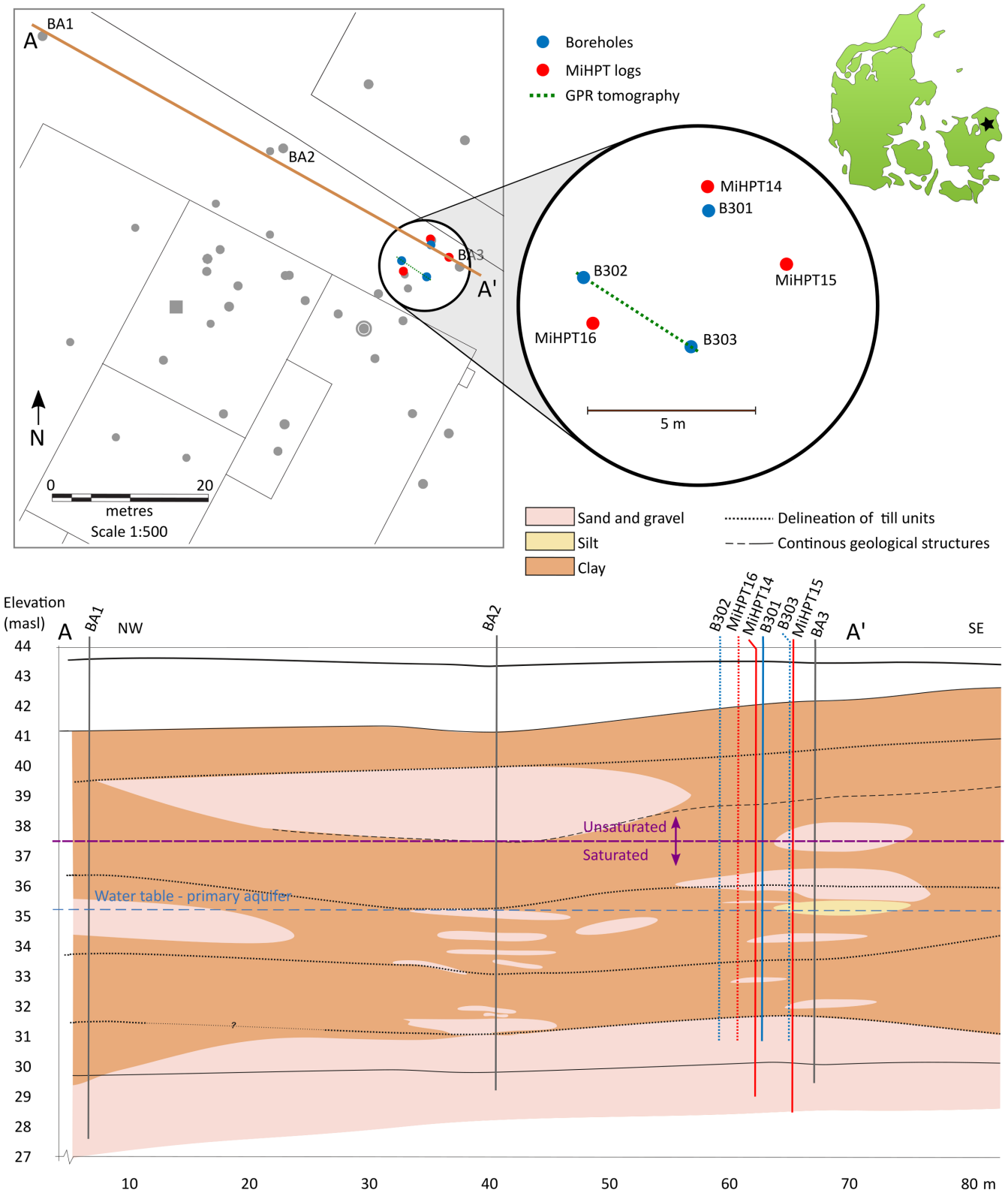


**Figure 1.** Upper: Overview of the field site in Vassingerød, Northern Zealand, Denmark (approximate location on map). The local area of investigation is shown in zoomed view (top) with the colored points that are considered in this study. The tomographic transect investigated by GPR is illustrated as the green dashed line. Lower: Geological profile for transect A-A'. The transect illustrates the general geology at the site, with sand lenses embedded in the clay till, underlain by a sandy aquifer. Transect adapted from NIRAS (2019). The approximate locations for MiHPT logs (red) and investigation wells (blue) are projected onto the transect.

analysis to better understand the overall lateral variability at the site. Approximate locations of boreholes B301-B303 and relative permeability logs have been projected onto the geological profile in Figure 1.

*Data Acquisition*

The relative permeability data were collected using the Membrane Interface and Hydraulic Profiling Tool (MiHPT), but only the HPT data will be used in this study

as a measure for the relative permeability of the subsurface (McCall et al. 2014; McCall and Christy 2020). Further details can be found in Data S1 and Rosenberg et al. (2022).

The grain size data is based on soil samples taken during the drilling of B301 to B303, every 0.5 m from 3 m below ground. As described by Lévy et al. (2022), the grain size distribution was analyzed using a sieve (0.063 to 2 mm) and a laser diffractometer (0.02 to 63  $\mu\text{m}$ ). The soil classification from the grain size samples follows the USDA particle size limit classification (e.g., Gee and Bauder 1986).

Crosshole GPR data were acquired using the PulseEKKO system from Sensors&Software with 100 MHz omnidirectional antennae and a sampling frequency of 0.2 ns. We used a 1000V transmitter and the Ultra Receiver. The antenna housing dimensions are  $\varnothing 29$  mm and 1.44 m long. The GPR equipment is shown in Figure 2. The boreholes were drilled as a part of the contaminated site investigation in 2019 and were equipped with plastic (PEH) casing tubes with an inner diameter of  $d=0.051$  m. The distance between B302 and B303 was 3.81 m. Since the casing tubes were screened at 13.0 m below ground, a specially designed packer system was installed in the boreholes to remove water from the casing tube before the GPR investigations. This was necessary, to prevent water from affecting the propagating EM wave, as investigated in Jensen et al. (2022b).

Zero-offset-profile (ZOP) data were collected by employing the transmitter in borehole B302 and the receiver in B303, then moving the transmitting and receiving antenna simultaneously in vertical increments of 0.25 m from 1.5 to 12.0 m below-ground level. The data acquisition geometry is illustrated in Figure 2, where the lines indicate the straight wave paths for the propagating EM signal between a given transmitter and receiver position. The ZOP data are used to obtain a 1D profile of water content and amplitude variations along the borehole depths. The ZOP acquisition time was 15 min.

Multi-offset-gather (MOG) data were collected by fixing the transmitting antenna at one depth in B302 while lowering the receiving antenna in vertical increments of

0.25 m along the borehole depth in B303. The data acquisition geometry for MOG measurements is illustrated in Figure 2. The receiver positions were chosen so the collected data span  $\pm 45^\circ$  from horizontal relative to the transmitter position, to avoid recording high-angle traces as they would be discarded in the post-processing (Peterson 2001). The transmitter was then moved 1 m down and the procedure was repeated. When the transmitter had covered the entire borehole depth, the receiver was moved in increments of 1 m, while the transmitter was moved in increments of 0.25 m. The MOG data are used in a geophysical inversion to estimate 2D subsurface models of water content and bulk electrical conductivity variations along the borehole depth and in the area between the boreholes. The MOG acquisition time was approximately 3 h.

Calibration gathers in air were acquired before and after recording the ZOP data as well as before, between and after each half MOG dataset, to calibrate the travelttime data for the zero-time of emitting the radar pulse, following the procedure described in Oberrohrmann et al. (2013). The field campaign took 1 d, which included installation and testing of the packer system, calibration gathers, ZOP and MOG data collection, and was carried out in June 2022.

#### Post-Processing of GPR Data

The travelttime and amplitude data were identified in the recorded waveform data and picked using a semi-automated approach. The first-arrival travelttime data were picked using cross-correlation between a reference wavelet and the acquired waveform data (Molyneux and Schmitt 1999; Hansen et al. 2013). The amplitude data were picked as the peak-to-peak waveform amplitude value in a defined window. No gain was applied to the data. The critically refracted EM wave traveling along the ground affected the shallower traces, and the first usable trace was obtained 2.75 m below ground. Prior to inversion, the measured MOG amplitude data were corrected for geometrical spreading of the energy, radiation patterns of the antenna and the antenna gain effect,  $A_0$ . See, for



**Figure 2.** Left: Photo of the field site with the GPR equipment. Antennas are laid out on ground during warm up of the equipment. Middle: Schematic illustration of GPR transmitter and receiver boxes connected to the 100 MHz antenna <https://www.sensoft.ca/products/pulseekkopro/borehole-gpr/> (with permission from Sensors&Software). Right: Data acquisition geometry of ZOP data and MOG data. Asterisks indicate transmitter positions and circles indicate receiver positions. The lines indicate the straight wave paths for the propagating EM signal between a given transmitter and receiver position.

example, Holliger et al. (2001) and Jensen et al. (2022a) for details on amplitude corrections. Traveltime data were time-zero corrected using the time-zero correction factor,  $t_0$ , estimated from the acquired calibration lines. We obtained a MOG dataset of 464 traces in total. We also investigated using a subset of this full dataset, omitting all data from transmitter and receiver positions between 6.5 and 8.5 m below ground, resulting in a reduced dataset of 232 traces. The data geometry for the reduced dataset can be found in Data S1.

## Inversion

The corrected MOG data were used in a tomographic geophysical inversion to obtain estimates of the 2D subsurface parameter distribution. The measured amplitude data were inverted to obtain tomograms for subsurface attenuation and the measured traveltime data were inverted to obtain the subsurface slowness (inverse velocity) distribution (as described in e.g., Giroux et al. 2007). We use a probabilistic linear inversion with a geostatistical Gaussian prior model included and we account for the forward modeling errors arising from choosing a linear scheme. The method is described in detail by Jensen et al. (2022a). The obtained tomograms presented here are the mean of all the equally likely subsurface representations that are consistent with the a priori information and the data. These mean results are overly smooth compared to each subsurface representation and the parameter value range is dampened (Tarantola 2005; Hansen et al. 2008; Looms et al. 2010). Further information on inversion parameters can be found in Data S1.

The obtained slowness distribution,  $s$ , from traveltime inversion can be related to the water content,  $\theta_v$ , through the dielectric permittivity,  $\epsilon_r$ , and a petrophysical relation, for example, the empirical Topp's equation (Topp et al. 1980):

$$\theta_v = -5.3 \times 10^{-2} + 2.92 \times 10^{-2} \epsilon_r - 5.5 \times 10^{-4} \epsilon_r^2 + 4.3 \times 10^{-6} \epsilon_r^3,$$

where the permittivity can be estimated from  $\epsilon_r = s^2 c^2$ , and  $c$  is the speed of light in vacuum ( $c = 0.2998 \text{ m/ns}$ ).

The obtained attenuation distribution,  $\alpha$ , from amplitude inversion can be related to the electrical conductivity,  $\sigma$ , through (e.g., Annan 2005):

$$\sigma = \frac{2 \alpha \sqrt{\epsilon_r}}{Z_0}, Z_0 = \sqrt{\frac{\mu_0}{\epsilon_0}},$$

where the dielectric permittivity,  $\epsilon_r$ , is estimated from the traveltime inversion as described above and  $Z_0$  is the free space impedance ( $\approx 377 \Omega$ ) given by the free space magnetic permeability,  $\mu_0 = 1.25 \times 10^{-6} \text{ H/m}$ , and the permittivity of free space,  $\epsilon_0 = 8.89 \times 10^{-12} \text{ F/m}$ .

## Results

### Existing Information

We construct a geological model for the area between the boreholes B302-B303 from an interpretation of the existing

geological information in the area of investigation (Figure 3, right). Overall, we interpret two till units, consistent with the large-scale geological model for the area (Figure 1), separated by a silt layer at approximately 36 masl.

The silt layer is interpreted as coherent, however thinning toward B302. This interpretation is mainly based on borehole logs as the discrete grain size analyses from B302 has two silt peaks and it is difficult to verify the thinning from the sampling distance of 0.5 m intervals. The low required pressure observed between 37 and 35 masl in HPT15 and at 36 to 37 in HPT16 is indicative of a more permeable layer, such as silt, but this is not identified in HPT14. Furthermore, the thickness of the silt layer appears overestimated in the HPT15 log, compared to the borehole and grain size logs. This could be a result of sparse fracture networks in the transition between the upper and the lower till units, separated by the silt layer.

Below the silt layer, the variance between the data types (HPT logs, borehole, and grain size logs) from B301, B302, and B303, is low, and the till unit seems more uniform laterally. The lower till unit is perhaps divided into an upper and lower part, where the upper subsection above 34 masl has a higher sand content, as identified in the grain size logs, and the lower is more clayey. The subdivision of the lower till unit into a sandier upper and a more clayey lower part is not observable in the HPT logs or indicated in the borehole logs. A transition zone toward the sandy aquifer with an increasing amount of sand from approximately 32.5 masl, is apparent in all data types. A slight dip of the top of the transition zone toward B303, is interpreted from grain size logs, and is also evident in the borehole logs.

The data from the upper till unit is inconclusive. The grain size log from B303 suggests a more sandy till in the entire depth interval 40 to 36 masl, which is contradictory to HPT data that indicate a geology with higher required pressure (lower relative permeability), that is, higher clay content, at least in the depth interval 37 to 38 masl. The borehole log for B303 suggests an interval of more sandy till between 37.2 to 38.8 masl.

The grain size log from B302 suggests an interval with higher clay and silt content at approximately 37.5 masl, which is supported by the high pressures recorded in the HPT logs in this depth interval, and a more sandy till above 38 masl. However, the borehole log does not reflect this variation in geology. In order to synthesize a geological model for the upper till, we mainly base our interpretation on the grain size data, since it can be challenging to evaluate small changes in, for example, sand content on site from a visual and mechanical inspection of a sample.

The interpolation between B302 and B303 is challenged by the differences in the data, which results in a highly uncertain conceptualized geological model in the depth interval 36.5 to 40 masl (Figure 3, right). We have included small heterogeneities in the interpretation of the upper till to honor this uncertainty as well as the grain size data.

### GPR Results

#### 1D Profiles (Zero-Offset-Profiling Data)

1D profiles obtained from zero-offset-profile acquisition of GPR data between boreholes B302 and B303

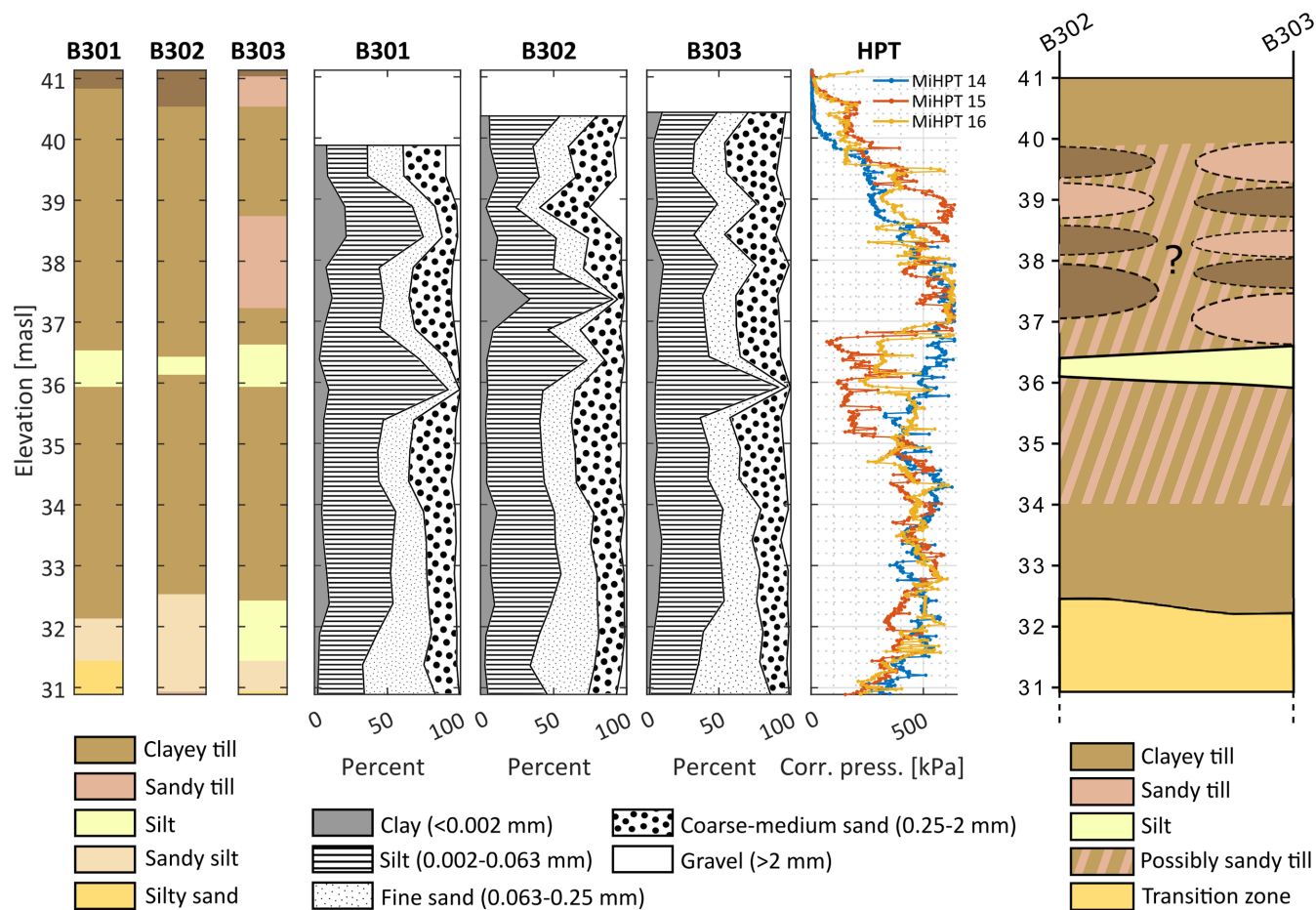


**Figure 3.** Existing information: Borehole logs for B301 to B303, grain size analyses for B301 to B303 and HPT logs from MiHPT14-16, see Figure 1 for locations. Interpreted geological model between boreholes B302 and B303 from existing data (right).

are presented in Figure 4. The recorded waveform data is equivalent to what can be seen in the field during data acquisition, and contains information on (1) traveltime ( $x$  axis), hence radar propagation velocity that can be translated to subsurface water content, as well as (2) signal strength identified as waveform amplitude (colorscale), hence attenuation of the radar wave, which provides additional information on subsurface bulk electrical conductivity.

The EM wave velocity, calculated by dividing the ray path length with the time-zero corrected traveltime data, and the picked waveform amplitude is shown in Figure 4b and 4c, respectively.

The transition from the unsaturated to the saturated zone is seen as a substantial decrease in EM velocity (i.e., an increase in water content) between 40.5 and 39.5 masl (Figure 4b). The exact location of the water table in the formation is difficult to determine from the GPR data due to the retention properties of the formation that create a capillary fringe zone. The silt layer at approximately 36 masl clearly impacts the velocity data, which is low in the layer, due to the high water-saturated porosity of the layer. The silt layer appears to act as a low-velocity waveguide, which traps the propagating EM wave. This is confirmed when inspecting the raw waveform data. Waveguide effects are seen as high-amplitude arrivals

later in the signal in the waveguide depth interval (marked in Figure 4a), as well as destructive signal interference for receiver positions close to both the upper and lower boundaries of the waveguide, similar to observations in Klotzsche et al. (2012). This interference arises from different wavefronts arriving simultaneously at the receiver. These depths are indicated with asterisks in Figure 4c.

The observed transition zone to the sandy aquifer is identified from the increase in signal amplitude below 33 masl, that is, lower attenuation hence lower electrical conductivity, which is interpreted as a decrease in clay content. The velocity data is only affected to a lesser degree due to lack of variation in water content. The 1D GPR data support the original geological model in Figure 3 suggesting that the lower till unit can be subdivided into an upper more sandy interval and a lower, more clayey interval. This is interpreted from a section of higher amplitudes from just above 35 masl down to 34 masl, indicating lower electrical conductivity, and lower amplitudes around 34 to 33 masl, indicating higher electrical conductivity. The 1D GPR data does not inform on the uncertain interpretation of the upper till unit in the original geological model. We observe intermediate GPR amplitudes around 4 mV at 37 masl, indicating a lower clay content, but a predominant layer of sandier clay till is not interpreted at this depth in the original model. The

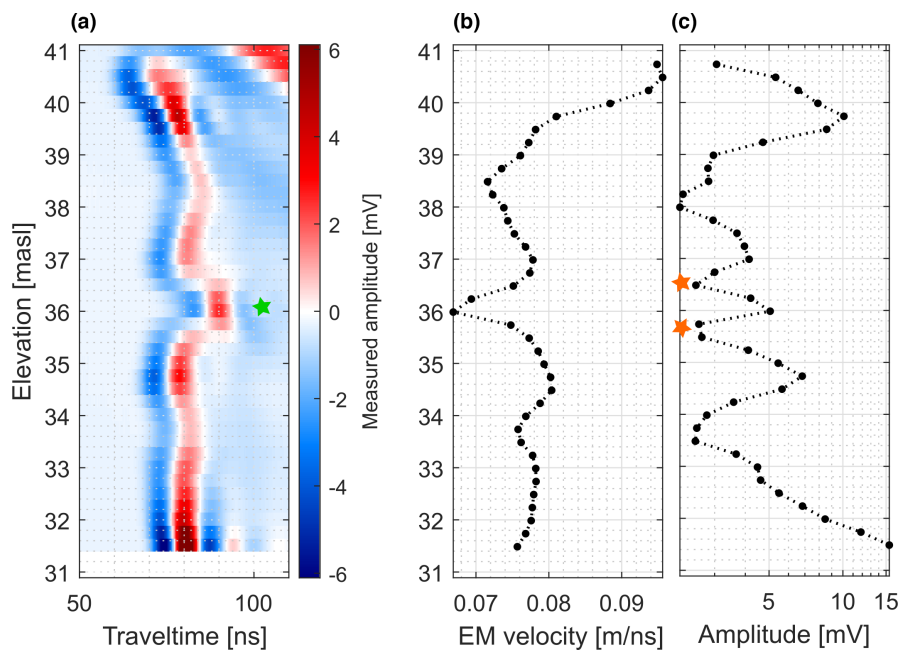


**Figure 4.** Zero-offset-profiling (ZOP) data collected between B302 and B303: (a) Recorded waveform data (radargram). Green asterisk indicates high amplitude arrivals later in the signal. (b) EM velocity. (c) Amplitude data, obtained from the raw waveform data. The orange asterisks marks destructive signal interference at both the upper and lower boundary of the silt layer. The ZOP data can be considered a 1D model, representing the average subsurface between the transmitter and receiver locations.

high amplitudes above 39 masl could be caused by either an increase in sand content, a decrease in water filled porosity or both.

The reason that the GPR method does not show abrupt changes is due to the sensitivity kernel of the propagating EM wave, that is, the propagating radar wave is affected by a volume of at least 0.5 m to all sides along the travel path of the radar wave, causing a smoothing of the recorded signal.

#### 2D Tomograms (Multi-Offset-Gather Data)

The results from the inversion of MOG traveltime and amplitude data collected at the field site between boreholes B302 and B303 are shown in Figure 5a and 5b. The water content tomogram in Figure 5a and 5c is estimated from the obtained slowness tomogram (not shown) and the electrical conductivity (EC) tomogram in Figure 5b and 5d is estimated from the obtained attenuation tomogram (not shown).

We observe diagonal streaking in the EC tomogram throughout the model area, most noticeable around 34 to 36 masl as indicated by the arrow in Figure 5b. These artifacts as well as the observed high contrasts in radar wave velocity caused by the silt layer, suggests that the linear inversion approach is challenged due to the presence of the low-velocity waveguide.

To avoid waveguide effects caused by the silt layer, we repeated the inversion with a reduced dataset. The water content and EC tomograms obtained from inversion of the reduced dataset are shown in Figure 5c and 5d, respectively. The area with no data coverage is cross-hatched and the variations in the tomograms at these depths are only a consequence of the chosen a priori information included in the inversion. The diagonal streaking is greatly reduced compared to the

full dataset tomogram and the structures recovered with the reduced dataset now correspond to the structures in the water content tomogram. The mean value of the water content tomogram is slightly shifted due to the large amount of data that are removed, but the recovered structures are consistent with the full dataset tomogram in Figure 5a.

We base our geological interpretation of the GPR results on the tomograms shown in Figure 5a and 5d. Overall, the vertical variations captured in the water content tomogram, Figure 5a, correspond well with the variations observed in the 1D velocity profile in Figure 4b. The transition from unsaturated to saturated conditions is again observed from the water content model between 40.5 and 39.5 masl, and the silt layer is recovered and clearly delineated as a layer with high water content at 36 masl. The estimated water content ranges between approximately 0.25 and 0.35 in the clay till, and 0.40 in the silt layer. In the saturated zone, the water content translates directly to porosity. The added information of the 2D water content tomograms, is primarily the thinning of the silt layer toward B302 that supports the observations in the borehole logs and the suggestion of a layer with higher water content, possibly connected, at 38.0 to 38.5 masl in B302 and at 38.5 to 39.0 masl in B303.

From the EC tomogram, Figure 5d, the subdivision of the lower till unit is confirmed, with a coherent layer of higher clay content (higher conductivity) at 34.3 to 33.3 masl and higher sand content (lower conductivity) above 34.3 masl. The transition zone to the sandy aquifer is not as evident as in the ZOP results (Figure 4). Above the silt layer, the high EC values above 20 mS/m at 38.0 to 38.5 masl in B302 and at 38.5 to 39.0 masl in B303, suggest a possibly connected layer. Apart from this, we do not see clear structure in the top till unit.

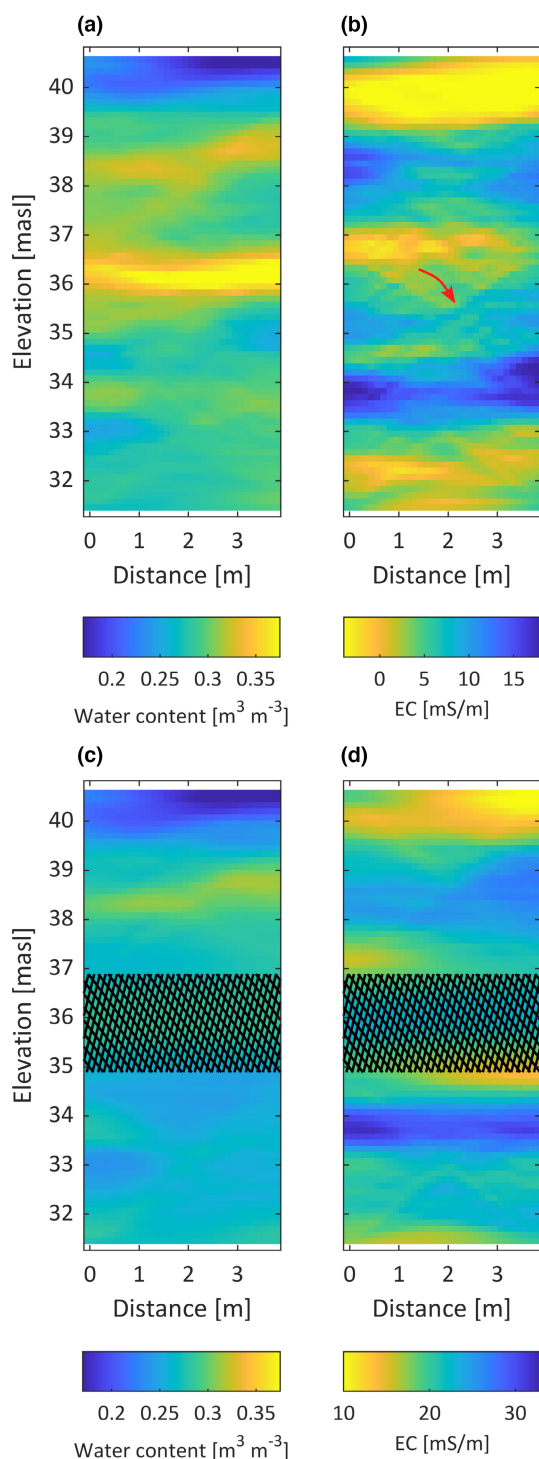


**Figure 5.** Two-dimensional tomograms obtained from inversion of Multi-Offset-Gather (MOG) data. Estimated water content tomogram and estimated electrical conductivity (EC) tomogram. Tomograms (a) and (b) are results from full dataset inversion. An area with diagonal streaking artifacts is indicated with the red arrow. Tomograms (c) and (d) are results from reduced dataset inversion where data between 34.9 and 36.9 masl are omitted to avoid influence from the silt layer.

### Updated Local Geological Model

An updated geological model between boreholes B302 and B303 was constructed based on the interpretation of the 1D GPR profiles as well as the 2D tomograms for water content and electrical conductivity. The updated model is

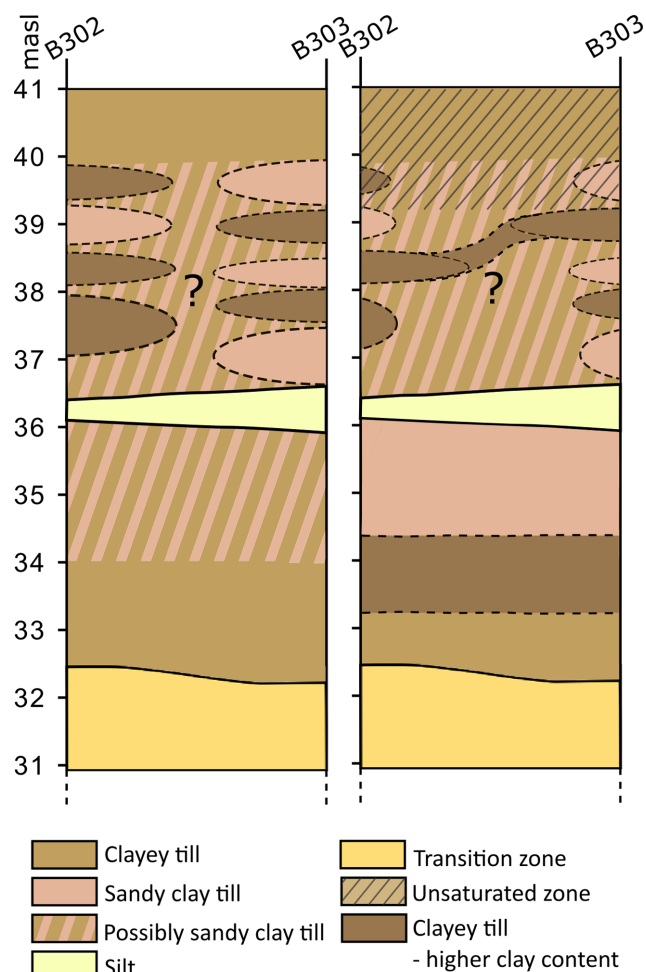


**Figure 6.** Original geological model (left) and updated conceptual geological model constructed on the basis of knowledge obtained from GPR data (right).

seen alongside the original interpretation in Figure 6. The silt layer coherency between the boreholes B302 and B303 and thinning toward B302, is confirmed from inversion of GPR travelttime data. The subdivision of the lower till unit is supported by the GPR amplitude data with a sandier clay till above 34.3 masl and a coherent layer of clayey till with higher clay content between 34.3 and 33.3 masl. The original interpretation of the transition zone below 32.5 masl is confirmed mainly by the GPR ZOP results.

In the upper till, the GPR results and the grain size data from the boreholes do not concur, and we therefore evaluate that these heterogeneities are not large enough to be resolved by GPR data. The size of these lenses has, therefore, been reduced in the updated geological model.

The only exception to the above is the layer observed at approximately 38 to 39 masl that is visible in both the water content and the EC tomogram. Whether the increase in EC is caused by either an increase in porosity, clay content, or both, is difficult to determine from the GPR data. However, the depth of this layer coincides with observations of higher clay/silt content in the grain size analyses from both boreholes. We therefore interpret a possibly connected clayey layer at this depth.

## Discussion

### The Use of Crosshole GPR to Refine the Geological Model

We used the results from the GPR data analysis to update the original interpretation of the geology and connect the borehole information as the GPR data provided valuable information on the subsurface geology between wells and thus allowed for a robust interpretation of the lateral connectivity. This study illustrated the added value of obtaining both a water content and an electrical conductivity tomogram. The two-dimensional water content model provided essential information about the subsurface porosity, and the obtained porosity values for the clay till are in line with reported values for clay till in Denmark (Aamand et al. 2022). The water content tomogram aided the delineation of the silt layer due to its high porosity, which arises from the well-sorted material. The water content tomogram did however not inform substantially on the geological variations of the remaining subsurface due to the fairly constant porosity in these areas. In contrast, the conductivity tomogram showed larger variability in these areas, which we interpreted as a result of variation in the clay content. Using this information, we were able to identify a continuous section with high clay content in the lower till unit, as well as sections less likely to be continuous in the upper till unit.

We did, however, observe challenges with the simple inversion routine, as the high contrast in water content (i.e., in EM velocity) was not included in the prior description and therefore caused artifacts in the conductivity tomogram (Hansen et al. 2014). To solve this, we omitted the data most affected by waveguide effects in the inversion. The subsurface area with no data coverage was therefore not resolved in the conductivity tomogram, instead, the water content tomogram informed on the geology in this depth interval. The consistency between the full and reduced water content tomograms implies that the linear inversion of traveltimes data is robust, even in the presence of pronounced velocity contrasts in the subsurface. Waveform data with late-arriving and high-amplitude elongated wave trains occur when a low-velocity layer is embedded in a geology with higher EM velocity (Klotzsche et al. 2012) and the waveguide effects therefore contain important information about the geology. Klotzsche et al. (2013) presented an amplitude analysis approach where the presence of waveguides as well as their upper and lower boundaries can be identified from direct analysis of the recorded waveform amplitudes, i.e. without the need for inversion of the data. This approach could be employed in this and future studies when low-velocity waveguides are suspected.

The investigated area between boreholes B302 and B303 is quite small compared to the area of the field site. This study is intended as a pilot study, and for future applications, the possibility of larger field scale GPR investigations should be explored. For this particular site, the lateral extension of the silt layer could be investigated across the site since it is easily detected in the ZOP data, given that boreholes with appropriate distances exist (up to 4 to 8 m depending on the geology). The depth of investigation is

limited by borehole depth and the GPR cable length, which is 30 m for the equipment used in this study.

Another cross-borehole geophysical method, frequently used for environmental application, is electrical resistivity tomography (ERT), often used in combination with induced polarization (IP). Similarly to the crosshole GPR method, crosshole resistivity methods have been applied for various purposes such as monitoring of in-situ remediation (e.g., Mao et al. 2016; Bording et al. 2021; Lévy et al. 2022) and mapping of possible contaminant flow paths in clay till (Bording et al. 2019). As mentioned previously, the resolution of resistivity tomography is, in contrast to GPR tomography, highest close to the boreholes (Day-Lewis et al. 2005). Crosshole resistivity and radar methods can therefore be used in combination since they provide complementary information for inversion and hydrogeological interpretation (e.g., Linde et al. 2006; Winship et al. 2006; Looms et al. 2008; Haarder et al. 2012; Cassiani et al. 2014). The electrodes used for ERT methods must be installed in specially made boreholes, and high contact resistance in the boreholes can negatively affect the data quality (Bording et al. 2019). While the initial installation of electrodes may be expensive and time-consuming, ERT data can be obtained almost autonomously after electrode installation. This allows for long-term monitoring campaigns as, for example, Lévy et al. (2022), where 10 data acquisition rounds were carried out over 2 years to monitor spreading of a remediation agent. Contrarily, crosshole GPR can be used in existing investigation wells, which make GPR attractive as a low-cost method to obtain additional information in ongoing site investigations.

### Method Advantages and Limitations

#### *Antennae Separation*

One limitation to consider when applying GPR at a contaminated site is the distance between the boreholes, since the signal is attenuated as it travels through the formation. In this study we measured a sufficient signal-to-noise level at a borehole distance of 3.81 m. Even for high angle traces in the MOG gather where the traveled distance is at least 5.3 m, the signal was sufficient. We estimate that in this type of geology, the boreholes could have been up to 6 m apart for ZOP investigations and 4.5 m for MOG investigations.

#### *Water in Wells*

The presence of water in the screened wells enforced the need for installing a packer system before conducting the GPR measurements. Dry boreholes are important for obtaining high-resolution tomograms in the saturated zone in clay till settings as the water downshifts the frequency content of the traveling EM wave and therefore reduces the possible resolution (Jensen et al. 2022b). The boreholes were pumped dry using a packer system that was made especially for this field campaign using off-the-shelf products and deployment was a bit tedious and time consuming. We consider the development of a packer system that is easy to install in existing, screened wells as an important step



toward field scale use of GPR at contaminated sites. Alternatively, an additional sealed inner tube could be inserted in the well given that the inner diameter of the well casing allows it. The antenna housing diameter is Ø29 mm and the minimum recommended borehole diameter is 33 mm. Despite this limitation, the fact that GPR can be deployed in existing investigation wells (with non-metallic casing), is a clear advantage.

#### *On-Site Evaluation of Data*

An advantage of the method when applied in the context of contaminated site investigations is the fast data acquisition and the possibility to obtain information about the subsurface between boreholes directly in the field, by visual inspection during data collection of one-dimensional ZOP data. Subsequent preliminary data processing of the 1D ZOP data can be done in 10 to 15 min.

#### *Equipment*

The GPR equipment is compact and easily transported. It fits into the back of a standard SUV, and can be set up in 10 to 15 min (see <https://youtu.be/VJDFdJBLvJ0>). The equipment can even be used indoors if required, for example, within a storage facility.

#### *Reproducibility*

Lastly, the GPR data are consistent when measurements are repeated. We evaluated the reproducibility of GPR data by plotting overlapping data acquired from (1) the first and (2) the second half of the MOG data acquisition against (3) the acquired ZOP data. The overlapping data were recorded approximately 1.5 h apart. The data fell along a straight line, as expected, and a linear model was fitted to the traveltime and amplitude data, respectively. For the traveltime data fit  $R^2 = 0.994$  and for the amplitude data fit  $R^2 = 0.993$ . This confirms that the acquired GPR data are reproducible and are not arbitrarily affected by industrial installations or by small deviations in antenna position and orientation.

## Conclusions

Crosshole GPR measurements were carried out at a contaminated site in a clay till setting to evaluate whether the GPR data analysis can provide valuable information about the geology between two selected boreholes located in a source zone. The GPR data analysis provided a strong guide for interpretation and validation of the existing data types (HPT data, grain size logs, borehole logs), and the analysis confirmed presumptions about the continuity of structures between boreholes in the lower till unit. The GPR data analysis resulted in a better understanding of the geological heterogeneity in the upper till.

The original interpretation of the geology between the boreholes was updated on the basis of the GPR results and the uncertainty of the conceptual geological model in our local investigation area was reduced, however not eliminated. The GPR investigation conducted at this site provides information that could be used to design a more targeted

uncertainty analysis of the hydraulic properties of the two till units and their impact on transport pathways.

With this pilot study, we show that the use of crosshole GPR at contaminated sites with complex geology can provide high-resolution information about the geology between the boreholes. The fast data acquisition and the novel efficient data processing make GPR investigations attractive to use as a low-cost additional source of information in ongoing contaminated sites investigations. Furthermore, GPR can be used at industrial and urban sites where infrastructure, such as pipes and electrical installations, can pose a challenge to other geophysical methods.

A pilot study like this could be extended by upscaling of the GPR method and the results could, as a logical next step, be related to contaminant transport at clayey till sites.

## Acknowledgments

This work was funded by the Capital Region of Denmark and the Innovation Fund DK under the Industrial PhD Program, Grant #7091-00007B. We thank Espen Bing Svendsen, Peer Jørgensen, Paul Christiansen, and Simon Hansen for invaluable technical assistance in the field.

## Supporting Information

Additional Supporting Information may be found in the online version of this article. Supporting Information is generally not peer reviewed.

**Data S1.** Details on HPT data, grain size analyses and inversion.

## References

- Aamand, J., N. Badawi, P.R. Jakobsen, P.R.R. Jørgensen, K. Mosthaf, L. Trolborg, and M. Rolle. 2022. Mapping groundwater vulnerability to pesticide contamination through fractured clays – CLAYFRAC. Pesticides Research No. 206. Danish Environmental Protection Agency.
- Alumbaugh, D., P.Y. Chang, L. Paprocki, J.R. Brainard, R.J. Glass, and C.A. Rautman. 2002. Estimating moisture contents in the vadose zone using cross-borehole ground penetrating radar: A study of accuracy and repeatability. *Water Resources Research* 38, no. 12: 45-1-45-12. <https://doi.org/10.1029/2001wr000754>
- Annan, A.P. 2005. GPR methods for hydrogeological studies. In *Hydrogeophysics*, 185-213. Dordrecht: Springer. [https://doi.org/10.1007/1-4020-3102-5\\_7](https://doi.org/10.1007/1-4020-3102-5_7)
- Bording, T., A.K. Kühn, G. Fiandaca, J.F. Christensen, A.V. Christensen, and E. Auken. 2021. Cross-borehole geoelectrical time-lapse monitoring of in situ chemical oxidation and permeability estimation through induced polarization. *Near Surface Geophysics* 19, no. 1: 43-58. <https://doi.org/10.1002/nsg.12131>
- Bording, T.S., G. Fiandaca, P.K. Maurya, E. Auken, A.V. Christensen, N. Tuxen, K. Erik, et al. 2019. Cross-borehole tomography with full-decay spectral time-domain induced polarization for mapping of potential contaminant flow-paths. *Journal of Contaminant Hydrology* 226: 103523. <https://doi.org/10.1016/j.jconhyd.2019.103523>
- Cassiani, G., A. Binley, A. Kemna, M. Wehrer, A.F. Orozco, R. Deiana, J. Boaga, M. Rossi, P. Dietrich, U. Werban, L. Zschornack, A. Godio, A. JafarGandomi, and G.P. Deidda. 2014. Noninvasive characterization of the Trecate (Italy) crude-oil contaminated

- site: Links between contamination and geophysical signals. *Environmental Science and Pollution Research* 21, no. 15: 8914–8931. <https://doi.org/10.1007/s11356-014-2494-7>
- Chang, P.Y., D. Alumbaugh, J. Brainard, and L. Hall. 2006. Cross-borehole ground-penetrating radar for monitoring and imaging solute transport within the vadose zone. *Water Resources Research* 42, no. 10: 1–16. <https://doi.org/10.1029/2004WR003871>
- Damgaard, I., P.L. Bjerg, J. Bælum, C. Scheutz, D. Hunkeler, C.S. Jacobsen, N. Tuxen, and M.M. Broholm. 2013. Identification of chlorinated solvents degradation zones in clay till by high resolution chemical, microbial and compound specific isotope analysis. *Journal of Contaminant Hydrology* 146: 37–50. <https://doi.org/10.1016/j.jconhyd.2012.11.010>
- Day-Lewis, F.D., K. Singha, and A.M. Binley. 2005. Applying petrophysical models to radar travel time and electrical resistivity tomograms: Resolution-dependent limitations. *Journal of Geophysical Research Atmospheres* 110, no. 8: 1–17. <https://doi.org/10.1029/2004JB003569>
- Eppstein, M.J., and D.E. Dougherty. 1998. Efficient three-dimensional data inversion: Soil characterization and moisture monitoring from cross-well ground-penetrating radar at a Vermont test site. *Water Resources Research* 34, no. 8: 1889–1900. <https://doi.org/10.1029/98WR00776>
- Gee, G.W., and J.W. Bauder. 1986. Particle-size analysis. In *Methods of Soil Analysis, Part 1: Physical and Mineralogical Methods*, ed. A. Klute. Madison, WI, USA: Soil Science Society of America. <https://doi.org/10.2136/SSABOOKSER5.1.2ED.C15>
- Giroux, B., E. Gloaguen, and M. Chouteau. 2007. Bh\_tomo-a Matlab borehole Georadar 2D tomography package. *Computers and Geosciences* 33, no. 1: 126–137. <https://doi.org/10.1016/j.cageo.2006.05.014>
- Gueting, N., T. Vienken, A. Klotzsche, J. van der Kruk, J. Vanderborght, J. Caers, H. Vereecken, and A. Englert. 2017. High resolution aquifer characterization using crosshole GPR full-waveform tomography: Comparison with direct-push and tracer test data. *Water Resources Research* 53, no. 1: 49–72. <https://doi.org/10.1002/2016WR019498>
- Haarder, E.B., A. Binley, M.C. Looms, J. Doetsch, L. Nielsen, and K.H. Jensen. 2012. Comparing plume characteristics inferred from cross-borehole geophysical data. *Vadose Zone Journal* 11, no. 4. <https://doi.org/10.2136/vzj2012.0031>
- Hansen, T.M., K.S. Cordua, B.H. Jacobsen, and K. Mosegaard. 2014. Accounting for imperfect forward modeling in geophysical inverse problems—Exemplified for Crosshole tomography. *Geophysics* 79, no. 3: H1–H21. <https://doi.org/10.1190/geo2013-0215.1>
- Hansen, T.M., K.S. Cordua, M.C. Looms, and K. Mosegaard. 2013. SIPPI: A Matlab toolbox for sampling the solution to inverse problems with complex prior information: Part I—methodology. *Computers and Geosciences* 52: 470–480. <https://doi.org/10.1016/j.cageo.2012.09.004>
- Hansen, T.M., M.C. Looms, and L. Nielsen. 2008. Inferring the subsurface structural covariance model using cross-borehole ground penetrating radar tomography. *Vadose Zone Journal* 7, no. 1: 249–262. <https://doi.org/10.2136/vzj2006.0144>
- Harrington, G.A., M. Jim Hendry, and N.I. Robinson. 2007. Impact of permeable conduits on solute transport in aquitards: Mathematical models and their application. *Water Resources Research* 43, no. 5: 5441. <https://doi.org/10.1029/2005WR004144>
- Holliger, K., M. Musil, and H.R. Maurer. 2001. Ray-based amplitude tomography for crosshole georadar data: A numerical assessment. *Journal of Applied Geophysics* 47: 285–298.
- Houmark-Nielsen, M. 2010. Extent, age and dynamics of marine isotope stage 3 glaciations in the southwestern Baltic Basin. *Boreas* 39, no. 2: 343–359. <https://doi.org/10.1111/j.1502-3885.2009.00136.x>
- Høyser, A.S., K.E.S. Klint, G. Fiandaca, P.K. Maurya, A.V. Christiansen, N. Balbarini, P.L. Bjerg, T.B. Hansen, and I. Møller. 2019. Development of a high-resolution 3D geological model for landfill leachate risk assessment. *Engineering Geology* 249, no. January: 45–59. <https://doi.org/10.1016/j.enggeo.2018.12.015>
- Hubbard, S.S., J. Chen, J. Peterson, E.L. Majer, K.H. Williams, D.J. Swift, B. Mailloux, and Y. Rubin. 2001. Hydrogeological characterization of the south oyster bacterial transport site using geophysical data. *Water Resources Research* 37, no. 10: 2431–2456. <https://doi.org/10.1029/2001WR000279>
- Huisman, J.A., S.S. Hubbard, J.D. Redman, and A.P. Annan. 2003. Measuring soil water content with ground penetrating Radar: A review. *Vadose Zone Journal* 2, no. 4: 476–491. <https://doi.org/10.2113/2.4.476>
- Jensen, B.B., T.M. Hansen, L. Nielsen, K.S. Cordua, N. Tuxen, A. Tsitonaki, and M.C. Looms. 2022a. Accounting for modeling errors in linear inversion of crosshole ground-penetrating radar amplitude data: Detecting sand in clayey till. *Journal of Geophysical Research: Solid Earth* 127, no. 10: e2022JB024666. <https://doi.org/10.1029/2022JB024666>
- Jensen, B.B., L. Rosenberg, L. Nielsen, N. Tuxen, A. Tsitonaki, T.M. Hansen, and M.C. Looms. 2022b. The impact of water-filled boreholes on GPR data in a clayey-till environment. In *Global Meeting Abstracts*, 119–122. Golden, CO, USA: Society of Exploration Geophysicists. <https://doi.org/10.1190/GPR2022-061.1>
- Jørgensen, P.R., M. Hoffmann, J.P. Kistrup, C. Bryde, R. Bossi, and K.G. Villholth. 2002. Preferential flow and pesticide transport in a clay-rich till: Field, laboratory, and modeling analysis. *Water Resources Research* 38, no. 11: 28–1–28–15. <https://doi.org/10.1029/2001WR000494>
- Kessler, T.C. 2012. *Hydrogeological Characterization of Low-Permeability Clayey Tills – The Role of Sand Lenses*. Lyngby, Denmark: Technical University of Denmark.
- Kessler, T.C., K.E.S. Klint, B. Nilsson, and P.L. Bjerg. 2012. Characterization of sand lenses embedded in tills. *Quaternary Science Reviews* 53: 55–71. <https://doi.org/10.1016/j.quascirev.2012.08.011>
- Klint, K.E.S., B. Nilsson, L. Trolldborg, and P.R. Jakobsen. 2013. A poly morphological landform approach for hydrogeological applications in heterogeneous glacial sediments. *Hydrogeology Journal* 21, no. 6: 1247–1264. <https://doi.org/10.1007/S10040-013-1011-2/FIGURES/13>
- Klotzsche, A., J. van der Kruk, N. Linde, J. Doetsch, and H. Vereecken. 2013. 3-D characterization of high-permeability zones in a gravel aquifer using 2-D crosshole GPR full-waveform inversion and waveguide detection. *Geophysical Journal International* 195, no. 2: 932–944. <https://doi.org/10.1093/gji/ggt275>
- Klotzsche, A., J. van der Kruk, G. Meles, and H. Vereecken. 2012. Crosshole GPR full-waveform inversion of waveguides acting as preferential flow paths within aquifer systems. *Geophysics* 77, no. 4: H57–H62. <https://doi.org/10.1190/geo2011-0458.1>
- Lévy, L., R. Thalund-Hansen, T. Bording, G. Fiandaca, A.V. Christiansen, K. Rügge, N. Tuxen, M. Hag, and P.L. Bjerg. 2022. Quantifying reagent spreading by cross-borehole electrical tomography to assess performance of groundwater remediation. *Water Resources Research* 58, no. 9: e2022WR032218. <https://doi.org/10.1029/2022WR032218>
- Linde, N., A. Binley, A. Tryggvason, L.B. Pedersen, and A. Revil. 2006. Improved hydrogeophysical characterization using joint inversion of cross-hole electrical resistance and ground-penetrating radar traveltimes data. *Water Resources Research* 42, W12404. <https://doi.org/10.1029/2006WR005131>
- Looms, M.C., A. Klotzsche, J. van der Kruk, T.H. Larsen, A. Edsen, N. Tuxen, N. Hamburger, J. Keskinen, and L. Nielsen. 2018. Mapping sand layers in clayey till using crosshole

- ground-penetrating radar. *Geophysics* 83, no. 1: A21–A26. <https://doi.org/10.1190/GEO2017-0297.1>
- Looms, M.C., T.M. Hansen, K.S. Cordua, L. Nielsen, K.H. Jensen, and A. Binley. 2010. Geostatistical inference using crosshole ground-penetrating radar. *Geophysics* 75, no. 6: J29–J41. <https://doi.org/10.1190/1.3496001>
- Looms, M.C., A. Binley, K.H. Jensen, L. Nielsen, and T.M. Hansen. 2008. Identifying unsaturated hydraulic parameters using an integrated data fusion approach on cross-borehole geophysical data. *Vadose Zone Journal* 7, no. 1: 238–248. <https://doi.org/10.2136/vzj2007.0087>
- Mao, D., L. Lu, A. Revil, Y. Zuo, J. Hinton, and Z.J. Ren. 2016. Geophysical monitoring of hydrocarbon-contaminated soils remediated with a bioelectrochemical system. *Environmental Science and Technology* 50, no. 15: 8205–8213. <https://doi.org/10.1021/acs.est.6b00535>
- Maurya, P.K., N. Balbarini, I. Møller, V. Rønde, A.V. Christiansen, P.L. Bjerg, E. Auken, and G. Fiandaca. 2018. Subsurface imaging of water electrical conductivity, hydraulic permeability and lithology at contaminated sites by induced polarization. *Geophysical Journal International* 213, no. 2: 770–785. <https://doi.org/10.1093/GJI/GGY018>
- McCabe, A.M. 1987. Quaternary deposits and glacial stratigraphy in Ireland. *Quaternary Science Reviews* 6, no. 3–4: 259–299. [https://doi.org/10.1016/0277-3791\(87\)90008-4](https://doi.org/10.1016/0277-3791(87)90008-4)
- McCall, W., and T.M. Christy. 2020. The hydraulic profiling tool for hydrogeologic investigation of unconsolidated formations. *Groundwater Monitoring & Remediation* 40, no. 3: 89–103. <https://doi.org/10.1111/gwmr.12399>
- McCall, W., T.M. Christy, D. Pipp, M. Terkelsen, A. Christensen, K. Weber, and P. Engelsen. 2014. Field application of the combined membrane-Interface probe and hydraulic profiling tool (MiHpt). *Groundwater Monitoring & Remediation* 34, no. 2: 85–95. <https://doi.org/10.1111/gwmr.12051>
- McKay, L.D., J.A. Cherry, and R.W. Gillham. 1993. Field experiments in a fractured clay till: 1. Hydraulic conductivity and fracture aperture. *Water Resources Research* 29, no. 4: 1149–1162. <https://doi.org/10.1029/92WR02592>
- Molyneux, J.B., and D.R. Schmitt. 1999. First-break timing: Arrival onset times by direct correlation. *Geophysics* 64, no. 5: 1492–1501. <https://doi.org/10.1190/1.1444653>
- NIRAS. 2019. *Afgrænsende Forureningsundersøgelse Industrivej 2, 3540 Lyngby*. Hillerød, Denmark: Region Hovedstaden.
- Oberröhrmann, M., A. Klotzsche, H. Vereecken, and J. Van Der Kruk. 2013. Optimization of acquisition setup for cross-hole GPR full-waveform inversion using checkerboard analysis. *Near Surface Geophysics* 11, no. 2: 197–209. <https://doi.org/10.3997/1873-0604.2012045>
- Peterson, J.E. 2001. Pre-inversion corrections and analysis of radar tomographic data. *Journal of Environmental and Engineering Geophysics* 6, no. 1: 1–18. <https://doi.org/10.4133/JEEG6.1.1>
- Reynolds, J.M. 2011. *An Introduction to Applied and Environmental Geophysics*, 2nd ed. West Sussex, UK: Wiley-Blackwell.
- Rosenberg, L., K. Mosthaf, M.M. Broholm, A.S. Fjordbøge, N. Tuxen, I.H. Kernn-Jespersen, V. Rønde, and P.L. Bjerg. 2023. A novel concept for estimating the contaminant mass discharge of chlorinated ethenes emanating from clay till sites. *Journal of Contaminant Hydrology* 252: 104121. <https://doi.org/10.1016/J.JCONHYD.2022.104121>
- Rosenberg, L., M.M. Broholm, N. Tuxen, I.H. Kernn-Jespersen, G. Lilbæk, and P.L. Bjerg. 2022. Vertical hydraulic gradient estimation in clay till, using MiHPT advanced direct-push technology. *Groundwater Monitoring & Remediation*. John Wiley & Sons, Ltd., 42: 29–37. <https://doi.org/10.1111/gwmr.12470>
- Shaw, J. 1987. Glacial sedimentary processes and environmental reconstruction based on lithofacies. *Sedimentology* 34, no. 1: 103–116. <https://doi.org/10.1111/J.1365-3091.1987.TB00563.X>
- Slater, L., A.M. Binley, W. Daily, and R. Johnson. 2000. Cross-hole electrical imaging of a controlled saline tracer injection. *Journal of Applied Geophysics* 44, no. 2–3: 85–102. [https://doi.org/10.1016/S0926-9851\(00\)00002-1](https://doi.org/10.1016/S0926-9851(00)00002-1)
- Stelman, C.M., J.R. Meyer, P. Wanner, B.J. Swanson, O. Conway-White, and B.L. Parker. 2020. The importance of transects for characterizing aged organic contaminant plumes in groundwater. *Journal of Contaminant Hydrology* 235: 103728. <https://doi.org/10.1016/J.JCONHYD.2020.103728>
- Svendsen, E.B., L. Nielsen, B. Nilsson, K.H. Kjær, and M.C. Looms. 2023. Crosshole ground-penetrating radar in clay-rich quaternary deposits: Towards characterization of high-loss media. *Journal of Geophysical Research: Solid Earth* 128: e2022JB025909. <https://doi.org/10.1029/2022JB025909>
- Tarantola, A. 2005. *Inverse Problem Theory and Methods for Model Parameter Estimation*. Philadelphia: Society for Industrial and Applied Mathematics. <https://doi.org/10.1137/1.9780898717921>
- Topp, G.C., J.L. Davis, and A.P. Annan. 1980. Electromagnetic determination of soil water content: Measurements in coaxial transmission lines. *Water Resources Research* 16, no. 3: 574–582. <https://doi.org/10.1029/WR016i003p00574>
- Wang, Y., and Y. Rao. 2006. Crosshole seismic waveform tomography-I. Strategy for real data application. *Geophysical Journal International* 166: 1224–1236. <https://doi.org/10.1111/j.1365-246X.2006.03030.x>
- Winship, P., A. Binley, and D. Gomez. 2006. Flow and transport in the unsaturated Sherwood sandstone: Characterization using cross-borehole geophysical methods. *Geological Society Special Publication* 263: 219–231. <https://doi.org/10.1144/GSL.SP.2006.263.01.12>
- Zhou, Z., A. Klotzsche, T. Hermans, F. Nguyen, J. Schmäck, P. Haruzi, H. Vereecken, and J. Van Der Kruk. 2020. 3D aquifer characterization of the Hermalle-Sous-Argenteau test site using crosshole ground-penetrating radar amplitude analysis and full-waveform inversion. *Geophysics* 85, no. 6: H133–H148. <https://doi.org/10.1190/geo2020-0067.1>

## Biographical Sketches

**Bolette Badsberg Jensen**, corresponding author, is at WSP, 2630 Taastrup, Denmark; [bolette.jensen@wsp.com](mailto:bolette.jensen@wsp.com).

**Louise Rosenberg**, is at the Technical University of Denmark, Department of Environmental and Resource Engineering, 2800 Kgs. Lyngby, Denmark.

**Aikaterini Tsitonaki**, is at WSP Denmark, 2630 Taastrup, Denmark.

**Nina Tuxen**, is at the Capital Region of Denmark, 3400 Hillerød, Denmark.

**Poul L. Bjerg**, is at the Technical University of Denmark, Department of Environmental and Resource Engineering, 2800 Kgs. Lyngby, Denmark.

**Lars Nielsen**, is at Geological Survey of Denmark and Greenland, 1350 Kbh K, Denmark.

**Thomas M. Hansen**, is at Aarhus University, Department of Geosciences, 8000 Århus, Denmark.

**Majken C. Looms**, is at University of Copenhagen, Department of Geosciences and Natural Resource Management, 1350 Kbh K, Denmark.







# IV

## Quantification of Contaminant Mass Discharge from Point Sources in Aquitard/Aquifer Systems based on Vertical Concentration Profiles and 3D Modeling

Klaus Mosthaf, Louise Rosenberg, Mette M. Broholm, Gro Lilbæk, Anders. G. Christensen, Annika S. Fjordbøge, Poul L. Bjerg

Submitted

1  
2 **Quantification of contaminant mass discharge from point sources in**  
3 **aquitard/aquifer systems based on vertical concentration profiles and 3D modeling**  
4

5 **Klaus Mosthaf<sup>1,\*</sup>, Louise Rosenberg<sup>1</sup>, Mette M. Broholm<sup>1</sup>, Annika S. Fjordbøge<sup>1</sup>,**  
6 **Gro Lilbæk<sup>2</sup>, Anders G. Christensen<sup>2</sup>, Poul L. Bjerg<sup>1</sup>**

7  
8 <sup>1</sup> Department of Environmental and Resource Engineering, Technical University of Denmark,  
9 Bygningstorvet, 2800 Kgs. Lyngby, Denmark.

10 <sup>2</sup> NIRAS, Sortemosevej 19, 3450 Allerød, Denmark.

11  
12 Corresponding author: Klaus Mosthaf ([klmos@dtu.dk](mailto:klmos@dtu.dk))  
13  
14  
15  
16  
17  
18  
19  
20  
21  
22  
23  
24  
25  
26  
27  
28  
29  
30  
31

32 **Key Points: (3 points, max 140 characters each)**

- 33
- 34 • 3D solute transport modeling of comprehensive field data covering a chlorinated ethene  
contamination source in a clayey till and the plume
  - 35 • Vertical concentration profiles and modeling quantify contaminant mass discharge,  
36 infiltration rate, and vertical hydraulic conductivity
  - 37 • Contaminant leaching from a clayey till with or without fractures causes very different  
38 evolution of the plume in the underlying aquifer  
39



**40 Abstract (max 250 words)**

41 Point sources with contaminants, such as chlorinated solvents or pesticides, are often located in  
42 low-permeability aquitards, where they can act as long-term sources and threaten underlying  
43 groundwater resources. We demonstrate the use of a 3D numerical model integrating  
44 hydrogeological and contamination data to determine the contaminant mass discharge (CMD)  
45 from a point source in a clayey-till aquitard. The quantitative determination is facilitated by  
46 model calibration to high-resolution vertical concentration profiles obtained by advanced direct-  
47 push sampling techniques in the aquifer downgradient of the chlorinated solvent source zone.  
48 The concentration profiles showed a characteristic plume sinking with distance from the source  
49 caused by the interplay between infiltrating water and horizontal groundwater flow. The  
50 combination of 3D solute transport modeling and high-resolution data was utilized to interpret  
51 measurements and determine the infiltration rate, hydraulic conductivity in the clayey till, and,  
52 ultimately, the CMD. The model could consistently reproduce the plume sinking with distance  
53 from the source. Different source zone conceptualizations demonstrated the effects of fractures  
54 and sorption in the source zone on the CMD and the temporal development of the contamination  
55 in the aquifer. The presence of fractures in the aquitard had a minor influence on the currently  
56 determined CMD. Still, a thorough characterization of the source zone conditions is key for  
57 shedding light on the probable future development of the contamination.

**58 1 Introduction**

59 Clean groundwater is a scarce resource in many places worldwide. It is under pressure  
60 from overexploitation and ubiquitous contamination from diffuse sources and point sources of  
61 organic and inorganic pollutants. Contaminated sites with point sources of dissolved pollutants  
62 originating from spills or industrial activity can be found all over the world and pose a severe  
63 threat to the quality of groundwater resources. Often, dissolved contaminants are stored and  
64 leach slowly from low-permeability soils (aquitards) like clayey tills due to sorption, slow  
65 advective transport, and matrix diffusion into less conductive zones. These processes can lead to  
66 a long-term contaminant release to an adjacent aquifer (Chambon et al., 2010; Chapman &  
67 Parker, 2005; Falta, 2005; Muniruzzaman & Rolle, 2021) and pose substantial mass-transfer  
68 limitations for remedial actions at contaminated sites (Seyedabbasi et al., 2012). Hydrogeological  
69 settings with an aquitard overlying an aquifer are widespread in many countries in the northern  
70 hemisphere, e.g., in Canada, China, Denmark, Italy, Poland, USA (Chapman et al., 2018;  
71 Filippini et al., 2020; Harrison et al., 1992; Klint et al., 2013; Szymkiewicz et al., 2019; Young et  
72 al., 2019).

73 Solute transport models are valuable tools for studying contaminant transport processes  
74 in the subsurface from point sources. They have been applied in 1D, 2D, or even 3D to a  
75 multitude of subsurface contamination applications, such as leaching from a NAPL source zone  
76 (Basu et al., 2008; L. Yang et al., 2018), sorption and degradation (Højberg et al., 2005;  
77 Prommer et al., 2006) and geochemical reactions in aquifers (Kruisdijk & van Breukelen, 2021;  
78 Muniruzzaman & Rolle, 2019). Of particular interest for this paper, Chapman & Parker (2005)  
79 simulated concentration profiles of a dissolved chlorinated ethene DNAPL source. The focus  
80 was on contaminant back-diffusion from an underlying aquitard to the aquifer. Prommer et al.  
81 (2006, 2009) applied a 2D reactive transport model to interpret BTEX and PAH degradation in a  
82 plume combining modeling and vertical concentration profile data from downgradient of the  
83 source zone. They considered an immobile NAPL source in the aquifer with mass transfer to the

84 aqueous phase. The studies mentioned above reported on either the source zone or the plume, did  
85 not consider the interplay between aquitard and underlying aquifer, did not encompass fractures  
86 in the aquitard, and were typically in 2D.

87 The further advancement of computer technologies and modeling tools increasingly  
88 permitted to study flow and transport processes in all three dimensions. Already in 1987 Burnett  
89 and Frind (1987) pointed out the importance of studying point sources in 3D. Parker & Park  
90 (2004) used a heterogeneous 3D percolation model to simulate the development of a DNAPL  
91 spill in the source zone. Recently, Parker et al. (2022) simulated a field experiment to determine  
92 effective diffusion coefficients of chlorohydrocarbons in natural clays, and Yang et al. (2022)  
93 investigated the effect of permeable reactive barriers on groundwater flow and contaminant  
94 transport using 3D numerical models. None of these studies has applied a 3D transport model in  
95 combination with depth-discrete contaminant concentration profiles to determine the  
96 contaminant mass discharge (CMD) from a point source, focusing on both the source zone in an  
97 aquitard and the plume in the aquifer.

98 The hydraulic conditions in the source zone have a crucial influence on the contaminant  
99 spreading in the aquifer (Gueting & Englert, 2013). Low-permeability soils like clayey tills are  
100 often heterogeneous and may contain hydraulically active fractures (Fredericia, 1990; Jørgensen,  
101 Helstrup, et al., 2004; Kessler et al., 2012; Mckay & Fredericia, 1995) that can act as preferential  
102 transport pathways for contaminants. Numerical models can account for fractures in different  
103 ways, either in a volume-averaged manner (e.g., dual-continuum models) or resolving them as  
104 discrete features (Berkowitz, 2002; Berre et al., 2019; Flemisch et al., 2017; Helmke et al.,  
105 2005). Discrete fracture-matrix (DFM) models include fractures as geometric entities embedded  
106 in the matrix domain and have been widely used to simulate flow and transport in fractured  
107 porous media (Blessent et al., 2014; Hu et al., 2022; Mosthaf et al., 2021; Therrien & Sudicky,  
108 1996). Such models can be used for a detailed representation of flow and transport in fractured  
109 soils, as they simulate the processes in both fractures and matrix and account for the mutual  
110 exchange fluxes. In DFM models, the cubic law (Snow, 1969; Witherspoon et al., 1980) is  
111 typically used to describe the relation between fracture hydraulic aperture and fracture hydraulic  
112 conductivity and, thus, flux in the fracture.

113 The CMD from a contaminant source is useful for assessing the risk a contaminated site  
114 poses to the groundwater (Horst et al., 2021). Several methods to determine the CMD have been  
115 proposed (Einarson & Mackay, 2001; Newell et al., 2011). Usually, a transect with a series of  
116 sampling wells is installed downgradient of the contaminant source to measure concentrations,  
117 hydraulic head gradients, and hydraulic conductivities in a control plane (Brusseau et al., 2013;  
118 Einarson et al., 2010; Troldborg et al., 2010), and the local fluxes are added up. Direct-push tools  
119 like the membrane interface probe hydraulic profiling tool, MiHPT (McCall & Christy, 2020),  
120 the Waterloo™ Advanced Profiling System (APS) (Adamson et al., 2015), or the groundwater  
121 profiler system (GWP) from Geoprobe® can be used for a detailed shallow subsurface  
122 characterization (e.g., in the upper 10-15 m). Such tools can provide valuable data about the  
123 depth-discrete distribution of hydraulic properties and contaminant concentrations (McCall et al.,  
124 2014) at a high resolution in a time-efficient manner.

125 The CMD from a point source strongly depends on the vertical water fluxes through the  
126 source zone; thus, an accurate determination of the local net infiltration rate is key for  
127 determining the CMD from an aquitard. Infiltration rates to aquitards can be determined at a  
128 larger scale in water balance models (Cherkauer, 2004; Manghi et al., 2009). The rates can be

129 highly variable in time and space (Waldowski et al., 2023). A more local determination requires  
130 knowledge of the local hydrogeologic conditions, including the vertical hydraulic conductivity  
131 and vertical hydraulic gradient. However, the physical testing to determine these properties in  
132 aquitards can be challenging and take a long time due to the low hydraulic conductivity of the  
133 aquitard and inherent heterogeneities and fractures (Chapman et al., 2018; Keller et al., 1989;  
134 Young et al., 2021). The determination of vertical hydraulic gradients in aquitards usually  
135 requires short well screens at different depths. Recently, Rosenberg et al. (2022) have used a  
136 direct-push hydraulic profiling tool (McCall et al., 2014; Sale et al., 2013) instead to determine  
137 vertical hydraulic gradients across a clayey-till layer.

138 The objective of this study was to demonstrate the strength and capability of a 3D  
139 numerical solute transport model to quantitatively characterize the contaminant leaching and  
140 spreading from a contamination source in a water-saturated, low-permeability geological layer  
141 (aquitard) into an underlying groundwater aquifer. In particular, the study aims to (1)  
142 demonstrate the use of a 3D solute transport model combined with depth-discrete concentration  
143 measurements to investigate transport processes in an aquitard/aquifer system; (2) apply a 3D  
144 model to determine CMD, as well as the relation between source concentrations, hydraulic  
145 properties and the CMD; and (3) demonstrate the effects of the specific conceptualization of the  
146 source zone in the aquitard (fractures, sorption properties) on the temporal development of the  
147 contamination in the aquifer.

148 We applied and extended the approach presented in Rosenberg et al. (2023) to quantify  
149 the CMD based on the measurement of vertical concentration profiles in a contaminant plume  
150 and numerical modeling. In Rosenberg et al. (2023), 2D modeling was applied, and a screening  
151 method was developed. Here, we included a more comprehensive set of hydrogeological and  
152 contaminant data in a detailed 3D model encompassing both the source zone and plume in an  
153 aquitard/aquifer system. The calibrated solute transport model was used to simultaneously  
154 determine the infiltration rate, vertical hydraulic conductivity in the aquitard, and CMD from the  
155 source to downgradient locations in the aquifer. The 3D model, in combination with submodels  
156 of the source zone, also demonstrated the potential effect of fractures in the aquitard on source  
157 depletion, plume evolution, and CMD.

## 158 **2 Materials and Methods**

### 159 **2.1 Field site, hydrogeological and contaminant data**

160 The extensive field and laboratory investigations of a trichloroethylene (TCE)  
161 contaminated site located in an industrial area about 30 km north of Copenhagen, Denmark  
162 (**Figure 1a**), were used as background for the 3D solute transport modeling in this study. At the  
163 site, a Styrofoam factory hall was completed in 1971. TCE was released close to the factory hall  
164 to the subsurface, likely caused by handling a pre-polymer containing TCE. The release resulted  
165 in a source zone with high TCE concentrations ( $> 3000 \mu\text{g/L}$ ) in the clayey till. It led to the  
166 evolution of a long and relatively narrow contaminant plume in the underlying sandy aquifer  
167 (**Figure 1b-d**), which passed by underneath the factory building. The handling of the pre-  
168 polymer stopped in 1996 and the storage barrels for the pre-polymer were removed. Thus, the  
169 period of TCE input to the subsurface was assumed to have happened over approximately 26  
170 years (1971-1996).

## 171 2.2 Geological and hydrogeological setting

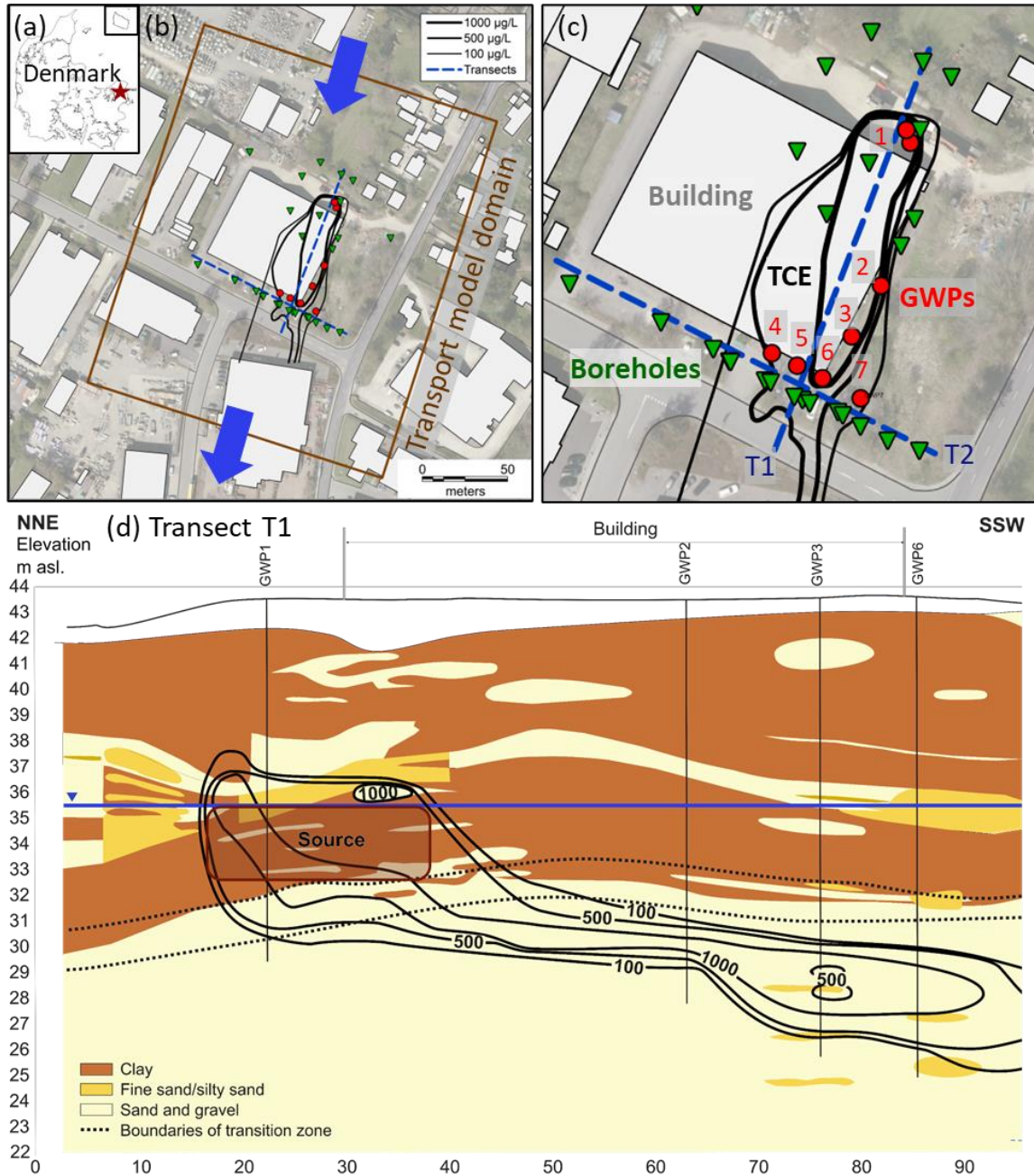
172 The geological setting considered in this study consists of a clayey-till aquitard overlying  
173 a confined sandy aquifer with strong hydraulic conductivity contrast. The thickness of the  
174 saturated clayey-till layer is 4-5 m, while the sandy aquifer is more than 35 m thick, underlain by  
175 a limestone aquifer. A thin sand layer and sandy inclusions can be found on top of the saturated  
176 clayey till. In the center of the factory hall and in the source zone in front of the factory building,  
177 multilevel wells with screens in the sand layer on top of the clayey till and in the aquifer were  
178 used to determine vertical hydraulic gradients below and around the building. The flow field was  
179 determined in synchronous monitoring well soundings in a larger area around the source zone.  
180 Infiltrating water caused predominantly vertical flow in the clayey-till aquitard, while horizontal  
181 flow prevailed in the aquifer. The average horizontal hydraulic gradient and the average flow  
182 direction at the site were determined with the spreadsheet tool described in Devlin (2015).

183 The cross-section of the studied field site in the flow direction (**Figure 1d**, transect T1)  
184 gives an overview of the considered geological setting, with a transition zone between clayey till  
185 and sandy aquifer with a varying thickness of 1-2 meters. The interpretation of the geological  
186 setting at the site was based on a rich set of measurements, including borehole logs, analysis of  
187 soil core samples, slug tests, soil samples, and MiHPT logs (see SI for details of the methods).  
188 The latter include electrical conductivity (EC), photoionization detector (PID), flame ionization  
189 detector (FID), halogen-specific detector (XSD), and HPT measurements. The MiHPT logs can  
190 be found in the Supporting Information (SI).

## 191 2.3 Determination of hydraulic properties

192 The piezometric head was measured in monitoring wells at the site and a larger area  
193 around it. The groundwater table was about 8 to 9 m below the ground surface (bgs.) in the  
194 source zone (**Figure 1d**) in 2022. The temporal change of the hydraulic head was recorded with  
195 pressure transducers, which had been installed in several monitoring wells over approximately  
196 1.5 years. The long-term monitoring showed an annual variation of the groundwater table by  
197  $\pm 0.25$  m and a relatively stable flow direction. The vertical hydraulic gradients between sandy  
198 inclusions/layer in the upper region of the clayey till and the aquifer and the source zone geology  
199 have been characterized in an earlier study (Rosenberg et al., 2022). The surface sealing by the  
200 factory building led to a lower vertical hydraulic gradient across the clayey-till aquitard (sand  
201 lenses to aquifer) below the building than in the source zone in front of the building. The  
202 existence of a vertical gradient below the building indicates lateral flow in the unsaturated zone  
203 and sand layer above the clayey till.

204



205  
 206 **Figure 1:** (a) Location of the study site. (b) and (c) Map showing the location of monitoring wells (green triangles), direct-push  
 207 GWP measurements (red dots and numbers), and the plume (black concentration contour lines for 1000, 500 and 100 µg/L). The  
 208 brown rectangle in (b) indicates the transport model domain. The dashed dark-blue line shows transect T1 in the flow direction  
 209 and transect T2 perpendicular to the flow. (d) Transect T1 with interpreted geology and TCE concentration isolines (in µg/L)  
 210 based on measurements. The approximate location of the groundwater table is shown with a blue line at 35.5 m asl. The dotted  
 211 lines show the interpreted top and the bottom of the transition layer.

212 The hydraulic conductivity in the aquifer was determined using falling head vacuum slug  
 213 tests (Hinsby et al., 1992). The change of the hydraulic head was measured at a high frequency  
 214 (10 Hz) in 56 well screens located primarily within the sandy aquifer. One slug test was

215 conducted in the transition zone. Furthermore, grain size analysis (GSA) was conducted on 71  
216 soil samples from below the groundwater table, representing the main hydrogeological units at  
217 the site. Due to the low hydraulic conductivity of the clayey till, it was considered very difficult  
218 to conduct reliable slug tests in a reasonable time frame; hence the hydraulic conductivity in this  
219 hydrogeological unit was estimated based on the GSA. The porosities of soil samples from the  
220 clayey till, the transition layer, and the aquifer were determined based on oven-drying of the  
221 initially water-saturated soil samples. For a detailed description of the methods mentioned above,  
222 see SI.

223 Values considered typical for the hydraulic fracture apertures and spacings in clayey till  
224 were selected based on a comprehensive review of glacial clayey tills from eight field sites  
225 (Aamand et al., 2022). In the review, fractures with hydraulic apertures larger than 25  $\mu\text{m}$  were  
226 hardly observed at depths larger than 5 m bgs. The fracture spacing showed a tendency to  
227 decrease with depth. Below 5 m bgs, fracture spacings from several cm to more than 2 m were  
228 observed. In this study, a spacing of 0.5 m was chosen as representative spacing for connected  
229 fractures in the upper 10 meters of a fractured glacial clayey till.

#### 230 2.4 Contamination

231 Comprehensive site investigations were conducted involving MiHPT logs, sampling of  
232 single- and multilevel monitoring wells, determination of pore air concentrations, and analyses of  
233 soil samples throughout the field site. The measurements were used to determine the spatial  
234 extent of the source, as well as to get an initial image of the vertical distribution of the  
235 contamination. In previous site investigations, the CMD was determined with a traditional  
236 transect method in a balance plane perpendicular to the groundwater flow approximately 50 m  
237 downgradient of the source zone.

238 The source zone extent in the clayey till was determined as 20 m in the flow direction and  
239 16 m in the transverse direction. A part of the source zone was located below the factory  
240 building, and the plume passed by underneath the building. Peak concentrations of up to 4900  
241  $\mu\text{g/L}$  were measured in water samples from the deeper part of the source zone. In 2021, the  
242 concentration measurements of the pore water and soil samples did not indicate the presence of a  
243 separate TCE phase, as the concentrations were far below TCE solubility in all measurements  
244 (Pankow & Cherry, 1996). The contamination in the source zone and the plume consisted mainly  
245 of TCE, and sequential degradation, potentially happening under anaerobic conditions, was  
246 hardly observed under the redox conditions at the site (Ottosen et al., 2021). For this study, the  
247 sum of chlorinated ethenes as TCE equivalents was used for the comparison between model  
248 simulations and concentration data, as only very low concentrations of degradation products  
249 were detected.

250 Distribution coefficients,  $K_d$ , were determined on soil samples to characterize the sorption  
251 behavior of TCE in the different geologic units (clayey till, transition zone, and aquifer), using  
252 linear sorption isotherms. The  $K_d$  values of TCE determined in the laboratory were considered in  
253 the upper range compared to actual field conditions, which usually provide less contact surface  
254 and have rate-limited mass-transfer processes between stagnant zones and zones with advective  
255 flow (Ball & Roberts, 1991; Brusseau et al., 1989). The lowest  $K_d$  values determined in the  
256 laboratory in each unit were used in the numerical modeling. Soil samples collected from the  
257 source zone were analyzed for the total TCE concentration. The measured total concentrations,

258 the determination of the total organic and a detailed description of the data mentioned in this  
 259 section content can be found in the SI.

### 260 2.5 Groundwater Profiler tool (GWP)

261 Of particular interest for this study, we performed high-resolution measurements with the  
 262 direct-push tool Groundwater Profiler (GWP, Geoprobe ®) (Dutta et al., 2021), which yielded  
 263 the concentration distribution of TCE and its degradation products at a high vertical resolution.  
 264 The profiles were obtained at seven locations (**Figure 1c**), aiming for five profiles at the  
 265 centerline and two at the outer edges of the plume. Four of the profiles (GWP4-GWP7) were  
 266 placed in a plane perpendicular to the flow direction, close to the downgradient transect where  
 267 the CMD had been determined with a transect method. Water samples were extracted with a  
 268 syringe pump located in the head of the probe right above the ports. The samples were analyzed  
 269 at a certified laboratory (ALS Danmark).

270 The combined information from the monitoring wells and the direct-push measurements  
 271 was used to create a transect in the flow direction (T1, **Figure 1d**). Interpreted isolines of the  
 272 sum of dissolved chlorinated concentration based on measurements in sampling wells, MiHPT  
 273 and GWP measurements are presented in top view in **Figure 1b/c** and in cross-section view in  
 274 **Figure 1d**.

### 275 3 Flow and transport modeling

276 A numerical 3D solute transport model was set up to simulate flow and transport in the  
 277 aquitard and aquifer. The model extends from the groundwater table (ca. 35.5 m asl, bounded by  
 278 a sandy layer on top of the clayey till in the source zone) down to a limestone layer located  
 279 below the sandy aquifer. The model was implemented in COMSOL Multiphysics v6.1  
 280 (COMSOL AB, 2022), using Darcy's law and the transport of diluted species interfaces. The  
 281 model solved a steady-state equation for saturated groundwater flow based on the typical (time-  
 282 average) flow conditions at the site, assuming a stationary flow field. The transient solute  
 283 transport model used the flow field to calculate advective and dispersive transport.

284 The water fluxes were described by Darcy's law in combination with a mass balance:

$$286 \nabla \cdot \mathbf{q} = \nabla \cdot (-\mathbf{K}\nabla h) = 0$$

285 with the anisotropic hydraulic conductivity tensor  $\mathbf{K}$  and the hydraulic head  $h$  (primary variable).

287 Solute transport was described by a transient transport equation, which accounts for  
 288 advection, dispersion, and sorption:

$$296 \phi R \frac{\partial c}{\partial t} + \nabla \cdot (\phi c \mathbf{v}) - \nabla \cdot (\phi \mathbf{D}_{\text{eff}} \nabla c) = 0$$

289 with the porosity  $\phi$ , the retardation factor  $R = 1 + \rho_b K_d / \phi$ , the bulk density  $\rho_b = (1 - \phi) \rho_s$   
 290 and the density of the dry soil material  $\rho_s$ , the concentration of TCE equivalents  $c$  (primary  
 291 variable), the distribution coefficient  $K_d$  assuming linear sorption (sorbed concentration  $c_s =$   
 292  $K_d * c$ ), the seepage velocity  $\mathbf{v} = \mathbf{q} / \phi$ , and the effective hydrodynamic dispersion tensor  $\mathbf{D}_{\text{eff}}$ , as  
 293 defined in Burnett & Frind (1987) and assuming the tortuosity to be equal to the porosity.  
 294 Degradation was not included, and the sum of chlorinated solvents was considered, as discussed  
 295 in section 2.4.

297 A first-order Finite Element method with linear shape functions on an unstructured  
298 tetrahedral mesh was used as a discretization scheme for both flow and transport. The nonlinear  
299 system of equations was solved with a dampened Newton algorithm and Pardiso (Bollhöfer et  
300 al., 2020) as solver for the linearized system of equations. The time discretization used variable-  
301 order variable-step-size backward differentiation formulas to adaptively determine time-step  
302 sizes.

### 303 3.1 Nested 3D model setup

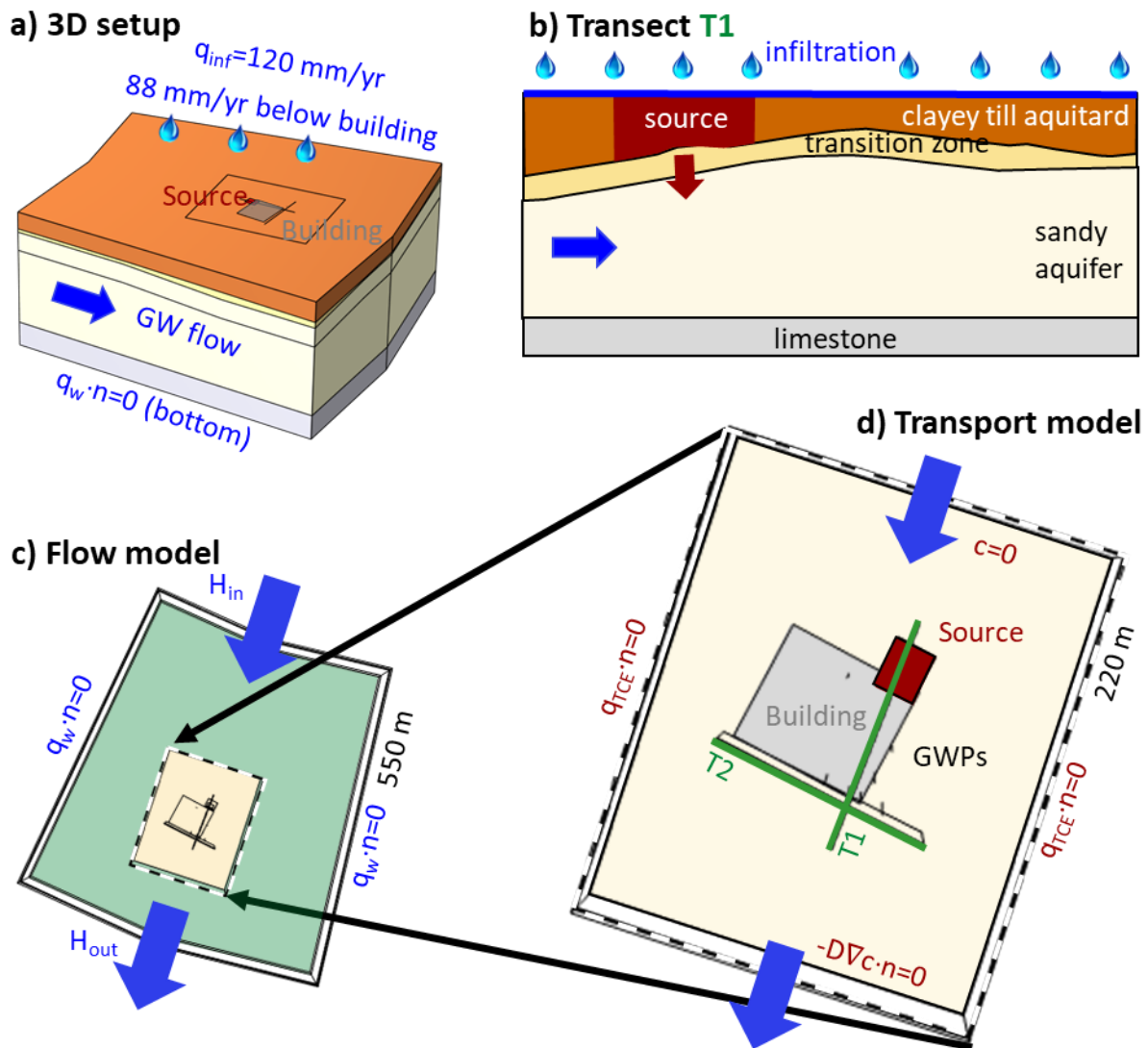
304 Relatively stable flow conditions were assumed, supported by the long-term hydraulic  
305 head monitoring at several locations within the model domain at the site. This allowed for the  
306 delineation of the flow model domain based on observed isopotential lines and streamlines and  
307 the use of a steady-state flow model. The focus for delineating the model domain was on  
308 obtaining a good representation of the hydraulic gradient and the overall flow direction in the  
309 aquifer at the location of the source zone and in the direction of the plume propagation. The 3D  
310 flow model was approximately 550 m long, 400 m wide, and 51 m deep (**Figure 2a**). A nested  
311 setup of the flow and transport domain was chosen, where a larger-scale flow model  
312 encapsulated a smaller-scale transport model to limit the computational efforts without losing  
313 accuracy in areas relevant to transport. The model geometry can be found in the data repository.

314 The vertical composition of four hydrogeological units formed the model domain: a  
315 clayey-till aquitard layer on top, followed by a 1-3 m thick transition zone, then a sandy aquifer  
316 layer, which is underlain by a limestone layer (**Figure 2b**). The transition zone was included as a  
317 layer with interpolated top and bottom surfaces based on the geologic characterization (data from  
318 HPT logs and borehole logs, **Figure 1c**). The values of the hydraulic parameters in the transition  
319 zone were determined to be in between the ones from the two adjacent hydrogeological units.  
320 This composed model domain is an idealized setup that does not resolve all small-scale  
321 heterogeneities and conductivity variations in the different hydrogeological units. It represents  
322 the strong hydraulic conductivity contrast between major hydrogeological units, particularly  
323 between clayey-till aquitard (source zone) and aquifer.

324 At the top model boundary (upper bounding surface of the saturated clayey till), a  
325 constant water flux was set to accommodate the vertical water influxes (infiltration). As the  
326 hydraulic head measurements had shown a stronger vertical hydraulic gradient outside the  
327 building (0.4) than below the building (0.3), the geometry of the building was included on the  
328 top boundary. A lower infiltration rate was set at the location of the building, calibrated to the  
329 vertical gradients around and below the building with a ratio of the vertical water fluxes ( $q_{inf}$ ) of  
330 approximately 4:3 (120 and 88 mm/yr). Two fixed hydraulic head boundaries on the up- and  
331 downgradient sides of the sandy aquifer and limestone layer established the horizontal  
332 groundwater flow according to the local flow conditions (time-averaged horizontal hydraulic  
333 gradient and flow direction) at the side. All other boundaries of the flow model were set to no-  
334 flow (**Figure 2c**).

335





336  
 337 **Figure 2:** (a) 3D model setup of the flow and transport model. (b) Simplified geological transect in the flow direction (T1, **Figure**  
 338 **1**), as used in the model. (c) top view of the 3D flow model with boundary conditions for flow. (d) Top view of the transport model  
 339 nested in the flow domain with respective boundary conditions and location of the building, source zone, and of transects.

340 The nested transport model domain had a length of approximately 220 m, a width of  
 341 180 m, and a depth of approximately 32 m (**Figure 2d**). The chlorinated solvent source (TCE  
 342 equivalents) was in a first step realized as an initial concentration distributed uniformly  
 343 throughout the thickness of the clayey-till layer (ca. 4 m) in a rectangular area of  $20 \times 16$  m<sup>2</sup>  
 344 according to the observed extent of the source zone. The TCE concentration in the inflowing  
 345 water from the top boundary and the upstream side boundary was set to 0  $\mu\text{g/L}$  (clean water). An  
 346 outflow condition was assigned to the downgradient boundary of the transport model, and all  
 347 other boundaries were set to no flux of TCE across these boundaries. The employed model  
 348 parameters are summarized in **Table 1**.

349 The travel time for TCE through the clayey till (both the saturated and the unsaturated  
 350 parts) until leaching from that layer to the aquifer had started was estimated based on simulations  
 351 of transport through the clayey till with a 2D submodel and a distribution coefficient of

352 0.55 L/kg. The simulations showed a travel time of about 20 years after the likely start of the  
 353 spill of TCE in 1971 (see Fig. S1 in the SI). Thus, 1991 was used as a starting point for the  
 354 models with an initially uniform concentration distribution in the source zone throughout the  
 355 clayey till.  
 356

357 *Table 1: Overview of model parameters in the base case with an initial concentration in the source zone.*

<b>Compartment / Parameter</b>	<b>Symbol</b>	<b>Value</b>	<b>Unit</b>	<b>Source</b>
Initial source concentration	$C_0$	1000*	µg/L	Initial guess
Soil material density	$\rho_s$	2650	kg/m <sup>3</sup>	Freeze & Cherry (1979)
Source extent	$L_s$	20×16	m <sup>2</sup>	This study
Infiltration rate	$I$	120 / 88	mm/yr	Calibrated
Free diffusion coefficient TCE (10° C)	$D_w$	$7.1 \cdot 10^{-10}$	m <sup>2</sup> /s	Wilke & Chang (1955)
<b>Aquitard (clayey till)</b>				
Vertical head gradient	$i_v$	0.4 / 0.3	m/m	Measured
Vertical conductivity	$K_v$	$9.6 \cdot 10^{-9}$	m/s	Calibrated
Anisotropy	$K_v/K_h$	0.25		Chapuis & Gill (1989)
Porosity	$n_{clay}$	0.25		Measured
Longitudinal dispersivity	$\alpha_l$	0.01	m	Estimate**
Transverse dispersivity	$\alpha_t$	0.002	m	Estimate**
Vertical dispersivity	$\alpha_v$	0.001	m	Estimate**
Thickness	$T_{clay}$	4-6	m	Measured
Sorption coefficient TCE	$K_{d,clay}$	0.55	L/kg	Measured
<b>Transition zone (silty sand)</b>				
Horizontal conductivity	$K_h$	$6.9 \cdot 10^{-7}$	m/s	Measured
Anisotropy	$K_v/K_h$	0.25		Chapuis & Gill (1989)
Porosity	$n_{tz}$	0.31		Measured
Longitudinal dispersivity	$\alpha_l$	0.5	m	Estimate**
Transverse dispersivity	$\alpha_t$	0.02	m	Estimate**
Vertical dispersivity	$\alpha_v$	0.005	m	Estimate**
Thickness	$T_{clay}$	1-2	m	Measured
Sorption coefficient TCE	$K_{d,clay}$	0.3	L/kg	Measured
<b>Aquifer (sand)</b>				
Horizontal head gradient	$i_h$	2.0	‰	Measured
Horizontal conductivity, upper	$K_h$	$3.5 \cdot 10^{-5}$	m/s	Measured
Horizontal conductivity, lower	$K_h$	$2.3 \cdot 10^{-5}$	m/s	Measured
Anisotropy	$K_v/K_h$	0.25		Chapuis & Gill (1989)
Porosity	$n_{aq}$	0.32		Measured
Longitudinal dispersivity	$\alpha_l$	0.5	m	Estimate**
Transverse dispersivity	$\alpha_t$	0.02	m	Estimate**
Vertical dispersivity	$\alpha_v$	0.005	m	Estimate**
Sorption coefficient TCE	$K_{d,aaq}$	0.11	L/kg	Measured

358 \*The initial source concentration was readjusted according to the concentrations in the vertical profiles.

359 \*\* Chosen within an interval of literature values (Chambon et al., 2010; e.g., Locatelli et al., 2019; Mosthaf et al., 2021;  
 360 Prommer et al., 2006; Schulze-Makuch, 2005).

361 A tetrahedral mesh was used, with a higher mesh resolution within the transport domain  
 362 than in the surrounding part of the flow domain. The hydraulic conductivity in the sandy aquifer

363 was more than two orders of magnitude higher than in the clayey till. To resolve the strong  
 364 conductivity contrast and to minimize the influence of numerical dispersion, the mesh was  
 365 refined particularly at the interfaces between clayey till, transition zone, and aquifer and at the  
 366 surfaces that delineate the source zone (resolution of several cm). The mesh elements were  
 367 vertically scaled, with a ten times higher vertical mesh resolution than in the horizontal direction.  
 368 The mesh had a total of 17.6 million tetrahedral mesh elements.

### 369 3.2 Calibration of the 3D model and data integration

370 A series of simulations with different parameter combinations showed that the location of  
 371 the maximum concentration in the vertical profiles was mainly controlled by the interplay of the  
 372 infiltrating vertical water flux and the horizontal groundwater flow, as confirmed by a global  
 373 sensitivity analysis with a similar 2D model setup (Rosenberg et al., 2023). Determining the  
 374 vertical hydraulic conductivity in clayey tills, which restricts the water fluxes and the advective  
 375 contaminant transport, can be tedious and requires special measurement techniques (Chapman et  
 376 al., 2018; Jørgensen et al., 2019; Sidle et al., 1998). The hydraulic conditions in the sandy aquifer  
 377 were considered more accessible and more accurately identifiable than in the clayey till.

378 Thus, the measured aquifer hydraulic conductivity and head gradient were used as fixed  
 379 values in the calibration process, whereas the vertical water fluxes through the aquitard (net  
 380 infiltration  $q_{inf}$ ) were used as the main calibration parameter for the 3D model (**Figure 2**) to  
 381 match the measured and simulated depths of the maximum concentration in the profiles. Once  
 382 the net infiltration was calibrated, an average vertical hydraulic conductivity in the clayey till  
 383 could be determined using the measured vertical hydraulic gradient.

384 The calibration process of the 3D flow and transport model entailed the following steps:

- 385 1. Setup of the steady-state 3D flow model, using the measured/estimated hydraulic  
 386 conductivities in all units (**Table 1**), the horizontal hydraulic gradient in the aquifer, and a  
 387 first realistic estimate of the infiltration rate to the clayey till (e.g., 200 mm/year)
- 388 2. Simulation of the contaminant transport and variation of infiltration rate to calibrate the  
 389 depth and the shape of the simulated concentration profiles to the measured ones
- 390 3. Calculation of the vertical hydraulic conductivity of the clayey till to match the measured  
 391 vertical hydraulic gradient across the clayey till around and below the building for the  
 392 infiltration rate determined in step 2
- 393 4. Determination of the ratio of the concentrations in the simulated and measured  
 394 concentration profiles that lead to a good fit at most profiles
- 395 5. Calculation of the initial concentration in the source zone and of the CMD by  
 396 multiplication by the ratio determined in step 4, exploiting the proportionality between  
 397 concentrations in the downgradient profiles and the initial source zone concentration

398 The TCE concentrations in the downgradient profiles and the rest of the plume were  
 399 linearly proportional to the average initial concentration  $c_0$  in the source zone. The simulated  
 400 concentrations in the profiles were based on an average initial concentration of 1000  $\mu\text{g/L}$ . The  
 401 concentrations in the model could thus be multiplied by a conversion factor that gives the  
 402 relation between measured and simulated concentrations in the vertical profiles, e.g., the average  
 403 maximum concentration in the measured profile divided by  $c_0$ . This factor was also used to

404 calculate the average initial concentration in the source zone in the clayey till at the beginning of  
 405 the leaching process and determine the CMD.

### 406 3.3 Clayey-till submodels as input functions from source and link to 3D model

#### 407 3.3.1 Setup and calibration of clayey-till source submodels

408 A 2D submodel was developed (**Figure 3**) to study the possible temporal development of  
 409 the contaminant leaching using different source-zone conceptualizations with and without  
 410 fractures while limiting the computational efforts. The submodel simulated a 6 m deep and 2.5 m  
 411 wide vertical cross-section of the source zone in the aquitard (clayey till) extending from the  
 412 water table in a 1 m thick sandy layer (saturated conditions) down to 1 m below the clayey-till  
 413 bottom, with vertical transport of TCE through 4 m of clayey till. This setup was simulated with  
 414 different distribution coefficients and fracture patterns to generate contaminant input functions  
 415 for the 3D model based on the effluent concentrations at the bottom of the clayey till in the 2D  
 416 submodel. The submodel was used as a proxy for the larger source zone in the clayey till (20 m ×  
 417 16 m × 4 m) and determined the input concentrations to the top boundary of the transition zone  
 418 in the larger-scale 3D model (**Figure 2a/b**).

419 Three different source-zone conceptualizations were simulated to study the influence of  
 420 the conditions in the aquitard on the CMD:

- 421 1. no fractures, variation of the distribution coefficient of TCE (0 to 0.8 L/kg),
- 422 2. five vertical fractures in the clayey till with uniform apertures (values of 8, 12, 15, and  
 423 18.5 μm were simulated), and a distribution coefficient of 0.55 L/kg,
- 424 3. five vertical fractures in the clayey till with an aperture distribution (apertures of 20, 5,  
 425 25, 5, and 20 μm), and a distribution coefficient of 0.55 L/kg.

#### 426 3.3.2 Discrete fracture-matrix model (DFM) as source zone submodel

427 In the fractured setups, a uniform and periodic distribution of the fractures with a spacing  
 428 of 0.5 m in the source zone was assumed (**Figure 3**), and different aperture distributions between  
 429 0 μm (no fractures) and 25 μm were included, which corresponds to fracture conditions  
 430 considered typical at a depth below 5 m below ground surface (bgs.) in similar clayey tills  
 431 (Aamand et al., 2022). The inclusion of vertical fractures in the DFM submodel was used to  
 432 study their effects on the leaching from the source zone in the aquitard under the influence of  
 433 fracture transport, matrix diffusion and sorption.

434 For the simulation of flow in fractures, the local cubic law was used to calculate the  
 435 fracture hydraulic conductivity

$$436 K_f = \frac{d_f^2 \rho_w g}{12 \mu_w}$$

437 and Darcy's law was used to describe the fluxes in the discrete, lower-dimensional fractures

$$438 q_f = -d_f K_f \nabla_T h$$

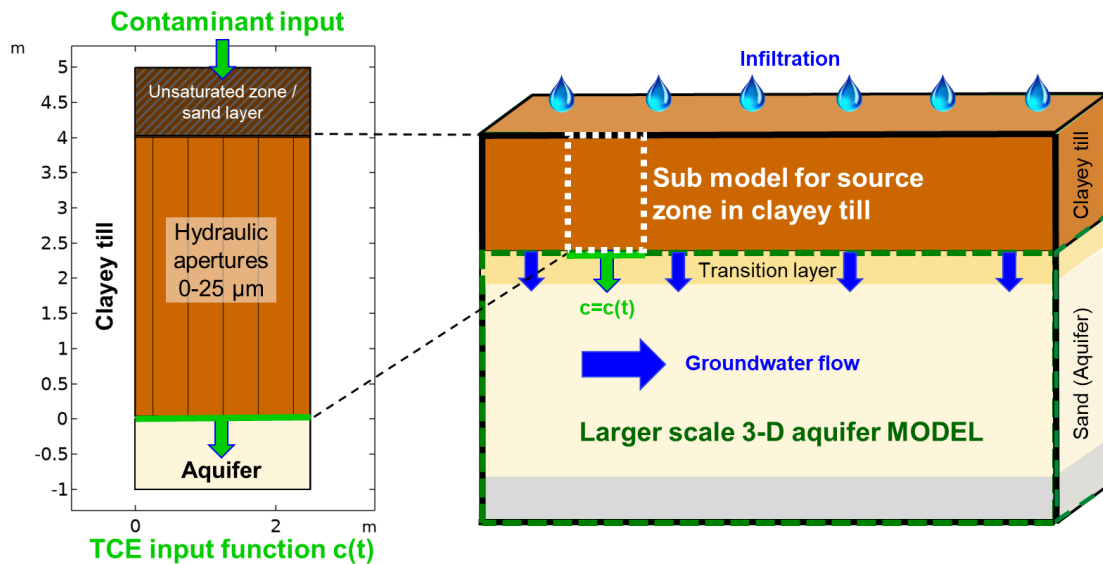
439 with the hydraulic fracture aperture  $d_f$ , the density  $\rho_w$  and dynamic viscosity  $\mu_w$  of water at  
 440 10°C (the approximate temperature of the groundwater in Denmark), the gravity constant  $g$ , and  
 441 the gradient tangential to the fracture  $\nabla_T$ .

442 The mass balance of TCE in the fractures was implemented as in Mosthaf et al. (2021)

443 
$$d_f(R_f \frac{\partial c}{\partial t} + \nabla \cdot (v_f c - D_f \nabla_T c) = 0$$

444 with the retardation factor  $R_f$  and the hydrodynamic dispersion coefficient in the fracture  $D_f$ .  
 445 The DFM model ensures the continuity of hydraulic heads, concentrations, and fluxes at the  
 446 fracture-matrix interface.

447



448 **Figure 3:** Setup of the 2D DFM submodel (left) to simulate the contaminant depletion from the source in a low-permeable layer  
 449 with and without fractures. The submodel is used to create input functions for the larger-scale 3D aquifer model (simplified setup  
 450 figure on the right), in which the clayey till is replaced by the submodel input, assuming a periodic fracture system in the  
 451 aquitard.  
 452

453 To resolve occurring strong concentration gradients at the fracture-matrix interfaces and  
 454 matrix diffusion correctly (Weatherill et al., 2008), the mesh of the submodel was strongly  
 455 refined with a very fine boundary layer mesh next to the fractures, and at the interface to the  
 456 aquifer and the sand layer above. For each fracture aperture setup, the matrix hydraulic  
 457 conductivity was calibrated so that the average vertical hydraulic gradient across the clayey till  
 458 still matched the measured gradient when applying the same infiltration rate as in the calibrated  
 459 3D model (see SI, Table S7). This was done using an automated, derivative-free Bound  
 460 Optimization by quadratic approximation (BOBYQA) optimization algorithm. The same low  
 461 dispersivities as in the clayey till were used in this thin layer. The sandy layer ensured a correct  
 462 redistribution of the flow into the fractures and matrix in the clayey till according to the  
 463 hydraulic conductivity in the fractured scenarios. A constant influx of TCE equivalents through  
 464 the top boundary was simulated over a period of 26 years, which covers the time in which a  
 465 TCE-containing substance was handled in the Styrofoam factory. This period was followed by  
 466 clean water infiltration without further TCE input into the clayey till from the top boundary. The  
 467 development of the average concentration right below the clayey till was determined with a

468 boundary probe as space-averaged concentrations relative to the input concentration at the top of  
469 the clayey till (dimensionless), varying between 0 and 1.

### 470 3.3.3 Source submodel integration in 3D model and CMD determination

471 As the water-fluxes from the clayey till to the aquifer remained unchanged, the same  
472 calibrated 3D flow model as for the simulations with an initially uniform concentration  
473 distribution in the clayey till (**Figure 2c**) was used. In the transport model, the clayey-till layer  
474 was deactivated, and the TCE input was realized by a time-dependent flux condition on the upper  
475 boundary of the transition layer in an area corresponding to the source zone ( $20 \times 16 \text{ m}^2$ ), as  
476 schematically shown in **Figure 3**. The flux condition applied the dimensionless input functions  
477 from the submodels to control the TCE input to the transition layer, using a maximum input  
478 concentration  $c_0$  of  $1000 \text{ } \mu\text{g/L}$  in the base case. The approach of integrating input functions from  
479 a submodel to a larger scale model presumes that the flow and transport through the aquitard is  
480 not restricted by the hydraulic conditions in the aquifer, which is justified by the given  
481 comparably high hydraulic conductivity in the aquifer.

482 Again, proportionality between input concentrations and concentrations in the  
483 downgradient profiles was exploited. The concentrations in the model domain based on a  $c_0$  of  
484  $1000 \text{ } \mu\text{g/L}$  were, as in the case of an initially uniform distribution in the source zone before,  
485 multiplied by a conversion factor to obtain a good match with the measured concentration values  
486 from the vertical GWP profiles. To determine the conversion factor, the shape and maximum  
487 concentration at the vertical concentration profiles, mainly at GWP6, were used, and the  
488 concentration levels were calibrated to the observed ones. This allowed determining the  
489 inflowing average source concentration and, ultimately, the CMD for the different source  
490 conceptualizations.

## 491 4 Results

492 The following sections present the measured hydrogeological data and the depth-discrete  
493 concentration profiles. The data integration into the 3D model, the model calibration, and the  
494 determination of CMD are discussed. Furthermore, the effects of different source  
495 conceptualizations, represented by input functions in the 3D model, on the temporal evolution of  
496 the CMD are presented. The results are assessed together with a discussion of the combination of  
497 high-resolution vertical concentration profiles with 3D modeling of the contaminant source zone  
498 and plume.

### 499 4.1 Integration of hydrogeological data and concentration data in the 3D model

#### 500 4.1.1 Hydraulic gradients and properties

501 The overall horizontal hydraulic gradient in the aquifer was evaluated at different times  
502 in the year. It was relatively stable in a range between 1.6 and 2.4 ‰ with an average of 2 ‰ and  
503 a main flow direction towards the south-southwest. The 58 slug tests and 71 GSAs from the  
504 saturated zone yielded hydraulic conductivity values, which were, based on the geological  
505 characterization, location of the screen, and description of the soil samples, classified into three  
506 hydrogeological units (**Table 2**): clayey till, transition zone, and aquifer. The hydraulic  
507 conductivities in the aquifer were two orders of magnitude higher than in the aquitard.

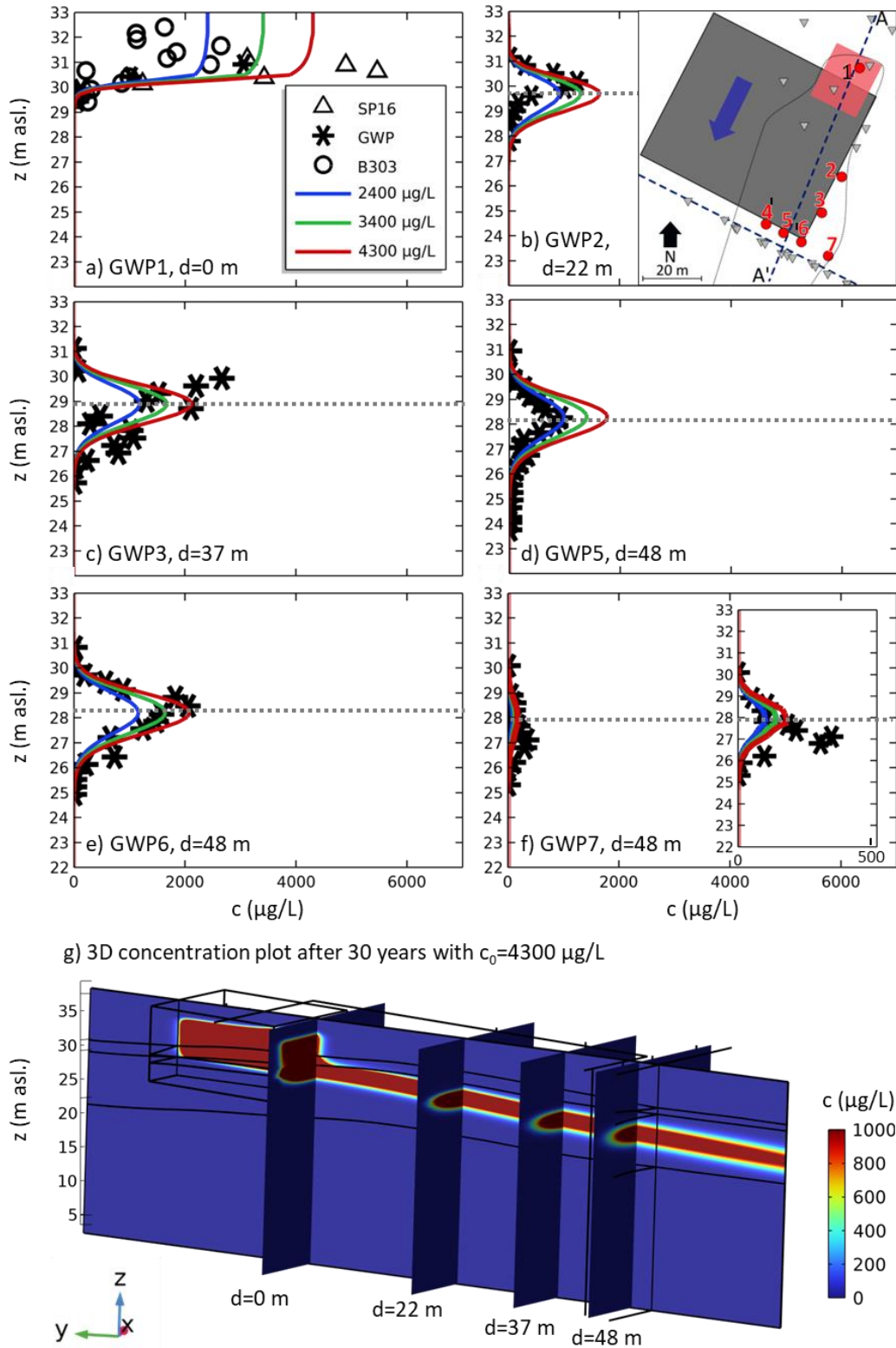
508 **Table 2:** Geometric mean ( $K_g$ ) of hydraulic conductivities ( $K$ ) determined by slug tests and GSA. The results are classified  
 509 according to the hydrogeological layers/intervals. The following parameters are given: the number of performed tests ( $N_K$ ), the  
 510 geometric mean ( $K_g$ ), the interval of the estimated hydraulic conductivity (Interval), and the variance of  $\ln(K)$  ( $\sigma^2 \ln(K)$ ). For  
 511 some of the soil samples, the porosity was determined. The number of samples ( $N_\phi$ ), the average porosity, and the observed  
 512 porosity intervals are listed.

Method and geological unit (level in m asl.)	$N_K$	$K_g$ (m/s)	$K$ interval (m/s)	$\sigma^2 \ln(K)$	$N_\phi$	Porosity [interval]
<b>Slug tests</b>						
Upper aquifer (24.2 - 31.4)	52	$3.52 \cdot 10^{-5}$	$8.00 \cdot 10^{-6} - 1.30 \cdot 10^{-4}$	0.45		
Lower aquifer (21.1 - 23.2)	6	$2.26 \cdot 10^{-5}$	$1.20 \cdot 10^{-5} - 4.11 \cdot 10^{-5}$	0.16		
<b>GSA</b>						
Aquifer (sand)	33	$1.81 \cdot 10^{-5}$	$1.05 \cdot 10^{-7} - 8.17 \cdot 10^{-5}$	3.73	15	0.32 [0.25-0.42]
Transition zone (silted sand)	11	$6.90 \cdot 10^{-7}$	$8.22 \cdot 10^{-8} - 3.82 \cdot 10^{-6}$	3.63	12	0.31 [0.27-0.37]
Sandy clayey till	27	$1.87 \cdot 10^{-7}$	$5.27 \cdot 10^{-8} - 6.44 \cdot 10^{-7}$	0.56	21	0.25 [0.22-0.33]

513 The hydraulic conductivities determined by slug tests in the sandy aquifer were further  
 514 classified into two depth intervals, one comprising the upper 7 m of the aquifer (where the plume  
 515 mainly spread) and the other interval covering the lower part of the sandy aquifer. The geometric  
 516 mean hydraulic conductivities in the upper 7 m were slightly higher than in the lower part of the  
 517 aquifer. Despite the different determination methods, the GSA and the slug tests yielded similar  
 518 conductivities in the aquifer. The values obtained from the slug tests were used in the modeling,  
 519 as they were considered a more direct measurement under in-situ conditions, had a lower  
 520 variance, and comprised a larger sampling volume. The determined porosities (**Table 2**) were in  
 521 a typical range for clayey tills and sandy aquifers.

#### 522 4.1.2 High-resolution vertical concentration profiles

523 The depth-discrete GWP sampling resulted in high-resolution vertical concentration  
 524 profiles (symbols in **Figure 4a-f**, see also data repository). The highest concentrations were  
 525 measured at the source zone, with concentrations up to 5500  $\mu\text{g/L}$  (SP16) and 2600  $\mu\text{g/L}$  (GWP).  
 526 The profiles show a downward dislocation of the maximum concentrations within the aquifer  
 527 with distance from the source zone, which can also be seen in the cross sections shown in **Figure**  
 528 **4g**. The distances of GWP2 and GWP3 from the downgradient edge of the source zone were 22  
 529 m and 37 m. GWP5 and GWP6 were in a transect perpendicular to the flow direction 48 m from  
 530 the source zone. The location of the maximum concentration shifted from about 30 m above sea  
 531 level (asl.) at GWP2 to about 28 m asl. in GWP5 and GWP6, driven by water infiltration from  
 532 the aquitard. GWP5 and GWP6 were only 6.7 m apart, and they were expected to be both in the  
 533 centerline of the plume, thus having similar concentrations. However, with around 2000  $\mu\text{g/L}$   
 534 TCE equivalents, the maximum concentration in GWP6 was about twice as high as in GWP5.  
 535 The lower concentrations in GWP5 could be caused by local heterogeneities or indicate that the  
 536 plume center was closer to GWP6.



537  
 538 **Figure 4:** Depth-discrete concentrations from GWP logs (symbols, measurements from 2021) and simulated concentration  
 539 profiles (lines) for three different initial concentrations below the source zone (a) and at five downgradient locations (b-f).  $d$   
 540 in the figures denotes the distance of the profile from the downgradient edge of the source zone. The inset in (b) shows the location  
 541 of the wells in top view. The dashed lines show the approximate center of the simulated plume (g) shows several cross sections  
 542 from the 3D model simulations 30 years after the simulation start (corresponds approximately to 2021).



543 Despite being closer to the source zone, the concentrations measured at GWP2 were  
544 lower than at some GWPs further downgradient of GWP2. The lower concentration can be  
545 explained by the location of GWP2, which was not in the plume centerline. A more central  
546 placement was impossible due to the factory building. The concentrations at the other GWPs  
547 decreased from the source zone in the downgradient direction. The continuous decrease shows  
548 that the source zone was not yet depleted and still actively contributed TCE to the plume. The  
549 vertical plume extent increased with distance from the source zone from about 4 m at GWP3 to  
550 5 m at GWP6.

#### 551 4.1.3 Model calibration to vertical profiles

552 The 3D flow and transport model was calibrated to the observed vertical concentration  
553 profiles from the GWP measurements, as described in Section 3.2. The match between simulated  
554 and measured profiles in the year 2021 (when the GWP measurements were conducted) was  
555 manually evaluated and found to compare very well for an infiltration rate of 120 mm/year  
556 outside the building and 88 mm/year below the building. These infiltration rates led to a  
557 consistent simulated plume depth at most vertical concentration profiles in 2021. With the  
558 infiltration rate and vertical hydraulic gradients fixed, the average vertical hydraulic conductivity  
559 in the clayey till could be determined as  $9.6 \cdot 10^{-9}$  m/s.

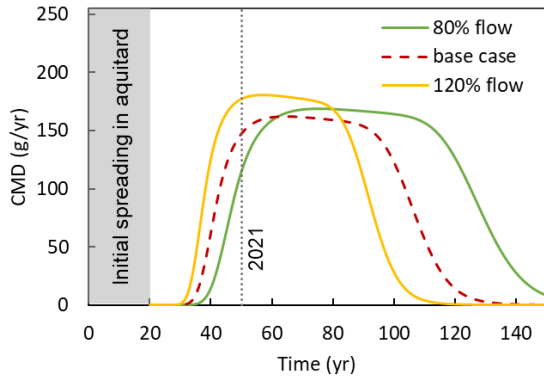
#### 560 4.2 CMD determination from model simulations

561 Determining the CMD was the ultimate goal of the simulations and depth-discrete  
562 concentration measurements. As the concentrations in the simulated profiles were proportional to  
563 the initial source concentration  $c_0$ , the simulated concentrations were recalculated using the ratio  
564 between measured and simulated concentrations in the vertical profiles in 2021 as a conversion  
565 factor to obtain a consistent match at the GWPs. Initial concentrations in the source zone  
566 between 2400 and 4300  $\mu\text{g/L}$  yielded a suitable match at the six presented GWPs (**Figure 4a-f**).  
567 The lowest value of 2400  $\mu\text{g/L}$  led to a good fit only at GWP5, which is likely not located in the  
568 centerline of the plume. According to visual comparison, a  $c_0$  of 3400 to 4300  $\mu\text{g/L}$ , which is in  
569 the range of maximum concentrations measured in the source zone in 2021, led to a good fit of  
570 the maximum values and shapes in the other profiles. A  $c_0$  of 4300  $\mu\text{g/L}$  was considered an upper  
571 limit for  $c_0$  for the selected infiltration rate and chosen as the base case, which was used to  
572 compare different setups in the sequel. The CMDs, obtained originally with an initial model  
573 concentration of 1000  $\mu\text{g/L}$ , were multiplied by the conversion factor of 4.3, respectively.

574 With uniform initial TCE concentrations in the source zone of 3400 to 4300  $\mu\text{g/L}$ , a  
575 CMD of 117 to 148 g/year was determined. This is in good agreement with a CMD estimate of  
576 143 g/year based on the determination with a traditional transect method (NIRAS, 2019) at  
577 transect T2 with a similar distance from the source zone as GWP5 and GWP6. The simulations  
578 did not lead to notable TCE concentrations at GWP4, while the measurements showed low TCE  
579 concentrations (see SI). These can possibly be attributed to an additional contaminant source that  
580 was detected west of the modeled source, which was not included in the model and was not  
581 investigated further here.

582 The simulated temporal development of the CMD in the downgradient transect T2  
583 (**Figure 5**, base case, red dashed line) showed increasing concentrations in 2002, around 31 years  
584 after the assumed start of the TCE spill in 1971. The maximum CMD of 160 g/year occurred  
585 after 58 years (2029), followed by a period of 40-50 years with a relatively constant discharge

586 until the CMD shows a stronger decrease after about 90 years. According to the presented  
 587 simulations, the CMD would not decrease considerably until several decades after 2021.



588  
 589 **Figure 5:** Breakthrough curves at the downgradient transect T2 for the base case and the vertical and horizontal flow scaled by  
 590 80% and 120%. Time 0 corresponds to the start of the spill (1971). The vertical dashed line shows approximately the year 2021  
 591 (GWP measurements). The first 20 years of initial spreading in the clayey till were not simulated, and the simulation started with  
 592 uniformly distributed TCE in the source zone in the clayey till.

593

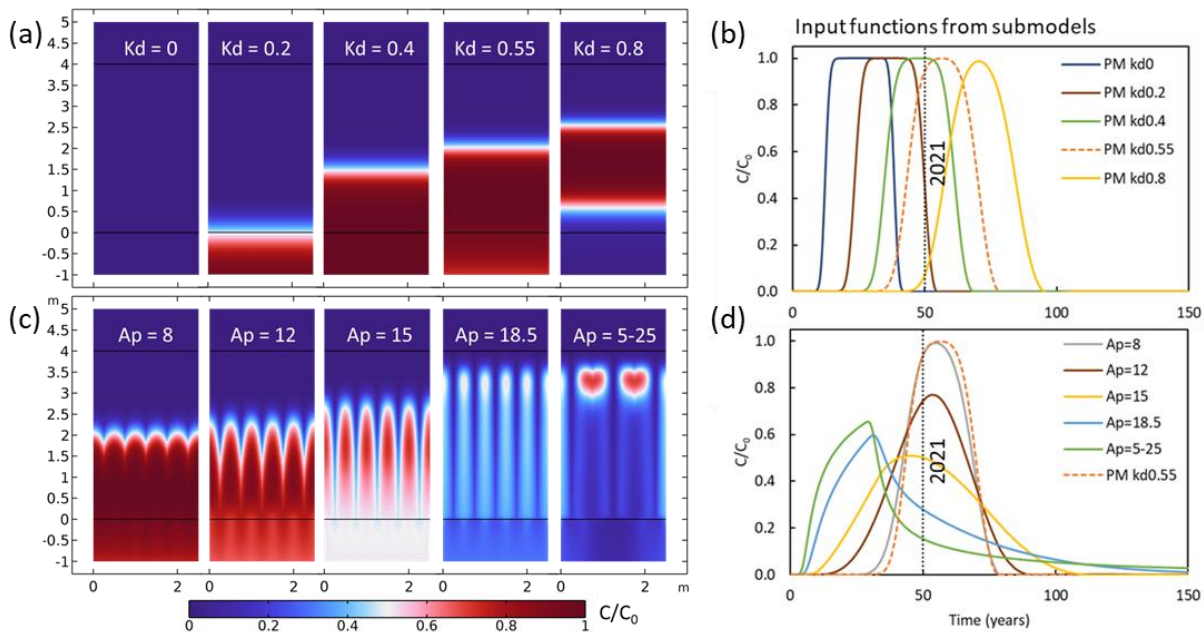
594 The sensitivity of the CMD to the infiltration rate and the hydraulic conductivity in the  
 595 aquifer was investigated. For this purpose, the hydraulic conductivity in the aquifer, which is  
 596 proportional to the groundwater flux, was varied by  $\pm 20\%$ . A constant ratio between infiltration  
 597 rate and horizontal groundwater flow maintained the simulated depth of the maximum  
 598 concentrations in the plume. Thus, the infiltration rate was changed at the same time as the  
 599 groundwater flux by  $\pm 20\%$  to keep the ratio between infiltrating water and horizontal  
 600 groundwater flux constant, leading to 96 mm/yr,  $K_{h,aq} = 2.8 \cdot 10^{-5}$  m/s in the case of 80% flow and  
 601 144 mm/yr,  $K_{h,aq} = 4.2 \cdot 10^{-5}$  m/s for 120% flow. Then, the initial source concentrations were  
 602 readjusted with individual conversion factors to match the measured profiles. An initial source  
 603 zone concentration of 5600  $\mu\text{g/L}$  for 80% flow and 4000  $\mu\text{g/L}$  for 120% flow led to almost  
 604 identical vertical profiles as in the base case.

605 With 80% flow, a CMD of 87 to 116 g/yr in 2021 was determined (**Figure 5**), while it  
 606 was 138 to 178 g/yr with a 20 % stronger infiltration rate and groundwater flow. Thus, the  
 607 determined CMD differed by  $\pm 15\text{-}25\%$ . The maximum concentration was reached earlier for  
 608 stronger flow (159  $\mu\text{g/L}$  after 74 years with 80% flow vs. 173  $\mu\text{g/L}$  after 54 years with 120%  
 609 flow). The determined CMD scaled almost linearly with the water fluxes, mainly because a  
 610 steady-state discharge had not yet been reached at transect T2 in 2021; however, the simulated  
 611 concentration profiles used to determine the conversion factors and the CMD were almost  
 612 identical. The depth of the maximum concentration and the shape of the simulated profiles  
 613 showed only very minor differences in the three scenarios. The differences in the determined  
 614 CMD would be smaller in a period with a relatively constant TCE discharge. The duration of the  
 615 TCE discharge through transect T2 was longer for the 80% flow scenario. The higher initial  
 616 source concentration  $c_0$  in the 80 % flow scenario compared to the base case resulted in more  
 617 contaminant mass in the system (CMD integrated over time).

618 4.3 Plume evolution with different source zone conceptualizations

619 Contaminant input functions for the 3D model were created with the 2D submodels  
 620 described in Section 3.3, following the goal of investigating the effects of the source zone  
 621 conceptualization in the aquitard (fractures, sorption properties) on the temporal development of  
 622 the plume and CMD. The simulated concentration distributions in 2021 in the vertical clayey-till  
 623 cross sections without fractures, applying different distribution coefficients, are shown in **Figure**  
 624 **6a**. With a  $K_d$  of 0.8 L/kg, which is the average value determined in laboratory experiments on  
 625 clayey till samples from the site, the TCE was in a narrow depth interval in the aquitard in 2021.  
 626 The TCE had not yet arrived at the bottom of the clayey-till layer in 2021, about 50 years after  
 627 the first release of the contaminant. Lower distribution coefficients led to a faster and deeper  
 628 migration of the TCE and spreading over a greater vertical distance in the clayey till. In the case  
 629 of no sorption ( $K_d = 0$  L/kg), the TCE had been entirely washed out from the clayey-till profile  
 630 by 2021, which is opposed to field observations.

631 The TCE breakthrough curves for the clayey till with different linear distribution  
 632 coefficients (**Figure 6b**) demonstrate the retarding effect of the sorption on the simulated  
 633 concentrations at the bottom of the clayey till. The first arrival of TCE at the clayey-till bottom  
 634 varies significantly, between 10 years for  $K_d = 0$  L/kg and 50 years for  $K_d = 0.8$  L/kg.



635 **Figure 6:** Concentration profiles in clayey till without fractures and different distribution coefficients in L/kg (a) and  
 636 fractures with different hydraulic apertures in  $\mu\text{m}$  (c) after 50 years of leaching. (b) Input functions of the concentration relative  
 637 to the input concentration on top of the clayey till from an unfractured porous medium (PM) submodel with different distribution  
 638 coefficients ( $K_d$  in L/kg), and (d) from a fractured submodel with different apertures ( $A_p$  in  $\mu\text{m}$ ). The result from the scenario  
 639 without fractures (PM  $kd_{0.55}$ ) is shown as a reference. The dashed vertical lines indicate the year 2021, about 50 years after the  
 640 spill had begun.  
 641

642 The concentration plots after 50 years with the different simulated fracture aperture  
 643 realizations are depicted in **Figure 6c**. A constant  $K_d$  value of 0.55 L/kg and TCE input with  
 644 concentration  $c_0$  over 26 years were used in these simulations. Hydraulic fracture apertures of 8  
 645 and 12  $\mu\text{m}$  led to relatively uniform leaching through the profile and TCE transport mainly  
 646 through matrix advection, with a minor influence of the fractures on the TCE distribution. The

647 concentration plot resembled the scenario with no fractures and a  $K_d$  value of 0.55 L/kg. At  
648 apertures of 15 to 18.5  $\mu\text{m}$ , the transport was shifted more and more from the matrix towards the  
649 fractures. Preferential flow and fracture transport gained importance, with co-occurring matrix  
650 diffusion and slow advective transport through the matrix. The large fracture apertures of up to  
651 25  $\mu\text{m}$  in the mixed case (Ap5-25) showed the most decisive impact on the TCE transport in the  
652 2D concentration plots. The contaminant spread quickly along the major fractures while  
653 diffusing into the matrix, followed by back-diffusion when the concentrations in the inflowing  
654 water decreased.

655 Fractures with small apertures, here smaller than 8  $\mu\text{m}$  and a fracture spacing of 0.5 m,  
656 revealed almost no effect on the TCE breakthrough curves at the bottom of the 4 m clayey-till  
657 profile (**Figure 6d**) compared to the unfractured scenario. Larger fractures, however, lead to a  
658 significantly earlier arrival and to tailing in the breakthrough curve. Note that, in contrast to the  
659 unfractured scenarios and the scenarios with small-aperture fractures, the concentrations relative  
660 to the input concentration  $c_0$  do not reach 1 for the setups with fractures larger than 8  $\mu\text{m}$ , i.e., the  
661 effluent concentrations are not reaching the maximum influent concentrations. The relative  
662 effluent concentrations smaller than 1 are due to the retarding effect of the matrix diffusion,  
663 sorption, and slow transport through the matrix.

664 The input functions from the submodels were applied as a boundary condition at the top  
665 of the transition layer in the 3D model, replacing the uniform concentration  $c_0$  throughout the  
666 source zone in the clayey till. This led to a difference in the concentration profiles at GWP1  
667 in the source zone (**Figure 7a**). However, the depth and shape of the downgradient concentration  
668 profiles did not change (GWP6, **Figure 7b**).

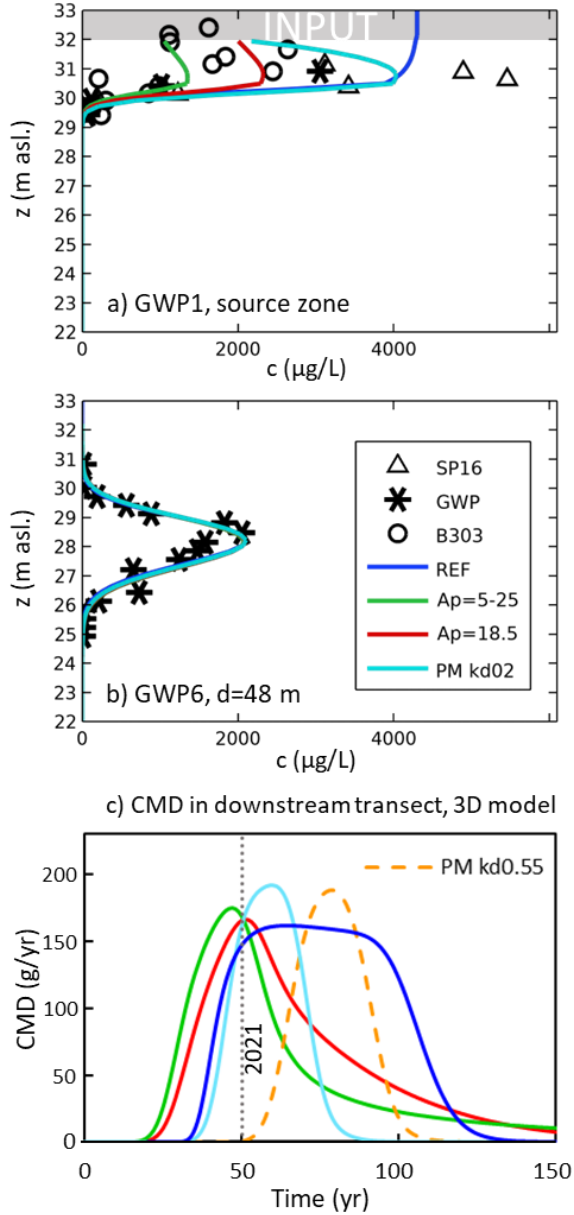
669 The simulated breakthrough curves (**Figure 7c**) demonstrate the transient evolution of the  
670 CMD in the downgradient transect T2 approximately 50 m from the source zone. In the  
671 unfractured scenario, a  $K_d$  value of 0.55 L/kg led to a strong and unrealistic delay in the plume  
672 arrival at the downgradient transect. According to the simulation, the plume would not have  
673 arrived 50 years after the spill started. A lower distribution coefficient of 0.20 L/kg led to an  
674 earlier arrival at T2 and a CMD comparable to the base case after 50 years with an initial  
675 concentration in the source zone. In that case, the simulated CMD increased further in the years  
676 after 2021.

677 The input from the fractured setups with relatively large apertures (18.5  $\mu\text{m}$  or 5-25  $\mu\text{m}$ )  
678 led to plausible CMDs 50 years after the start of the TCE spill and to a good fit of the vertical  
679 concentration profiles at GWP1 and GWP6 (**Figure 7a** and **Figure 7b**). The peak CMD of  
680 160 g/year could be observed after 45-50 years (2016-2021) using an input concentration to the  
681 top of the submodel of 6500  $\mu\text{g/L}$ . The breakthrough curves with the large apertures (5-25  $\mu\text{m}$ )  
682 show a considerable influence on the contaminant fluxes at the downgradient transect and led to  
683 an earlier increase and a long tailing of the CMD curves. The effect of fractures with apertures  
684 smaller than 18.5  $\mu\text{m}$  was not further evaluated in the 3D model, as the results would resemble  
685 those from the model without fractures according to the input functions (**Figure 6d**).

686 The comparison of the CMD evolution in the different submodel scenarios with the setup  
687 with an initially uniform TCE distribution (**Figure 7c**) showed that assuming an initially uniform  
688 distribution of TCE throughout the depth of the clayey till would lead to a longer estimated  
689 duration of the period with a high CMD in the downgradient transect. In the fractured scenarios,  
690 the breakthrough curves at the downgradient transect show a long tailing. In contrast to the

691 scenarios without fractures, the CMD after 150 years (around the year 2121) would still not be  
 692 close to 0 g/year. The value of the CMD in the year of the GWP measurements (2021) is,  
 693 however, in a narrow range in the different scenarios.

694



695 **Figure 7:** Measured and simulated profiles after 50 years with an initially uniformly distributed concentration in the source zone  
 696 (REF) and different input functions from the fractured/non-fractured submodels at (a) GWP1 (source zone) and (b) GWP 6. Note  
 697 that the simulated curves in (b) are on top of each other. (c) Evolution of the CMD at transect T2 over time in the different  
 698 scenarios.  
 699

## 700 4.4 Discussion and perspectives

## 701 4.4.1 Comparison of field-derived parameters with model-calibrated parameters

702 This study demonstrated that the concept of calibrating a 3D numerical transport model  
703 to high-resolution vertical concentration profiles could be successfully applied to determine  
704 fluxes and the CMD of a dissolved chlorinated hydrocarbon plume in an aquitard/aquifer system.  
705 We found that the interplay between vertical water fluxes through the aquitard and the horizontal  
706 groundwater fluxes in the aquifer controlled the vertical plume dislocation, thus defining the  
707 depth of the concentration maximum. Identifying a setup that integrated the hydrogeological data  
708 and reproduced the plume sinking with distance from the source led to consistent results at the  
709 locations of the vertical profiles (GWPs) and allowed for the determination of the CMD. Based  
710 on the model and the measurements, the CMD at the considered field site to the underlying  
711 aquifer was 117-148 g/year, which is in good agreement with the CMD determined with a  
712 traditional transect approach (NIRAS, 2019) and in Rosenberg et al. (2023).

713 The most important measurements for using this concept were the horizontal conductivity  
714 in the aquifer, the horizontal gradient in the groundwater, the source zone extent, and the high-  
715 resolution concentration profiles downgradient of the source, as well as the geological  
716 characterization of the site. The horizontal groundwater fluxes could be constrained by the  
717 hydraulic gradient and the hydraulic conductivity in the aquifer, quantities that can be easier  
718 determined than the fluxes and hydraulic properties in the clayey till.

719 The simultaneous variation of the infiltration rate and the hydraulic conductivity in the  
720 aquifer by  $\pm 20\%$  led to similar profiles at the GWPs, while the determined CMD differed by  
721  $\pm 15-25\%$ . An independent and reliable determination of the groundwater fluxes (hydraulic  
722 conductivity and gradient) in the aquifer is thus crucial for a good CMD approximation using the  
723 presented approach, particularly if the CMD is not at a steady state at the location of the CMD  
724 evaluation. Furthermore, the shape of the simulated vertical concentration profiles can be  
725 influenced by the vertical dispersivity in the aquifer. With low values of the transverse and  
726 vertical dispersivities, as often determined for plumes in relatively homogeneous sandy geologies  
727 (Cirpka et al., 2006; Garabedian & LeBlanc, 1991; Jensen et al., 1993; Prommer et al., 2006), the  
728 influence of the vertical dispersivity on the determined CMD is considered small. This is  
729 supported by the results of the global sensitivity analysis presented in Rosenberg et al. (2023).

730 We used a simplified hydrogeological setup with four uniform layers to limit  
731 computational costs. The possible influence of thin inclusions/lenses in the clayey till was tested  
732 (results not shown here), and it was found that isolated higher-permeability heterogeneities had a  
733 minor effect on the vertical transport and the determined CMD. The contrast between aquitard  
734 and aquifer was considered more influential for the contaminant leaching than the variations and  
735 small-scale heterogeneities within the clayey till. Future studies could further explore the impact  
736 of heterogeneous conductivity distributions in the clayey till on the contaminant leaching, similar  
737 to L. Yang et al. (2018), who modeled heterogeneous DNAPL source zones using geostatistically  
738 generated hydraulic permeability fields.

739 The model calibration with the simplified hydrogeological setup allowed for the  
740 determination of an average vertical hydraulic conductivity of the aquitard. The hydraulic  
741 conductivity is close to the value obtained in Rosenberg et al. (2022) and in the medium range of  
742 hydraulic conductivities found in similar clayey tills in the literature (Chapman et al., 2018;

743 Ferris et al., 2020; Fredericia, 1990; Jørgensen et al., 2002; Jørgensen, McKay, et al., 2004).  
744 However, it is by a factor of about 20 lower than the geometric mean of the values determined by  
745 GSA methods. GSA can be useful to determine the hydraulic properties of coarse and relatively  
746 uniform soils like sands or gravels (Devlin, 2015) but may give poor estimates of in-situ  
747 conditions for fine-grained, heterogeneous materials like clayey tills (Van der Kamp, 2001). A  
748 GSA typically determines the isotropic hydraulic conductivity values for a disturbed sample and  
749 does not account for pore connectivity, small-scale heterogeneities and fractures, and possible  
750 anisotropy. Hydraulic tests like slug tests or pumping tests cover a larger sampling volume but  
751 may represent more the horizontal hydraulic conductivity in the case of an application in  
752 traditional vertical wells. In addition, the low conductivity in the aquitard may complicate  
753 conducting slug or pumping tests (Butler, 2019). The average vertical hydraulic conductivity  
754 determined by the model calibration is considered representative of in-situ conditions relevant to  
755 the contaminant leaching from the aquitard.

#### 756 4.4.2 Influence of fractures on contaminant transport

757 The model simulations without fractures and with a sorption coefficient in the clayey till  
758 of 0.55 L/kg or higher did not reproduce the observed spreading of the TCE contamination in the  
759 aquifer, as the contamination had just arrived at the bottom of the clayey till and not yet reached  
760 the downgradient GWPs. This indicates that the applied sorption coefficient was too high, the  
761 infiltration rate was too low and/or the presence of preferential flow paths like fractures or  
762 textural heterogeneities in the aquitard. Discrete-fracture simulations with a simple fracture  
763 geometry and constant spacing demonstrated the effects of fractures on the evolution of the  
764 CMD. With fractures, the current distribution in the aquifer could be reproduced. The influence  
765 of more complex fracture geometries and aperture distributions (also along a fracture) and of  
766 macropores (Makedonska et al., 2016; Mosthaf et al., 2021; Rosenbom et al., 2009), as well as  
767 textural heterogeneities (Kessler et al., 2013), on the leaching could be further investigated. This  
768 was, however, outside the scope of this paper.

769 Moreover, the simulations in this study demonstrated that fractures in an aquitard with  
770 small hydraulic apertures ( $<10\text{-}15\ \mu\text{m}$ ) had a minor to negligible influence on the TCE  
771 distribution and leaching from the clayey till. In contrast, larger fracture apertures showed a  
772 substantial impact on the arrival times of TCE at the bottom of the clayey till and on the duration  
773 of the leaching period, influenced by matrix diffusion and sorption. The study outcomes  
774 highlight the value of developing and using advanced characterization methods to analyze the  
775 nature of the source zone (e.g., hydraulic fracture properties, matrix hydraulic conductivity,  
776 sorption characteristics) for a good approximation of the source depletion and the temporal  
777 development of CMD. For the determination of the CMD in 2021 with the presented concept, the  
778 hydraulic conditions in the source zone were, however, less influential, as the determined CMD  
779 was the same for the different fracture scenarios and the base case without fractures.

#### 780 4.4.3 Transient conditions and varying concentrations

781 In the presented simulations, a steady-state flow field was considered as observed  
782 variations in the hydraulic heads were small. However, groundwater table variations can be more  
783 pronounced and the groundwater flow direction can show spatial patterns. Such patterns could  
784 lead to temporal variations in the contaminant input and more mixing in the aquifer, thus  
785 widening the plume. These temporal variations were small at the considered study site, and the

786 model with a steady-state flow field yielded a good agreement between simulated and measured  
787 profiles and plume extend. Strong temporal variations of the flow field can complicate the  
788 determination of the CMD as presented in the study, as they would require, e.g., using a transient  
789 flow model.

790 The modeling used knowledge of the source location and extent and assumed uniform  
791 concentrations in the source zone instead of a spatially variable concentration distribution. This  
792 assumption can be justified by the age of the contamination of about 50 years, in which diffusion  
793 has led to the spreading of the contaminant and a decrease of steep concentration gradients over  
794 time. However, a more random distribution of the concentrations in the source zone was  
795 observed. Therefore, a model setup with higher concentrations in the source center in the  
796 horizontal plane and a circular source was also tested in supplementing simulations. A more  
797 complex source concentration distribution led to only slight differences in the downgradient  
798 vertical concentration profiles and determined CMD. A long horizontal distance compared to the  
799 source zone extent makes the exact entry point of the contaminant from within the source zone to  
800 the aquifer less important for the determined CMD as long as the input area and the average  
801 source zone concentration are roughly the same. Integrating a more detailed vertical  
802 concentration distribution in the source zone in the model could result in a more accurate  
803 determination of the possible future development of the CMD. In this study, a uniform  
804 contaminant source setup based on the determined source extent was considered better suited to  
805 study the influence of the individual parameters and processes.

806 Despite the simplifications of the source zone and geology, the computational time and  
807 effort to run the 3D solute transport model were high. Thus, the fit of the simulated results to the  
808 measured vertical concentration profiles was manually evaluated. In future studies, calibration or  
809 inverse modeling methods similar to those used in Yin et al. (2015) and Essouayed et al. (2021)  
810 could be applied to optimize the goodness of fit and quantify uncertainties.

#### 811 4.4.4 Reactive transport and application to other compounds

812 At the considered field site, no substantial degradation of TCE was observed. When  
813 degradation happens, it must be included in the model to obtain realistic CMD estimates. For  
814 TCE, sequential degradation by reductive dechlorination (Chambon et al., 2010) could be  
815 considered under anaerobic conditions. Sequential degradation in the source zone would lead to  
816 lower TCE concentrations and a lower CMD with time and could shorten the duration of the  
817 contaminant leaching from the source zone. However, it would lead to increased concentrations  
818 of the degradation products (dichloroethylene, vinyl chloride).

819 The presented approach can also be beneficial for investigations with substances other  
820 than chlorinated solvents, such as BTEX/PAHs (Prommer et al., 2009), PFAS (Gerardu et al.,  
821 2023), or pesticides (Mosthaf et al., 2021), in aquitard-aquifer systems with a similar  
822 hydrogeological setting. For aerobically degrading compounds, aerobic degradation in the  
823 aquifer could lead to a decrease in the concentrations at the top of the plume (in the upper areas  
824 of the aquifer). Additionally, if unsaturated conditions are investigated, the transfer and transport  
825 of volatile substances in the soil air must be accounted for. A mixture of simultaneously  
826 occurring processes could, however, make it more difficult to calibrate a model and determine  
827 the CMD in such systems.



## 828           4.4.5 Final remarks

829           Field datasets of contaminated sites are often not as comprehensive as presented in this  
830 study for a contaminated site, preventing the development of a complex 3D model to determine  
831 the CMD. In cases with less data availability, the concept described in Rosenberg et al. (2023)  
832 could be instrumental for practical application and screening purposes. It employs a simplified  
833 2D model setup in combination with vertical concentration profiles. It also exploits the  
834 characteristic sinking of the plume and a limited number of measurement points to obtain an  
835 estimate of the CMD from a contaminated site in an aquitard-aquifer system. Fractures in the  
836 aquitard, however, are not considered, so exploring the effects of fractures as done in this study  
837 adds crucial new conceptual understanding of the leaching out of the aquitard, the corresponding  
838 vertical profiles in the underlying aquifer and the temporal development of breakthrough curves.

839   **5 Summary and conclusions**

840           This work demonstrated the strength and capability of a 3D model to quantitatively  
841 characterize the contaminant leaching and spreading from a contamination source in a water-  
842 saturated, low-permeability geological layer (aquitard) into an underlying groundwater aquifer.  
843 The high-resolution concentration profiles obtained from direct-push measurements revealed a  
844 vertical dislocation of the dissolved TCE plume with distance from the source. The observed  
845 depth-discrete concentration profiles and plume sinking could be reproduced in the model using  
846 vertical water fluxes through the clayey till as the main calibration parameter. Based on the  
847 calibration of the 3D model and knowledge of the average hydraulic conductivity and hydraulic  
848 gradient in the aquifer, the CMD from the point source in the clayey-till aquitard could  
849 successfully be determined. Additionally, the presented approach allowed for the determination  
850 of an average vertical hydraulic conductivity and the vertical water fluxes (net infiltration) in the  
851 clayey-till aquitard.

852           The results of 3D modeling integrating source input functions from a 2D submodel  
853 demonstrated the effects of the specific conceptualization of the source zone (sorption, fractures)  
854 on the temporal development of the TCE leaching in the aquifer. The differences in CMD  
855 determined for the year of the measurements (2021) were small for the tested source  
856 conceptualizations. However, different sorption properties in the source zone and fractures with  
857 hydraulic apertures larger than 10-15  $\mu\text{m}$  led to very different temporal developments of the  
858 CMD. Thus, a correct source conceptualization is key for evaluating the possible future CMD  
859 evolution from a contaminated site. This also highlights the need for elaborate characterization  
860 methods for the aquitard, e.g., regarding the transport and hydraulic properties and the presence  
861 and properties of fractures and macropores.

862   **Acknowledgments**

863           The authors are grateful for inspiring discussions and support from Vinni Rønde,  
864 Henriette Kern-Jespersen, Nina Tuxen (Capital Region of Denmark), as well as for the  
865 geological interpretations and the input by Klaus Weber, Peter Tyge and Charlotte Riis (NIRAS).  
866 The technicians Bent Henning Skov and Jens Schaarup Sørensen participated in the field  
867 sampling, sample characterization, and chemical analyses. These contributions are gratefully  
868 acknowledged. This work was funded by the Capital Region of Denmark and the Technical  
869 University of Denmark.

870 **Open Research**

871 The measured concentration profiles and the model geometries are available in a data  
 872 repository (<https://doi.org/10.11583/DTU.22884035>). Relevant model parameters are provided in  
 873 the manuscript. Total organic carbon and hydraulic conductivity data, the data from sorption  
 874 capacity experiments, coordinates of the GWP measurements, and the logs from MiHPT  
 875 measurements can be found in the supporting information (SI).

876 Temporary link to the data repository: <https://figshare.com/s/6aac3a72643dba3874bf>

877 **References**

- 878 Aamand, J., Badawi, N., Jakobsen, P. R., Jørgensen, P. R., Mosthaf, K., Troldborg, L., & Rolle, M. (2022). *Mapping*  
 879 *Groundwater Vulnerability to Pesticide Contamination through Fractured Clays - CLAYFRAC*. Retrieved  
 880 from <https://mst.dk/service/publikationer/publikationsarkiv/2022/feb/clayfrac/>
- 881 Ball, W. P., & Roberts, P. v. (1991). Long-Term Sorption of Halogenated Organic Chemicals by Aquifer Material.  
 882 1. Equilibrium. *Environmental Science and Technology*, 25(7), 1223–1237.  
 883 [https://doi.org/10.1021/ES00019A002/ASSET/ES00019A002.FP.PNG\\_V03](https://doi.org/10.1021/ES00019A002/ASSET/ES00019A002.FP.PNG_V03)
- 884 Barr, D. W. (2001). Coefficient of Permeability Determined by Measurable Parameters. *Ground Water*, 39(3), 356–  
 885 361. <https://doi.org/10.1111/j.1745-6584.2001.tb02318.x>
- 886 Basu, N. B., Rao, P. S. C., Falta, R. W., Annable, M. D., Jawitz, J. W., & Hatfield, K. (2008). Temporal evolution of  
 887 DNAPL source and contaminant flux distribution: Impacts of source mass depletion. *Journal of Contaminant*  
 888 *Hydrology*, 95(3–4), 93–109. <https://doi.org/10.1016/j.jconhyd.2007.08.001>
- 889 Berkowitz, B. (2002). Characterizing flow and transport in fractured geological media: A review. *Advances in Water*  
 890 *Resources*, 25(8–12), 861–884. [https://doi.org/10.1016/S0309-1708\(02\)00042-8](https://doi.org/10.1016/S0309-1708(02)00042-8)
- 891 Berre, I., Doster, F., & Keilegavlen, E. (2019). Flow in Fractured Porous Media: A Review of Conceptual Models  
 892 and Discretization Approaches. *Transport in Porous Media*, 130(1), 215–236. [https://doi.org/10.1007/s11242-](https://doi.org/10.1007/s11242-018-1171-6)  
 893 018-1171-6
- 894 Blessent, D., Jørgensen, P. R., & Therrien, R. (2014). Comparing Discrete Fracture and Continuum Models to  
 895 Predict Contaminant Transport in Fractured Porous Media. *Groundwater*, 52(1), 84–95.  
 896 <https://doi.org/10.1111/gwat.12032>
- 897 Bollhöfer, M., Schenk, O., Janalik, R., Hamm, S., & Gullapalli, K. (2020). State-of-the-Art Sparse Direct Solvers. In  
 898 *Parallel Algorithms in Computational Science and Engineering* (pp. 3–33).
- 899 Brusseau, M. L., Jessup, R. E., & Rao, P. S. C. (1989). Modeling the transport of solutes influenced by multiprocess  
 900 nonequilibrium. *Water Resources Research*, 25(9), 1971–1988. <https://doi.org/10.1029/WR025I009P01971>
- 901 Brusseau, M. L., Matthieu, D. E., Carroll, K. C., Mainhagu, J., Morrison, C., McMillan, A., et al. (2013).  
 902 Characterizing long-term contaminant mass discharge and the relationship between reductions in discharge  
 903 and reductions in mass for DNAPL source areas. *Journal of Contaminant Hydrology*, 149, 1–12.  
 904 <https://doi.org/10.1016/j.jconhyd.2013.02.011>
- 905 Burnett, R. D., & Frind, E. O. (1987). Simulation of contaminant transport in three dimensions: 2. Dimensionality  
 906 effects. *Water Resources Research*, 23(4), 695. <https://doi.org/10.1029/WR023i004p00695>
- 907 Butler, J. J. Jr. (2019). *The Design, Performance, and Analysis of Slug Tests* (2nd Edition). CRC Press.
- 908 Chambon, J. C., Broholm, M. M., Binning, P. J., & Bjerg, P. L. (2010). Modeling multi-component transport and  
 909 enhanced anaerobic dechlorination processes in a single fracture-clay matrix system. *Journal of Contaminant*  
 910 *Hydrology*, 112(1–4), 77–90. <https://doi.org/10.1016/j.jconhyd.2009.10.008>
- 911 Chapman, S. W., & Parker, B. L. (2005). Plume persistence due to aquitard back diffusion following dense  
 912 nonaqueous phase liquid source removal or isolation. *Water Resources Research*, 41(12), 1–16.  
 913 <https://doi.org/10.1029/2005WR004224>
- 914 Chapman, S. W., Cherry, J. A., & Parker, B. L. (2018). Multiple-scale hydraulic characterization of a surficial  
 915 clayey aquitard overlying a regional aquifer in Louisiana. *Journal of Hydrology*, 558, 546–563.  
 916 <https://doi.org/10.1016/j.jhydrol.2018.01.059>
- 917 Chapuis, R. P., & Gill, D. E. (1989). Hydraulic anisotropy of homogeneous soils and rocks: influence of the  
 918 densification process. *Bulletin of the International Association of Engineering Geology*, 39(1), 75–86.  
 919 <https://doi.org/10.1007/BF02592538>

- 920 Cherkauer, D. S. (2004). Quantifying Ground Water Recharge at Multiple Scales Using PRMS and GIS. *Ground*  
 921 *Water*, 42(1), 97–110. <https://doi.org/10.1111/J.1745-6584.2004.TB02455.X>
- 922 Cirpka, O. a., Olsson, Å., Ju, Q., Rahman, M. A., & Grathwohl, P. (2006). Determination of transverse dispersion  
 923 coefficients from reactive plume lengths. *Ground Water*, 44(2), 212–221. [https://doi.org/10.1111/j.1745-](https://doi.org/10.1111/j.1745-6584.2005.00124.x)  
 924 [6584.2005.00124.x](https://doi.org/10.1111/j.1745-6584.2005.00124.x)
- 925 COMSOL AB. (2022). COMSOL Multiphysics®. Retrieved from [www.comsol.com](http://www.comsol.com)
- 926 Devlin, J. F. (2015). HydrogeoSieveXL: an Excel-based tool to estimate hydraulic conductivity from grain-size  
 927 analysis. *Hydrogeology Journal*, 23(4), 837–844. <https://doi.org/10.1007/s10040-015-1255-0>
- 928 Dutta, S., Christy, T. M., McCall, W., & Kurup, P. (2021). Field evaluation of 1.75 groundwater profiler and field  
 929 screening device for on-site contamination profiling of chromium(VI) in groundwater. *Environmental Earth*  
 930 *Sciences*, 80(7), 1–19. <https://doi.org/10.1007/s12665-021-09568-9>
- 931 Einarson, M. D., & Mackay, D. M. (2001). Predicting Impacts of Ground Water Contamination. *Environmental*  
 932 *Science & Technology*, 35(3), 66–73. Retrieved from <https://pubs.acs.org/sharingguidelines>
- 933 Einarson, M. D., Mackay, D. M., & Bennett, P. J. (2010). Sampling transects for affordable, high-resolution plume  
 934 characterization and monitoring. *Ground Water*, 48(6), 805–808. [https://doi.org/10.1111/j.1745-](https://doi.org/10.1111/j.1745-6584.2010.00755.x)  
 935 [6584.2010.00755.x](https://doi.org/10.1111/j.1745-6584.2010.00755.x)
- 936 Essouayed, E., Ferré, T., Cohen, G., Guiserix, N., & Atteia, O. (2021). Application of an iterative source localization  
 937 strategy at a chlorinated solvent site. *Journal of Hydrology X*, 13.  
 938 <https://doi.org/10.1016/J.HYDROA.2021.100111>
- 939 Falta, R. W. (2005). Dissolved chemical discharge from fractured clay aquitards contaminated by DNAPLs. In  
 940 *Geophysical Monograph Series* (Vol. 162, pp. 165–174). Blackwell Publishing Ltd.  
 941 <https://doi.org/10.1029/162GM15>
- 942 Ferris, D. M., Potter, G., & Ferguson, G. (2020). Characterization of the hydraulic conductivity of glacial till  
 943 aquitards. *Hydrogeology Journal*, 28(5), 1827–1839. <https://doi.org/10.1007/S10040-020-02161-7>
- 944 Filippini, M., Parker, B. L., Dinelli, E., Wanner, P., Chapman, S. W., & Gargini, A. (2020). Assessing aquitard  
 945 integrity in a complex aquifer – aquitard system contaminated by chlorinated hydrocarbons. *Water Research*,  
 946 171, 115388. <https://doi.org/10.1016/j.watres.2019.115388>
- 947 Flemisch, B., Berre, I., Boon, W., Fumagalli, A., Schwenck, N., Scotti, A., et al. (2017). Benchmarks for single-  
 948 phase flow in fractured porous media, 1–33. Retrieved from <http://arxiv.org/abs/1701.01496>
- 949 Fredericia, J. (1990). Saturated hydraulic conductivity of clayey tills and the roles of fractures. *Nordic Hydrology*,  
 950 21, 119–132.
- 951 Freeze, R. Allan., & Cherry, J. A. (1979). *Groundwater*. Englewood Cliffs, N.J.: Prentice-Hall.  
 952 Retrieved from <https://findit.dtu.dk/en/catalog/2304905336>
- 953 Garabedian, S. P., & LeBlanc, D. (1991). Large-scale natural gradient tracer test in sand and gravel, Cape Cod,  
 954 Massachusetts. 2. Analysis of spatial moments for a nonreactive tracer, 27(5), 911–924.
- 955 Geoprobe. (2023). SP16 Groundwater Sampler.
- 956 Gerardu, T., Dijkstra, J., Beeltje, H., van Renesse van Duivenbode, A., & Griffioen, J. (2023). Accumulation and  
 957 transport of atmospherically deposited PFOA and PFOS in undisturbed soils downwind from a fluoropolymers  
 958 factory. *Environmental Advances*, 11. <https://doi.org/10.1016/J.ENVADV.2022.100332>
- 959 Gueting, N., & Englert, A. (2013). Hydraulic conditions at the source zone and their impact on plume behavior.  
 960 *Hydrogeology Journal*, 21(4), 829–844. <https://doi.org/10.1007/s10040-013-0962-7>
- 961 Harrison, B., Sudicky, E. A., & Cherry, J. A. (1992). Numerical analysis of solute migration through fractured  
 962 clayey deposits into underlying aquifers. *Water Resources Research*, 28(2), 515–526.  
 963 <https://doi.org/10.1029/91WR02559>
- 964 Helmke, M. F., Simpkins, W. W., & Horton, R. (2005). Simulating conservative tracers in fractured till under  
 965 realistic timescales. *Ground Water*, 43(6), 877–889. <https://doi.org/10.1111/j.1745-6584.2005.00129.x>
- 966 Hinsby, K., Bjerg, P., Andersen, L., Skov, B., & Clausen, E. (1992). A mini slug test method for determination of a  
 967 local hydraulic conductivity of an unconfined sandy aquifer. *Journal of Hydrology*, 136(1–4), 87–106.  
 968 [https://doi.org/10.1016/0022-1694\(92\)90006-H](https://doi.org/10.1016/0022-1694(92)90006-H)
- 969 Højberg, A. L., Engesgaard, P., & Bjerg, P. L. (2005). Pesticide transport in an aerobic aquifer with variable pH -  
 970 Modeling of a field scale injection experiment. *Journal of Contaminant Hydrology*, 78(3), 231–255.
- 971 Horst, J., Schnobrich, M., Divine, C., Curry, P., Sager, S., & Horneman, A. (2021). Mass Flux Strategies 20 Years  
 972 On—Getting the Sand Out of the Gears. *Groundwater Monitoring and Remediation*, 41(4), 13–21.  
 973 <https://doi.org/10.1111/gwmr.12491>

- 974 Hu, Y., Xu, W., Zhan, L., Zou, L., & Chen, Y. (2022). Modeling of solute transport in a fracture-matrix system with  
 975 a three-dimensional discrete fracture network. *Journal of Hydrology*, *605*, 127333.  
 976 <https://doi.org/10.1016/j.jhydrol.2021.127333>
- 977 Hvorslev, M. Juul. (1951). *Time lag and soil permeability in ground-water observations* (Vol. 36.). U.S.Army,  
 978 Corps of engineers, Waterways experiment station,.
- 979 Jensen, K. H., Bitsch, K., & Bjerg, P. L. (1993). Large-scale dispersion experiments in a sandy aquifer in Denmark:  
 980 Observed tracer movements and numerical analyses. *Water Resources Research*, *29*(3), 673–696.  
 981 <https://doi.org/10.1029/92WR02468>
- 982 Jørgensen, P. R., Hoffmann, M., Kistrup, J. P., Bryde, C., Bossi, R., & Villholth, K. G. (2002). Preferential flow and  
 983 pesticide transport in a clay-rich till : Field, laboratory, and modeling analysis. *Water Resources Research*,  
 984 *38*(11). <https://doi.org/10.1029/2001WR000494>
- 985 Jørgensen, P. R., McKay, L. D., & Kistrup, J. P. (2004). Aquifer vulnerability to pesticide migration through till  
 986 aquitards. *Ground Water*, *42*(6), 841–855. <https://doi.org/10.1111/j.1745-6584.2004.t013-x>
- 987 Jørgensen, P. R., Helstrup, T., Urup, J., & Seifert, D. (2004). Modeling of non-reactive solute transport in fractured  
 988 clayey till during variable flow rate and time. *Journal of Contaminant Hydrology*, *68*(3–4), 193–216.  
 989 [https://doi.org/10.1016/S0169-7722\(03\)00146-3](https://doi.org/10.1016/S0169-7722(03)00146-3)
- 990 Jørgensen, P. R., Mosthaf, K., & Rolle, M. (2019). A Large Undisturbed Column Method to Study Flow and  
 991 Transport in Macropores and Fractured Media. *Groundwater*, *57*(6), 951–961.  
 992 <https://doi.org/10.1111/gwat.12885>
- 993 Van der Kamp, G. (2001). Methods for determining the in situ hydraulic conductivity of shallow aquitards - An  
 994 overview. *Hydrogeology Journal*, *9*(1), 5–16. <https://doi.org/10.1007/S100400000118>
- 995 Keller, C. K., Van Der Kamp, G., & Cherry, J. A. (1989). A multiscale study of the permeability of a thick clayey  
 996 till. *Water Resources Research*, *25*(11), 2299–2317. <https://doi.org/10.1029/WR025i011p02299>
- 997 Kessler, T. C., Klint, K. E. S., Nilsson, B., & Bjerg, P. L. (2012). Characterization of sand lenses embedded in tills.  
 998 *Quaternary Science Reviews*, *53*(C), 55–71. <https://doi.org/10.1016/j.quascirev.2012.08.011>
- 999 Kessler, T. C., Comunian, A., Oriani, F., Renard, P., Nilsson, B., Klint, K. E., & Bjerg, P. L. (2013). Modeling fine-  
 1000 scale geological heterogeneity-examples of sand lenses in tills. *Groundwater*, *51*(5), 692–705.  
 1001 <https://doi.org/10.1111/j.1745-6584.2012.01015.x>
- 1002 Klint, K. E. S., Nilsson, B., Trolldborg, L., & Jakobsen, P. R. (2013). A poly morphological landform approach for  
 1003 hydrogeological applications in heterogeneous glacial sediments. *Hydrogeology Journal*, *21*(6), 1247–1264.  
 1004 <https://doi.org/10.1007/s10040-013-1011-2>
- 1005 Kruisdijk, E., & van Breukelen, B. M. (2021). Reactive transport modelling of push-pull tests: A versatile approach  
 1006 to quantify aquifer reactivity. *Applied Geochemistry*, *131*. <https://doi.org/10.1016/j.apgeochem.2021.104998>
- 1007 Locatelli, L., Binning, P. J., Sanchez-Vila, X., Søndergaard, G. L., Rosenberg, L., & Bjerg, P. L. (2019). A simple  
 1008 contaminant fate and transport modelling tool for management and risk assessment of groundwater pollution  
 1009 from contaminated sites. *Journal of Contaminant Hydrology*, *221*, 35–49.  
 1010 <https://doi.org/10.1016/j.jconhyd.2018.11.002>
- 1011 Lu, C., Bjerg, P. L., Zhang, F., & Broholm, M. M. (2011). Sorption of chlorinated solvents and degradation products  
 1012 on natural clayey tills. *Chemosphere*, *83*(11), 1467–1474. <https://doi.org/10.1016/j.chemosphere.2011.03.007>
- 1013 Makedonska, N., Hyman, J. D., Karra, S., Painter, S. L., Gable, C. W., & Viswanathan, H. S. (2016). Evaluating the  
 1014 effect of internal aperture variability on transport in kilometer scale discrete fracture networks. *Advances in*  
 1015 *Water Resources*, *94*, 486–497. <https://doi.org/10.1016/j.advwatres.2016.06.010>
- 1016 Manghi, F., Mortazavi, B., Crother, C., & Hamdi, M. R. (2009). Estimating regional groundwater recharge using a  
 1017 hydrological budget method. *Water Resources Management*, *23*(12), 2475–2489.  
 1018 <https://doi.org/10.1007/S11269-008-9391-0>
- 1019 McCall, W., & Christy, T. M. (2020). The Hydraulic Profiling Tool for Hydrogeologic Investigation of  
 1020 Unconsolidated Formations. *Groundwater Monitoring and Remediation*, *40*(3), 89–103.  
 1021 <https://doi.org/10.1111/gwmr.12399>
- 1022 McCall, W., Christy, T. M., Pipp, D., Terkelsen, M., Christensen, A., Weber, K., & Engelsen, P. (2014). Field  
 1023 Application of the Combined Membrane-Interface Probe and Hydraulic Profiling Tool (MiHpt). *Groundwater*  
 1024 *Monitoring & Remediation*, *34*(2), 85–95. <https://doi.org/10.1111/gwmr.12051>
- 1025 McKay, L. D., & Fredericia, J. (1995). Distribution, origin, and hydraulic influence of fractures in glacial deposit.  
 1026 *Canadian Geotechnical Journal*, *32*, 957–975.
- 1027 Mosthaf, K., Rolle, M., Petursdottir, U., Aamand, J., & Jørgensen, P. R. (2021). Transport of tracers and pesticides  
 1028 through fractured clayey till: Large Undisturbed Column (LUC) experiments and model-based interpretation.  
 1029 *Water Resources Research*, *57*, 1–18. <https://doi.org/10.1029/2020WR028019>

- 1030 Muniruzzaman, M., & Rolle, M. (2019). Multicomponent Ionic Transport Modeling in Physically and  
 1031 Electrostatically Heterogeneous Porous Media With PhreeqcRM Coupling for Geochemical Reactions. *Water*  
 1032 *Resources Research*, (II). <https://doi.org/10.1029/2019WR026373>
- 1033 Muniruzzaman, M., & Rolle, M. (2021). Impact of diffuse layer processes on contaminant forward and back  
 1034 diffusion in heterogeneous sandy-clayey domains. *Journal of Contaminant Hydrology*, 237.  
 1035 <https://doi.org/10.1016/j.jconhyd.2020.103754>
- 1036 Newell, C. J., Farhat, S. K., Adamson, D. T., & Looney, B. B. (2011). Contaminant Plume Classification System  
 1037 Based on Mass Discharge. *Ground Water*, 49(6), 914–919. <https://doi.org/10.1111/j.1745-6584.2010.00793.x>
- 1038 NIRAS. (2019). *Afgrænsende Forureningsundersøgelse Industrivej 2, 3540 Lynge*. Allerød.
- 1039 Ottosen, C. B., Bjerg, P. L., Hunkeler, D., Zimmermann, J., Tuxen, N., Harrekilde, D., et al. (2021). Assessment of  
 1040 chlorinated ethenes degradation after field scale injection of activated carbon and bioamendments: Application  
 1041 of isotopic and microbial analyses. *Journal of Contaminant Hydrology*, 240.  
 1042 <https://doi.org/10.1016/j.jconhyd.2021.103794>
- 1043 Pankow, J. F., & Cherry, J. A. (1996). *Dense chlorinated solvents and other DNAPLs in groundwater: history,*  
 1044 *behavior, and remediation*. Waterloo Press.
- 1045 Parker, B. L., Cherry, J. A., & Wanner, P. (2022). Determining effective diffusion coefficients of  
 1046 chlorohydrocarbons in natural clays: Unique results from highly resolved controlled release field experiments.  
 1047 *Journal of Contaminant Hydrology*, 250(August), 104075. <https://doi.org/10.1016/j.jconhyd.2022.104075>
- 1048 Parker, J. C., & Park, E. (2004). Modeling field-scale dense nonaqueous phase liquid dissolution kinetics in  
 1049 heterogeneous aquifers. *Water Resources Research*, 40(5), 1–12. <https://doi.org/10.1029/2003WR002807>
- 1050 Prommer, H., Tuxen, N., & Bjerg, P. L. (2006). Fringe-controlled natural attenuation of phenoxy acids in a landfill  
 1051 plume: Integration of field-scale processes by reactive transport modeling. *Environmental Science and*  
 1052 *Technology*, 40(15), 4732–4738. <https://doi.org/10.1021/es0603002>
- 1053 Prommer, H., Anneser, B., Rolle, M., Einsiedl, F., & Griebler, C. (2009). Biogeochemical and isotopic gradients in a  
 1054 BTEX/PAH contaminant plume: Model-based interpretation of a high-resolution field data set. *Environmental*  
 1055 *Science and Technology*, 43(21), 8206–8212. <https://doi.org/10.1021/ES901142A>
- 1056 Rønne, V., McKnight, U. S., Sonne, A. T., Balbarini, N., Devlin, J. F., & Bjerg, P. L. (2017). Contaminant mass  
 1057 discharge to streams: Comparing direct groundwater velocity measurements and multi-level groundwater  
 1058 sampling with an in-stream approach. *Journal of Contaminant Hydrology*, 206, 43–54.  
 1059 <https://doi.org/10.1016/j.jconhyd.2017.09.010>
- 1060 Rosenberg, L., Broholm, M. M., Tuxen, N., Kern-Jespersen, I. H., Lilbæk, G., & Bjerg, P. L. (2022). Vertical  
 1061 Hydraulic Gradient Estimation in Clay Till, Using MiHPT Advanced Direct-Push Technology. *Groundwater*  
 1062 *Monitoring & Remediation*, 42(1), 29–37. <https://doi.org/10.1111/gwmr.12470>
- 1063 Rosenberg, L., Mosthaf, K., Broholm, M. M., Fjordbøge, A. S., Tuxen, N., Kern-Jespersen, I. H., et al. (2023). A  
 1064 novel concept for estimating the contaminant mass discharge of chlorinated ethenes emanating from clay till  
 1065 sites. *Journal of Contaminant Hydrology*, 252, 104121. <https://doi.org/10.1016/j.jconhyd.2022.104121>
- 1066 Rosenbom, A. E., Therrien, R., Refsgaard, J. C., Jensen, K. H., Ernsten, V., & Klint, K. E. S. (2009). Numerical  
 1067 analysis of water and solute transport in variably-saturated fractured clayey till. *Journal of Contaminant*  
 1068 *Hydrology*, 104, 137–152. <https://doi.org/10.1016/j.jconhyd.2008.09.001>
- 1069 Sale, T., Parker, B. L., Newell, C. J., & Devlin, J. F. (2013). *Management of Contaminants Stored in Low*  
 1070 *Permeability Zones: A State-of-the-Science Review*.
- 1071 Schulze-Makuch, D. (2005). Longitudinal dispersivity data and implications for scaling behavior. *Ground Water*,  
 1072 43(3), 443–456. <https://doi.org/10.1111/j.1745-6584.2005.0051.x>
- 1073 Seyedabbasi, M. A., Newell, C. J., Adamson, D. T., & Sale, T. C. (2012). Relative contribution of DNAPL  
 1074 dissolution and matrix diffusion to the long-term persistence of chlorinated solvent source zones. *Journal of*  
 1075 *Contaminant Hydrology*, 134–135, 69–81. <https://doi.org/10.1016/j.jconhyd.2012.03.010>
- 1076 Sidle, R. C., Nilsson, B., Hansen, M., & Fredericia, J. (1998). Spatially varying hydraulic and solute transport  
 1077 characteristics of a fractured till determined by field tracer tests, Funen, Denmark. *Water Resources Research*,  
 1078 34(10), 2515–2527. <https://doi.org/10.1029/98WR01735>
- 1079 Snow, D. T. (1969). Anisotropic permeability of fractured media. *Water Resources Research*, 5(6), 1273–1289.
- 1080 Switzer, A. D., & Pile, J. (2015). Grain size analysis. In I. Shennan, A. J. Long, & B. P. Horton (Eds.), *Handbook of*  
 1081 *Sea-level Research* (pp. 331–346). Wiley Blackwell. <https://doi.org/https://doi-org.proxy.findit.cvt.dk/10.1002/9781118452547.ch22>
- 1082
- 1083 Szymkiewicz, A., Savard, J., & Jaworska-Szulc, B. (2019). Numerical analysis of recharge rates and contaminant  
 1084 travel time in layered unsaturated soils. *Water (Switzerland)*, 11(3). <https://doi.org/10.3390/w11030545>

- 1085 Therrien, R., & Sudicky, E. A. (1996). Three-dimensional analysis of variably-saturated flow and solute transport in  
1086 discretely-fractured porous media. *Journal of Contaminant Hydrology*, 23, 1–44.  
1087 [https://doi.org/10.1016/0169-7722\(95\)00088-7](https://doi.org/10.1016/0169-7722(95)00088-7)
- 1088 Vukovic, M., & Soro, A. (1992). *Determination of hydraulic conductivity of porous media from grain-size*  
1089 *composition*. Littleton, Colorado, USA: Water Resources Publications.
- 1090 Waldowski, B., Sánchez-León, E., Cirpka, O. A., Brandhorst, N., Hendricks Franssen, H., & Neuweiler, I. (2023).  
1091 Estimating Groundwater Recharge in Fully Integrated *pde* -Based Hydrological Models. *Water Resources*  
1092 *Research*, 59(3). <https://doi.org/10.1029/2022WR032430>
- 1093 Weatherill, D., Graf, T., Simmons, C. T., Cook, P. G., Therrien, R., & Reynolds, D. A. (2008). Discretizing the  
1094 Fracture-Matrix Interface to Simulate Solute Transport. *Ground Water*, 46(4), 606–615.  
1095 <https://doi.org/10.1111/j.1745-6584.2007.00430.x>
- 1096 Wilke, C. R., & Chang, P. (1955). Correlation of diffusion coefficients in dilute solutions. *AIChE Journal*, 1(2),  
1097 264–270. <https://doi.org/10.1002/AIC.690010222>
- 1098 Witherspoon, P. A., Wang, J. S. Y., Iwai, K., & Gale, J. E. (1980). Validity of cubic law for fluid flow in a  
1099 deformable rock fracture. *Water Resources Research*, 16(6), 1016–1024.
- 1100 Yang, H., Liu, Q., Hu, R., Ptak, T., Taherdangkoo, R., Liu, Y., & Noubactep, C. (2022). Numerical case studies on  
1101 long-term effectiveness of metallic iron based permeable reactive barriers: Importance of porosity  
1102 heterogeneity of the barrier. *Journal of Hydrology*, 612(PB), 128148.  
1103 <https://doi.org/10.1016/j.jhydrol.2022.128148>
- 1104 Yang, L., Wang, X., Mendoza-Sanchez, I., & Abriola, L. M. (2018). Modeling the influence of coupled mass  
1105 transfer processes on mass flux downgradient of heterogeneous DNAPL source zones. *Journal of*  
1106 *Contaminant Hydrology*, 211, 1–14. <https://doi.org/10.1016/j.jconhyd.2018.02.003>
- 1107 Yin, Y., Sykes, J. F., & Normani, S. D. (2015). Impacts of spatial and temporal recharge on field-scale contaminant  
1108 transport model calibration. *Journal of Hydrology*, 527, 77–87. <https://doi.org/10.1016/j.jhydrol.2015.04.040>
- 1109 Young, N. L., Simpkins, W. W., Reber, J. E., & Helmke, M. F. (2019). Estimation of the representative elementary  
1110 volume of a fractured till: a field and groundwater modeling approach. *Hydrogeology Journal*, 28(2), 781–  
1111 793. <https://doi.org/10.1007/s10040-019-02076-y>
- 1112 Young, N. L., Simpkins, W. W., & Horton, R. (2021). Are Visible Fractures Accurate Predictors of Flow and Mass  
1113 Transport in Fractured Till? *Groundwater*, 59(1), 24–30. <https://doi.org/10.1111/gwat.13013>  
1114
- 1115  
1116  
1117

1  
2  
3  
4  
5  
6  
7  
8  
9  
10  
11  
12  
13  
14  
15  
16  
17  
18  
19  
20  
21  
22  
23  
24  
25  
26  
27  
28  
29  
30  
31  
32  
33

*Water Resources Research*

Supporting Information for

**Quantification of contaminant mass discharge from point sources in aquitard/aquifer systems based on high-resolution vertical concentration profiles and 3-D modeling**

Klaus Mosthaf<sup>1,\*</sup>, Louise Rosenberg<sup>1</sup>, Mette M. Broholm<sup>1</sup>, Annika S. Fjordbøge<sup>1</sup>, Gro Lilbæk<sup>2</sup>, Anders G. Christensen<sup>2</sup>, Poul L. Bjerg<sup>1</sup>

<sup>1</sup> Department of Environmental and Resource Engineering, Technical University of Denmark, Bygningstorvet, 2800 Kgs. Lyngby, Denmark.

<sup>2</sup> NIRAS, Sortemosevej 19, 3450 Allerød, Denmark.

\*Corresponding author (klmos@dtu.dk)

**Contents of this file**

- Text S1: Field-site investigations
- Figure S1: Timeline
- Figure S2: Multilevel samplers
- Figure S3-S6: Logs from the low-level MiHPTs (MiHPT04 to MiHPT07)
- Table S1: Hydraulic conductivities from slug tests
- Table S2: Hydraulic conductivities from grain size analysis
- Table S3: Content of organic carbon (TOC)
- Table S4: Results from sorption capacity tests
- Table S5: Coordinates used in the model
- Table S6: Vertical hydraulic matrix conductivities used in the DFM models

**Additional Supporting Information (Files uploaded separately)**

Table S7: Concentration\_profiles.csv in the data repository (<https://doi.org/10.11583/DTU.22884035>): Groundwater concentrations of sum of chlorinated solvents measured using SP16, multilevel samplers and GWP. The X and Y coordinates are according to the model coordinates.

34 **Introduction**

35 Supplementary information with a comprehensive description of the field site investigations,  
36 including:

- 37 - Site history, investigations, timeline
- 38 - Hydrogeology
- 39 - Hydraulic conditions
- 40 - Slug tests in groundwater wells
- 41 - Results from grain-size analysis
- 42 - Fraction of organic carbon of soil samples
- 43 - Contaminant status of the site
- 44 - Groundwater samples from screened wells
- 45 - Multilevel samplers
- 46 - Soil samples, porosity, results from sorption tests
- 47 - Coordinates important for the model setup

48 A table listing depth-discrete values of the concentrations measured in the profiles with the  
49 Groundwater Profiling tool (GWP) and the concentration measurements from multilevel samplers at  
50 the site can be found in the data repository (<https://doi.org/10.11583/DTU.22884035>).

51

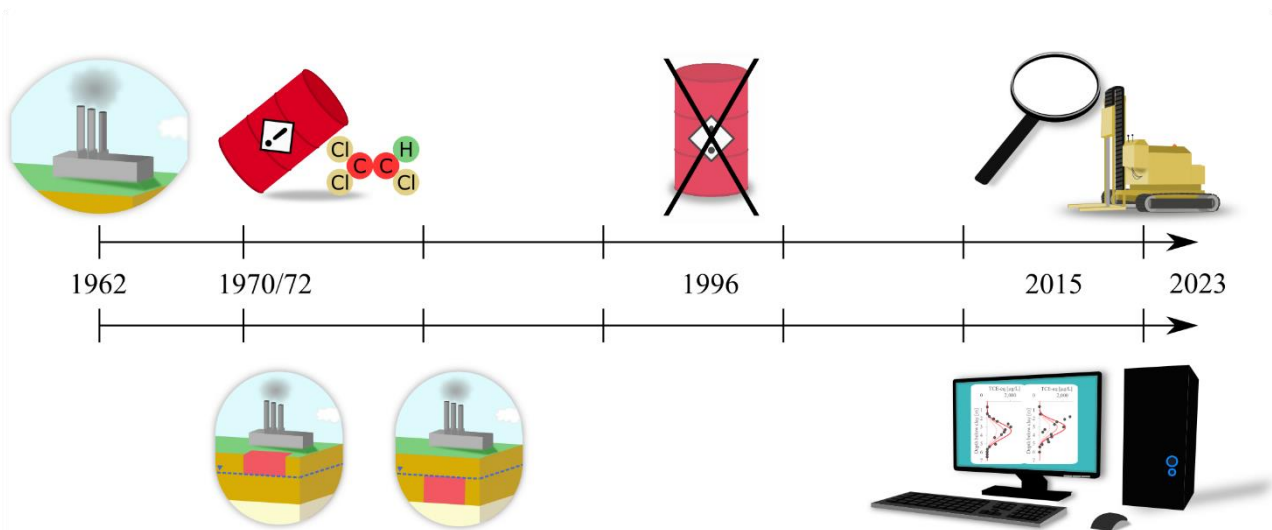


52

53 **Text S1: Field site investigations**

54 Site history and investigations

55 Field site investigations included groundwater samples (with screen lengths between 6 cm and  
56 2 m), soil samples, membrane interface probe hydraulic profiling tool (MiHPT), slug tests, and  
57 monitoring of the hydraulic head. The geology at the site consists of a clayey till layer of a varying  
58 thickness of 10-13 m with embedded sand lenses. Depth-discrete soil samples have shown through  
59 grain size analysis and the determination of the fraction of organic carbon that the clayey till  
60 consists of two separate packages; an upper clayey till and a lower clayey till, with an embedded  
61 sand layer in between. The upper clayey till is unsaturated (above the groundwater table), whereas  
62 the lower clayey till is saturated. Below the lower clayey till is a transition zone with a varying  
63 thickness of 1-2 meters and a sandy aquifer. A timeline of activities at the site, along with the  
64 timeline used for the modeling, is shown in Figure S1.  
65



66 **Figure S1. The top part of the figure depicts the contaminant activities at the contaminated sites using the**  
67 **knowledge of when the TCE was released at the site and when the input was stopped. The exact time is unknown,**  
68 **but the time interval in which the spill happened is known. The bottom part depicts the timeline used for the**  
69 **modelling of the contaminant spill.**  
70

71

72 Hydrogeology

73 The geology at the site was interpreted based on 43 borehole logs and 26 hydraulic profiles  
74 determined by the Hydraulic Profiling Tool (HPT) and performed across the site (plume scale).  
75 Furthermore, grain size analysis and fraction of organic carbon have been analyzed at six selected  
76 locations in the source and plume area.  
77

77

78 Slug tests in groundwater wells

79 In 56 of the screened groundwater wells falling head slug tests were performed to estimate  
80 the hydraulic conductivity of the aquifer. A pressure transducer was submerged into the well and  
81 the hydraulic head was recorded every 0.1 s (at 10 Hz). After the system had reached equilibrium,  
82 the water table was raised by approximately 1 m applying a vacuum. The vacuum was released and  
83 the falling hydraulic head was recorded (Hinsby et al. 1992) twice for each screen. The falling head  
84 curves were analyzed with the software AQTESOLV, using the Hvorslev method (Hvorslev 1951).

85 The estimated hydraulic conductivities based on the slug tests are shown in Table S1. The  
 86 results have been analyzed as a total and divided into five levels. Generally, the hydraulic  
 87 conductivities varied between  $0.80 \cdot 10^{-5}$  and  $13.0 \cdot 10^{-5}$  m/s with a total geometric mean ( $K_g$ ) of  
 88  $3.42 \cdot 10^{-5}$  m/s. The interval of the geometric mean in the five levels is narrow, varying between  
 89  $2.02 \cdot 10^{-5}$  and  $6.13 \cdot 10^{-5}$  m/s. The variance of the samples, both total and divided into the five levels,  
 90 is small as it does not exceed 0.5. However, the variance is generally smaller when the results are  
 91 divided into the five levels than the total variance, indicating a somewhat layered hydraulic  
 92 conductivity, though the interval of the geometric mean between the layers is small.

93  
 94 **Table S1. Geometric mean ( $K_g$ ) of estimated hydraulic conductivities ( $K$ ) from slug tests. The results are divided**  
 95 **into five different levels as well as a summarization of all 56 slug tests. For each level, the following parameters**  
 96 **are given: the number of performed slug tests ( $N$ ), the geometric mean ( $K_g$ ), the interval of the estimated**  
 97 **hydraulic conductivity (Interval), and the variance of  $\ln(K)$  ( $\sigma^2 \ln K$ ).**  
 98

Level (m above sea level)	$N$	$K_g$ ( $10^{-5}$ m/s)	Interval of $K$ ( $10^{-5}$ m/s)	$\sigma^2 \ln K$
30.05 – 31.35	18	3.83	0.80 – 7.93	0.25
26.69 – 27.51	17	6.13	0.82 – 13.0	0.49
24.21 – 25.16	15	2.53	1.05 – 3.55	0.13
22.95 – 23.16	4	2.02	1.93 – 2.69	0.13
21.11 – 21.16	2	2.82	1.93 – 4.11	(*)
Total	56	3.42	0.80 – 13.0	0.44

99 \*Too few slug tests to perform statistics on

### 100 Grain size analysis

101 The grain size distributions of 116 samples were analyzed, representing different geologic  
 102 units at the site. First, approximately 100 g sample was sieved to divide the sample into two  
 103 subsamples: with fractions larger and smaller than 0.063 mm. The subsample larger than 0.063 mm  
 104 was sieved through 9 different sieves varying in mesh size from 0.063 – 2.0 mm. For the subsample  
 105 smaller than 0.063 mm a laser diffraction particle size analyzer (Mastersizer2000) was used. The  
 106 Mastersizer2000 could measure grain sizes down to 0.0002 mm (Switzer and Pile 2015). The results  
 107 from the grain-size analysis were used to get an estimate of the hydraulic conductivity for the  
 108 different geological units. This was done using the HydrogeoSieveXL tool (Devlin 2015), an Excel  
 109 spreadsheet that uses 15 different equations to estimate the hydraulic conductivity based on grain-  
 110 size analysis. For all 116 samples, three of the 15 equations were applicable: Sauerbrei (from  
 111 (Vukovic and Soro 1992); Alyamani and Sen 1993; Barr 2005). However, for some of the samples  
 112 more than the three equations were applicable, but only the same three equations were used for all  
 113 samples to keep consistency. Applicable conditions for Sauerbrei are for sand and sandy clay with a  
 114  $d_{10} < 0.05$  cm, where  $d_{10}$  corresponds to the grainsize of which 10 % of the sample was smaller. For  
 115 Alyamani and Barr the applicable conditions are unspecified however, both of the articles are  
 116 focused on hydraulic conductivities in the interval  $10^{-4}$  –  $10^{-2}$  m/s, which is expected to be much  
 117 higher than what is found in a clayey till. Therefore, caution on the results must be taken for the  
 118 samples within the clayey till. With this in mind, the reported hydraulic conductivities for the 116  
 119 samples are a geometric mean of the result from the three equations.

120 In Table S2, the results for the 116 samples have been divided into five different layers based  
 121 on the geological description of the samples: Three of them within the clayey till, one in the

122 transition zone, and one in the aquifer. The hydraulic conductivity found for the sand/silt in  
 123 between the clayey tills is higher than those found for the two different clay packages. The upper  
 124 clayey till has a lower hydraulic conductivity than the lower, however, they are relatively close to  
 125 each other. The upper clayey till has a much higher interval and variance than the lower one,  
 126 indicating that the lower clayey till is more homogenous than the upper. Note that the  
 127 groundwater table was at the sand/silt between the two clayey till layers, and the upper clayey till  
 128 was not included in the modeling. The high variance of the sand/silt within the till, the transition  
 129 zone and the aquifer indicates some heterogeneities. However, the hydraulic conductivity of the  
 130 aquifer from the grain size analysis ( $1.81 \cdot 10^{-5}$  m/s) and that found from the slug tests ( $3.42 \cdot 10^{-5}$  m/s)  
 131 are fairly similar considering the different sampling sizes and techniques.

132  
 133 **Table S2. Geometric mean ( $K_g$ ) of estimated hydraulic conductivities ( $K$ ) from grain size analysis using three**  
 134 **different equations. The results are divided into five different geologies, three for the till, one for the transition**  
 135 **zone and one for the aquifer. For each geology, the following parameters are given: the number of samples ( $N$ ),**  
 136 **the geometric mean ( $K_g$ ), the interval of the geometric mean (Interval) and the variance of  $\ln(K_g)$  ( $\sigma^2 \ln K$ ).**

Geological description	$N$	$K_g$ ( $10^{-7}$ m/s)	Interval of $K$ (m/s)	$\sigma^2 \ln K$
Upper clayey till	24	0.82	$5.71 \cdot 10^{-10} - 3.22 \cdot 10^{-6}$	4.65
Sand/silt within the till	21	4.52	$4.09 \cdot 10^{-8} - 3.26 \cdot 10^{-6}$	4.51
Lower clayey till	27	1.87	$5.27 \cdot 10^{-8} - 6.44 \cdot 10^{-7}$	0.56
Sandy silt (transition zone)	11	6.90	$8.22 \cdot 10^{-8} - 3.82 \cdot 10^{-6}$	3.63
Silty sand/sand (aquifer)	33	181	$1.05 \cdot 10^{-7} - 8.17 \cdot 10^{-5}$	3.73

137

138 Fraction of organic carbon

139 The fraction of organic carbon ( $f_{oc}$ ) was analyzed for 62 samples representing the different  
 140 geologic units at the site. Firstly, the samples were crushed and cleaned for inorganic carbon using  
 141 phosphoric acid. Secondly, the samples were analyzed in a carbon determinator (LECO Induction  
 142 furnace CS-230). The LECO heats the sample to 850 °C while adding oxygen to burn the sample  
 143 completely. The gas from the combustion chamber was analyzed for the carbon content. Triplicates  
 144 were made for each sample. In Table S3, the results have been summarized by being divided into  
 145 five different geological units, as described in the section "Grain size analysis".

146  
 147 **Table S3. Content of organic carbon divided into five different geological layers, three in the clayey till, one in**  
 148 **the transition zone, and one in the aquifer. For each layer, the following parameters are given: the number of**  
 149 **samples ( $N$ ), the mean of the content of organic carbon (TOC), the interval of the content of organic carbon, and**  
 150 **the variance ( $\sigma^2$ ).**

Geological description	$N$	TOC (%)	Interval of TOC (%)	$\sigma^2$
Upper clayey till	14	0.084	0.039 – 0.240	0.237
Sand/silt within the till	10	0.068	0.027 – 0.121	0.189
Lower clayey till	11	0.180	0.111 – 0.219	0.193
Sandy silt (transition zone)	7	0.114	0.026 – 0.087	0.161
Silty sand/sand (aquifer)	20	0.045	0.011 – 0.145	0.188

151

152 Contaminant status

153 To investigate the contaminant status at the site, both soil and groundwater concentrations  
154 have been measured. All samples were analyzed at an accredited laboratory, either Eurofins or ALS  
155 Denmark A/S.

156 Initially, three volumes of standing water were purged from the screened wells and multilevel  
157 samplers (MLS) before the groundwater sampling. Furthermore, for all three types of groundwater  
158 samples, electrical conductivity (EC), redox potential, pH, oxygen, and temperature were monitored.  
159 When all parameters stabilized, the groundwater samples were taken as described in Rønne et al.  
160 (2017).

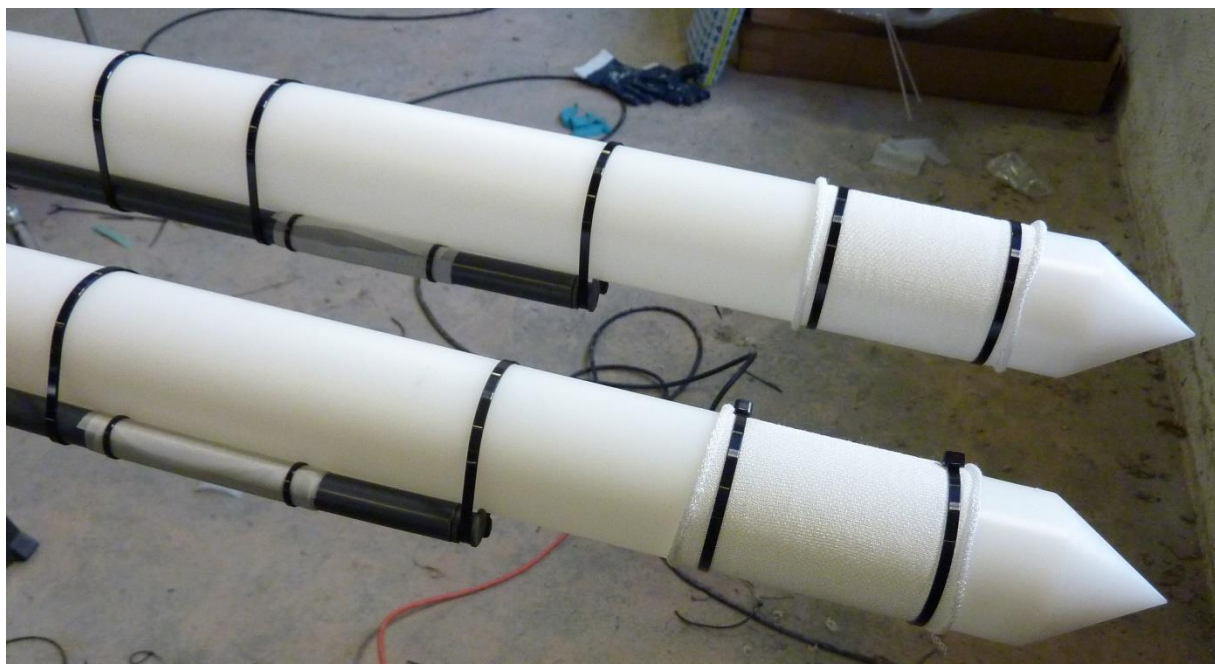
161 Groundwater samples from screened wells

162 The screened wells were sampled in November 2017. The screen length for most of the wells  
163 is two meters, however, some are one meter. In total, 35 screens were sampled. Furthermore, in  
164 June 2018, 32 samples were taken using the GeoProbe SP16 with a screen length of 1 meter,  
165 covering nine different locations. One SP16 was placed in the source zone (shown on figures in the  
166 main paper). The screen length of this SP16 was reduced to 14 cm. A description of the SP16  
167 system is available from (Geoprobe 2023).

168  
169 Multilevel samplers (MLS)

170 Three MLS were designed in the source zone area as a part of the investigation of the bottom  
171 of the clay, the transition zone and upper aquifer (approximately 29.5-32.5 m above sea level). Each  
172 MLS consisted of 12 16 mm Ø pipes attached to the outside of a 63 mm Ø pipe (Figure S2). Each  
173 pipe had a screen with a length of 6 cm with a fine masked sock outside the screen in order to  
174 prevent the fine silt and clay particles from clogging the screens. The distance between the screens  
175 was 25 cm, covering a depth of three meters. Each MLS was installed in individual boreholes. In  
176 total, 39 groundwater samples were taken from the three MLS in December 2020. Groundwater  
177 was sampled using an intertie pump. The results can be found in Table S7 (data repository).

178



179

180 **Figure S2. Multilevel samplers.**

181

## 182 Groundwater Profiler (GWP)

183 We performed high-resolution measurements with the direct-push method Groundwater  
184 Profiler tool (GWP) (Geoprobe<sup>®</sup>), which yielded the concentration distribution of TCE and its  
185 degradation products at a high vertical resolution. The profiles were obtained at seven locations,  
186 aiming for five profiles at the centerline and two at the outer edges of the plume. Four of the  
187 profiles were taken in a plane perpendicular to the flow direction. A GWP 1.75 Groundwater Profiler  
188 Geoprobe<sup>®</sup> system (Dutta et al., 2021) was employed. Water samples were extracted in 10 cm  
189 intervals by pushing a probe into the ground and circulating water through 20 ports (four rows  
190 with five ports on each side of the probe, spanning over 10 cm). While lowering the probe into the  
191 ground, deionized water was pumped through a low-density polyethylene tube into the formation  
192 through the ports. This was done to avoid clogging of the ports. Water samples were extracted  
193 with a syringe pump, which is located in the head of the probe right above the ports. Field  
194 measurements of pH, electrical conductivity (EC), oxygen content, redox parameters and  
195 temperature of the extracted water were performed. When the EC signal had stabilized (deionized  
196 water has a different electric conductivity than the formation water), the final groundwater samples  
197 were extracted. The samples were analyzed at a certified laboratory (ALS Danmark) for the  
198 concentrations of TCE and its degradation products. The results can be found in table S7 in the  
199 data repository.

200

## 201 Soil samples

202 Soil samples were taken every half meter from 3 m below ground level while drilling the  
203 boreholes B301-B303 in the source zone. The soil samples used for analyzing the soil  
204 concentrations were stored in Rilsan<sup>®</sup> bags; the samples used for grain size analysis were stored in  
205 regular plastic bags.

206

## 207 Porosity

208 Prior to the grain size analysis, the soil samples were dried to remove all of the water in the  
209 soil sample. The samples were weighed before and after the drying to investigate the mass of  
210 water,  $m_{water}$  in each sample:

211

$$m_{water} = m_{wet} - m_{dry}$$

212 where  $m_{wet}$  is the mass before the drying and  $m_{dry}$  is the mass after the drying. The percentage of  
213 the water in the sample,  $c_{water,\%}$  is found as:

214

$$c_{water,\%} = \frac{m_{water}}{m_{wet}} \cdot 100\%$$

215

For soil samples in the saturated zone, the porosity  $\phi$ , can be found from  $c_{water,\%}$  as:

216

$$\phi = \frac{\frac{c_{water,\%}}{\rho_w}}{\frac{100 - c_{water,\%}}{\rho_{soil}} + \frac{c_{water,\%}}{\rho_{soil}}}$$

217

where  $\rho_s$  is the density of the dry soil material 2.65 kg/L,  $\rho_w$  is the density of water.

218

219 Sorption

220 To investigate the retardation of the contaminant transport through the clayey till, transition  
221 zone and aquifer, the sorption capacity was tested for 17 different soil samples, covering the  
222 different soil types at the site. The experiment was carried out in a two-phase system following the  
223 OECD guidelines, as summarized in Lu et al. (2011). Initial aqueous concentrations were 4, 10 and  
224 20 mg/L, using a stock solution with a mix of TCE and cis-DCE. 4 mg/L is in the range that showed  
225 linearity in a previous sorption experiment with TCE, and 10-20 mg/L were within the fairly linear  
226 range in Lu et al. (2011). The higher concentrations are needed to accommodate the risk of  
227 remaining contamination in the clayey till. 30 g of soil was added to each 42.3 mL vial. The  
228 soil:water ratio is based on a desirable sorption of around 50 % ( $\pm 30$  %) that covers the expected  
229 *K<sub>d</sub>* range for sand to clayey till. The samples were rotated for 4 days at 10 °C. Triplicates were taken  
230 for each concentration level. When fitting the concentration levels, four of the samples were taken  
231 out, hence, only duplicates were used for four of the samples (see Table S4). The water phase was  
232 analyzed for TCE and cis-DCE on a GC-MS using the regular 85 °C program.

233 As there were issues with sample S2, no results were obtained from that.

234  
235  
236

**Table S4. The results of the sorption capacity experiments for 17 soil samples at the contaminated site, including the linear sorption coefficient ( $K_d$ ), the clay content and the TOC.**

Sample no.	Depth [m bgl]	Soil type	Points for fitting	$K_d$ [L/kg]		Comments	Clay content [%]	TOC [%]
				TCE [R <sup>2</sup> ]	cis-DCE [R <sup>2</sup> ]			
S1	4.5	Clayey till	3	0.34 [0.99]	0.21 [0.97]		7.22	0.039
S2	5	Clayey till	3	-	-			
S3	6	Clayey till	3	0.37 [0.92]	0.34 [0.95]		12.3	0.098
S4	6.5	Sandy till	3	0.41 [0.99]	0.31 [0.99]		7.15	0.042
S5	7	Sandy silt	3	0.42 [0.92]	0.14 [0.79]	Duplicates for middle cis-DCE	5	0.108
S6	7.5	Silt	3	0.66 [0.98]	0.35 [0.91]		5.82	0.121
S7	9	Clayey till	3	1.10 [0.88]	0.54 [0.89]		6.2	0.214
S8	9.5	Clayey till	3	0.96 [0.96]	0.47 [0.99]		7.28	0.198
S9	10	Clayey till	2	0.55 [0.99]	0.46 [0.98]		9.4	0.181
S10	11.5	Sandy silt	3	0.30 [0.96]	0.20 [0.93]	Duplicates for middle cis-DCE	9.2	0.137
S11	11.5	Sandy silt	3	0.80 [0.99]	0.49 [0.98]		5	0.105
S12	12	Sandy silt	3	0.62 [0.99]	0.37 [0.99]		2.65	0.105
S13	12	Silty sand	3	0.35 [0.94]	0.14 [0.64]		6.1	0.095
S14	12.5	Silty sand	3	0.67 [0.94]	0.58 [0.97]		10.8	0.145
S15	13	Silty sand	2	0.26 [0.99]	0.08 [0.74]	Duplicates for middle for both	3.5	0.044
S16	14	Sandy aquifer	3	0.11 [0.87]	0.08 [0.96]		0.95	0.021
S17	14	Sandy aquifer	3	0.34 [0.99]	0.26 [0.98]		0.92	0.016

237

### Coordinates important for the model set-up

Important coordinates used in the model are given in Table S5. The source area is 16 m wide and 20 m long and placed with a rotation of -28.2 degrees.

**Table S5. Coordinates used in the model for placement of the source zone and the two transects.**

	<b>X [m]</b>	<b>Y [m]</b>
Source center	1212.5	2235.5
Transect A	1220.4	2257.6
Transect A'	1182.4	2160.1
Transect B	1131.8	2207.3
Transect B'	1222.3	2161.3

### Hydraulic conductivities and apertures used in the DFM models

In the discrete fracture-matrix models, the matrix hydraulic conductivity was calibrated to obtain the same bulk vertical hydraulic conductivity and hydraulic gradient as in the setup without fractures.

**Table S6. Vertical hydraulic matrix conductivities used in the DFM models.**

<b>Aperture [<math>\mu\text{m}</math>]</b>	<b><math>K_{v,\text{mat}}</math> [<math>10^{-9}</math> m/s]</b>
8	8.88
12	7.38
15	5.34
18.5	1.70
5-25	1.65



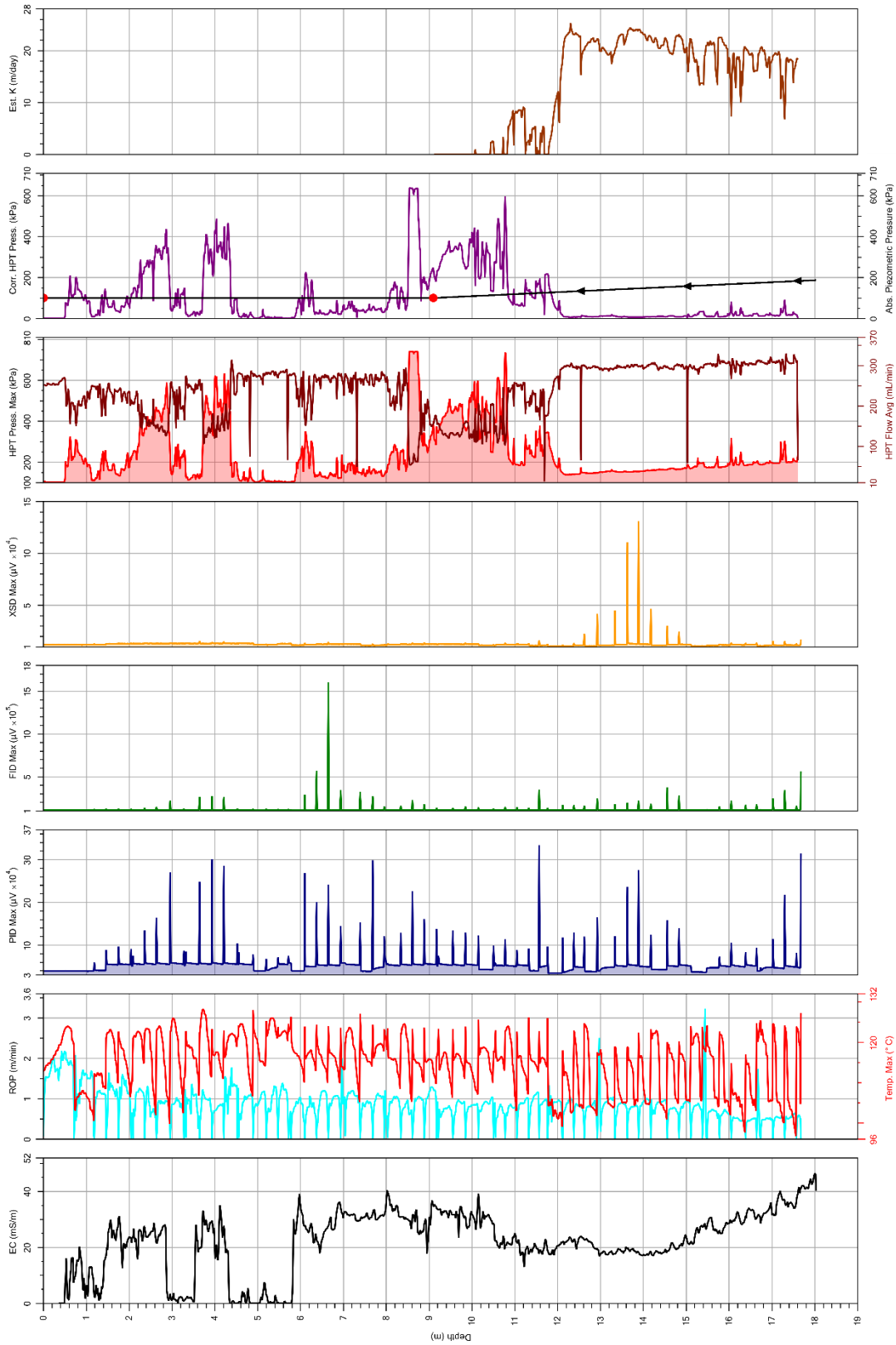


**Figure S3: Logs from the low-level MiHPT04 (LL-MiHPT), located at x=1208.2 m, y=2201.8 m, and z=43.587 m.**

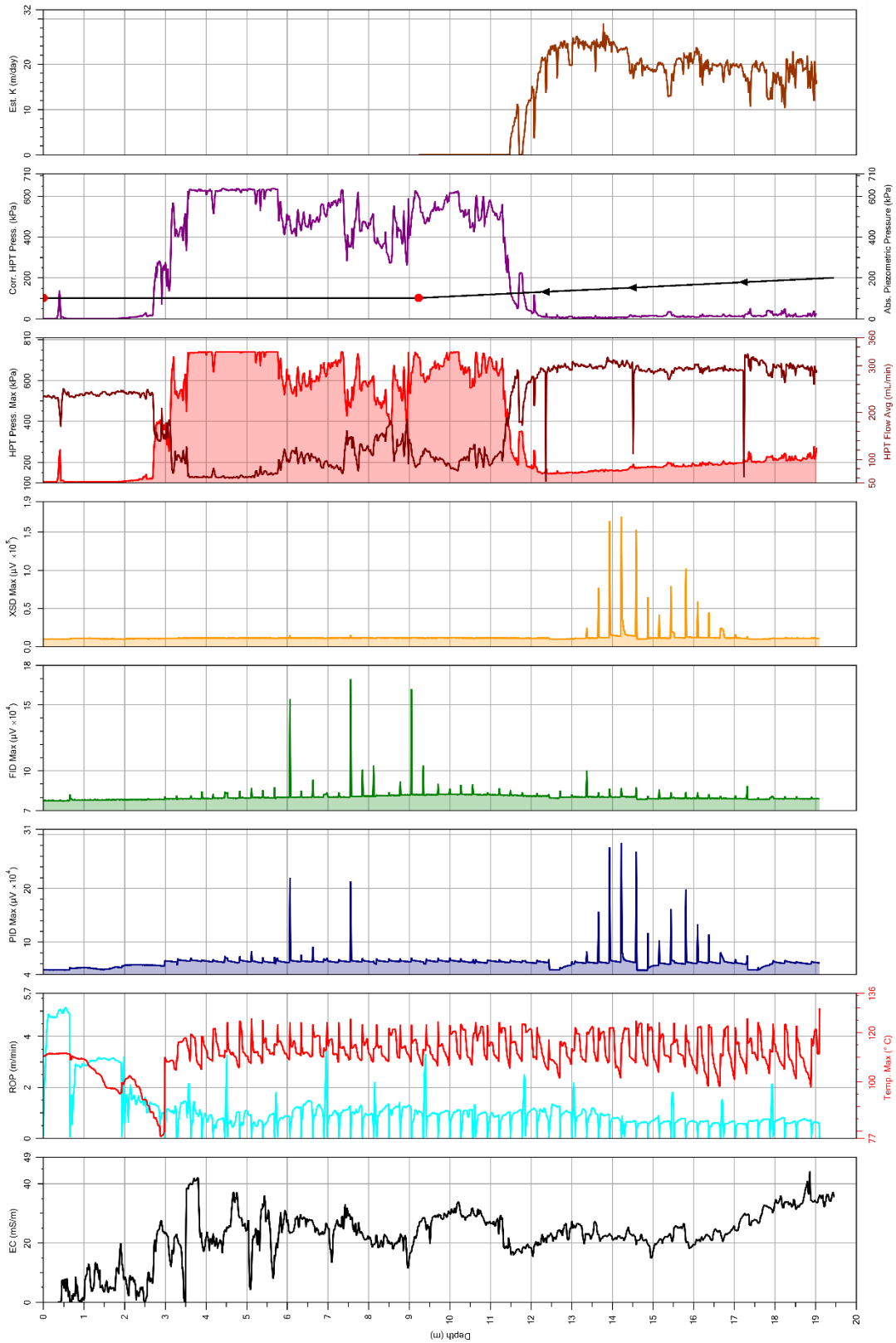


**Figure S4: Logs from the low-level MiHPT05 (LL-MiHPT), located at x=1201.7 m, y=2188.6 m, and z=43.639 m.**

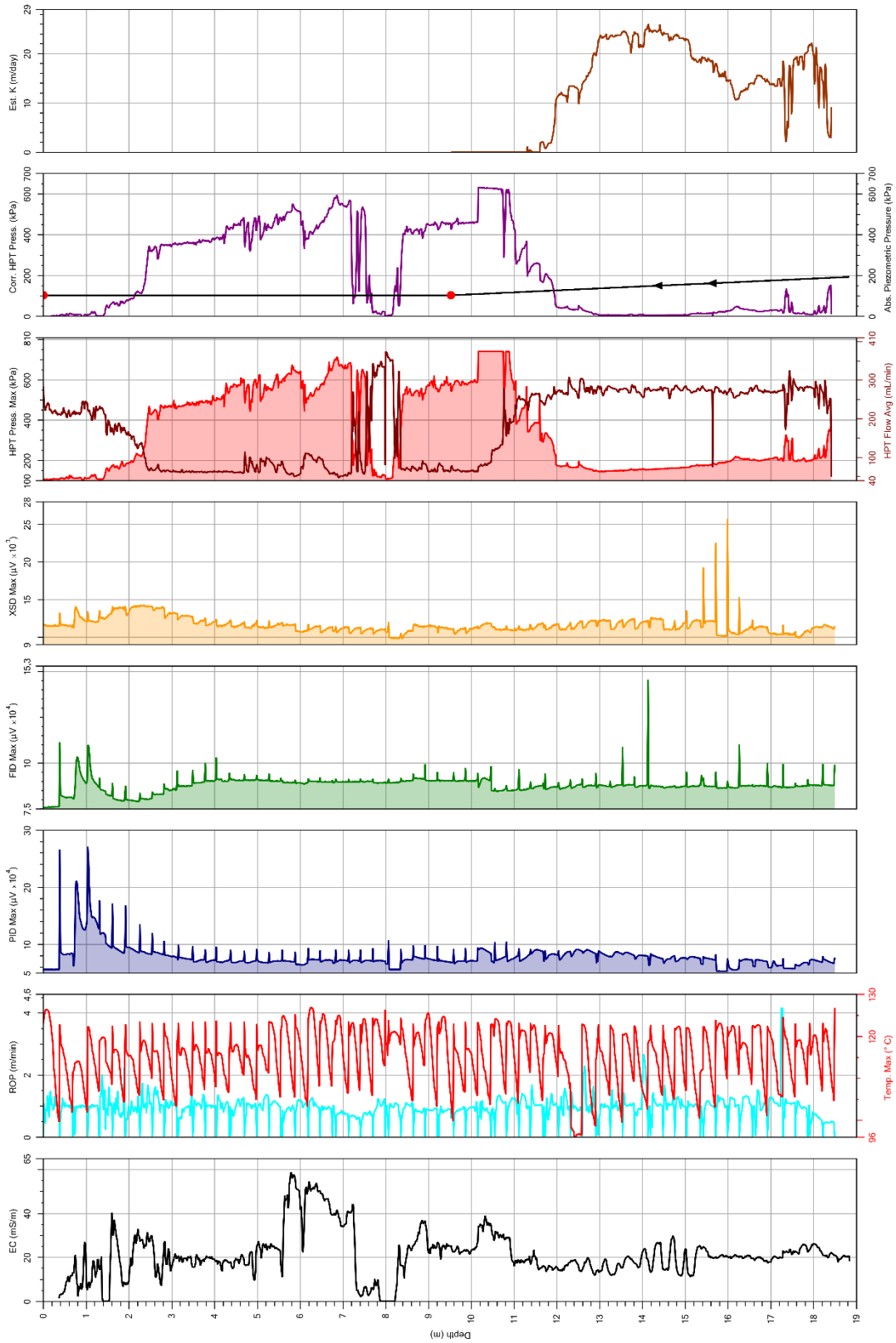


**Figure S5: Logs from the low-level MiHPT06 (LL-MiHPT), located at x=1179.2 m, y=2187.8 m, and z=43.607 m.**

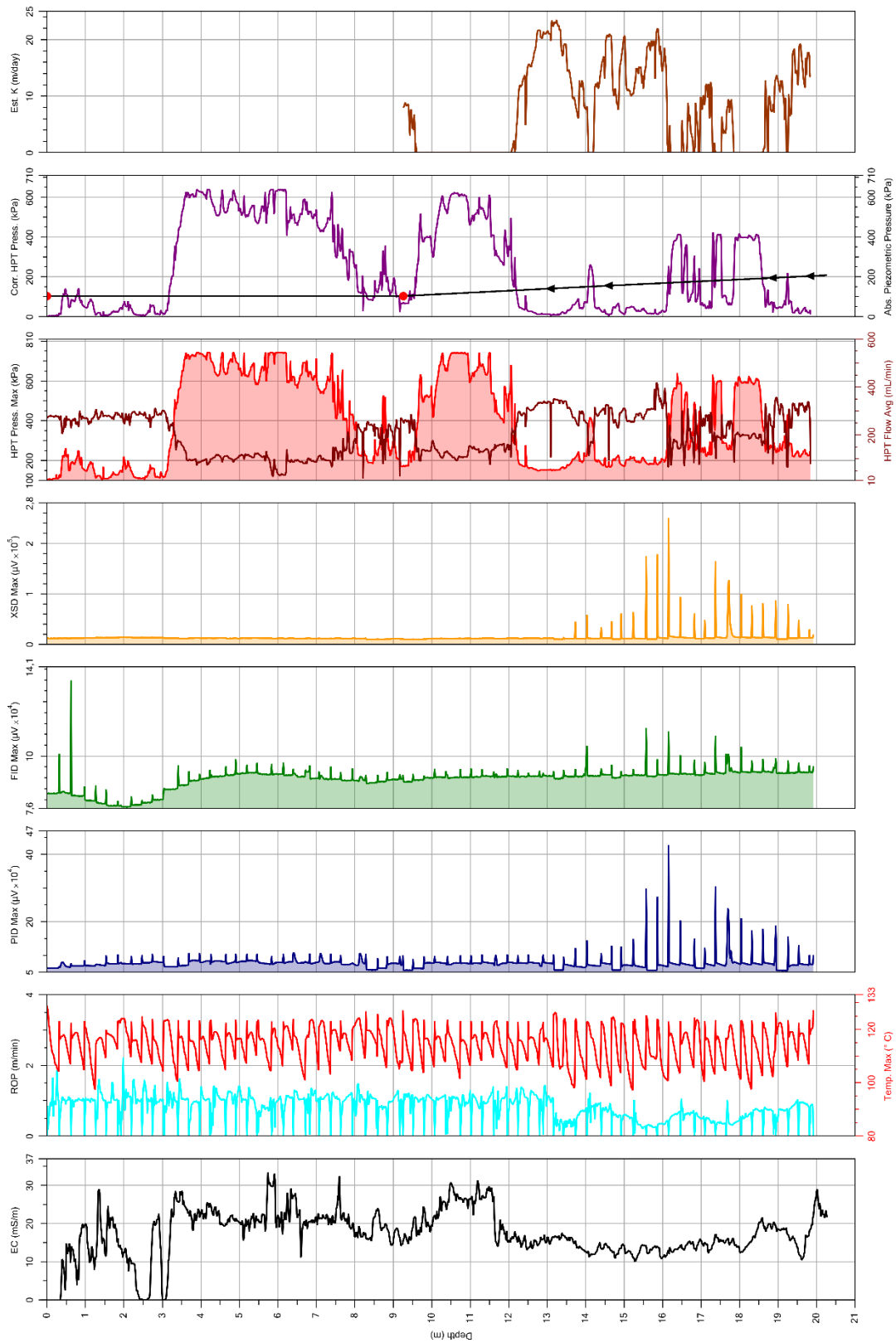


**Figure S6: Logs from the low-level MiHPT07 (LL-MiHPT), located at x=1196.3 m, y=2179.6 m, and z=43.571 m.**

Department of Environmental and Resource Engineering is one of the largest university departments specializing in environmental and resource engineering in Europe. The department conducts research, development & scientific advice and provides educational programs and service to society. We are working to develop new environmentally friendly and sustainable technologies, methods and solutions, and to disseminate this knowledge to society and future generations of engineers. The Department has approximately 300 staff of more than 30 nationalities.

Department of Environmental and Resource Engineering

Bygningstorvet, Building 115  
2800 Kgs. Lyngby  
Tel. +45 4525 1600

[www.sustain.dtu.dk](http://www.sustain.dtu.dk)

